Investigating the molecular basis of histidine catabolism in a human pathogenic bacterium *Pseudomonas aeruginosa* PAO1

A thesis presented in partial fulfilment of the

requirements for the degree of

Doctor of Philosophy

in

Microbiology & Genetics

at Massey University, Auckland,

New Zealand

Kiran Sreeja Jayan

2021

Abstract

Pseudomonas aeruginosa is an opportunistic and a nosocomial pathogen of significant medical concern, particularly for cystic fibrosis patients. The extensive metabolic flexibility coupled with an array of virulence factors make them ubiquitous and successful in causing persistent multi-drug resistant infections. Pathogens exploit nutrient-rich hosts, and thus nutrients can be considered as signals perceived by bacteria that allow host recognition and coordination of expression of metabolic and virulence genes for successful colonization. A deeper understanding of the metabolic pathways and host perception mechanisms are significant from a therapeutic perspective in the current era of antibiotic resistance.

Histidine is an amino acid that can serve as a source of carbon and nitrogen to many bacteria. Histidine catabolism in *Pseudomonas* spp., is widely known to occur via a 5-step enzymatic pathway, and the genes for histidine utilization (*hut*) are negatively regulated by HutC protein. The enteric bacteria and some others utilize a 4-step enzymatic pathway for histidine catabolism, which differs from the 5-step pathway in the direct conversion of intermediate formiminoglutamate (FIGLU) to glutamate. However, *P. aeruginosa* contains an additional operon (dislocated from the *hut* locus) encoding for formimidoylglutamase enzyme and its regulator, which can break down FIGLU similar to 4-step pathway. Previous studies report the accumulation of histidine metabolites, urocanate and FIGLU, in the mammalian tissues and reduced virulence of *P. aeruginosa* defective in histidine catabolism towards animal models. But the implications of the presence of two pathways for histidine catabolism or mechanisms associated with virulence remain elusive. This prompted us to examine the *hut* pathways and mechanisms that link *hut* with virulence in *P. aeruginosa* PAO1.

First, computational analysis identified a transporter gene (named *figT*) adjacent to formimidoylglutamase enzyme (FigA) and transcriptional regulator FigR. This led to a new hypothesis that the three genes (*figRAT*) are responsible for the uptake and utilization of FIGLU, and they are not involved in histidine utilization as previously thought. Genetic analyses utilizing site-directed mutagenesis and *lacZ* reporter fusions confirmed that *figT* encodes for a FIGLU-specific transporter whose expression is induced by FIGLU. The *figT* gene is co-transcribed with *figRA*, and its expression is activated by FigR. Furthermore, gene expression studies indicate that FIGLU is the physiological inducer of *fig* operon, while histidine and urocanate are indirect inducers (by virtue of conversion to FIGLU). Growth and fitness assays revealed that histidine is predominantly catabolised via the 5-step *hut* pathway (not via the FigRAT system). Together, our genetic and phenotypic data show that *fig* operon is involved in the direct utilization of FIGLU from the environment. Phylogenetic analysis

showed that *figRAT* genes are highly conserved and present in all completely sequenced strains of *P*. *aeruginosa*, but we found no evidence for horizontal gene transfer events.

Previous work in Zhang's laboratory suggests that urocanate derived from host tissues could serve as a signalling molecule, eliciting *P*. *aeruginosa* infections via interaction with the HutC regulator. Here, we aimed to seek further genetic, biochemical, and phenotypic evidence to improve our understanding of the global regulatory roles for HutC beyond histidine catabolism and determine their potential contribution to the colonization of eukaryotic hosts. Utilizing *in silico* analysis, we predicted 172 novel HutC-target sites in the genome of *P*. *aeruginosa* PAO1 with a *P* value less than 10^{-4}. Six selected candidates were subject to experimental verification for HutC binding by means of gel shift assays (EMSA) and/or DNAse I footprinting assays, and all were able to bind with purified $HutC_{his6}$ proteins. Further, a *hutC* deletion mutant was constructed by site-directed mutagenesis and subjected to phenotypic characterization. Phenotypic analyses revealed that *hutC* is involved in biofilm formation, tobramycin-induced biofilm formation, cell motility, and pyoverdine production. Significantly, we found that mutation of *hutC* resulted in reduced killing of *C*. *elegans* by *P*. *aeruginosa* PAO1.

Finally, we observed distinct binding patterns for HutC interaction with the *hutF* promoter DNAs in *P*. *aeruginosa* PAO1 and *P*. *fluorescens* SBW25 (a model plant-colonizing bacterium used for studies of histidine catabolism). Molecular investigations revealed that the differences were not caused by HutC proteins from either species, but HutC recognized a distinct site proximal to $hutF_{SBW25}$. This site displayed sequence similarity with the NtrC-binding site and was called the Pntr site. Functional analysis of the significance of Pntr site identified that Pntr site is necessary for the wild-type level production of HutF in *P*. *fluorescens* SBW25 during growth on histidine.

Overall, the results from this study enhance our understanding of *hut* catabolism in *Pseudomonas* and contribute to novel molecular mechanisms associated with the virulence of *P*. *aeruginosa* PAO1. The identification of *fig* operon for the utilization of FIGLU (accumulated in host tissues) and global regulatory role of HutC in gene expression have broader implications from a therapeutic perspective in treating *P*. *aeruginosa* PAO1 infections. The ability of HutC to recognise multiple distinct DNA-binding sites suggests complex modes of gene regulation mediated by HutC and promotes further studies to fully understand the functional significance of genes in the HutC regulon.

Acknowledgements

Undertaking this PhD was an impressive and challenging experience to me. Thank you, God! This journey would not have been possible without the guidance and support from many people.

Firstly, I would like to express my sincere gratitude to my mentor Associate Prof. Dr Xue-Xian Zhang for accepting me as a doctoral student. I developed many research skills from you, particularly troubleshooting and logical thinking/reasoning. Thank you for the enormous patience, continuous support, motivation, and guidance over all these years. Thank you for the constructive criticism which helped in improving my data analysis and scientific writing skills.

I thank Dr Sebastian Schmeier, my co-supervisor, for his support and encouragement. I extend my thanks to my laboratory colleague, Dr Naran Naren, for the initial training in the laboratory at the start of my study, valuable discussions, and sharing research information on *Pseudomonas fluorescens* SBW25. I am thankful to Dr Yunhao Liu and Dr Monica Gerth for use of some of their plasmids and strains involved in this study.

Thanks to all current and past members of Zhang lab, Hendrickson lab, and Rainey lab, who made the working place a happy and joyful one. Special thanks to Dr Daniel Rexin and Danielle Kok for maintaining laboratory and efforts in ordering consumables. Thanks to Farhad Golzar for useful tips on managing *Caenorhabditis elegans*.

I would like to express my special gratitude to my institute, School of Natural and Computational Sciences, and Massey University, for the scholarships that helped fund my studies and expenses in New Zealand.

I deeply thank my parents, P. Jayachandran Pillai and Sreeja Jayachandran Pillai for their love, trust, constant encouragement, patience, and additional financial support. I thank my brother, Saran Sreeja Jayan, for his constant encouragement throughout my studies. I must thank my wife, Manju Subhash Chandran, for being a good companion on this journey. I am grateful for your special late-night coffee that helped me stay awake. Thank you for the motivation and all the sacrifices you have made. I extend my thankfulness to all my family members, who were very supportive over these years.

Finally, I remember my grandma, Subhadra Itty Amma, who died last year. She was anxiously waiting for completion of my PhD study and return home.

Table of Contents

List of Figures

List of Supplementary Figures

List of Tables

List of Abbreviations

µg	Microgram
µl	Microlitre
µM	Micromolar
APS	Ammonium persulfate
Arr	Aminoglycoside response regulator
BSA	Bovine serum albumin
CCR	Carbon catabolite repression
CDS	Coding sequence
CF	Cystic fibrosis
CFTR	Cystic Fibrosis Transmembrane Conductance Regulator
Da	Dalton
DMSO	Dimethyl Sulfoxide
DNAse I	Deoxyribonuclease I
EMSA	Electrophoretic Mobility Shift Assay
EPS	Extracellular polymeric substance
FG	Formylglutamate
FIG	Figure
Fig. S	Supplementary figure
FIGLU	N-formimino-L-glutamate
g	Gram
Glu	Glucose
HAMPs	Host Associated Molecular Patterns
HEPES	4-(2-Hydroxyethyl)piperazine-1-ethanesulfonic acid
His	Histidine
Hut	Histidine utilization
IPTG	Isopropyl β-D-1-thiogalactopyranoside
KB	Kings medium B
K_d	Dissociation constant
kDa	Kilodaltons
LB	Luria-Bertani
M	Molar
mg	Milligram
MIC	Minimum Inhibitory Concentration
ml	Millilitre

mM	Millimolar
MOPS	4-Morpholinepropanesulfonic acid
MSM	Minimal salt medium
MW	Molecular weight
MWCO	Molecular eight cut-off
NAG	N-Acetyl-L-Glutamic acid
ncRNA	Non-coding Ribonucleic acid
ng	Nanogram
nm	Nanometre
nM	Nanomolar
PAGE	Polyacrylamide gel electrophoresis
Phut	HutC-binding inverted sequence (TGTA-N2-TACA)
PMSF	phenylmethylsulfonyl fluoride
Pntr	HutC-binding novel site in *hutF* promoter
QS	Quorum sensing
RE	Restriction enzyme
RFU	Relative fluorescence units
SDS	Sodium dodecyl sulfate
SOB	Super optimal broth
SOE	Splicing by overlap extension
sp.	species
SRC	Selection rate constant
Suc	Succinate
T3SS	Type 3 secretion system
T6SS	Type 6 secretion system
TBE	Tris-Borate-EDTA buffer
TEMED	Tetramethylethylenediamine
U	Units
UV	Ultraviolet
v/v	Volume by volume
w/v	Weight by volume
X-gal	5-bromo-4-chloro-3-indolyl ß-D-galactopyranoside

Chapter 1
Review of Literature

The fundamental basis for the association of bacteria with eukaryotic hosts is to acquire nutrients for their growth and proliferation. However, this is often challenged by host immune responses or competition from the resident microflora (Rohmer *et al.*, 2011, Abu Kwaik & Bumann, 2013). Hence, pathogenic bacteria have evolved mechanisms that coordinate expression of virulence factors and metabolic pathways as they move through multiple diverse environments to eukaryotic hosts (Balasubramanian *et al.*, 2013). Several studies indicate that the ability to utilize specific host-derived nutrients correlated with virulence and bacterial pathogenesis. The intracellular pathogen *Legionella pneumophila* requires amino acid threonine for their replication in phagosomes (Sauer *et al.*, 2005). Inactivation of the sialic acid catabolic pathway in a pathogenic strain of *Vibrio cholerae*, reduced their ability to colonize animal models (Almagro-Moreno & Boyd, 2009). In *Pseudomonas aeruginosa*, defects in the catabolism of amino acids such as alanine, tryptophan, and histidine correlated with reduced virulence (Boulette *et al.*, 2009, Shen *et al.*, 2008, Rietsch *et al.*, 2004). Also, *Pseudomonas fluorescens* mutants that are incapable of utilizing organic acids were found to be poor colonizers of the tomato roots, presumably due to competition from the resident microflora (Lugtenberg *et al.*, 1999, Somers *et al.*, 2004). Thus, in addition to being an energy source, nutrients may serve as signals allowing bacteria to sense suitable hosts and modulate virulence traits that trigger host-pathogen interactions (Rohmer *et al.*, 2011, Zhang *et al.*, 2014).

Besides, the gain and loss of metabolic pathways could also be related to site/niche specific infections. A good example is the ability to utilize tetrathionate, which is linked to the success of *Salmonella* Typhimurium in causing enteric infections. However, the related pathogens, *Salmonella* Typhi and Paratyphi that cause systemic infections appear to have lost this pathway (Rohmer *et al.*, 2011). Recently, researches have shifted focus towards directly targeting virulence factors for developing novel anti-microbials due to a rise in resistance to currently available antibiotics (Maurice *et al.*, 2018). In this regard, metabolic pathways could serve as potential therapeutic targets (Rohmer *et al.*, 2011). However, this requires a deeper understanding of the significance of metabolic pathways from a bacterial perspective and the underlying regulatory mechanisms that link specific metabolic pathways to virulence.

Research in our laboratory focuses on *hut* genes for the utilization of histidine in *Pseudomonas*. Histidine is an important amino acid that can serve as a source of nutrient and energy for many bacteria. Genetic studies on the characterisation of histidine utilization (*hut*)

genes and regulatory mechanisms dates to the 1950s, which discovered three paradigms: (i) carbon catabolite repression (CCR) for the preferential utilization of carbon sources, (ii) nitrogen dependent regulation of catabolic genes (NtrBC – two-component systems), and (iii) inducer-dependent autoregulation of transcriptional regulators (Itoh *et al.*, 2007, Bender, 2012). Recent work from our laboratory provided significant insights into the (i) mechanism of CCR acting on *hut* genes, (ii) the complex interplay of CCR and nitrogen regulation acting on *hut* genes, which requires to be carefully controlled to prevent *hut* system from stalling, and (iii) the involvement of *hut* transcriptional regulator (HutC) in the ecological success and global control of gene regulation in a plant-colonizing bacterium *Pseudomonas fluorescens* SBW25 (Zhang & Rainey, 2007b, Zhang & Rainey, 2008, Naren & Zhang, 2020, Naren & Zhang, 2021).

Accumulation of histidine metabolites, urocanate and formiminoglutamate (FIGLU), in eukaryotic tissues have been previously reported (Gibbs & Norval, 2011, Hibbard, 1964, Carey *et al.*, 1964, Perry *et al.*, 1975, Matsuda *et al.*, 1982, Stebbings & Lewis, 1986, Coulson & Hernandez, 1968). Urocanate is a good source of carbon and nitrogen and has been proposed as a cue for eliciting host-pathogen interactions through HutC regulator in *P. aeruginosa* PAO1 (Zhang *et al.*, 2014). Histidine catabolism also appears to be unusual in *P. aeruginosa* PAO1, because it was recently found to possess alternate enzymes to breakdown FIGLU (histidine metabolite) (Marti-Arbona *et al.*, 2006, Gerth *et al.*, 2012). In this review, we will first discuss the histidine catabolic pathways and their regulation in different bacterial genera. In the subsequent sections, we will discuss the potential global regulatory role of HutC that links histidine catabolism to virulence as a mechanism for how nutrients trigger host-pathogen interactions.

1.1 Histidine catabolic pathways in bacteria

Histidine is an amino acid that can serve as a good source of carbon, nitrogen, and energy for many bacteria. Hence, histidine catabolic pathway appears to be widely distributed among many bacterial genera but is not universal; for instance, *Escherichia coli* and *Shigella* do not contain *hut* operons (Bender, 2012). Depending on the bacterial genera, histidine catabolism proceeds via a 4-step or 5-step enzymatic pathway (Fig. 1.1). The first three enzymatic steps appear universal, where, histidine is sequentially converted to urocanate (and ammonia), 4-imidazolone-5-propionate, and N-formimino-L-glutamate (FIGLU) by HutH (histidase), HutU (urocanase), and HutI (Imidazolone propionate hydrolase), respectively (Itoh *et al.*, 2007, Bender, 2012). The histidine catabolic pathway branches at the intermediate FIGLU and has two fates. The enteric bacteria (*Salmonella enterica* and *Klebsiella pneumoniae*) and Gram-positive *Bacillus subtilis* break down histidine via 4-step pathway, wherein FIGLU is hydrolysed

to glutamate and formamide by formimidoylglutamase (HutG4: 4 denotes 4-step pathway enzyme) (Smith *et al.*, 1971, Rodriguez & West, 1984, Kimhi & Magasanik, 1970). Formamide is excreted as a waste product (Magasanik & Bowser, 1955). However, *Pseudomonas* spp. and *Streptomyces* sp. utilize a 5-step enzymatic pathway to break down histidine, wherein FIGLU is first hydrolysed to formylglutamate (and ammonia) by FIGLU deiminase (HutF), and formyglutamate is subsequently hydrolysed to glutamate and formate by formylglutamate amidohydrolase (HutG) (Tabor & Mehler, 1954, Lessie & Neidhardt, 1967, Hu *et al.*, 1987, Zhang & Rainey, 2007b, Kendrick & Wheelis, 1982, Kroening & Kendrick, 1987). An extra mole of ammonium produced from histidine catabolism via the 5-step pathway is widely thought to confer an advantage when growing under nitrogen limited conditions (Bender, 2012); however, this has been recently challenged in *P. aeruginosa* PAO1 (Gerth *et al.*, 2012). Nevertheless, carbon and energy required for growth is obtained from glutamate entering the Tricarboxylic acid cycle via conversion to α-ketoglutarate (Itoh *et al.*, 2007).

1.2 Histidine catabolic pathway in other domains of life

While a wealth of information is available on the *hut* pathways in bacteria, its presence is obscure in archaea. However, orthologs of histidase and urocanase have been identified in some archaeal species (Bender, 2012). This appears to be similar in other lower eukaryotes, while *Dictyostelium discoideum* may possess the *hut* pathway (Krichevsky & Love, 1964, Bender, 2012). The plant kingdom possesses a histidase-like protein but not urocanase; however, studies on histidine catabolism in plants appear to be lacking (Bender, 2012, Hildebrandt *et al.*, 2015).

In mammals, including humans, the initial enzymatic steps leading to the production of FIGLU from histidine catabolism are similar with bacteria. In the subsequent reactions, formimino group from FIGLU is transferred to tetrahydrofolate by the enzyme formiminotransferase cyclodeaminase (Fig. 1.1). This couples histidine catabolism with folate metabolism, which is required for the synthesis of nucleotides and other molecules (Solans *et al.*, 2000, Mao *et al.*, 2004). However, it has been observed that human skin lacks urocanase activity, and consequently urocanate accumulates and functions as natural sunscreen (Gibbs & Norval, 2011). The *hut* pathway seen in mammals also appears to exist in reptiles, fishes, birds, and amphibians (Itoh, 1970, Casu *et al.*, 2019, Bender, 2012).

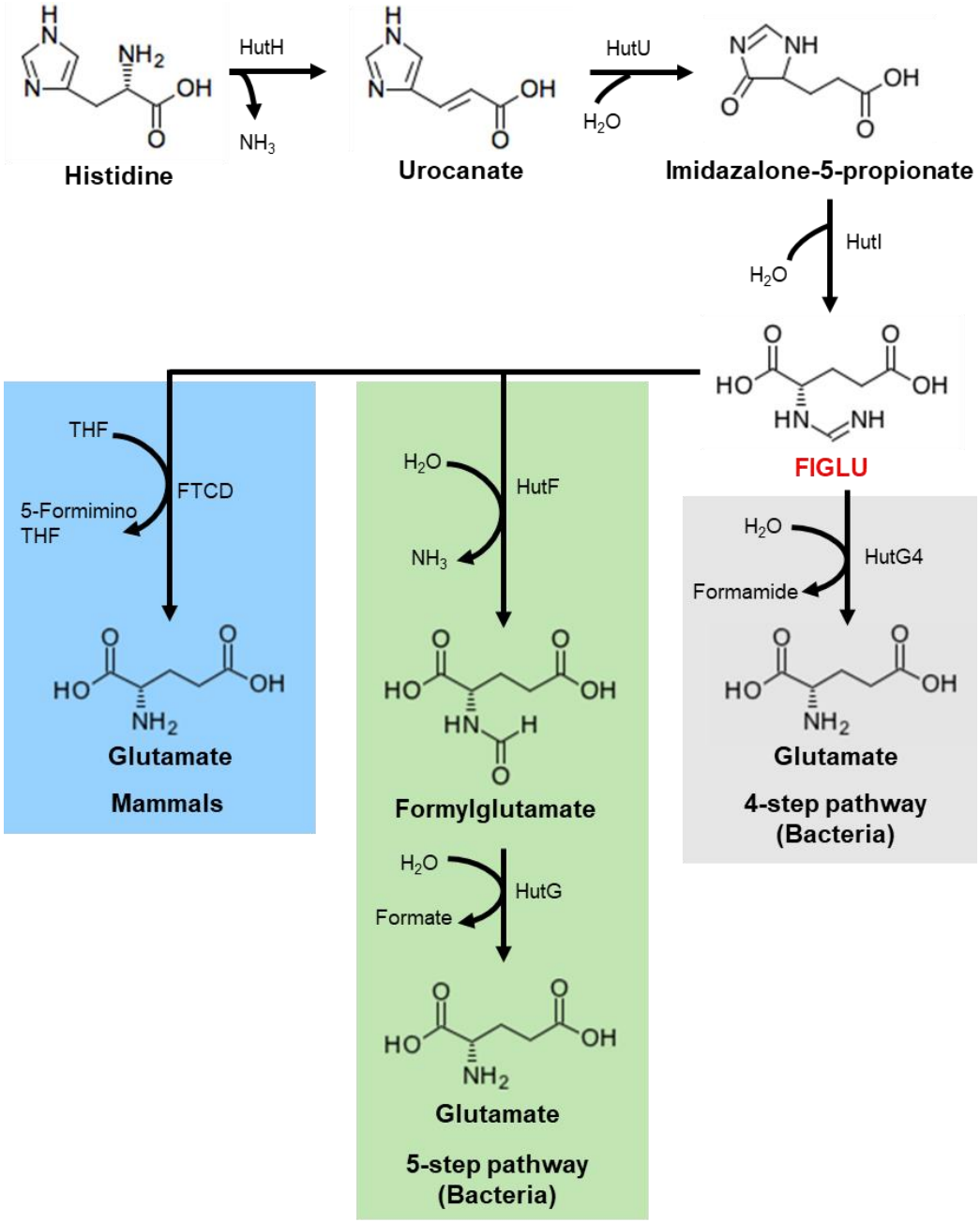

FIG 1.1 Histidine catabolic pathways in bacteria and mammals.
The first three enzymatic steps involved in the conversion of histidine to formiminoglutamate (FIGLU) are common in all organisms. The pathway branches at the intermediate FIGLU, and further breakdown of FIGLU varies depending on the organism. The enteric (*Salmonella enterica* and *Klebsiella pneumoniae*) and Gram-positive (*Bacillus subtilis* and *Corynebacterium resistens*) bacteria utilize the 4-step pathway, which produces 1 mole of ammonia per mole of histidine. *Pseudomonas* and *Streptomyces* utilize the 5-step pathway, which produces 2 mole of ammonia per mole of histidine. In mammals, further degradation of FIGLU is linked to folate catabolism, wherein FIGLU donates the formimino group to tetrahydrofolate (THF) catalysed by the enzyme formiminotransferase cyclodeaminase (FTCD). The enzymes involved in histidine catabolism are shown above the arrows: HutH (Histidase), HutU (Urocanase), HutI (Imidazolone propionate hydrolase), HutG4 (Formimidoylglutamase), HutF (FIGLU deiminase), HutG (Formylglutamate amidohydrolase). Compound structures (histidine [C00135], urocanate [C00785], Imidazalone-5-propionate [C03680], FIGLU [C00439], formylglutamate [C01045] and glutamate [C00025]) were obtained from KEGG compound database (Kanehisa *et al.*, 2017).

1.3 The *hut* operons and their expression in bacteria

1.3.1 *Klebsiella pneumoniae*

The enteric bacterium *K*. *pneumonia* utilizes a 4-step enzymatic pathway for the catabolism of histidine to glutamate and formamide (Fig. 1.1). The genes encoding for enzymes, transcriptional regulator, and transporter are organized in a single locus (Fig. 1.2) in the order of *hutIG4CUHT* (Boylan & Bender, 1984, Goldberg & Magasanik, 1975). The *hutU* and *hutH* genes form an operon and are transcribed from a promoter preceding *hutU* (Schwacha *et al.*, 1990, Nieuwkoop & Bender, 1988, Nieuwkoop *et al.*, 1984). Urocanate was shown to be the direct inducer of *hut* genes (Schlesinger *et al.*, 1965). By arranging *hutH* and *hutU* genes in a single operon, both histidase and urocanase activity can be coordinated for the induction of *hut* by urocanate, accumulated from histidine degradation. The *hutT* gene presumably encodes a urocanate specific transporter. Although its relative location suggests that *hutT* forms an operon with *hutUH* (Bender, 2012), the existence of an independent promoter has not been ruled out (Schlesinger & Magasanik, 1965). The *hutC* gene encodes for the transcriptional regulator HutC that negatively regulates *hut* genes (Goldberg & Magasanik, 1975). The *hutC* gene is independently transcribed from *hutG4*, while *hutI* and *hutG4* appear to be co-transcribed (Schwacha *et al.*, 1990). However, a further complexity here is that *hutIG4C* can be co-transcribed as well (Schwacha & Bender, 1990). The *hutC* gene may be independently transcribed to achieve a tighter repression of the *hutUH* operon relative to *hutIG4C* (Bender, 2012). *In vitro* analysis on HutC binding with *hut* promoter regions are lacking. But deletion analysis of the *hutUH* promoter regions identified a dyad symmetric sequence, ATGCTTGTATAGACAAGTAT, which is required to titrate HutC (Osuna *et al.*, 1994b). Indeed, this sequence is very similar to the HutC-binding site sequence in *Pseudomonas* spp. (see below), suggesting that the mechanism of HutC-mediated regulation of *hut* is conserved.

1.3.2 *Salmonella* Typhimurium

S. Typhimurium also utilizes a 4-step enzymatic pathway for histidine catabolism (Fig. 1.1). The order of *hut* gene arrangements is similar to that in *K*. *pneumonia* (Fig. 1.2), except that they lack *hutT*; a urocanate inducible transporter (Smith *et al.*, 1971). In contrast with *K*. *pneumonia*, *hutIG4C* is co-transcribed from a promoter preceding *hutI* in *S*. Typhimurium (Smith & Magasanik, 1971a, Bender, 2012). In the absence of histidine or urocanate, HutC occupies the operator sites of *hutUH* and *hutIG4C* operons and represses *hut* expression. However, this repression is relieved by the interaction of urocanate (inducer) with HutC protein, which dissociates HutC from the operator sites (Smith & Magasanik, 1971a, Smith & Magasanik, 1971b, Hagen & Magasanik, 1976). Here, HutC has a lower binding-affinity for

hutIG4C operator site compared to *hutUH* (Hagen & Magasanik, 1976). This suggests that HutC exerts a stronger repression of *hutUH* operon, while weakly repressing its own and *hutIG4* expressions. This appears to be significant for avoiding histidine poisoning from the non-coordinated expression of *hut* genes from two independently transcribed operons (Boylan & Bender, 1984, Hagen *et al.*, 1975).

1.3.3 *Bacillus subtilis*

Bacillus subtilis is a Gram-positive bacterium that utilizes a 4-step enzymatic pathway for histidine catabolism (Fig. 1.1). The enzymes involved in histidine catabolism share similarity with *hut* enzymes of Gram-negative bacteria (Bender, 2012). However, distinct differences in their transcription, induction, and mode of regulation have been observed.

The *hut* genes in *B. subtilis* are arranged in a single transcriptional unit in the order of *hutPHUIG4M* (Fig. 1.2) (Oda et al., 1988, Yoshida et al., 1995, Wray & Fisher, 1994). The *hutM* gene encodes for a transporter for histidine uptake, and *hutP* encodes for a positive regulator of the *hut* operon. The transcription of *hut* genes is initiated from a promoter preceding *hutP* (Oda et al., 1988). But under non-inducing conditions, a stem-loop structure within the intercistronic region between *hutP* and *hutH* terminates transcription of the *hut* structural genes (Wray & Fisher, 1994). Unlike in enteric bacteria and *Pseudomonas*, histidine is the physiological inducer of *hut* genes in *B. subtilis* (Chasin & Magasanik, 1968). Histidine induces the transcription of *hut* genes, during which a hexamer of HutP binds histidine and Mg^{2+} ions sequentially causing multiple confirmational changes. Subsequently, the HutP complex interacts with two sites of the GC-rich stem-loop structure and destabilizes the structure for the transcription to proceed (Kumarevel *et al.*, 2005).

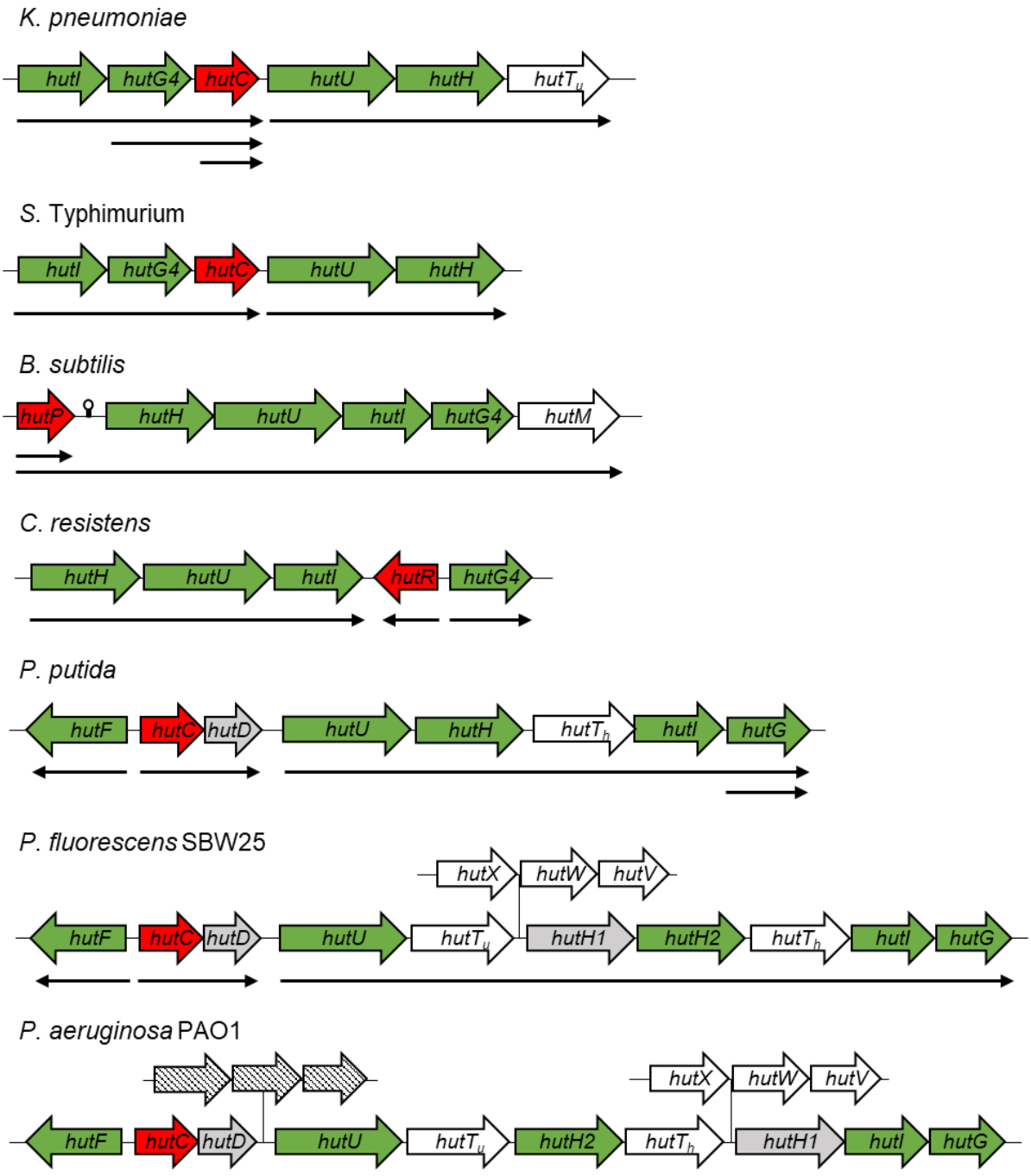

FIG 1.2 Genetic organization of histidine utilization (*hut*) genes in different bacterial genera.
Genes that encode regulators and enzymes for *hut* are shown in red and green respectively. Genes shown without colour encode for transporters of histidine or urocanate. Genes in gray are part of *hut* but precise function has not been determined. Genes represented by striped arrows are unrelated to *hut*. The stem loop structure in front of *hutP* in *Bacillus subtilis* is indicated by a lollipop structure. Genes with identical names are homologs and arrows below the genes indicate transcriptional units and directions. Figure is not drawn to scale.

1.3.4 Pseudomonads

Pseudomonas is widely known to utilize a 5-step enzymatic pathway for histidine catabolism, wherein FIGLU is sequentially broken down into Formylglutamate (FG) (and ammonia) and glutamate plus formate (Fig. 1.1). The *hut* genes are clustered at a single locus and the genetic organization is highly conserved among *Pseudomonas* spp. (Fig. 1.2) (Itoh et al., 2007, Bender, 2012). Both histidine and urocanate can induce *hut* expression, while urocanate is the physiological inducer.

In *P. fluorescens* SBW25, the *hut* genes are organized in three transcriptional units: *hutF*, *hutCD*, and *hutU-G* (Fig. 1.2). The *hutF* gene is transcribed in the opposite direction from *hutCD* and *hutU-G* genes. The *hutH2* gene encodes for histidase enzyme and is involved in the catalysis of histidine to urocanate. An additional copy of a gene (*hutH1*) encoding histidase-like protein is present adjacent to *hutH2*. HutH1 displays 36% amino acid sequence identity with HutH from *P. putida* but appears to lack functional histidase activity in *P. fluorescens* SBW25 (Zhang & Rainey, 2007b). Both histidine and urocanate specific transporters are encoded by the gene products of $hutT_h$ and $hutT_u$, respectively. The *hutXWV* genes encode for an ABC-type transporter that has a minimal role in histidine transport (Zhang *et al.*, 2012).

The *hutC* gene encodes for the transcriptional repressor of *hut* genes. DNA-Protein binding studies demonstrated that a 10-bp palindromic sequence (TGTA-N2-TACA) located downstream to the -12 elements of the *hutU* promoter was required for HutC binding with the DNA. Both the half-sites are equally important for the formation of HutC tetramers, via protein-protein interactions, and consequently for the stronger repression of *hutU* promoter. Urocanate abolished this interaction in a concentration dependent manner (Naren & Zhang, 2020). Considering the relative location of the palindrome within the promoter, HutC is deemed to repress *hutU-G* expression by acting as roadblock for the transcribing RNA polymerase. An identical palindromic sequence has been found in the divergently transcribed *hutF* and *hutC* genes, suggesting that HutC regulates its own and *hutF* expression by operating at a single site (Zhang & Rainey, 2007b). Indeed, gene expression studies using *lacZ* reporter fusions have shown that HutC represses its own and *hutF* expression (Zhang & Rainey, 2007b) in the absence of the inducer. However, *in vitro* binding data with purified HutC proteins are lacking for the precise mode of action of HutC on *hutF* and *hutC* promoter DNAs.

In *P. fluorescens* SBW25 and other *Pseudomonas* spp., an additional gene, *hutD* is located downstream of *hutC* in an overlapped manner (Fig. 1.2) (Zhang & Rainey, 2007b). The exact function of *hutD* encoded protein remains unknown. However, mutation of *hutD* in *P. fluorescens* SBW25 caused a slower growth phenotype, impaired fitness, and significantly

enhanced *hutU* transcript levels during growth on histidine. Thus, it has been proposed that HutD acts as a governor that limits the over-expression of *hut* pathway to circumvent toxicity from the accumulation of toxic metabolites, such as ammonia, produced from histidine catabolism (Zhang & Rainey, 2007b). Structural analyses indicate that HutD is a bicupin protein that is devoid of the conserved motifs, generally found in many cupins and bicupins, for metal binding. Docking and differential scanning fluorimetry analyses predicted that FG is a potential ligand of HutD. FG is also the final intermediate of the histidine catabolic pathway and potentially a good signal indicating over-activation of *hut* pathway. Thus, this prediction is in line with the proposed role of HutD as a governor of *hut* pathway expression (Gerth *et al.*, 2017).

In contrast with *P. fluorescens* SBW25, the *hut* operon of *P. putida* differs in the absence of *hutXVW* transporter, urocanate specific transporter ($hutT_U$), and *hutH1* (Fig. 1.2) (Bender, 2012). Genetic analysis revealed that the *hut* genes are transcribed in 4 transcriptional units (Hu & Phillips, 1988). Like in *P. fluorescens* SBW25, *hutF*, *hutC*, and *hutUHIG* are all induced by urocanate. However, *hutG* can also be transcribed from an independent promoter; inducible by both urocanate and FG (Hu *et al.*, 1987, Hu & Phillips, 1988). Crude extract of the HutC protein bound to three sites containing regulatory regions of *hutU*, *hutF*, and *hutG*. HutC-binding affinity was weaker for *hutG* regulatory region, and FG only inhibited this interaction but not others (Hu *et al.*, 1989, Allison & Phillips, 1990).

The *hut* operons of *P. aeruginosa* PAO1 is very similar to that of *P. fluorescens* SBW25 (Fig. 1.2), except that some rearrangements in the transporters have been observed (Bender, 2012, Winsor *et al.*, 2016). Interestingly, there is also an additional insertion of three genes between *hutD* and *hutU*, presumably encoding an ABC-transporter (Winsor *et al.*, 2016). Genetic analysis on *hut* gene transcription in *P. aeruginosa* is lacking. But considering a similar arrangement of *hut* genes, transcription could be similar to *hut* operons of *P. fluorescens* SBW25 and *P. putida* (Bender, 2012). Both histidine and urocanate can induce the expression of *hut* enzymes, but urocanate is the physiological inducer (Lessie & Neidhardt, 1967). The repressor role of HutC was demonstrated by enzyme studies, where inactivation of HutC resulted in a constitutive production of histidase and urocanase in media devoid of histidine or urocanate (Yuji, 2010). Currently, there is no published data available on the precise mode of action of HutC on *hut* operators in *P. aeruginosa* (Bender, 2012).

1.3.5 *Corynebacterium resistens*

Corynebacterium resistens is a Gram-positive bacterium and a human pathogen (Schröder *et al.*, 2012), which breaks down histidine via a 4-step enzymatic pathway (Schroder *et al.*, 2012).

But the mechanism of *hut* pathway regulation differs significantly from the enteric bacteria, pseudomonads, and *Bacillus subtilis*, described above.

The *hut* pathway genes are arranged in a single locus in the order of *hutH-hutU-hutI-hutR-hutG4*, with *hutR* gene transcribed divergently from *hutG4* (Fig. 1.2). Histidine induces the expression of *hut* genes, but whether urocanate induces *hut* gene expression is not known. The *hut* genes are transcribed in three transcriptional units: *hutHUI*, *hutR*, and *hutG4*. The *hutR* gene encodes for a transcriptional regulator that belongs to the IclR family of regulators. DNA-Protein binding assays revealed that HutR binds to a 14-bp DNA sequence, TCTGwwATwCCAGA (terminal ends are palindromic), located upstream of the -35 element of all three promoters. Neither histidine nor urocanate was able to dissociate the binding of HutR with the DNAs. Together, HutR is presumably thought to function as a transcriptional activator of *hut* genes (Schroder *et al.*, 2012).

1.4 Carbon and Nitrogen regulation of *hut*

Histidine can serve as a good source of carbon and nitrogen for many bacteria. However, histidine utilization is tightly regulated because (i) it is an expensive amino acid, requiring 20 high-energy phosphate bonds for its synthesis (Akashi & Gojobori, 2002); (ii) histidine degradation produces excess ammonia over carbon, which can be toxic for bacteria; and (iii) part of the histidine biosynthetic pathway feeds into purine biosynthetic pathway (Bender, 2012). Besides the substrate-specific induction and regulation by local transcriptional regulators (discussed above), additional regulatory mechanisms such as carbon catabolite repression (CCR) and nitrogen regulation of histidine utilization have been described (Itoh *et al.*, 2007, Bender, 2012). CCR is a regulatory mechanism that allows bacteria to preferentially utilize carbon sources by repressing the expression of genes involved in the utilization of secondary carbon sources. CCR is observed in many bacteria; however, the mechanism varies depending on the bacterial genera. In fact, it is the study of histidine utilization that provided the first evidence of carbon catabolite repression in bacteria (Magasanik, 1955, Bender, 2012). Histidine catabolism also serves as a model system for studying the coordination of carbon and nitrogen metabolism (Naren & Zhang, 2021). In the sections below, I will briefly discuss CCR and nitrogen regulatory mechanisms targeting histidine utilization in some model organisms.

1.4.1 *Klebsiella pneumoniae*

Much of our understanding of the CCR mechanisms in enteric bacteria stems from studies in *E. coli* and the key components involved appear to be similar in both *E. coli* and *K. pneumoniae* (Bender, 2012). Briefly, glucose is the preferred carbon source for *E. coli* and its uptake is

mediated by the phosphotransferase system (PTS), an active transport system. Glucose being translocated into the cell undergoes phosphorylation, coupled with dephosphorylation of the glucose specific transport protein $EIIA^{Glc}$. The unphosphorylated $EIIA^{Glc}$ interacts with and inhibits activities of transport proteins for non-PTS sugar uptake. In addition, they inactivate adenylate cyclase, a membrane-bound enzyme; consequently, lowering the intracellular levels of cAMP. This results in the inhibition of cAMP-CRP complex formation and subsequent transcriptional activation of many catabolic genes (Gorke & Stulke, 2008).

In *K*. *pneumoniae*, histidine degradation is repressed by glucose and many other carbon sources that allows faster growth than histidine (Magasanik, 1955, Magasanik, 1961). Expression of enzyme histidase is repressed in the presence of glucose and this repression is relieved by the addition of exogeneous cAMP into the growth medium (Prival & Magasanik, 1971). The cAMP-CRP complex directly activates transcription from *hutU* promoter by binding to two sites in the promoter region with varying affinities (Fig. 1.3). The high-affinity binding site, centred at -82.5 relative to transcription initiation site, is essential for the activation of *hutU* promoter. The second binding site, centred at -41.5, has a lower-affinity and is required for maximal activation (Osuna *et al.*, 1994a).

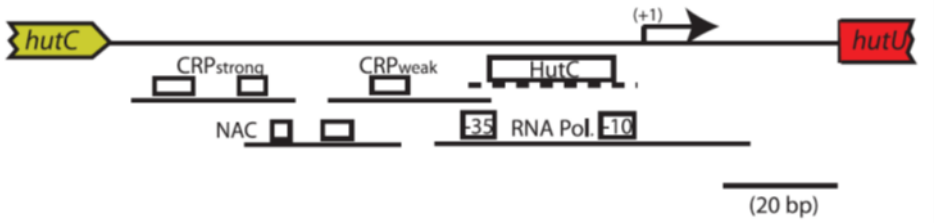

FIG 1.3 Regulatory sites in the *hutU* promoter region of *K*. *pneumoniae*.
The upper line represents the intergenic region between *hutC* and *hutU*, with +1 indicating the start of transcription of the *hutUHT* operon. Boxes represent matches to consensus sequences for known regulators of *hutUHT* transcription, and the lines beneath the boxes represent the extents of the footprints of those regulators on the DNA. The diagram was drawn approximately to scale. Figure from Bender (2012).

The glucose-mediated repression on histidine utilization in *K*. *pneumoniae* is de-repressed under growth in nitrogen limited conditions (Neidhardt & Magasanik, 1957, Prival & Magasanik, 1971). In response to nitrogen starvation, *hut* genes are transcriptionally activated by Nitrogen Assimilation Control (NAC) protein, by binding to a site centred at 64-bp upstream of the transcription start site of *hutUH* operon (Fig. 1.3) (Goss & Bender, 1995). NAC is also thought to activate the expression of *hutIG* in response to nitrogen limitation (Magasanik *et*

al., 1965, Bender, 2012). The expression of NAC is regulated by the NtrBC two-component system, which is a master regulator of cellular nitrogen metabolism. Nitrogen limitation is sensed by the NtrBC system, which activates expression of genes associated with nitrogen metabolism, including the NAC protein (Reitzer, 2003).

1.4.2 *Bacillus subtilis*

In *B*. *subtilis*, glucose is a preferred carbon source that can repress utilization of non-preferred carbon sources. In contrast with enteric bacteria, CCR in *B*. *subtilis* is achieved via transcriptional repression mediated by catabolite control protein A (CcpA) and the histidine-containing phosphocarrier protein (HPr). HPr is phosphorylated at Ser46 by HPrK (kinase) in the presence of high concentrations of phosphorylated glucose (Fructose-1,6-bisphosphate) (Gorke & Stulke, 2008). The phosphorylated HPr protein binds to CcpA protein and this complex represses transcription of catabolic genes by binding to sites called catabolite repression elements (*cre*) located within or downstream of promoter DNAs (Henkin, 1996).

The expression of *hut* genes in *B*. *subtilis* are also subject to CCR in the presence of glucose and other preferred carbon sources than histidine (Chasin & Magasanik, 1968). This is achieved via CcpA binding to the *cre* site present in the *hutP* (*hut* regulator) gene (Fig. 1.4) (Wray *et al.*, 1994). Although, direct binding of CcpA to the *cre* site in *hutP* gene has not been experimentally verified, the *cre* site in *hutP* resembles sites known to bind CcpA (Kim & Chambliss, 1997, Bender, 2012). Since the binding site is located within the *hutP* coding region, CcpA binding inhibits transcription of *hutP* (Bender, 2012), which functions as the transcriptional activator of *hut* operon (Oda *et al.*, 1988).

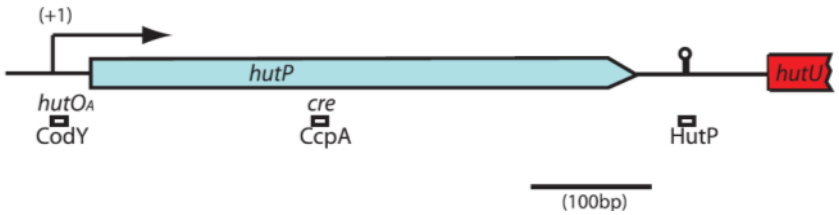

FIG 1.4 Regulatory sites in the control region of the *hut* operon of *B*. *subtilis*. The upper line represents the control region of the *hutHUIGM* operon, including the start of transcription (+1) and the *hutP* gene. Boxes below that line indicate the binding sites for the following regulatory proteins: CodY, a transcriptional repressor that binds to the $hutO_A$ site; CcpA, a protein that blocks transcription by binding at a *cre* site; and HutP, which prevents transcriptional termination at the site, indicated by the lollipop structure on the upper line. The diagram was drawn approximately to scale. Figure from Bender (2012).

In *B*. *subtilis*, regulation of genes involved in nitrogen metabolism in response to nutrient availability is controlled by three regulators: GlnR, TnrA, and CodY. GlnR and TnrA are homologues that bind similar DNA sequences and respond to nitrogen status of the cell. GlnR represses transcription of genes, promoters or enzymes during growth in excess nitrogen, while TnrA activates or represses transcription in response to nitrogen-limited growth (Fisher, 1999). CodY-dependent negative regulation occurs during growth in medium rich in amino acids (Atkinson *et al.*, 1990). The *hut* genes in *B*. *subtilis* are not regulated in response to nitrogen limitation, but instead *hut* genes are subject to amino acid repression mediated by CodY (Chasin & Magasanik, 1968, Fisher *et al.*, 1996). The transcription of *hut* genes was strongly repressed when cells were grown in the presence of 11 amino acids. CodY is thought to bind an operator site, $hutO_A$, located downstream of the promoter (Fig. 1.4) and presumably represses *hut* transcription by a roadblock mechanism (Fisher *et al.*, 1996, Wray & Fisher, 1994).

1.4.3 Pseudomonads

The components and mechanism of CCR in *Pseudomonas* spp. are entirely different from those identified in the enteric bacteria and *B*. *subtilis*. CCR in *Pseudomonas* does not involve the PTS system or cAMP (Phillips & Mulfinger, 1981). Interestingly, organic acids such as succinate are preferred carbon sources that elicit a strong CCR (Rojo, 2010). In *Pseudomonas*, CCR occurs at the post-transcriptional level and is mediated by the interplay between CbrAB (TCS), CrcZ/Y (ncRNAs), and Crc/Hfq proteins. Briefly, in the presence of preferred carbon sources, Crc/Hfq protein complex binds to a ‘CA’ motif (CAACAACAA) near the RBS binding site of mRNA transcripts and represses translation of catabolic genes associated with the utilization of non-preferred carbon sources (Sonnleitner & Blasi, 2014, Hernandez-Arranz *et al.*, 2013, Sonnleitner *et al.*, 2018, Liu *et al.*, 2017). However, in the absence of a preferred carbon source, CbrAB activates the expression of CrcZ/Y, which sequesters Crc/Hfq proteins; subsequently, derepressing genes associated with the utilization of less preferred carbon sources (Sonnleitner *et al.*, 2012, Valentini *et al.*, 2014, Liu *et al.*, 2017, Naren & Zhang, 2021).

The *hut* genes of *Pseudomonas* spp. are also subject to CCR and was first described in the late 1960s, where succinate was found to repress the *hut* pathway enzymes (Lessie & Neidhardt, 1967, Hug *et al.*, 1968). However, the mechanism of CCR acting on *hut* remained unknown for a long time (Bender, 2012). But recent studies from our laboratory provided detailed mechanism of CCR acting on *hut* gene expression in *P*. *fluorescens* SBW25 (Zhang & Rainey, 2008, Naren & Zhang, 2021). It has been shown that Crc/Hfq protein complexes bind to 6 sites in the *hutU-G* operon, targeting transporters for histidine ($hutT_h$) and urocanate

(*hutT*$_u$) and enzymes histdase and urocanase (Fig. 1.5). When histidine is the sole carbon source (in the absence of succinate), CbrAB directly activates *hutU-G* expression from a sigma-54 dependent promoter while derepressing Crc/Hfq mediated repression on *hut* translation via activation of CrcY and CrcZ (ncRNAs) (Zhang & Rainey, 2008, Naren & Zhang, 2021).

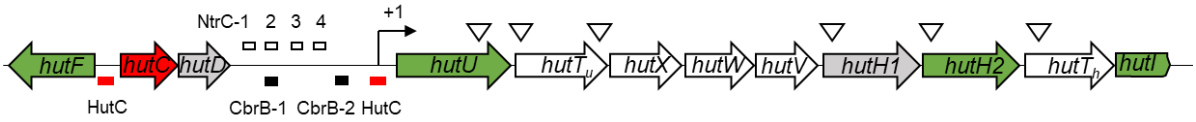

FIG 1.5 Regulatory features of the *hut* operons of *Pseudomonas fluorescens* SBW25.
The transcription start site is indicated as +1 with a bent arrow. The inverted triangles indicate location of the Crc/Hfq binding sites. The rectangular boxes indicate binding sites for NtrC (unfilled), CbrB (black filled), and HutC (red filled) regulator proteins in the *hut* operons.

However, studies in *P. fluorescens* SBW25 indicate that *hut* regulation is complex when histidine is the sole nitrogen source (succinate as carbon source). The presence of succinate induces repression of *hut* expression at the translational level, mediated by Crc/Hfq proteins. The CbrAB-mediated activation of *hut* transcription is weaker in this nutrient condition. At this stage, NtrBC plays a dominant role in the activation of *hut* transcription by directly binding to the *hutU-G* promoter region. The expression of NtrBC (TCS) is autoactivated in response to nitrogen starvation and this requires NtrC binding to the promoter *ntrBC*. The NtrBC-mediated expression of *hut* transcription needs to be tightly controlled because *hut* over-expression can cause accumulation of NH_4 that shuts off the NtrBC system; consequently, inhibiting *hut* transcription. Surprisingly, this is achieved by HutC whose concentration increases in response to histidine/urocanate and competes with the NtrC binding site in the *ntrBC* promoter. This helps in sustaining a nitrogen limited condition and maintain active expression of the NtrBC system (Fig. 1.6) (Zhang & Rainey, 2008, Naren & Zhang, 2020, Naren & Zhang, 2021).

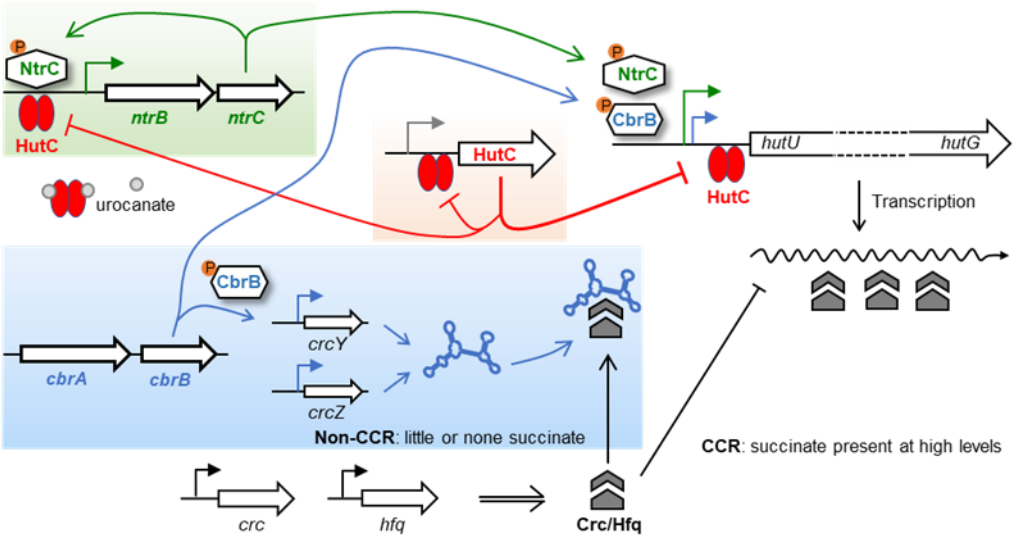

FIG 1.6 C/N homeostatic regulation of *hut* genes by CbrAB, NtrBC, and HutC.
When histidine is utilized as a N source, transcription of *hut* genes is predominantly activated by NtrBC whose expression is autoactivated and involves repression by HutC as a negative feedback loop. HutC thus coordinates the expression of *hut* genes, *hutC* itself and the NtrBC activator in a histidine concentration-dependent manner. Utilization of histidine as a C source is subject to succinate-induced CCR control. In succinate-deplete media, CbrAB activates *hut* transcription while de-repressing the translation of *hut* mRNA mediated by the Crc/Hfq complex, which is sequestrated by the CbrAB-activated ncRNAs (CrcY and CrcZ). Of note, the CbrA sensor kinase can potentially detect histidine availability.

Figure reused from Naren, N., and Zhang, X.X., Role of a local transcription factor in governing cellular carbon/nitrogen homeostasis in *Pseudomonas fluorescens* (2021), *Nucleic Acids Research*, 49(6), 3204-3216, by permission of Oxford University Press. License Number: 5162230223732.

1.5 Proposal for 4-step histidine catabolic pathway in *P. aeruginosa* PAO1

Histidine catabolism in *Pseudomonas* spp. is widely known to proceed via a 5-step enzymatic pathway (Itoh *et al.*, 2007, Bender, 2012). However, *P. aeruginosa* PAO1 possesses an additional enzyme, with formimidoylglutamase activity, that convert FIGLU directly to glutamate and formamide as seen in enteric bacteria (Marti-Arbona *et al.*, 2006). The gene encoding this enzyme (PA3175, *hutE*) is dislocated from the *hut* locus, and its expression is positively activated by a preceding IclR-type transcriptional regulator (PA3174, *hutR*) in response to histidine, urocanate or FIGLU (Gerth *et al.*, 2012). HutE (PA3175) was also found to possess a 20-fold lower affinity for FIGLU than HutF (PA5106) (Marti-Arbona *et al.*, 2006). A 5-step pathway mutant strain of *P. aeruginosa* PAO1 (Δ*hutF*), retained the ability to grow on histidine but required both *hutR* (PA3174) and *hutE* (PA3175) (Gerth *et al.*, 2012). Thus, it was proposed that both 4- and 5-step *hut* pathways co-exist in *P. aeruginosa* PAO1. The *hutR* and *hutE* genes are likely co-transcribed as an operon, and both genes were identified in *P. aeruginosa* (4 strains: PAO1, PA7, PA14 and LESB58), *P. fluorescens* Pf-5, and *P. mendocina* ymp (Gerth *et al.*, 2012).

Intriguingly, neither pathways conferred a fitness advantage growing under nitrogen limited or excess conditions (Gerth *et al.*, 2012). This finding was contrary to a previous hypothesis that the 5-step pathway may be beneficial under nitrogen limited conditions (Itoh *et al.*, 2007, Bender, 2012). However, when histidine was a source of carbon, histidine catabolism through HutR-HutE was found to be advantageous (Gerth *et al.*, 2012).

In this work, we identified a putative transporter gene (PA3176) immediate downstream of *hutE* (PA3175), so we tested a new hypothesis that this locus is dedicated to the utilization of FIGLU but not histidine as initially thought (see details in Chapter 2). Based on our findings, we renamed the genes in this locus as *figR* (PA3174), *figA* (PA3175), and *figT* (PA3176); involved in the direct utilization of FIGLU.

1.6 HutC plays a surprising role in global gene regulation

HutC is known to function as a transcriptional repressor of *hut* pathways in both *Pseudomonas* and enteric bacteria. However, recent studies from our laboratory and others indicate that HutC plays a significant role in the regulation of both metabolic and virulence genes beyond histidine catabolism.

In a recent work from our laboratory in *P. fluorescens* SBW25 (a plant growth-promoting bacterium), HutC was found to possess a governor role in the regulation of *ntrBC* (TCS), a global regulator of cellular nitrogen metabolism (Naren & Zhang, 2020, Naren & Zhang, 2021). Under nitrogen limited conditions, NtrBC activates its own expression through NtrC binding to its operator sites; consequently, activating genes involved in nitrogen assimilation. NtrBC directly activates *hut* expression when histidine is the sole nitrogen source. But when histidine is present at high concentrations, an excess build-up of ammonium from the 5-step *hut* pathway shuts off the *ntrBC* expression; consequently, inactivating *hut* gene expression. To circumvent this, HutC competes with NtrC for the same operator site in the *ntrBC* promoter and fine-tunes *ntrBC* expression, co-ordinating the expression levels of both *ntrBC* and *hut* genes to optimum (Fig. 1.6). HutC was also found to repress the expression of *plcC* gene for phosphatidylcholine catabolism, and RNA-seq data revealed differential regulation of genes associated with T3SS, T6SS, iron uptake, and pyoverdine synthesis among others (Naren & Zhang, 2020). Further, laboratory competition experiments on plant surfaces identified that mutation of *hutC* significantly reduced the ability of *P. fluorescens* SBW25 to colonize plant shoot and rhizosphere (Zhang & Rainey, 2007b). This observation complemented the RNA-seq data, suggesting that *hutC* plays a significant role beyond the regulation of *hut* pathways (Naren & Zhang, 2020).

A direct role for HutC in the expression of virulence determinants was established in the zoonotic pathogen *Brucella abortus*. *Brucella* is an intracellular pathogen, which requires the expression of Type IV secretion system (T4SS) encoded by the *virB* operon for survival and replication within host cells. Interestingly, HutC was found to co-activate the expression of *virB* operon by directly binding to a low-affinity site in the *virB* regulatory region (Sieira *et al.*, 2010). Also, HutC positively regulates the expression of *btaE* gene, encoding for a trimeric-autotransporter adhesin, by binding to their regulatory region. This is required for *Brucella* attachment to the HeLa cell lines (Sieira *et al.*, 2017).

In *Yersinia pseudotuberculosis*, *hutC* appears to play a significant role in biofilm formation and swimming motility phenotype. Mutation of *hutC* resulted in loss of biofilm formation on *Caenorhabditis elegans*. Further, HutC was found to regulate the expression of *flhDC* in gene expression studies. The expression of *flhDC*, encoding the motility master regulator, was 5-fold higher in the *hutC* mutant compared with the parent strain. Consistently, *hutC* mutant displayed a hyper-swimming phenotype suggesting that HutC functions as a motility repressor in *Y*. *pseudotuberculosis* (Joshua et al., 2015).

P. aeruginosa strain PAK carrying a transposon insertion in *hutC* was defective in swimming and swarming motility phenotypes (Yeung *et al.*, 2009). The expression of *hutC* was also reported to be downregulated by 1.4-fold in biofilms compared to the planktonic cells (Patell *et al.*, 2010). In *P*. *aeruginosa* PAO1, an excessive uptake and utilization of histidine caused a significant reduction in Type III secretion system (T3SS) mediated cytotoxicity (Rietsch *et al.*, 2004). The expression of exoenzyme S was abolished, and the strain was unable to lyse macrophages. The excessive histidine utilization phenotype was caused by a transposon insertion in the *hut* locus, which resulted in an overexpression of *hut* genes (Rietsch *et al.*, 2004). Here, the defects in the expression of virulence traits could be the consequence of HutC overexpression.

Taken together, our laboratory proposed that urocanate accumulated in the mammalian tissues such as skin acts as a signalling molecule eliciting *P*. *aeruginosa* infections via interaction with the HutC regulator (Zhang *et al.*, 2014). Urocanate is produced by the deamination of histidine; catalysed by histidase (HutH) enzyme. Human skin lacks urocanase (HutU) activity, required for the subsequent degradation of urocanate. Consequently, urocanate accumulates in the skin and function as a natural sunscreen (Gibbs & Norval, 2011). Furthermore, urocanate was found to stimulate the synthesis of alkaline protease in *Vibrio alginolyticus* (Bowden *et al.*, 1982). Urocanate triggers the expression of VjbR, a transcriptional regulator of virulence genes, in *Brucella abortus* (Arocena *et al.*, 2012). It has also been shown that certain parasitic nematodes sense urocanate accumulated in the

mammalian skin to cause infections (Safer *et al.*, 2007). Thus, we could predict that urocanate and HutC functions analogous to a one-component system, where HutC modulates the expression of both metabolic and virulence factors in response to urocanate (Zhang *et al.*, 2014).

1.6.1 Domain structure of HutC

HutC belongs to and represents the second largest sub-family of the GntR family of transcriptional regulators (Rigali *et al.*, 2002, Suvorova *et al.*, 2015). The GntR family of transcriptional regulators was first described in 1991 and named after the gluconate operon repressor in *Bacillus subtilis* (Haydon & Guest, 1991). Members of this family possess winged helix-turn-helix DNA-binding domain at their N-terminus and effector binding/oligomerization domain at their C-terminus (Rigali *et al.*, 2002, Resch *et al.*, 2010) . The N-terminal domain is formed by three α-helices and anti-parallel β-sheet cluster (Suvorova *et al.*, 2015). DNA-binding domains between the members appear to be highly similar, while heterogeneity in the effector binding and oligomerization domains formed the basis for their further classification into four main (FadR, HutC, MocR, and YtrA) and two minor (AraR and PlmA) sub-families (Rigali *et al.*, 2002, Suvorova *et al.*, 2015).

The HutC sub-family is named after HutC, the transcriptional repressor of *hut* pathway, from *P. putida* (Allison & Phillips, 1990). The HutC sub-family represents about 31% of the GntR family of transcriptional regulators, which are involved in various biological processes, including metabolism and conjugative plasmid transfer (Rigali *et al.*, 2002, Rigali *et al.*, 2006, Suvorova *et al.*, 2015). The effector and oligomerization binding domains of HutC sub-family protein is made of α-helical and β-sheets and adopts a chorismate lyase fold; but lacks catalytic activity. This suggests that the effector molecules bind to HutC-family proteins similar to substrate binding to chorismate lyase (Aravind & Anantharaman, 2003, Resch *et al.*, 2010).

The crystal structure of a full-length HutC has not been determined yet despite being the representative member of the HutC sub-family. Based on the domain structure, HutC repressor protein appears to function analogous to a one-component signal transduction system. Presumably, binding of urocanate to the effector domain induces a confirmational change in the DNA binding domain, which alters their affinity for DNA (Bender, 2012). Consistently, homology-based modelling of HutC from *P. fluorescens* SBW25 suggests that wHTH domain is projected towards the major groove, while wing domain is towards the minor grove in the *hutU* operator DNA (Naren & Zhang, 2020). HutC is capable of binding to each half-site of the consensus sequence as monomers. However, efficient repression is achieved only when HutC forms a dimer and simultaneously binds both the half-sites, subsequently undergoing oligomerization via protein-protein interactions to form a tetramer (Fig. 1.7) (Naren

& Zhang, 2020). The formation of a tetramer is important for the strong repression of the *hutU* promoter. Urocanate was found to dissociate HutC from the *hutU* operator site in a concentration dependent manner in the *in vitro* Protein-DNA binding assays (Naren & Zhang, 2020).

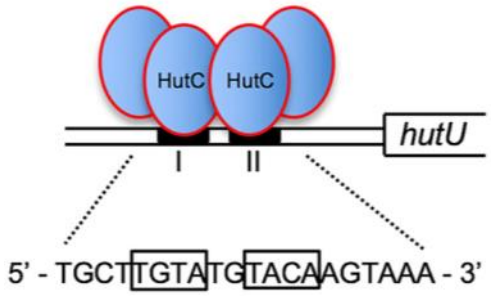

FIG 1.7 Proposed model for HutC binding to *hutU* promoter DNA in *P. fluorescens* SBW25. Schematic representation of the HutC tetramer bound with the P_{hutU} promoter. This involves direct interactions between the HutC dimer and P_{hutU} with the formation of a HutC tetramer via protein-protein interactions.

1.7 *Pseudomonas aeruginosa*

The name *Pseudomonas* was first described by professor Migula, a German botanist, in the late 19th century (Palleroni, 2010). *Pseudomonas* species are Gram-negative bacteria belonging to the phylum *Proteobacteria*. The genus *Pseudomonas* contains over 140 species (Gomila *et al.*, 2015). Of all the species in the genus, *Pseudomonas aeruginosa* is one of the most recognized species primarily due to their association with several human infections (Pendleton *et al.*, 2013).

P. aeruginosa is a motile, non-spore forming bacillus, classified as obligate aerobe. However, they are also capable of anaerobic growth by reducing nitrate or nitrite (Yahr & Parsek, 2006). *P. aeruginosa* is ubiquitous in natural environments and has been isolated from crude oil (Marin *et al.*, 2003), rivers (Pirnay *et al.*, 2005), open ocean (Khan *et al.*, 2007), soil, air (Panagea *et al.*, 2005), plants (Radhapriya *et al.*, 2015), and pharmaceutical and chemical products (Weiser *et al.*, 2019, Jimenez, 2007). *P. aeruginosa* is also capable of infecting a wide variety of hosts, including plants (Rahme *et al.*, 2000, Walker *et al.*, 2004) , nematodes (Tan & Ausubel, 2000), insects (Miyata *et al.*, 2003), and zebra fish (Clatworthy *et al.*, 2009), so they are used as models for studying bacterial pathogenesis. The ubiquitous nature of this

bacterium is explained by its large and expanding genome, usually varies in size between 5.5 and 7.5 Mbp, that confers metabolic flexibility (Silby *et al.*, 2011, Weiser *et al.*, 2019). Thus, it is not surprising that over 80 organic compounds can be utilized by *P. aeruginosa* as carbon and energy sources (Yahr & Parsek, 2006). A high degree of conservation in metabolic genes among clinical and environmental strains has been observed (Wolfgang *et al.*, 2003, Valot *et al.*, 2015). This partially explains the success of *P. aeruginosa* in switching between environmental habitats and causing infections in eukaryotes.

1.7.1 Clinical significance of *Pseudomonas aeruginosa*

P. aeruginosa is an important opportunistic and nosocomial pathogen of significant medical concern (Pendleton *et al.*, 2013). However, fatal infections in healthy individuals have also been reported (Hatchette *et al.*, 2000). In humans, *P. aeruginosa* causes a wide range of acute and chronic infections. These include burn wound infections, skin and soft-tissue infections, urinary tract infections, otitis media and externa, keratitis, septicaemia, and hospital-acquired pneumonia among others (Glik *et al.*, 2018, Nagoba *et al.*, 2017, Koulenti *et al.*, 2009, Streeter & Katouli, 2016). *P. aeruginosa* is also responsible for chronic infections in people with diabetic foot and cystic fibrosis (CF) of the lungs (Ertugrul *et al.*, 2017, Panagea *et al.*, 2005, Winstanley *et al.*, 2016).

CF is an inherited genetic condition resulting from mutations in the gene encoding for Cystic Fibrosis Transmembrane Conductance Regulator (CFTR) protein, which normally functions as a chloride transporter maintaining homeostasis. A defect in the CFTR protein causes thickening of the mucus, due to reduced mucociliary clearance, and provides a suitable environment for bacterial colonization (Cohen & Prince, 2012). *P. aeruginosa* is the most common pathogen isolated from CF patients, and it is the major cause of morbidity and mortality in CF patients due to accompanying respiratory failure (Lyczak *et al.*, 2000, Winstanley *et al.*, 2016). *P. aeruginosa* establishes chronic infections of the lungs by forming biofilms and adapting to the heterogeneous amino acid rich lung environment through genetic alterations, leading to a shift in metabolism, loss of virulence, and enhanced antibiotic tolerance (Winstanley *et al.*, 2016). It is often difficult to treat and eradicate *P. aeruginosa* upon establishing chronic infection.

The difficulty in treating *P. aeruginosa* infections is due to their intrinsic and acquired resistance to many antibiotics. The porins present in the outer membrane of *P. aeruginosa* possess low permeability to antibiotics, which makes *P. aeruginosa* naturally resistant to many antibiotics (Angus *et al.*, 1982). *P. aeruginosa* produces enzymes such as β-lactamases and cephalosporinase, encoded on their chromosome, that inactivate various antibiotics (Streeter & Katouli, 2016). Also, *P. aeruginosa* possesses multiple efflux pumps, such as MexAB-OprM,

MexCD-OprJ, MexEF-OprN, and MexXY-OprM, that expel antibiotics from the periplasm. They can also acquire resistance from selective pressure via mutations in efflux pumps or enzymes that cleave antibiotics, causing their overexpression (Pendleton *et al.*, 2013, Streeter & Katouli, 2016). Mutations in DNA gyrase and topoisomerase that confer resistance to fluoroquinolones have also been reported (Pendleton *et al.*, 2013). Both intrinsic and acquired resistance mechanisms have been identified as contributing factors for *P. aeruginosa* resistance to many classes of antibiotics: carbapenems, sulfonamides, β-lactams, cephalosporins, macrolides, and aminoglycosides (Pendleton *et al.*, 2013, Streeter & Katouli, 2016). There is an alarming rise in the multi-drug resistant *P. aeruginosa* infections. Thus, *P. aeruginosa* has been classified as a high priority pathogen by WHO for the development of novel therapeutics. We need to develop novel strategies to target *P. aeruginosa* that minimise selection for resistance. These include directly targeting metabolic pathways or virulence factors/mechanisms, such as biofilm formation or T3SS; some of these are currently under development (Rohmer *et al.*, 2011, Maurice *et al.*, 2018, Shaw & Wuest, 2020).

1.7.2 Major virulence factors and pathogenesis

P. aeruginosa possesses a myriad of virulence factors (Fig. 1.8) that help in host colonization by subverting immune responses (Gellatly & Hancock, 2013). The pathogenesis of *P. aeruginosa* is therefore multifactorial, showing remarkable differences in the expression of virulence factors between acute and chronic infections. *P. aeruginosa* strains isolated from chronic infections displayed reduced motility and expression of T3SS, while enhanced ability to form biofilms and antibiotic resistance were also observed (Jain *et al.*, 2004, Winstanley *et al.*, 2016). Hypervirulent isolates were found to be generally associated with acute infections (Gellatly & Hancock, 2013).

Flagella and type IV pili are two proteinaceous cell surface appendages of *P. aeruginosa* that play a significant role in motility, initial attachment to the host cell, and generating inflammatory responses. Each cell possesses a single polar flagellum and multiple type IV pili at the cell pole. The rotating flagellum helps cells to move through aqueous environment in a form of motility referred to as swimming (Gellatly & Hancock, 2013). Upon reaching a suitable infection site, flagellum mediates adherence to the host cell by binding to host cell receptors such as asialo GM1 (de Bentzmann *et al.*, 1996), which triggers a large inflammatory response. However, in chronic infections, expression of flagellar biosynthesis genes are repressed (Tart *et al.*, 2006) and a show reduced inflammatory response (Faure *et al.*, 2018). Type IV pili also mediate host attachment by binding to host cell glycoproteins and is important for cell motility, aggregation, and biofilm formation. Type IV pili help cells move along solid surfaces via pilus extension and retraction, like grappling hooks. This type of motility is referred to as ‘twitching’

(Gellatly & Hancock, 2013). *P. aeruginosa* defective in twitching motility displays reduced virulence, while enhanced twitching motility impairs biofilm formation (Burrows, 2012). Both flagella and type IV pili mediate another form of motility called 'swarming', where cells display a highly coordinated movement on semi-solid surfaces (Yeung *et al.*, 2009). Additionally, *P. aeruginosa* adherence to abiotic surfaces and biofilm formation is promoted by fimbriae (Vallet *et al.*, 2001).

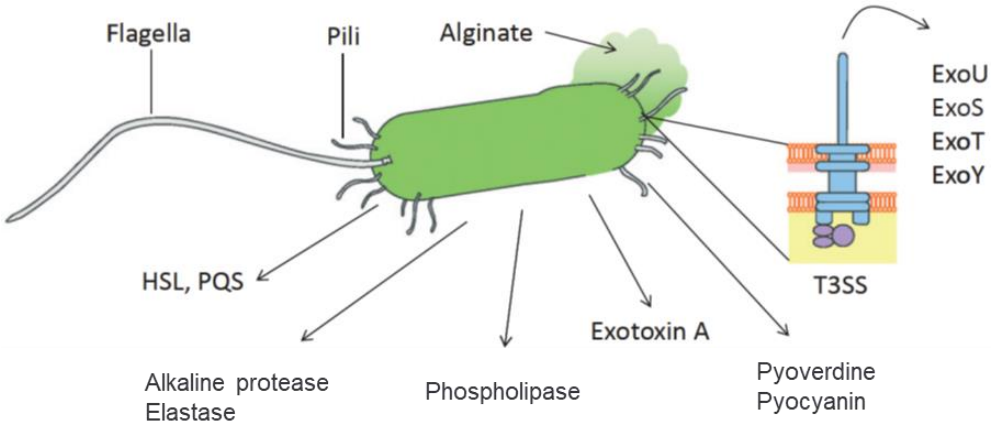

FIG 1.8 Major virulence factors produced by *Pseudomonas aeruginosa*.
Flagella and Pili are motility appendages that help in making initial contact with the host cell. Initial contact triggers the expression of T3SS, which injects various exotoxins into the host cell, that induces host cell death and impairs immune response. Secreted proteases and phospholipases degrade host complement proteins and host cellular components. Pyocyanin is a redox-active compound and a major virulence factor that can interfere with host cell electron transport chain. Pyoverdine functions as an iron scavenger from the host. Figure adapted from Gellatly and Hancock (2013).

T3SS are needle-like protrusions present in many pathogenic bacteria that facilitate the delivery of toxins/effector proteins directly into the eukaryotic cells (Hauser, 2009). In *P. aeruginosa*, T3SS is an important virulence determinant of acute infections such as pneumonia, burn, and blood stream infections. *P. aeruginosa* strains defective in T3SS are attenuated in virulence (Holder *et al.*, 2001, Lee *et al.*, 2003, Vance *et al.*, 2005). The expression of T3SS is triggered by initial contact with the host eukaryotic cells. *P. aeruginosa* possesses four effector proteins (ExoS, ExoT, ExoY and ExoU) that are injected directly into host eukaryotic cells. ExoS and ExoT are bifunctional enzymes, possessing both GTPase-activating protein and ADP-ribosyl transferase activities. They are involved in actin cytoskeletal rearrangements and inducing host eukaryotic cell death. ExoT also inhibits the wound healing process. ExoU possesses phospholipase activity and can cause rapid eukaryotic cell death (Hauser, 2009). ExoY is a nucleotidyl cyclase that was recently shown to be involved in impairing early immune responses and inducing host cell apoptosis (Kloth *et al.*, 2018). All four effector proteins work in concert to disrupt the epithelial and endothelial barriers causing bacterial dissemination into the blood stream, and consequently septic shock.

They also kill phagocytes and amplify the inflammatory responses (Hauser, 2009). In chronic infections, strains defective in T3SS are selected, presumably to reduce the inflammatory response that contribute to their enhanced persistence.

Many bacteria use a quorum sensing (QS) mechanism for cell-to-cell communication, which facilitates cell-density dependent regulation of gene expression for adaptation to environmental conditions. Bacteria constitutively produce signalling molecules called autoinducers, such as N-acyl-homoserine lactones (AHL) and autoinducer-2 (AI-2), whose accumulation above a threshold level is detected by specific receptors on the bacterial cell surface (Kariminik *et al.*, 2017). This activates signalling pathways, and subsequently modulate the expression of genes for a coordinated response. *P*. *aeruginosa* possesses at least three QS systems: LasI/LasR, RhlI/RhlR, and PQS. QS regulates nearly 10% of *P*. *aeruginosa* genes, many of which are involved in virulence, such as biofilm (rhamnolipids and eDNA [extracellular DNA]), cell motility, production of polysaccharides, and siderophores among others (Kariminik *et al.*, 2017, Gellatly & Hancock, 2013).

Biofilms are a special form of growth on surfaces (biotic and abiotic), wherein bacterial cells form communities by attaching to each other and to the surface. The cells are embedded in a matrix of Extra Polymeric Substances (EPS), which is composed of exopolysaccharides, biomolecules, eDNA, lipids, and proteins, that hold bacterial cells together (Balasubramanian *et al.*, 2013). Biofilms display enhanced resistance to antibiotics and disinfectants, due to their lower penetration through the EPS and presence of high concentrations of enzymes that cleave antibiotics (Drenkard, 2003). Biofilm mode of growth is a major medical concern because biofilms can also be formed on medical devices, such as catheters and endotracheal tubes. *P*. *aeruginosa* establishes chronic infections by biofilm formation. Interestingly, they have also evolved mechanisms that induce biofilm mode of growth in response to antibiotics (Hoffman *et al.*, 2005, Winstanley *et al.*, 2016).

Biofilm formation by *P*. *aeruginosa* is a complex multi-step process involving: (i) reversible attachment of cells onto a surface, (ii) irreversible attachment, (iii) formation of microcolonies, (iv) biofilm maturation, and (v) biofilm dispersal (Fig. 1.9) (Rasamiravaka *et al.*, 2015). The initial attachment to a surface is mediated by flagella, type IV pili, and fimbria. Following attachment, cells proliferate to form microcolonies and produce EPS matrix. Depending on the strain, three polysaccharides are produced: alginate, Pel, and Psl, that appears to be important for structural integrity of biofilms (Balasubramanian *et al.*, 2013). Subsequently, biofilms undergo maturation to form mushroom-shaped structures containing liquid-filled channels. These channels are important for supplying nutrients to and removing waste products produced by the cells. In the final stage, cells detach from biofilm, re-enter the

planktonic phase, and colonize a new site by re-initiating biofilm formation (Gellatly & Hancock, 2013). Regulation of biofilm formation is complex and involves multiple regulatory systems, including the QS, GacA/GacS two-component system, and c-di-GMP (bacterial second messengers), that directly or indirectly influence biofilm formation.

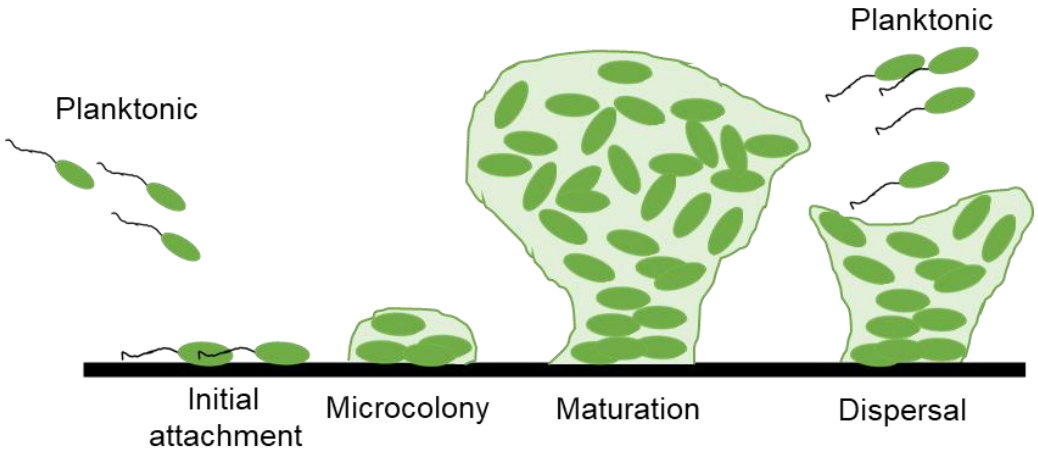

FIG 1.9 Schematic representation of biofilm development in *P. aeruginosa* PAO1.
The biofilm cycle begins with the initial attachment (reversible followed by irreversible) of planktonic cells to the surface, mediated by flagella and type IV pili. This is followed by microcolony formation and EPS production. Subsequently, the biofilms undergo maturation to form mushroom shaped structures. During dispersion, cells detach from biofilm and re-enter the planktonic phase.

P. aeruginosa also possesses several proteases that contribute to tissue damage and degradation of host immune components. Alkaline protease is a zinc metalloprotease that degrades host complement proteins (Laarman *et al.*, 2012). They also degrade Toll-like receptor 5 (TLR5) and flagellin-sensitive 2 (FLS2) receptors, present on cell surfaces of mammals and plants, that mediate the activation of host innate immune response by recognizing flagellin monomers (Bardoel *et al.*, 2011). LasA and LasB are two elastases produced by *P. aeruginosa*. LasB is secreted in large amounts and has been studied in detail. They are involved in the degradation of host tissue components such as collagen and fibrin, causing tissue damage. Additionally, they degrade complement proteins produced as consequence of host immune response (Everett & Davies, 2021). *P. aeruginosa* also secretes a serine protease called protease IV, which is a critical virulence factor for corneal infection (Caballero *et al.*, 2004).

1.8 Research aims and objectives

1.8.1 Objectives of this study

The overall aim of this thesis is to unravel the molecular basis of histidine catabolism in the human opportunistic pathogen *P. aeruginosa* and explore its linkage with bacterial virulence.

The first part of this research will focus on a genetic assessment of the 4- and 5-step histidine catabolic pathways, which were considered to be functionally redundant. Our results led to the discovery of a new catabolic pathway for the utilization of FIGLU, a histidine metabolite, accumulated in human tissues. The newly discovered pathway encoded by genes in the *fig* operon is not dedicated to the utilization of histidine as previously thought.

In the second part of this work, we aim to investigate the global regulatory role of HutC in the pathogenic bacterium *P. aeruginosa* PAO1. The global regulatory role of HutC has recently been described in Zhang's lab using the plant-associated bacterium *P. fluorescens* SBW25 as a model. Here, we extend our investigation to a human pathogen, with a particular focus on virulence traits.

Finally, we aim to provide a mechanistic insight into the precise modes of action of HutC in regulating *hutF* expression in *Pseudomonas*. HutC is known to recognize two distinct DNA binding sites (Phut and Pntr), which share little sequence similarity. Interestingly, both target sites are present in the P_{hutF} promoter of *P. fluorescens* SBW25; but the P_{hutF} promoter of *P. aeruginosa* PAO1 contains only the Phut site.

1.8.2 Specific aims of this study

The specific aims of this study are:

1. Define *fig* operon for the utilization of FIGLU in *P. aeruginosa* PAO1

- ❖ Determine the FIGLU specific transporter role of *figT* (PA3176).
- ❖ Determine if *figT* expression is induced by FIGLU and regulated by *figR* (PA3174).
- ❖ Determine if FIGLU utilization is subjected to carbon catabolite repression by targeting *figT* gene.
- ❖ Examine the effect of *fig* and *hut* pathways on histidine and FIGLU catabolism.
- ❖ Perform phylogenetic analysis to determine the origin of *fig* operon in *P. aeruginosa*.

2. Investigate the global regulatory role of HutC in *P. aeruginosa* PAO1

- ❖ Predict the novel HutC-target sites in the genome by *in silico* analysis.
- ❖ Examine the molecular interaction of purified HutC proteins with *hut* promoter and *in silico* predicted selected HutC-target sites. Also, determine and compare the binding affinities of these interactions.
- ❖ Examine biofilm, tobramycin-induced biofilm, motility, and pyoverdine phenotypes of *hutC* with respect to the functions of novel HutC regulated candidate genes.
- ❖ Determine the role of *hutC* in *P. aeruginosa* virulence using a model host organism, *Caenorhabditis elegans.*

3. Dissect the regulatory role of HutC in *hutC* and *hutF* expression in *Pseudomonas*

- ❖ Examine the molecular interaction of purified HutC proteins with *hutF* promoter from *P. aeruginosa* PAO1 and *P. fluorescens* SBW25.
- ❖ Determine the functional significance of the novel HutC-binding Pntr site identified in the *hutF* promoter region in *P. fluorescens* SBW25.

Chapter 2

Identification of *fig* operon for the utilization of Formiminoglutamate and its impact on histidine catabolism in *Pseudomonas aeruginosa*

2.1 Abstract

Histidine is catabolised in bacteria through either a 4- or 5-step enzymatic pathway, which differ in the breakdown of formiminoglutamate (FIGLU), and are best described in enteric bacteria and pseudomonads, respectively. However, previous studies revealed that the two pathways co-exist in the human opportunistic pathogen *Pseudomonas aeruginosa*. *P. aeruginosa* PAO1 contains an additional operon (dislocated from the *hut* locus) encoding for formimidoylglutamase enzyme and its regulator, which can break down FIGLU like the 4-step pathway in a functionally redundant manner. Here, we genetically identified a transporter gene (named *figT*) adjacent to the genes encoding for formimidoylglutamase enzyme (FigA) and its transcriptional regulator FigR. Site-directed mutagenesis combined with *lacZ* reporter fusions showed that FigT functions as a FIGLU-specific transporter whose expression is activated by FigR in response to the presence of FIGLU. The *figT* gene is co-transcribed with *figRA*. Expression of the three gene operon was also induced by histidine and urocanate, but the induction was indirect by virtue of intracellular conversion to FIGLU. Growth and fitness assays revealed that histidine is predominantly catabolised via the 5-step *hut* pathway but not via the FigRAT pathway. Together, our genetic and phenotypic data show that *fig* operon is dedicated to the utilization of FIGLU but not histidine or urocanate as previously thought. Phylogenetic analysis showed that *figRAT* homologues are highly conserved and present in all completely sequenced strains of *P. aeruginosa* but revealed no evidence of recent horizontal gene transfer within the genus of *Pseudomonas*.

2.2 Introduction

Pseudomonas aeruginosa is an important opportunistic and a major nosocomial pathogen of significant medical concern (Pendleton *et al.*, 2013). In humans, *P. aeruginosa* causes burn wound infections, skin and soft-tissue infections (Glik *et al.*, 2018, Nagoba *et al.*, 2017), ventilator-associated pneumonia (Koulenti *et al.*, 2009), and is responsible for chronic lung infections in cystic fibrosis patients (Winstanley *et al.*, 2016, Panagea *et al.*, 2005). *P. aeruginosa* is also capable of infecting plants (Walker *et al.*, 2004, Rahme *et al.*, 2000), nematodes (Tan & Ausubel, 2000), insects (Miyata *et al.*, 2003), zebra fish (Clatworthy *et al.*, 2009), and are used as models for studying infection pathogenesis. *P. aeruginosa* can be isolated from diverse environments, including crude oil (Marin *et al.*, 2003), rivers (Pirnay *et al.*, 2005), open ocean (Khan *et al.*, 2007), air (Panagea *et al.*, 2005), and pharmaceutical and chemical products (Weiser *et al.*, 2019). The ubiquitous nature of *P. aeruginosa* is partially explained by its metabolic versatility conferred by the large genome (usually >6 Mbp). Comparative genomic analysis of clinical and environmental isolates shows a high degree of conservation of metabolic genes (Wolfgang *et al.*, 2003, Valot *et al.*, 2015), enabling *P. aeruginosa* to switch between eukaryotic hosts and environmental niches.

P. aeruginosa preferentially utilizes organic acids (succinate) and amino acids over others (Rojo, 2010). Metabolic genes contribute significantly to their virulence (Panayidou *et al.*, 2020) and niche adaptation (La Rosa *et al.*, 2019). *P. aeruginosa* strains defective in the catabolism of amino acids such as tryptophan, alanine, and histidine were shown to have reduced virulence in animal models (Bortolotti *et al.*, 2016, Boulette *et al.*, 2009, Rietsch *et al.*, 2004). Thus, a clear understanding of *P. aeruginosa* metabolism and the metabolic pathways are significant: (i) from a therapeutic perspective in identifying novel target sites and (ii) in developing biocontrol strains for environmental biotechnology applications, such as to clean up oil spills.

Histidine is an important amino acid that serves as source of carbon, nitrogen, and energy for *Pseudomonas* spp. and many other bacteria. Histidine catabolic pathway is highly conserved among bacteria, and the catabolism proceeds via a 4-step or 5-step enzymatic pathway depending on the bacterial genera (Fig. 1.1, Chapter 1). The first three enzymatic steps appear universal, where, histidine is sequentially converted to urocanate (and ammonia), 4-imidazolone-5-propionate, and formiminoglutamate (FIGLU) by HutH (histidase), HutU (urocanase), and HutI (Imidazolone propionate hydrolase), respectively (Itoh *et al.*, 2007, Bender, 2012). The histidine catabolic pathway branches at the intermediate FIGLU and has two fates. In the 4-step catabolic pathway utilized by enteric bacteria (*Salmonella enterica* and *Klebsiella pneumoniae*) and *Bacillus subtilis*, FIGLU is hydrolysed to glutamate and formamide

by formimidoylglutamase (HutG4: 4 denotes 4-step pathway enzyme) (Kimhi & Magasanik, 1970, Smith *et al.*, 1971, Rodriguez & West, 1984). Formamide is excreted as a waste product (Magasanik & Bowser, 1955). However, in the 5-step pathway utilized by *Pseudomonas* spp. and *Streptomyces* sp., FIGLU is first hydrolysed to formylglutamate (and ammonia) by FIGLU deiminase (HutF), and formyglutamate is hydrolysed to glutamate and formate by formylglutamate amidohydrolase (HutG) (Tabor & Mehler, 1954, Lessie & Neidhardt, 1967, Hu *et al.*, 1987, Zhang & Rainey, 2007b, Kendrick & Wheelis, 1982, Kroening & Kendrick, 1987). The 5-step pathway produces an extra mole of ammonium that may provide an advantage for *Pseudomonas* spp. growing under nitrogen limited conditions (Itoh *et al.*, 2007). Together, the observation that HutF (5-step pathway) has higher affinity for FIGLU (Marti-Arbona *et al.*, 2006) than HutG4 (4-step pathway) (Kaminskas *et al.*, 1970) led some to suggest that the 4-step pathway was ancestral in *Pseudomonas* spp., later replaced by HutF-HutG pair (Bender, 2012).

The genes for histidine utilization (*hut*) in *Pseudomonas* spp. including *P*. *putida*, *P*. *fluorescens*, and *P*. *aeruginosa* are clustered together in a single locus in 3 or 4 transcriptional units (Fig. 1.2, Chapter 1). The *hut* genes are subject to negative transcriptional regulation by a urocanate (inducer) responsive HutC (GntR-family) repressor protein. Similarly, *hut* genes in non-*pseudomonas* spp. are also repressed by HutC protein; a notable exception is *Bacillus subtilis* (Zhang & Rainey, 2007b, Bender, 2012, Naren & Zhang, 2020). Additionally, the *hut* genes are subject to carbon catabolite repression (CCR) in the presence of a preferred carbon source (Itoh *et al.*, 2007, Bender, 2012). Recent work from our lab in *P. fluorescens* SBW25 shows that CCR on *hut* genes is mediated by the interplay of CbrAB-CrcYZ-Crc/Hfq regulators at the transcriptional and translational levels (Zhang & Rainey, 2008, Naren & Zhang, 2021).

Intriguingly, *P*. *aeruginosa* PAO1 possesses an additional enzyme with formimidoylglutamase activity (Marti-Arbona *et al.*, 2006) that is found in organisms utilizing histidine via the 4-step pathway. The gene encoding for this enzyme (*hutE*, PA3175) is dislocated from the *hut* locus (Stover *et al.*, 2000), and its expression is activated by a preceding IclR-type transcriptional regulator (*hutR*, PA3174) in response to histidine, urocanate or FIGLU (Gerth *et al.*, 2012). Thus, it was proposed that both 4- and 5-step *hut* pathways co-exist in *P*. *aeruginosa* PAO1. The 4-step pathway was dispensable in the presence of 5-step pathway, and neither pathways conferred a fitness advantage growing under nitrogen limited or excess conditions (Gerth *et al.*, 2012). Indeed, this was contrary to a previous hypothesis that the 5-step pathway may be beneficial under nitrogen limited conditions. Nevertheless, the co-existence of both pathways was surprising since no other *Pseudomonas* spp. or bacterial genera is known to possess both pathways (Zhang & Rainey, 2007b, Bender, 2012, Itoh *et al.*, 2007). However, upon a careful examination of the gene neighbourhoods of *hutR* (PA3174) and *hutE* (PA3175), we

identified a putative transporter gene PA3176 (Fig. 2.1A) that is located 37-bp downstream of *hutE* (Winsor *et al.*, 2016, Stover *et al.*, 2000). Surprisingly, this three-gene organization is conserved across all *Pseudomonas* spp. possessing the homologs of *hutR* and *hutE*. The presence of a transporter together with a regulator (*hutR*) and an enzyme (*hutE*) involved in the degradation of FIGLU led us to hypothesize that PA3176 acts as a FIGLU specific transporter, and the three-gene cassette is dedicated for the direct utilization of FIGLU accumulated in host tissues/environment. However, this operon may have an impact on histidine utilization via the 5-step (*hutFG*) pathway.

Considering that metabolic flexibility is a key strength of *P. aeruginosa*, investigating the relevance of PA3174-PA3175-PA3176 operon in the direct utilization of FIGLU is of significant interest from an infection control and therapeutic perspective. Indeed, FIGLU appears to be widespread in the diverse ecological niches of *P. aeruginosa*. FIGLU is produced as an intermediate of histidine catabolism in humans. Although the initial enzymatic steps leading to the production of FIGLU are similar with bacteria, FIGLU donates its formimino group to tetrahydrofolate coupling histidine catabolism to folate metabolism (Fig. 1.1, Chapter 1), required for the synthesis of nucleotides and other molecules (Mao *et al.*, 2004, Solans *et al.*, 2000). Elevated levels and increased urinary excretion of FIGLU occur with folate and vitamin B12 deficiencies, certain anaemia and neoplastic diseases, histidinaemia, liver cirrhosis, and other hepatic disorders in humans (Hibbard, 1964, Carey *et al.*, 1964, Perry *et al.*, 1975, Majumdar *et al.*, 2017, Hilton *et al.*, 2003, Mohamed & Roberts, 1966, Luhby *et al.*, 1959, Matsuda *et al.*, 1982). Similarly, urinary excretion of FIGLU also occurs in animals and fishes associated with folate and vitamin B12 deficiencies (Stebbings & Lewis, 1986, Quirk & Norton, 1988, Casu *et al.*, 2019). Interestingly, FIGLU appears to be the end-product of histidine catabolism in reptiles and is excreted (Herbert, 1968, Coulson & Hernandez, 1968).

In this study, utilizing genetic techniques, we first investigated the FIGLU specific transporter role of PA3176 from *P. aeruginosa* PAO1. We found that PA3176 is induced by FIGLU in a dose-dependent manner and is required for growth on FIGLU. The three genes (PA3174, PA3175, and PA3176) are co-transcribed, and their expression is activated by PA3174 in response to FIGLU. Henceforth, these genes for FIGLU uptake and catabolism are referred to as *figR* (PA3174), *figA* (PA3175), and *figT* (PA3176). FIGLU utilization is subject to carbon catabolite repression, and *figT* appears to be the target of Crc/Hfq mediated repression. Further studies examined the effect of FigRAT and HutFG pathways (5-step *hut* pathway) on histidine and FIGLU catabolism in *P. aeruginosa* PAO1 and a plant growth promoting bacterium *P. fluorescens* SBW25 (Bailey *et al.*, 1995, Zhang & Rainey, 2007b). Histidine or urocanate by itself are incapable of inducing the *figRAT* operon, and our *in vivo* experimental data indicate that histidine is predominantly catabolised via the HutFG pathway. *In silico*

analysis suggests that there is no cross-regulation between FigRAT and *hut* pathways. Together, our data indicate that *figRAT* operon is dedicated for the direct utilization of FIGLU but not histidine. The intact *figRAT* operon is highly conserved among all *P. aeruginosa* strains, found in other *Pseudomonas* spp., and other bacterial genera. HGT events within *Pseudomonas* spp. were identified. Finally, we report for the first time the presence of *hut* operons for catabolism of histidine via 4-step enzymatic pathway in some *Pseudomonas* spp.

2.3 Results

2.3.1 Genetic identification of PA3176 (*figT*) as a FIGLU specific transporter

The *figT* gene encodes for a predicted protein of 404 amino acids in length and belongs to the Glutamate:Na^+ symporter (ESS) family (Pfam03616, E-value: $6.38e^{-137}$). Computational hydropathy analysis, using the TMHMM Server v. 2.0 (Moller *et al.*, 2001), predicted that FigT possesses 11 transmembrane domains (Fig. S2.1). Based on the computational prediction and proximity with *figRA* (Fig. 2.1A), we proposed that FigT functions as a transporter for FIGLU uptake. First, we showed that wild-type *P. aeruginosa* PAO1 can grow on minimal salts medium containing FIGLU as the sole source of carbon and nitrogen (Fig. 2.1C). Next, to test the predicted role of FigT in FIGLU uptake, an isogenic *figT* deletion mutant (MU52-86) was constructed and assayed growth on FIGLU as the sole source of carbon and nitrogen. Consistent with our expectation, the mutant strain MU52-86 (Δ*figT*) was unable to grow on FIGLU (Fig. 2.1C). Further, a complementation strain was constructed by re-introducing *figT* on a plasmid vector (pME6010) into MU52-86 (Δ*figT*). The complemented *figT* mutant (MU4A4-38) partially recovered growth on FIGLU (Fig. 2.1C). However, transferring the empty vector (pME6010) into MU52-86 (Δ*figT*) had no effect (data not shown). Of note, a small initial increase in the absorbance observed for the *figT* deletion mutant (MU52-86) is likely caused by growth on glutamate derived from the degradation of some unstable FIGLU in the medium (Fig. 2.1C). Consistently, *figA* (encoding for formimidoylglutamase enzyme) deletion mutant (strain PBR1020) also displayed a similar increase in the absorbance indicating that the growth was independent of FIGLU (Fig. 2.1C).

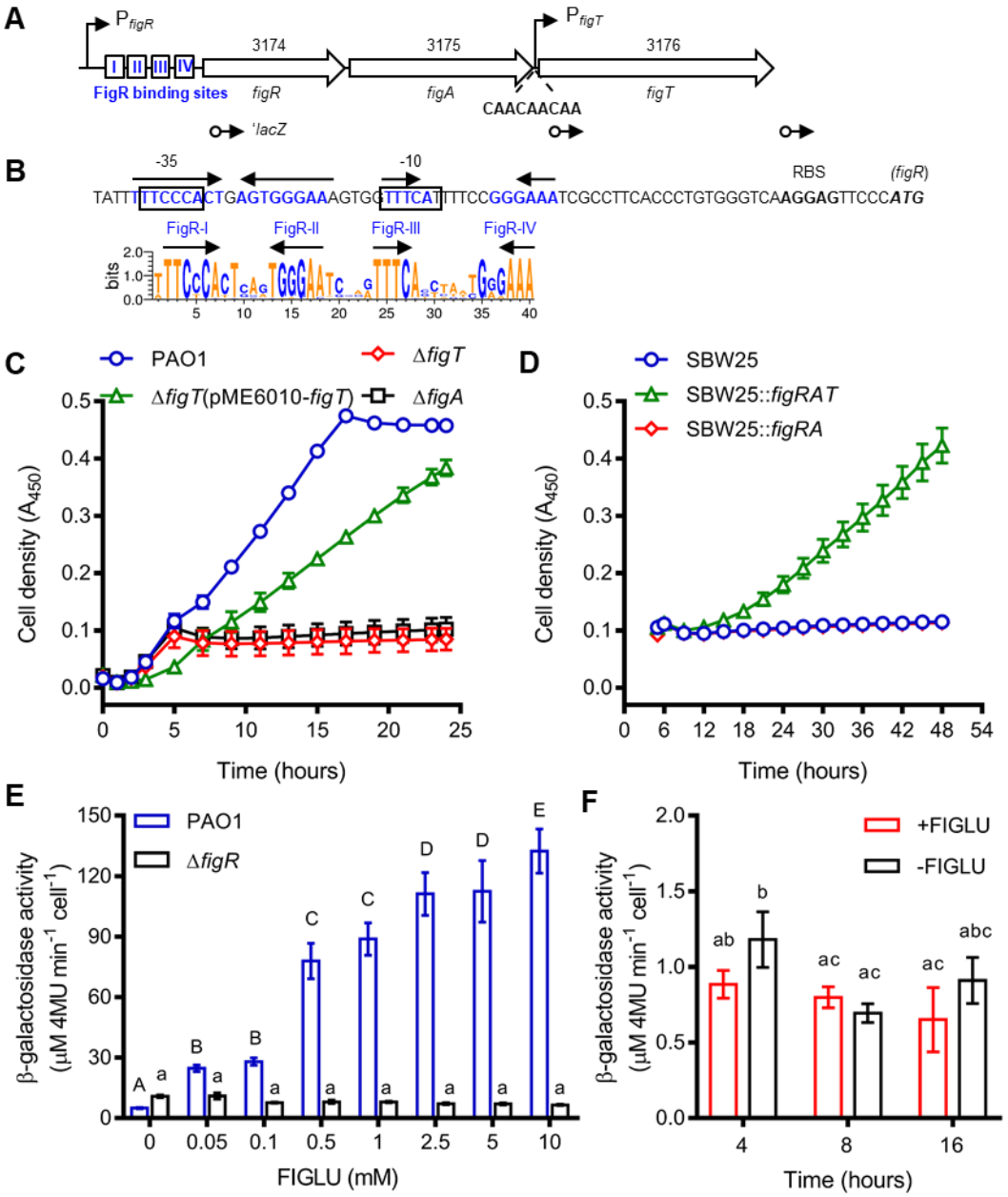

FIG 2.1 Genetic organization of the *fig* operon and identification of FigT as a FIGLU specific transporter.
(A) Schematic representation of the *fig* locus in *P. aeruginosa* PAO1. Location and orientation of the predicted promoters are indicated by bent arrows. Positions of the *lacZ* fusions are shown by open circles with arrow attached.
(B) Details of the *figR* promoter region in *P. aeruginosa* PAO1. The putative -10 and -35 promoter sequences are boxed. The predicted FigR binding sites are shown in blue boldface with arrows representing inverted repeats. Sequence logo generated from the alignment of P_{figR} from promoters of 30 *Pseudomonas* strains.
(C) Growth dynamics of wild-type PAO1, MU52-86 (Δ*figT*), MU4A4-38 (*figT* complementation), and PBR1020 (Δ*figA*) in minimal salts medium (MSM) containing FIGLU (10 mM) as C and N source. Data are means ± standard errors for two independent experiments (at least 4 replicate cultures per experiment).
(D) Growth dynamics of wild-type SBW25, MU36-55 (SBW25::*figRAT*), and MU43-79 (SBW25::*figRA*) in MSM containing FIGLU (10 mM) as C and N source. Data are means ± standard errors for 2 to 3 independent experiments (at least 5 replicate cultures per experiment).
(E) Dosage response of *figT* to FIGLU measured using *figT-lacZ* fusion strains MU4A4-55 (wild-type background) and MU4A4-64 (Δ*figR*). Data from each fusion strain was analysed separately by Tukey's test ($P < 0.05$), and bars that are not connected by identical upper- or lower-case letters are significant.
(F) Promoter activity in the *figA-figT* intergenic region measured using the P_{figT}- *lacZ* fusion strain MU46-9 (wild-type PAO1 background) in response to FIGLU (10 mM)**.** Bars that are not connected by the same letter are statistically significant as determined by Tukey's test ($P < 0.05$).
β-galactosidase activity was assayed for cells grown in MSM containing succinate (20 mM)+NH_4Cl (1 mg/ml) supplemented with FIGLU. Data are means ± standard deviations of four independent cultures.

P. *fluorescens* SBW25 does not contain the homologs of *figRAT*, therefore, suggesting that FIGLU cannot be catabolized. We next wanted to test if an introduced copy of *figRAT* from *P*. *aeruginosa* PAO1 would confer *P*. *fluorescens* SBW25 growth on FIGLU. First, we cloned the intact *figRAT* cassette from *P*. *aeruginosa* PAO1 into vector pUC18-mini-Tn7T-Gm-GW and introduced into *P*. *fluorescens* SBW25, where it is integrated into the chromosome at the neutral *attB* site. The resultant strain MU36-55 (SBW25::*figRAT*) was then examined for growth on FIGLU. Indeed, the wild type was incapable of growth on FIGLU; however, MU36-55 (SBW25::*figRAT*) gained the ability to grow on FIGLU (Fig. 2.1D). Additionally, strain MU43-79 (SBW25::*figRA*) generated by introducing *figRA* (without *figT*) into *P*. *fluorescens* SBW25 was also incapable of growth on FIGLU (Fig. 2.1D). Together, the genetic data consistently suggest that FigT functions as a FIGLU specific transporter.

2.3.2 Expression of *figT* is activated by FigR in a FIGLU dependent manner

To determine if *figT* expression can be induced by FIGLU and this requires *figR*, a chromosomally integrated *figT-lacZ* transcriptional fusion was constructed in the genetic background of wild-type *P*. *aeruginosa* PAO1 (fusion strain MU4A4-55) and the *figR* mutant (fusion strain MU4A4-64). β-galactosidase activity was then monitored in the presence of increasing concentrations of FIGLU (Fig. 2.1E). We observed a concentration dependent FigT expression response to FIGLU in the wild-type background (fusion strain MU4A4-55). However, *figT* remained uninducible at all FIGLU concentrations tested in the *figR* mutant (fusion strain MU4A4-64) background. Thus, we conclude that FIGLU induces *figT* expression, and FigR is required to activate FIGLU-induced expression of *figT*.

We next asked whether *figT* is co-transcribed with *figRA* and expressed from a previously identified promoter (Gerth *et al.*, 2012) preceding *figR*. To test for the possible presence of an additional promoter in the *figA-figT* intergenic region (P_{figT}), we constructed a P_{figT}-*lacZ* translational fusion and introduced into the genetic background of wild-type *P*. *aeruginosa* PAO1 (fusion strain MU46-9). β-galactosidase activity was then monitored in the presence and absence of FIGLU. FIGLU was not able to induce the expression of *lacZ* (Fig. 2.1F) in MU46-9, indicating a lack of promoter activity in the *figA-figT* intergenic region. Furthermore, an inspection of the *figA-figT* intergenic sequences did not identify a standard Ribosome Binding Site (RBS) for FigT translation, probably suggesting translational coupling with FigA. Together, we conclude that *figT* is co-transcribed with *figRA* in response to FIGLU.

2.3.3 FigRAT is not involved in the utilization of N-Acetyl-L-Glutamic acid

A previous study reported that the disruption of *figT* by transposon mutagenesis in *P. aeruginosa* PAO1 resulted in a reduced growth on N-Acetyl-L-Glutamic (NAG) acid as the sole nitrogen source (Johnson *et al.*, 2008). To test this, we compared the growth of wild type and *figT* deletion mutant (MU52-86) on NAG acid as the sole nitrogen source. Intriguingly, we found that the growth of MU52-86 (Δ*figT*) was similar to the wild-type PAO1, and no defect in growth was observed (Fig. 2.2A). Similar results were also observed with a *figA* deletion mutant (strain PBR1020) (Fig. 2.2A) and for growth on NAG acid as the sole carbon source (data not shown).

Additionally, to test whether NAG acid could induce *figT* expression, β-galactosidase activity was measured in a *figT-lacZ* fusion strain MU4A4-55 (wild-type background) in response to NAG acid and FIGLU (positive control). Consistent with our expectation, *figT* remained uninducible in response to NAG acid, whilst FIGLU was able to induce *figT* expression (Fig. 2.2B). Taken together, our data suggest that *figT* is not involved in the transport of NAG acid, and *fig* operon is not associated with the utilization of NAG acid.

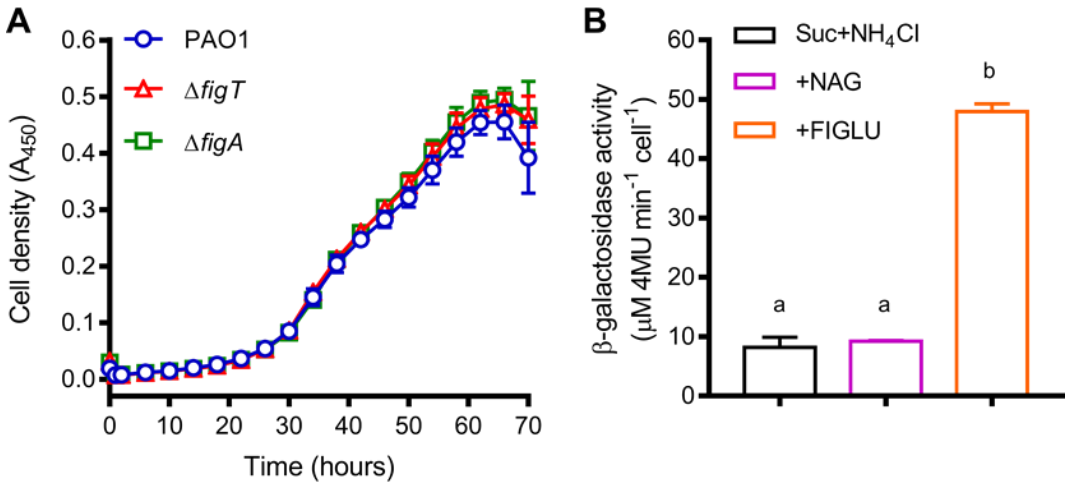

FIG 2.2 N-Acetyl-L-Glutamic acid (NAG) uptake and utilization in *P. aeruginosa* PAO1 does not involve *figT* or *fig* operon.
(A) Growth dynamics of wild-type PAO1, MU52-86 (Δ*figT*), and PBR1020 (Δ*figA*) on NAG acid as the sole nitrogen source. Cells were grown in minimal salts medium (MSM) containing NAG acid (5 mM) and succinate (20 mM) as carbon source. Data are means ± standard deviations of at least 4 independent cultures. If not visible, error bars are contained within the symbol.
(B) Induction of *figT* in response to NAG acid and FIGLU was monitored using the *figT-lacZ* fusion strain MU4A4-55. β-galactosidase activity was assayed after 8 hours of cell growth in MSM containing succinate (20 mM)+NH_4Cl (1 mg/ml) supplemented with NAG (10 mM) or FIGLU (10 mM). Data are means ± standard deviations of 3 independent cultures. Representative data from two independent fusions (P_{figR}-*lacZ* fusion also shows similar results). Bars that are not connected by the same letter are statistically significant as determined by Tukey's test ($P < 0.05$).

2.3.4 Expression of *figRAT* is subjected to Crc/Hfq-mediated Carbon Catabolite Repression

Carbon Catabolite Repression (CCR) is a regulatory mechanism that allows bacteria to utilize preferred carbon sources by repressing the expression of genes associated with the utilization of alternative carbon sources. In *Pseudomonas* spp., Crc/Hfq protein binds to a 'CA' motif (CAACAACAA) near the RBS binding site of mRNA transcripts to repress the expression of genes encoding for enzymes or regulators associated with the utilization of less preferred carbon sources. In the *figRAT* operon of *P. aeruginosa* PAO1, we identified a 'CA' rich motif in the *figA-figT* intergenic region (Fig. 2.1A) but not in the vicinities of *figR* or *figA* translational start site. This suggests that the transporter (*figT*) for FIGLU uptake is subjected to Carbon Catabolite Repression (CCR), rather than the catabolic enzyme or the regulator.

To determine if CCR regulates the *figRAT* operon, we first sought to examine whether Hfq_{his6} protein is capable of binding to the predicted 'CA' motif in the *figA-figT* intergenic region. The EMSA binding assay described below was carried out by Dr Yunhao Liu, a former PhD student in the Zhang lab. Briefly, a biotin labelled RNA probe (138 nucleotides in length) possessing the predicted 'CA' motif was synthesized using T7 RNA polymerase and subjected to EMSA analysis with purified Hfq_{his6}. We observed a significant shift in the biotin labelled RNA probe with increasing concentrations of Hfq_{his6} (Fig. 2.3A, lanes 2-7). RNA retardation was abolished when unlabelled RNA probe was added in 200-fold molar excess, indicating that the RNA-protein interaction is specific. The Hfq_{his6} dissociation constant (K_d) was estimated to be 183.4 ± 7.1 nM. The *in vitro* data strongly suggests that *figT* expression is subject to the Crc/Hfq-mediated CCR control.

Succinate is one of the most preferred carbon sources for *Pseudomonas* spp. and elicits a strong CCR in *P. aeruginosa*. To determine the effect of succinate on bacterial growth on FIGLU, we examined the growth of wild-type *P. aeruginosa* PAO1 on different FIGLU containing media (Fig. 2.3B). A rapid and biphasic growth was observed when cells were growing in the presence of succinate; suggestive of CCR. The first phase of the biphasic growth overlapped with growth on succinate and ammonium, suggesting utilization of succinate prior to FIGLU. Contrary to previous studies reporting that ammonium augmented succinate provoked CCR (Collier *et al.*, 1996), we observed that supplementing ammonium enhanced bacterial growth on FIGLU regardless of the presence of succinate (Fig. 2.3B).

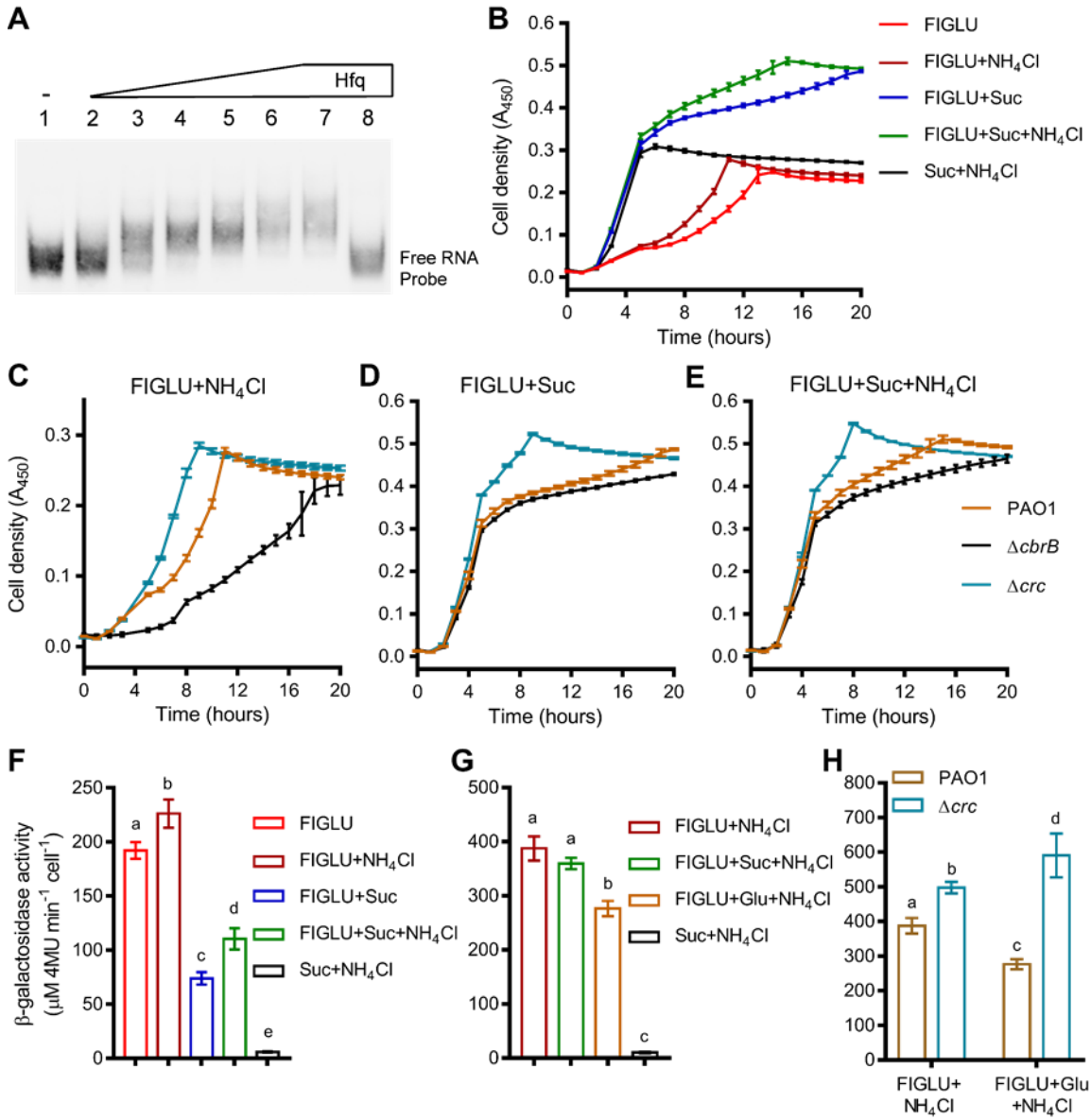

FIG 2.3 FIGLU utilization is subjected to Carbon Catabolite Repression (CCR).
(A) EMSA experiment showing specific binding of Hfq to the FigT transcript. EMSA was performed with 0.1 μM biotin-labeled RNA probe, synthesized in vitro using T7 RNA polymerase. Purified Hfq_{His6} was added at a final concentration of 0, 0.1, 0.2, 0.4, 0.8, 1.2, 1.6, and 1.6 μM in lanes 1 to 8, respectively. A 200-fold molar excess of unlabeled probe was added in lane 8 as a competitor RNA to examine protein-RNA specific interactions.
(B) Growth dynamics of wild-type PAO1 on minimal salts medium (MSM) containing FIGLU (5 mM), succinate (5 mM), and NH_4Cl (1 mg/ml) as indicated in the figure.
(C,D,E) Growth dynamics of wild-type PAO1, MU43-93 (Δ*cbrB*), and MU43-92 (Δ*crc*) on MSM containing FIGLU (5 mM), succinate (5 mM), and NH_4Cl (1 mg/ml) as indicated in the figure. Growth data are the means ± standard deviations of 4 independent cultures. Hourly absorbance readings are shown for clarity.
(F) Expression of FigT, measured using the *figT-lacZ* transcriptional fusion strain MU4A4-55 (wild-type PAO1 background), in response to FIGLU (10 mM) supplemented with succinate (20 mM) and/or NH_4Cl (1 mg/ml) as indicated in the figure.
(G) Expression of FigR, measured using the P_{figR}-*lacZ* fusion strain MU46-18 (wild-type PAO1 background), in response to FIGLU (10 mM) supplemented with succinate (20 mM), glucose (20 mM), and NH_4Cl (1 mg/ml) as indicated in the figure.
(H) Expression of FigR measured using the P_{figR}-*lacZ* fusion strains MU46-18 (wild-type background) and MU46-21 (Δ*crc* background) of PAO1 in MSM containing FIGLU (10 mM) and NH_4Cl (1 mg/ml) supplemented with glucose (20 mM) as indicated in the figure.
Expression data are means ± standard deviations of 4 independent cultures. Bars that are not connected by the same letter are statistically significant as determined by Tukey's test ($P < 0.05$).

The CCR regulatory cascade involves the interplay between *cbrAB*, *crcZ*, and *crc*/*hfq*. The CbrAB two-component system induces the expression of CrcZ, which sequesters Crc/Hfq; consequently, derepressing genes associated with the utilization of less preferred carbon sources. To determine the effects of *cbrAB* and *crc* on FIGLU utilization in *P*. *aeruginosa* PAO1, we compared the growth profiles of wild-type and mutant strains MU43-93 (Δ*cbrB*, [high CCR]) and MU43-92 (Δ*crc*, [no CCR]) on FIGLU in the presence of succinate and/or ammonium. We observed that the mutant strain MU43-93 (Δ*cbrB*) displayed a slower growth on FIGLU supplemented with ammonium (Fig. 2.3C). However, MU43-92 (Δ*crc*) had a growth advantage (Fig. 2.3C) and higher fitness than wild type (SRC = 0.765 ± 0.06 day^{-1} [mean ± SE; n=6], $P < 0.0001$). Similar results were also obtained with the mutant strains when growing on FIGLU without ammonium (data not shown). Thus, our growth data coupled with *in vitro* data (EMSA) indicate that FIGLU utilization is subject to CbrAB-CrcZ-Crc/Hfq regulation. Both wild type and *cbrB* mutant (MU43-93) showed a biphasic growth in the presence of succinate, and MU43-93 displayed a minor growth defect in the second log phase (during FIGLU utilization) as expected. We also observed that MU43-92 (Δ*crc*) had a growth advantage over wild type (Fig. 2.3D & E).

Considering that FigT is the predicted target of Crc/Hfq, we would expect to see a succinate mediated repression in *figT* expression when grown under CCR conditions. To test this, β-galactosidase activity was measured in a *figT-lacZ* transcriptional fusion strain MU4A4-55 (wild-type background) grown on FIGLU, or that supplemented with succinate and/or ammonium. Consistent with our expectation, *figT* expression was significantly repressed in the presence of succinate. However, addition of ammonium resulted in a slightly higher expression regardless of the presence of succinate, suggesting that ammonium does not pose any repression in *figT* expression (Fig. 2.3F).

We next asked if *figR* is subjected to CCR. To test this, expression of *figR* was measured using a P_{figR}-*lacZ* transcriptional fusion in the genetic background of wild-type *P*. *aeruginosa* PAO1 (fusion strain MU46-18) and *crc* mutant (fusion strain MU46-21) during growth on FIGLU under CCR conditions. Interestingly, we observed that *figR* expression in the MU46-18 (wild-type background) was repressed in the presence of glucose but not succinate (Fig. 2.3G). Moreover, this glucose mediated repression was relieved in the Δ*crc* background (fusion strain MU46-21) (Fig. 2.3H). Indeed, this repression is an indirect effect of CCR targeting *figT* expression which results in a reduced uptake of FIGLU, and consequently lower induction of *figR* expression.

2.3.5 Examining the effects of *hut* pathway on FigRAT-mediated FIGLU catabolism

We first tested the possible effects of *hut* genes (*hutF* and *hutG*) on FIGLU catabolism in *P. aeruginosa* PAO1 by comparing the growth profiles of wild type and mutants MU4A4-48 (Δ*hutF*), MU4A4-47 (Δ*hutG*), and PBR1021 (Δ*hutF* Δ*hutG*) on FIGLU as the sole carbon and nitrogen source. Intriguingly, we observed that deletion of *hutF* or *hutFG* conferred better growth for the mutants MU4A4-48 and PBR1021 on FIGLU compared to the wild type (Fig. 2.4A). The Δ*hutF* and Δ*hutFG* mutants showed a higher growth rate (0.484 ± 0.019 h^{-1} and 0.513 ± 0.051 h^{-1}) than the wild type (0.317 ± 0.023 h^{-1}). However, deletion of *hutG* (strain MU4A4-47) had no effect on growth on FIGLU; the growth rate of strain MU4A4-47 was 0.317 ± 0.038 h^{-1}) similar to the wild type (Table S2.1). Indeed, PBR1021 (Δ*hutF* Δ*hutG*) displayed a higher fitness than the wild type in a direct competition assay on FIGLU as the sole source of carbon or both carbon and nitrogen (Table 2.1). Together, the data imply that *hutFG* pose a disadvantage on FIGLU catabolism via the FigRAT pathway. It is of note that we did not observe a higher fitness for the mutant PBR1021 (Δ*hutF* Δ*hutG*) relative to wild type growing on FIGLU as a nitrogen source (Table 2.1). This is possibly due to the lower flux required to supply nitrogen for bacterial growth.

Table 2.1 Fitness of PAO1 mutant PBR1021 (Δ*hutF* Δ*hutG)* relative to the *lacZ* marked wild-type *P. aeruginosa* PAO1.

Growth condition[a]	Selection rate constant (day^{-1})[b]
FIGLU	0.606 ± 0.074*
FIGLU+NH_4Cl	0.482 ± 0.104*
Succinate+FIGLU	-0.202 ± 0.106
Succinate+NH_4Cl	-0.159 ± 0.084

[a]Strains were grown in minimal salts medium containing FIGLU (10 mM), succinate (20 mM), and NH_4Cl (18.7 mM) as indicated in the table.

[b]Data (means ± standard errors of at least 4 independent cultures) are differences in the Malthusian parameters for each competitor, and asterisks indicate significant difference from zero as determined by student's t-test ($P < 0.05$).

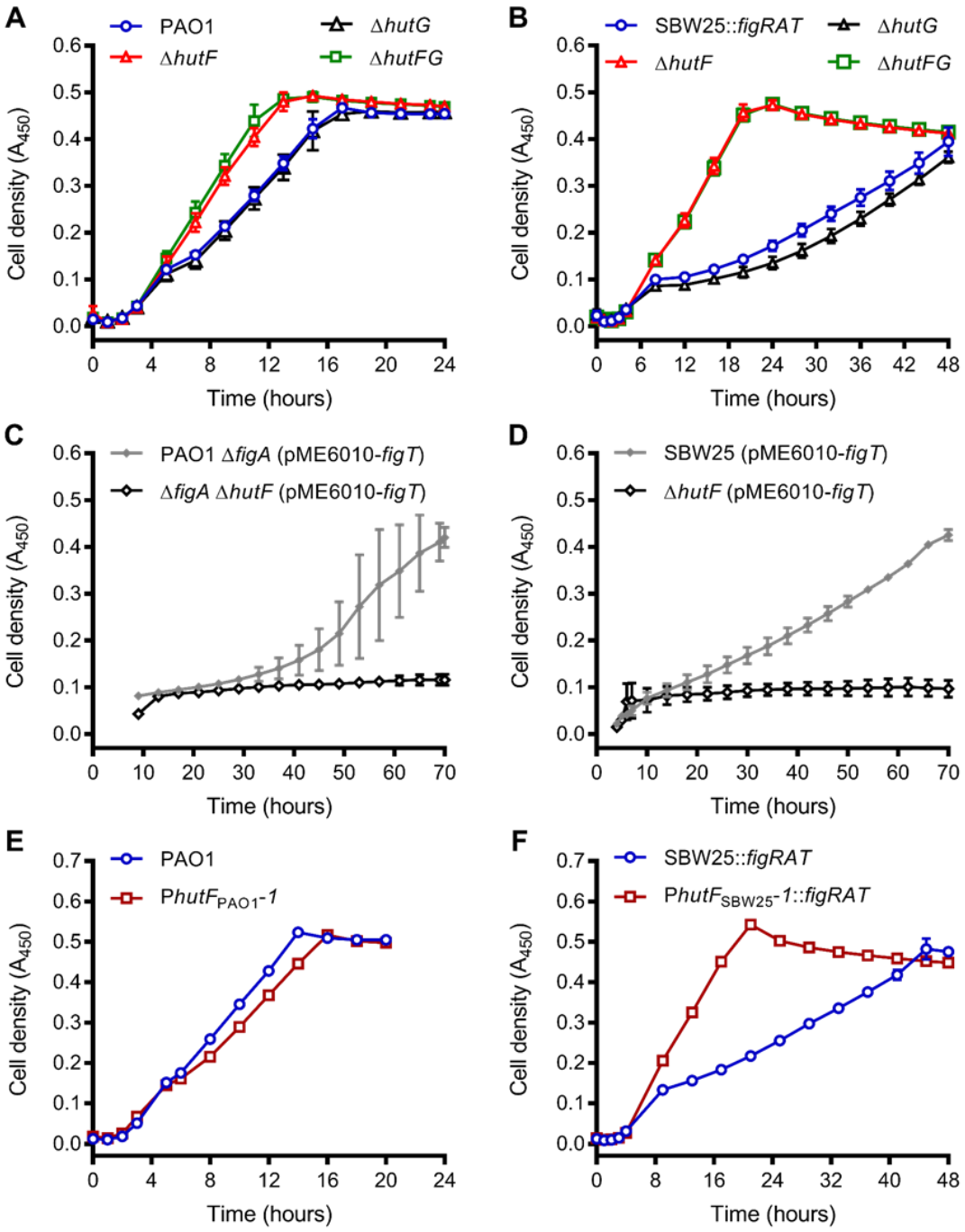

FIG 2.4 Presence of HutFG pathway is disadvantageous for FIGLU catabolism via FigRAT pathway.
(A) Growth dynamics of wild-type PAO1 and *hut* mutants MU4A4-48 (Δ*hutF*), MU4A4-47 (Δ*hutG*), and PBR1021 (Δ*hutF* Δ*hutG*). Data represent means ± standard errors for 2 to 3 independent experiments.
(B) Growth dynamics of SBW25 *hut* mutants carrying the *fig* operon: MU36-55 (SBW25::*figRAT*), MU36-57 (Δ*hutF*::*figRAT*), MU36-59 (Δ*hutF* Δ*hutG*::*figRAT*), and MU43-76 (Δ*hutG*::*figRAT*). Data represent means ± standard errors for 2 to 3 independent experiments.
(C) Growth dynamics of PAO1 mutants MU57-88 [Δ*figA*(pME6010-*figT*)] and MU57-94 [Δ*figA* Δ*hutF*(pME6010-*figT*)]. Data represent means ± standard deviations for 4 independent cultures. Absorbance readings every 4-hr are shown.
(D) Growth dynamics of SBW25 strains MU35-45 [SBW25(pME6060-*figT*)] and MU59-46 [Δ*hutF* (pME6010-*figT*)]. Data represent means ± standard errors for 2 independent experiments.
(E) Growth dynamics of wild-type PAO1 and MU59-96 ($PhutF_{PAO1}$-*1*; carrying Pntr site). Data represent means ± standard deviations for 4 independent cultures. Error bars are contained within the symbol.
(F) Growth dynamics of SBW25 strains MU36-55 (SBW25::*figRAT*) and MU62-1 ($PhutF_{SBW25}$-*1*; variant devoid of Pntr site and carries *figRAT*). Data represent means ± standard deviations of 3 biologically independent mutant samples. If not visible, error bars are contained within the symbol.
Cells were grown in MSM containing FIGLU (10 mM) as the sole source of carbon and nitrogen.

Further, we extended our investigation on the effect of *hutFG* on FIGLU catabolism in *P. fluorescens* SBW25, since they do not possess the homologs of *figRAT* and might explain the growth disadvantage in *P. aeruginosa* PAO1. First, *figRAT* from *P. aeruginosa* PAO1 was introduced into the genetic backgrounds of wild-type *P. fluorescens* SBW25 and *hut* pathway mutants: Δ*hutF*, Δ*hutFG*, and Δ*hutG*. Subsequently, growth dynamics of the resultant strains MU36-55 (SBW25::*figRAT*), MU36-57 (Δ*hutF*::*figRAT*), MU36-59 (Δ*hutF* Δ*hutG*::*figRAT*), and MU43-76 (Δ*hutG*::*figRAT*) were compared on FIGLU as the sole source of carbon and nitrogen. Consistent with the observation above, deletion of *hutF* or *hutFG* conferred a faster growth for the mutants MU36-57 (Δ*hutF*::*figRAT*) and MU36-59 (Δ*hutF* Δ*hutG*::*figRAT*), while mutation in *hutG* resulted in a slightly slower growth for MU43-76 (Δ*hutG*::*figRAT*), relative to MU36-55 (SBW25::*figRAT*) (Fig. 2.4B). Intriguingly, the effect of *hutFG* on FIGLU catabolism in *P. fluorescens* SBW25 was much larger than that observed in *P. aeruginosa* PAO1 (Fig. 2.4A). This was confirmed in a competitive fitness assay, where MU36-57 (Δ*hutF*::*figRAT*) and MU36-59 (Δ*hutF* Δ*hutG*::*figRAT*) had a large fitness advantage than SBW25::*figRAT* on FIGLU utilization (Table 2.2). Consistent with the growth data (Fig. 2.4B), MU43-76 (Δ*hutG*::*figRAT*) had a reduced fitness on FIGLU (Table 2.2).

Table 2.2 Fitness of *P. fluorescens* SBW25 *hut* pathway mutants relative to the *lacZ* marked strain MU58-32 (SBW25::*figRAT*) on FIGLU.

Strain (genotype)[a]	Selection rate constant (day^{-1})[b]
MU36-57 (Δ*hutF*::*figRAT*)/MU58-32	1.527 ± 0.077*
MU36-59 (Δ*hutF* Δ*hutG*::*figRAT*)/MU58-32	1.415 ± 0.069*
MU43-76 (Δ*hutG*::*figRAT*)/MU58-32	-0.404 ± 0.046*

[a]Cells were grown in minimal salts medium containing FIGLU (10 mM) as the sole source of carbon and nitrogen.

[b]Data (means ± standard errors of 6 independent cultures from 3 biologically independent samples) are differences in the Malthusian parameters for each competitor, and asterisks indicate significant difference from zero as determined by student's t-test ($P < 0.05$).

We next asked whether the growth disadvantage posed by *hutFG* on FIGLU catabolism was due to a lower flux through the HutFG pathway. To test this, *figT* was first introduced into wild-type *P. fluorescens* SBW25 and *hutF* deletion mutant on a plasmid vector pME6010. The resultant strains MU35-45 [SBW25(pME6010-*figT*)] and MU59-46 [Δ*hutF*(pME6010-*figT*)] were subsequently assayed growth on FIGLU. Consistent with our prediction, MU35-45 [SBW25(pME6010-*figT*)] was able to grow on FIGLU and the growth was dependent on *hutF*; MU59-46 [Δ*hutF*(pME6010-*figT*)] remained Fig^- (Fig. 2.4D). This indicates that FIGLU can be catabolized via the HutFG pathway in *P. fluorescens* SBW25.

Next, we tested whether this is true in *P*. *aeruginosa* PAO1 by generating mutants carrying pME6010-*figT*: MU57-88 [Δ*figA*(pME6010-*figT*)] and MU57-94 [Δ*figA* Δ*hutF*(pME6010-*figT*)], and assaying growth on FIGLU. We observed a poor growth for MU57-88 on FIGLU via the HutFG pathway (Fig. 2.4C), while MU57-94 remained Fig$^-$. However, we found that the poor growth of MU57-88 [Δ*figA*(pME6010-*figT*)] was caused by mutations and is not a phenotype of this mutant (data not shown); suggesting that FIGLU may not be able to induce *hutF* expression in wild-type *P*. *aeruginosa* PAO1. This further explains the more pronounced *hutFG* mediated growth disadvantage observed in *P*. *fluorescens* SBW25 (Fig. 2.4B) in contrast to *P*. *aeruginosa* PAO1 (Fig. 2.4A).

We predicted that this phenotypic difference between *P*. *fluorescence* SBW25 and *P*. *aeruginosa* PAO1 could be attributed to the presence of a Pntr site in *hutF* promoter in *P*. *fluorescence* SBW25 but not in *P*. *aeruginosa* PAO1 (Chapter 4). In chapter 4, we report that HutC (transcriptional repressor of *hut* genes) can recognise a distinct binding site (termed the Pntr site) in *hutF* promoter; Pntr site has poor similarity with the canonical HutC-binding site consensus sequence. We found that this Pntr site was required to produce wild-type levels of *hutF* during growth on histidine (Chapter 4).

Next, to determine the effect of Pntr site on FIGLU catabolism, we generated two mutants in the genetic background of *P*. *aeruginosa* PAO1 and *P*. *fluorescens* SBW25: MU59-96 (PAO1 P_{hutF} introduced with Pntr site [strain carries variant P$hutF_{PAO1}$-*1*]) and MU62-1 (SBW25::*figRAT* with mutation in P_{hutF} Pntr site [strain carries P$hutF_{SBW25}$-*1* variant]). The details of Pntr site variant construction are detailed in Chapter 4, Fig. 4.5. Subsequently, MU59-96 and wild-type PAO1, and MU62-1 and MU36-55 (SBW25::*figRAT*) were assayed growth on FIGLU. We observed that *P*. *fluorescens* SBW25 strain MU62-1 (P$hutF_{SBW25}$-*1* variant), carrying mutation in the Pntr site, displayed enhanced growth compared to MU36-55 (SBW25::*figRAT*) (Fig. 2.4F). However, *P*. *aeruginosa* PAO1 strain MU59-96 (P$hutF_{PAO1}$-*1*), carrying the Pntr site in P_{hutF}, had a minor growth disadvantage on FIGLU relative to wild type (Fig. 2.4E).

2.3.6 Examining the effects of *figRAT* on histidine catabolism

In *P*. *aeruginosa* PAO1, the *figRAT* expression can be induced by histidine, urocanate, and FIGLU; however, the physiological inducer of *fig* operon remains elusive. Here, we sought to investigate if histidine, urocanate, imidazalone propionate or FIGLU (histidine metabolites) is the direct inducer of *figRAT* expression. This was determined in the *P. fluorescens* SBW25 background, since all the required *hut* mutants were previously constructed in our laboratory. *P. fluorescens* SBW25 does not contain the homologs of *figRAT*. Therefore, we first introduced

figRAT from *P. aeruginosa* PAO1 into wild-type *P*. *fluorescens* SBW25 and three mutants that are defective in histidine catabolism: (i) Δ*hutH*$_2$ (ii) Δ*hutH*$_2$ Δ*hutU*, and (iii) Δ*hutI*. Subsequently, a *figT-lacZ* transcriptional fusion at the *fig* locus was constructed (by insertion-duplication) in these four backgrounds: MU56-45 (fusion strain, SBW25::*figRAT*), MU56-48 (fusion strain, Δ*hutH*$_2$::*figRAT*), MU58-73 (fusion strain, Δ*hutH*$_2$ Δ*hutU*::*figRAT*), and MU58-63 (fusion strain, Δ*hutI*::*figRAT*). Briefly, the Δ*hutH*$_2$ mutant lacks histidase activity and is unable to breakdown histidine (histidine accumulates in the cell) via the *hut* pathway. Similarly, Δ*hutH*$_2$ Δ*hutU* double mutant lacks both histidase and urocanase activities; thus, both histidine and urocanate accumulate in the cell. Histidine and urocanate are broken down to imidazalone propionate in the Δ*hutI* mutant but further degradation is blocked.

β-galactosidase activity was then monitored by growing cells in minimal salts medium containing glutamate supplemented with histidine, urocanate or FIGLU (Fig. 2.5A). FIGLU induced expression of *figRAT* was observed in all fusion strains: MU56-45, MU56-48, MU58-73, and MU58-63. Histidine induced expression of *figRAT* was observed only in MU56-45 (fusion strain, SBW25::*figRAT*) but not in the Δ*hutH*$_2$, Δ*hutH*$_2$ Δ*hutU* or Δ*hutI* genetic background. Urocanate induced expression of *figRAT* was observed in MU56-45 (fusion strain, SBW25::*figRAT*) and MU56-48 (fusion strain, Δ*hutH*$_2$::*figRAT*) but not in the Δ*hutH*$_2$ Δ*hutU* or Δ*hutI* genetic background. Urocanase activity is unaffected in strain MU56-48, hence urocanate is further broken down via the *hut* pathway. Our results indicate that histidine and urocanate are not capable of directly inducing *figRAT* expression. Histidine induced expression of *figRAT* observed in MU56-45 (fusion strain, SBW25::*figRAT*), and urocanate induced expression of *figRAT* observed in MU56-45 (fusion strain, SBW25::*figRAT*) and MU56-48 (fusion strain, Δ*hutH*$_2$::*figRAT*) are by virtue of their conversion to FIGLU via the *hut* pathway. Further, imidazolone propionate accumulated in the Δ*hutI* mutant (fusion strain MU58-63) was unable to induce *figRAT* expression, indicating none of the *hut* pathway inducers or intermediates (except FIGLU) can directly induce *figRAT* expression. Thus, our results indicate that FIGLU is the direct inducer of *fig* operon, whilst histidine and urocanate are indirect inducers.

Of note, we observed that the FIGLU induced expression levels of *figRAT* was >2-fold higher in MU56-48 (fusion strain, Δ*hutH*$_2$::*figRAT*) and MU58-73 (fusion strain, Δ*hutH*$_2$ Δ*hutU*::*figRAT*) compared to MU56-45 (fusion strain, SBW25::*figRAT*) and MU58-63 (fusion strain, Δ*hutI*::*figRAT*) (Fig. 2.5A). This could be associated with mutation of *hutH*$_2$. However, the exact reasons for the observed differences are not clear at this stage of the study.

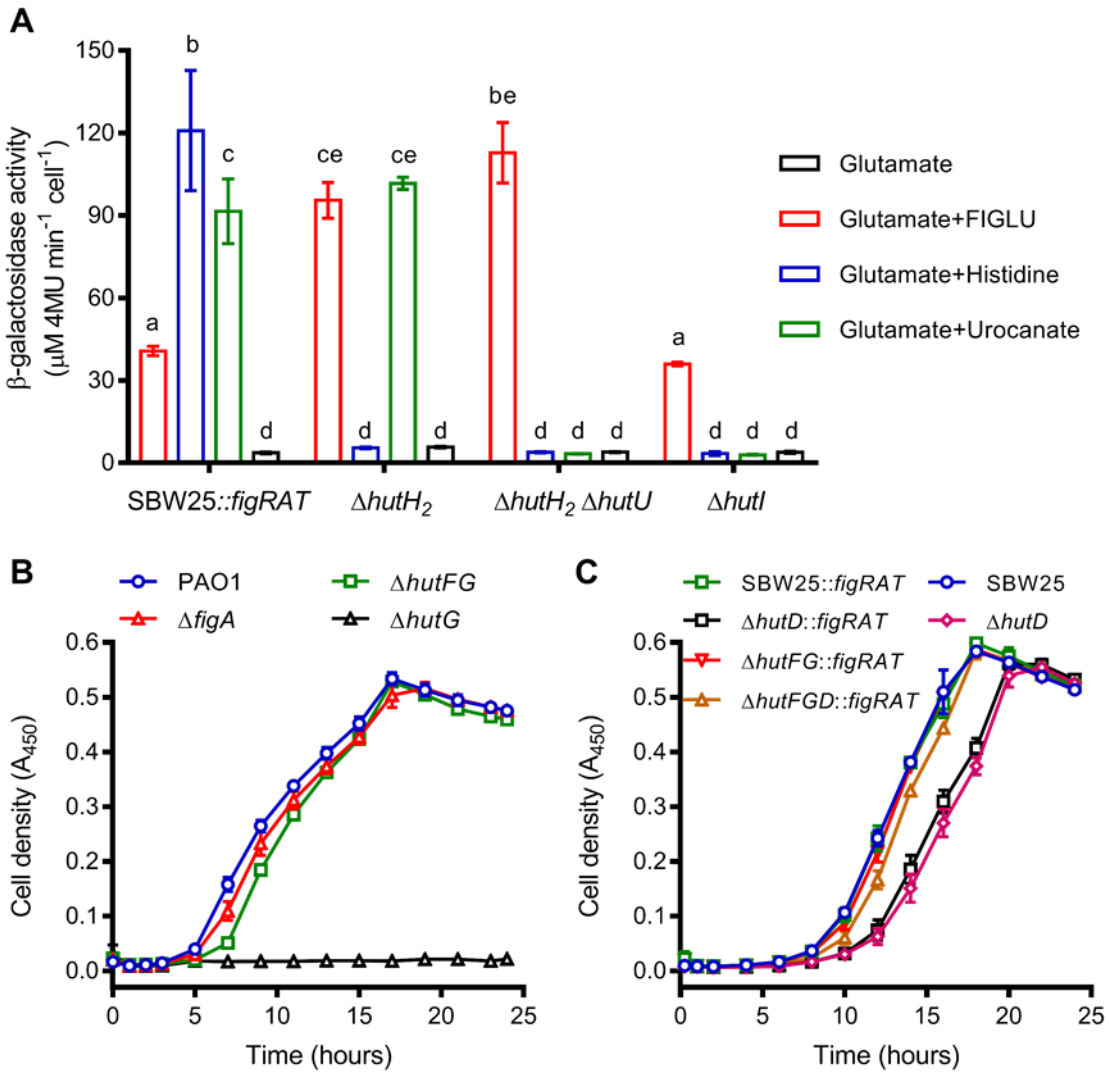

FIG 2.5 Role of *figRAT* operon in the utilization of histidine.
(A) FIGLU is the physiological inducer of *figRAT* operon, while histidine and urocanate are indirect inducers. Induction of *fig* operon in *P. fluorescens* SBW25 was measured using the *figT-lacZ* fusion strains MU56-45 (SBW25::*figRAT*), MU56-48 (Δ*hutH*$_2$::*figRAT*), MU58-73 (Δ*hutH*$_2$ Δ*hutU*::*figRAT*), and MU58-63 (Δ*hutI*::*figRAT*). β-galactosidase activity was assayed for cells grown in minimal salts medium (MSM) containing glutamate (10 mM) supplemented with FIGLU, histidine or urocanate at 10 mM. Data are means ± standard deviations of four independent cultures. Bars that are not connected by the same letter are statistically significant as determined by Tukey's test ($P < 0.05$).
(B) Growth dynamics of wild-type PAO1, PBR1020, (Δ*figA*), MU4A4-47 (Δ*hutG*), and PBR1021 (Δ*hutF* Δ*hutG*). Cells were grown in minimal salts medium containing histidine (10 mM) as the sole source of carbon and nitrogen. Data are means ± standard errors of 3 independent experiments (at least 4 replicate cultures per experiment). If not visible, error bars are contained within the symbol.
(C) Growth dynamics of wild-type SBW25, PBR806 (Δ*hutD*), MU36-55 (SBW25::*figRAT*), MU56-22 (Δ*hutD*::*figRAT*), MU36-59 (Δ*hutF* Δ*hutG*::*figRAT*), and MU56-16 (Δ*hutF* Δ*hutG* Δ*hutD*::*figRAT*). Cells were grown in minimal salts medium containing histidine (10 mM) as the sole source of carbon and nitrogen. Data are means ± standard errors of 2 independent experiments (4 replicate cultures per experiment). If not visible, error bars are contained within the symbol.

We next tested the effect of FigRAT pathway on histidine catabolism (via the *hut* pathway) in *P. aeruginosa* PAO1 by comparing the growth profiles of wild type and mutants PBR1020 (Δ*figA*), PBR1021 (Δ*hutF* Δ*hutG*), and MU4A4-47 (Δ*hutG*) on histidine as the sole source of carbon and nitrogen (Fig. 2.5B). We observed that the growth rates of wild type [0.481 ± 0.040

h^{-1}; Mean ± SE] and the mutants PBR1020 (Δ*figA*) [0.456 ± 0.048 h^{-1}] and PBR1021 (Δ*hutF* Δ*hutG*) [0.461 ± 0.037 h^{-1}] were similar. The mutant PBR1020 (Δ*figA*) had a slightly longer lag time [5.61 ± 0.10 h; *P* = 0.027] compared to the wild type [5.02 ± 0.084 h]. However, the mutant PBR1021 (Δ*hutF* Δ*hutG*) had a significantly longer lag time [6.67 ± 0.152 h; *P* = 0.0001] compared to the wild type. Accumulation of formylglutamate is deleterious to bacterial growth (Xue-Xian Zhang, unpublished data), explains why MU4A4-47 (Δ*hutG*) is unable to grow on histidine despite having the *figRAT* operon.

To further analyse the growth phenotypes, fitness assays were performed to determine the competitive ability of *hut* or *fig* pathway mutants relative to the wild-type background during growth on histidine as the sole source of carbon and nitrogen. We found that the fitness of the mutant PBR1021 (Δ*hutF* Δ*hutG*) was significantly reduced than wild type (Table 2.3). Similarly, fitness of the mutant MU4A4-48 (Δ*hutF*) was also found to be significantly impaired. The mutant PBR1020 (Δ*figA*), however, had a minor reduction in fitness compared to wild type (Table 2.3). Furthermore, when strains harbouring individual pathway (HutFG or FigA) were competed against each other, HutFG pathway was found to have higher fitness over FigA pathway (Table 2.3). These results suggest that histidine is efficiently catabolized via the HutFG pathway.

Table 2.3 Fitness of *P. aeruginosa* PAO1 *fig* or *hut* pathway mutants during growth on histidine.

Strain (genotype)[a]	Selection rate constant (day^{-1})[b]
MU4A4-48 (Δ*hutF*)/ PBR1023 (PAO1::*lacZ*)	-0.559 ± 0.033*
PBR1021 (Δ*hutFG*)/ PBR1023 (PAO1::*lacZ*)	-0.628 ± 0.029*
PBR1020 (Δ*figA*)/ PBR1023 (PAO1::*lacZ*)	-0.169 ± 0.046*
PBR1020 (Δ*figA*)/MU3U2-99 (Δ*hutFG::lacZ*)	0.241 ± 0.025*
PBR1021 (Δ*hutFG*)/ PBR1024 (Δ*figA*::*lacZ*)	-0.450 ± 0.048*

[a]Cells were grown in minimal salts medium containing histidine (10 mM) as the sole source of carbon and nitrogen.

[b]Data (means ± standard errors of 6 independent cultures) are differences in the Malthusian parameters for each competitor, and asterisks indicate significant difference from zero as determined by student's t-test (*P* < 0.05).

Next, to determine the effect of *figRAT* on histidine catabolism in *P. fluorescens* SBW25, we compared the growth dynamics of wild-type SBW25 (contains only HutFG pathway) and mutants MU36-55 (SBW25::*figRAT*, contains both pathways), MU36-59 (Δ*hutF* Δ*hutG*::*figRAT*), and MU43-76 (Δ*hutG*::*figRAT*) on histidine. We observed that growth characteristics such as the growth rate of strain MU36-55 possessing both HutFG and FigRAT pathways was similar to wild-type SBW25 possessing only the HutFG pathway. However, strain MU36-59 (Δ*hutF* Δ*hutG*::*figRAT*) possessing only the *figRAT* pathway had a slightly

higher growth rate relative to wild type and MU36-55 (Fig. S2.2 and Table S2.2). The mutant strain MU43-76 (Δ*hutG*::*figRAT*) was unable to grow on histidine despite having the *figRAT* operon likely due to the accumulation of toxic formylglutamate (Fig. S2.2).

We next performed fitness assays to determine the competitive ability of each pathway, HutFG or FigRAT, relative to the presence of both pathways. We observed that strains MU36-57 (Δ*hutF*::*figRAT*) and MU36-59 (Δ*hutFG*::*figRAT*) possessing only the FigRAT pathway was found to be equally fit as a strain possessing both FigRAT and HutFG pathways in head-to-head competition assays when grown on histidine as the sole source of carbon and nitrogen (Table 2.4). However, wild-type SBW25 possessing only the HutFG pathway was found to have a minor reduction in fitness compared to that possessing both HutFG and FigRAT pathways (Table 2.4) and was not detected in the growth assays (Fig. S2.2). Thus, our data suggest that histidine can be efficiently catabolized via both pathways in *P*. *fluorescens* SBW25. However, the large reduction in fitness associated with *hutFG* mutant observed above in *P*. *aeruginosa* PAO1 is not clear (Table 2.3).

Table 2.4 Fitness of *fig* or *hut* pathway relative to *P. fluorescens* SBW25 possessing both pathways.

Strain (genotype)[a]	Selection rate constant (day^{-1})[b]
MU36-57 (Δ*hutF*::*figRAT*)/MU58-32	-0.034 ± 0.111
MU36-59 (Δ*hutFG*::*figRAT*)/MU58-32	0.002 ± 0.023
Wild type/MU58-32	-0.170 ± 0.031*

[a]Cells were grown in minimal salts medium containing histidine (10 mM) as the sole source of carbon and nitrogen. MU58-32:*lacZ* marked strain of SBW25::*figRAT*.

[b]Data (means ± standard errors of 6 independent cultures from 3 biologically independent samples) are differences in the Malthusian parameters for each competitor, and asterisk indicates significant difference from zero as determined by student's t-test ($P < 0.05$).

We identified above that histidine is capable of inducing *figRAT* expression by virtue of conversion to FIGLU, and hypothetically FIGLU produced can be catabolized via either FigRAT or HutFG pathway. This promoted us to investigate whether both HutFG and FigRAT pathways are simultaneously utilized for breaking down FIGLU produced during histidine catabolism. To determine this, we exploited the slower growth phenotype of *hutD* associated with histidine utilization, via the HutFG pathway, in *P*. *fluorescens* SBW25. The *hutD* gene is co-transcribed with *hutC* and is thought to function as a governor for *hut* induction (Zhang & Rainey, 2007b). If histidine is predominantly catabolized via the HutFG pathway, we would then expect to see a *hutD* associated phenotype in the presence of both pathways (HutFG and FigRAT).

To test this, we first introduced *figRAT* from *P*. *aeruginosa* PAO1 into Δ*hutD* and Δ*hutF* Δ*hutG* Δ*hutD* (triple) mutants of *P*. *fluorescens* SBW25. The resultant strains MU56-22 (Δ*hutD*, contains both HutFG and FigRAT pathways) and MU56-16 (Δ*hutFGD*, contains only FigRAT pathway) along with wild-type SBW25 (contains only HutFG pathway), PBR806 (Δ*hutD*, contains only HutFG pathway), MU36-55 (SBW25::*figRAT*, contains FigRAT and HutFG pathways), and MU36-59 (Δ*hutF* Δ*hutG*::*figRAT*, contains only FigRAT pathway) were assayed growth on histidine as the sole source of carbon and nitrogen. Consistent with our prediction, we observed a *hutD* arbitrated growth defect associated with (i) HutFG pathway (wild type vs PBR806) and (ii) HutFG and FigRAT pathways (MU36-55 vs MU56-22). But such a defect was not observed with FigRAT pathway (MU36-59 vs MU56-16), Fig. 2.5C. Deletion of *hutD* from strains possessing only the HutFG pathway and both HutFG and FigRAT pathways significantly lowered growth rates and extended lag times by ~ 3 hr relative to their *hutD*$^+$ counterparts. However, deletion of *hutD* from strain possessing only the *figRAT* pathway had no significant effect (Table S2.2).

The growth assay results were further confirmed by fitness assays (Table 2.5). Consistent with the growth data, *hutD* mutants possessing only the HutFG (strain PBR806) pathway or both HutFG and FigRAT (strain MU56-22) pathways were observed to have significantly lower fitness compared to their *hutD*$^+$ counterparts. Indeed, *hutD* mutant possessing only the FigRAT pathway (strain MU56-16) was equally fit as a strain possessing both HutFG and FigRAT pathways, which was equally fit as strain (MU36-59) possessing only the FigRAT pathway (Table 2.5). Thus, our results strongly indicate that histidine is predominantly catabolized via the HutFG pathway in the presence of both pathways.

Table 2.5 Fitness effect of *hutD* mutation on histidine catabolism via Hut and FigRAT pathways in *P*. *fluorescens* SBW25.

Strain (genotype)[a]	Selection rate constant (day^{-1})[b]
PBR806 (Δ*hutD*)/SBW25-*lacZ*	-1.761 ± 0.145*
MU56-22 (Δ*hutD*::*figRAT*)/MU58-32	-1.627 ± 0.065*
MU36-59 (Δ*hutFG*::*figRAT*)/MU58-32	0.102 ± 0.04
MU56-16 (Δ*hutFG* Δ*hutD*::*figRAT*)/MU58-32	-0.041 ± 0.033

[a]Cells were grown in minimal salts medium containing histidine (10 mM) as the sole source of carbon and nitrogen. SBW25-*lacZ* carrying only the HutFG pathway; MU58-32: *lacZ* marked strain of SBW25::*figRAT* carrying both HutFG and FigRAT pathways.

[b]Data (means ± standard errors of 6 independent cultures) are differences in the Malthusian parameters for each competitor, and asterisks indicate significant difference from zero as determined by student's t-test ($P < 0.05$).

2.3.7 FigR consensus sequence prediction and cross-regulation of *hut* and *figRAT* operons

Having identified above that histidine is predominantly catabolized via the HutFG pathway, we asked if there is any cross-regulation between FigRAT and *hut* pathways. To determine this, we computationally analysed the *figRAT* and *hut* operons for the presence of their respective regulator binding sites. Considering the HutC recognition sequences is already known, we first predicted the FigR recognition sequences utilizing the below described *in silico* approach.

First, we aligned the putative *figR* promoter regions from 30 *Pseudomonas* strains representing 19 species to identify conserved sequences. Interestingly, we identified two highly conserved inverted repeat sequences (TTCYCAYT-N3-TGGGAA, and TTTCA-N6-GRGAAA) in the promoter regions, likely constituting the FigR binding site (Fig. 2.1A & S2.3). We designated the corresponding half-sites of the inverted repeat sequences in *figR* promoter as FigR-I, FigR-II, FigR-III, and FigR-IV, respectively (Fig. 2.1A). Sequences (TTCCCA-N16-TTTCAT) displaying similarity to the -35 (TTGaCc) and -10 (TAtAAT) consensus elements of *P*. *aeruginosa* promoter were identified in the regulatory regions, suggesting that *figR* expression is subject to sigma-70 regulation. The predicted -35 and -10 elements were also found to overlap with the putative FigR-I and FigR-III sites, respectively.

We next queried the *hut* operons for the presence of FigR binding site using a probability matrix of the FigR consensus sequence, generated in MEME suite package. Indeed, no significant hits were identified in the *hut* operons (P-value $<10^{-3}$), suggesting that *hut* operons are not subjected to FigR mediated regulation. Similarly, we queried the *figRAT* operon for the presence of HutC binding site (TGTA-N2-TACA) to determine if HutC is involved in the cross-regulation of *figRAT* operon. However, no significant hits were returned, suggesting that HutC does not cross-regulate the *figRAT* operon.

2.3.8 Phylogenetic analyses of *fig* genes

In the previous study (Gerth *et al.*, 2012), FigA was reported to be found exclusively in *P*. *aeruginosa* (strains PAO1, PA7, PA14, and LESB58), *P. fluorescens* Pf-5 (now updated to *P*. *protegens* Pf-5), and *P*. *mendocina* ymp. Interestingly, FigA from *P*. *mendocina* ymp was found to be distantly related to the homologous protein from *P*. *aeruginosa* PAO1, and they proposed that FigA was acquired by multiple independent horizontal gene transfer (HGT) events. Having witnessed a rapid increase in the whole genome sequencing over the recent years, we sought to investigate the origin of *figRAT* operon in *Pseudomonas* spp.

2.3.8.1 Prevalence of *figRAT* operon and relatedness of *figA* within *P. aeruginosa* strains

To decipher HGT events, we first asked whether all *P. aeruginosa* strains contain the *figRAT* operon and are all FigA proteins closely related. There are now 190 completely genome sequenced *P. aeruginosa* strains available in the Pseudomonas.com database (last accessed 28th August 2020).

To determine if all *P. aeruginosa* strains contain the *figRAT* operon, we performed a BLASTP search (built-in Pseudomonas.com database) for FigA against each genome using amino acid sequences from *P. aeruginosa* PAO1. The presence of linked genes *figR* and *figT* were confirmed by examining the *figA* locus. The *figA* gene was identified in all 190 completely sequenced *P. aeruginosa* strains. In all *P. aeruginosa* strains, we observed that *figA* was always flanked by an IclR-type transcriptional regulator and a sodium:glutamate symporter (as in *P. aeruginosa* PAO1), representing *figR* and *figT* genes, respectively. This indicates that the three gene organization is highly conserved.

Of note, we identified four *P. aeruginosa* strains with anomalies in *figR*, *figA*, and *figT*. The *figR* gene from *P. aeruginosa* 1334/14 and *P. aeruginosa* 97 have a transition mutation (G → A) at position 149 resulting in a stop codon and predicted truncated protein. In *P. aeruginosa* PAK, *figT* has multiple short stretches of deletions and uncalled bases at position 484 resulting in a frameshift and stop codons immediate downstream. The *figA* gene from *P. aeruginosa* AK6U has an insertion of a nucleotide at position 698 resulting in a frameshift and stop codon further downstream. However, other *fig* genes remained intact in these strains.

FigA sequences from all *P. aeruginosa* strains are of identical length (311 amino acids) and share 82.3% identical sites. To determine the relatedness of FigA amongst *P. aeruginosa* strains, we constructed a Neighbour-Joining phylogenetic tree. In the phylogeny, all FigA are grouped in closely related sister clades. About 93.7% (178/190) were grouped in a single clade, while 6.3% (12/190) formed smaller closely related clades (Fig. S2.4). In the phylogeny, we also observed divergence of FigA within the *P. aeruginosa* strains.

2.3.8.2 *In silico* identification of 4-step histidine catabolic pathway in *Pseudomonas*

Histidine catabolism in *Pseudomonas* spp. is widely known to proceed via a 5-step enzymatic pathway, involving *hutF* and *hutG* genes. FIGLU produced from histidine catabolism is converted into formylglutamate by HutF and is further broken down into formate and glutamate by HutG.

Co-incidentally, BLASTP search for FigA (utilizing sequences from *P. aeruginosa* PAO1) homologs in *Pseudomonas* spp., identified an enzyme with formidoylglutamase activity in the *hut* locus of several *Pseudomonas* spp. This enzyme is involved in the 4-step pathway histidine catabolism in enteric bacteria, where FIGLU is directly broken down to glutamate and formamide. Indeed, this is the first evidence for the existence of a 4-step histidine catabolic pathway in *Pseudomonas* spp. Henceforth, we refer to this *figA* homolog in the *hut* locus as *hutG4* (4 denotes 4-step *hut* pathway enzyme). Indeed, all the remaining *figA* homologs were flanked by *figR* and *figT* genes, constituting the *figRAT* operon. The *hutG4* gene was identified in the *hut* locus of *P. alcaligenes* NEB 585, *P. alcaliphila* JAB1, *P. fulva* 12-X, *P. mendocina* ymp, *P. oryzae* KCTC 32247, *P. oryzihabitans* USDA-ARS-USMARC-56511, *P. pseudoalcaligenes* CECT 5344, *P. sihuiensis* KCTC 32246, and 5 unclassified species of *Pseudomonas* (whose complete genomic sequences are available). Intriguingly, we have also identified a handful of *Pseudomonas* strains with incomplete genomic sequences (scaffold or contigs) possessing both *hutG4* (in *hut* locus) and *figRAT* operon (data not shown). This indicates that the presence of *figRAT* is independent of *hut* pathways, and further consolidates our hypothesis that *figRAT* is dedicated to the direct utilization of FIGLU present in the environment or host.

2.3.8.3 Phylogenetic analyses of FigA, HutG4, FigR, and FigT

To determine the relationship of FigA with HutG4, infer HGT events, and investigate the source of origin of *fig* genes, phylogenies of FigA and HutG4, FigR, and FigT were constructed with homologs identified from BLASTP search in *Pseudomonas* and non-*Pseudomonas* spp. HutG4 from *Salmonella* Typhimurium LT2 was additionally included in the FigA and HutG4 phylogeny and was chosen as the outgroup.

In the FigA and HutG4 phylogeny, all *Pseudomonas* FigA and HutG4 are grouped separately in two distant clusters (Fig. 2.6). All *Pseudomonas* HutG4 are grouped in a single cluster and do not have a recent common ancestor with FigA. This indicates that both FigA and HutG4 in *Pseudomonas* spp. are less related and serve different purposes. The previously reported FigA homolog in *P. mendocina* ymp (Gerth *et al.*, 2012) also clustered with HutG4 from other *Pseudomonas* spp. Surprisingly, HutG4 from *Corticimicrobacter populi* (belonging to b-proteobacteria) clustered with HutG4 from *Pseudomonas* spp. However, *Corticimicrobacter* species are not closely related to *Pseudomonas*.

All *Pseudomonas* FigA are grouped in a single cluster and displayed close relatedness with homologs from *Halomonas* spp., *Oceanimonas* spp., *Oceanisphaera* spp., and *Vibrio algivorus* (Fig. 2.6). These species including *Pseudomonas* belong to g-proteobacteria. It is possible that *Pseudomonas* spp. may have acquired FigA from these species or vice-versa.

We next examined the genomic locus of the FigA homologs in these species and found that both FigR and FigT homologs flanked FigA. Interestingly, we also observed homologous proteins from some of these species in distant clades but closer to *Pseudomonas* HutG4, suggesting that they may also contain HutG4. This prompted us to examine the genomic locus of all the FigA homologs in the phylogeny to differentiate FigA from HutG4. Indeed, we found that they contained both *figA* (in the *fig* operon) and *hutG4* (in the *hut* locus) genes. Further, *figRAT* operon was identified in the members of *Providencia* spp., *Wohlfahrtiimonas chitiniclastica*, *Arthrobacter castelli*, *Nocardiopsis alba*, *Chromobacterium haemolyticum*, *Chromobacterium rhizoryzae*, *Novispirillum itersonii*, and *Thauera humireducens*.

FigA from *Providencia* spp. and *Wohlfahrtiimonas chitiniclastica* clustered separately from *Pseudomonas* FigA (Fig. 2.6). Their most common ancestor appears to be near the base of the tree. FigA from *Chromobacterium* spp., *Novispirillum itersonii*, and *Thauera humireducens* clustered closer to HutG4. However, FigA from *Arthrobacter castelli* and *Nocardiopsis alba* were found to cluster with HutG4 from *Rhodococcus agglutinans*. It is possible that the two proteins had a common ancestor in the past, but a definite conclusion cannot be drawn based on the present evidence. Overall, FigA appears to be well separated from HutG4.

In the FigR phylogeny (Fig. S2.5), all *Pseudomonas* FigR are grouped in a single cluster. FigR from *Pseudomonas* spp. displayed close relatedness with FigR from *Halomonas* spp., *Oceanimonas* spp., *Oceanisphaera* spp., and *Vibrio algivorus*. We also found FigR from *Chromobacterium* spp., *Novispirillum itersonii*, and *Thauera humireducens* grouped in this cluster. This presumably suggests that these three groups had a common ancestor. However, FigR from *Providencia* spp. and *Wohlfahrtiimonas chitiniclastica,* and *Arthrobacter castelli* and *Nocardiopsis alba* clustered separately in a distant clade. We observed a similar pattern for FigA in these organisms (Fig. 2.6). Not surprisingly, we also observed a similar clustering of organisms for FigT in the FigT phylogeny (Fig. S2.6). The similar clusterings observed for FigA, FigR, and FigT presumably suggest that *figRAT* was transferred into *Pseudomonas* as an operon.

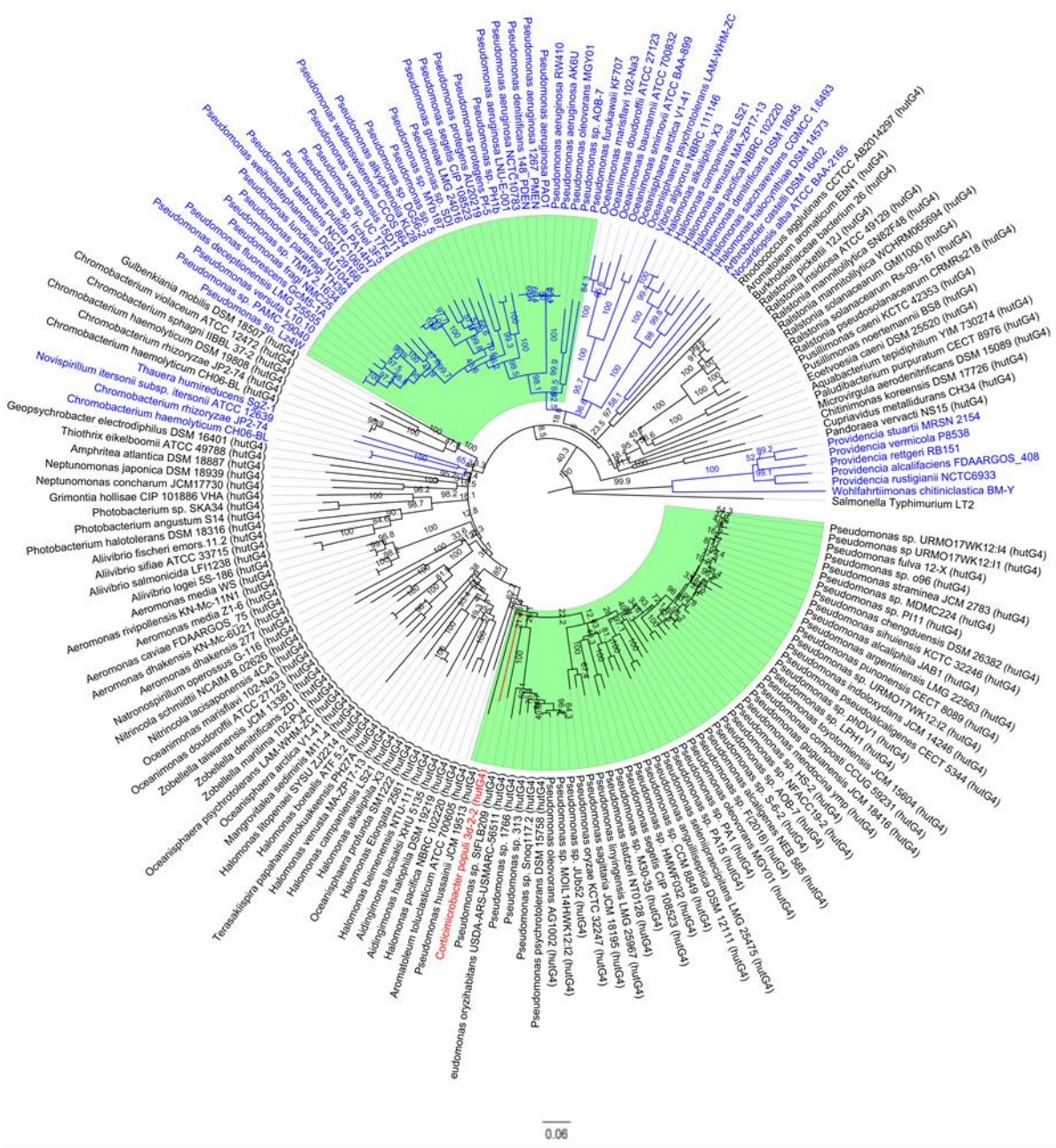

FIG 2.6 Neighbour-Joining consensus phylogenetic tree for FigA and HutG4 proteins constructed using amino acid sequences of the homologs identified in *Pseudomonas* spp. and non-*Pseudomonas* spp. *Salmonella* Typhimurium LT2 was chosen as the outgroup. FigA protein homologs are marked in blue to differentiate FigA from HutG4. Clades of *Pseudomonas* spp. are highlighted in green. Note that HutG4 from *Corticimicrobacter populi* (marked in red) is nested with the *Pseudomonas* HutG4 clade. Branch support values shown above branches are based on bootstrapping (1000 replicates).

To infer HGT events, we first re-constructed phylogenies of FigA, FigR, and FigT, with organisms possessing the *figRAT* operon. We next compared the individual protein phylogenies with their 16S rDNA gene phylogeny (Fig. 2.7-2.9). There is no apparent evidence for HGT of FigA, FigR or FigT into *Pseudomonas* spp. from other genus. However, in all three comparisons, we identified a few instances of HGT within *Pseudomonas* spp.; notably between, *P*. *deceptionensis* LMG 25555 and *P*. *fluorescens* GcM5-1A, *P*. *guineae* LMG 24016

and *P*. *segetis* CIP 108523, and *P*. *alkylphenolia* KL28, *Pseudomonas* spp. DG56-2 and *Pseudomonas* sp. 5.

The FigA, FigR, and FigT phylogenies have very similar clustering of organisms and topology. This further indicates that FigR, FigA, and FigT are maintained and transferred as an operon. We next constructed a phylogeny of concatenated FigRAT proteins and compared with the 16S rDNA profile. Indeed, we identified same instances of HGT within *Pseudomonas* spp. (Fig. S2.7) as observed in the individual protein phylogenies (Fig. 2.7-2.9). Further comparisons of the concatenated FigRAT tree with individual protein trees also revealed near identical clustering of organisms (data not shown) indicating lack of evidence for recombination events.

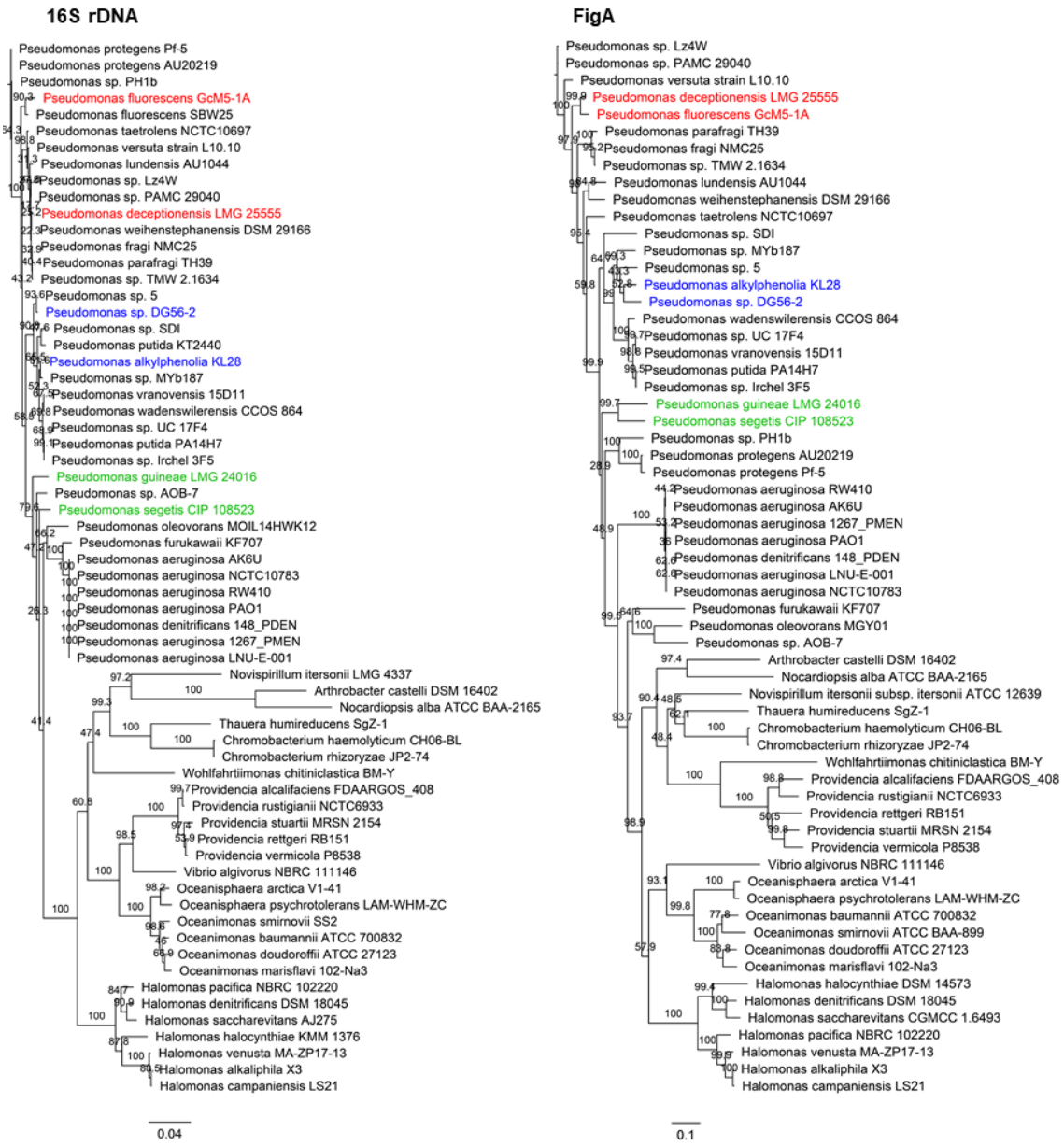

FIG 2.7 Neighbour-Joining consensus phylogenies of 16S rDNA and FigA protein.
Putative instances of HGT within *Pseudomonas* spp. are marked in identical colours on the 16S rDNA and protein trees. Branch support values shown above branches are based on bootstrapping (1000 replicates).

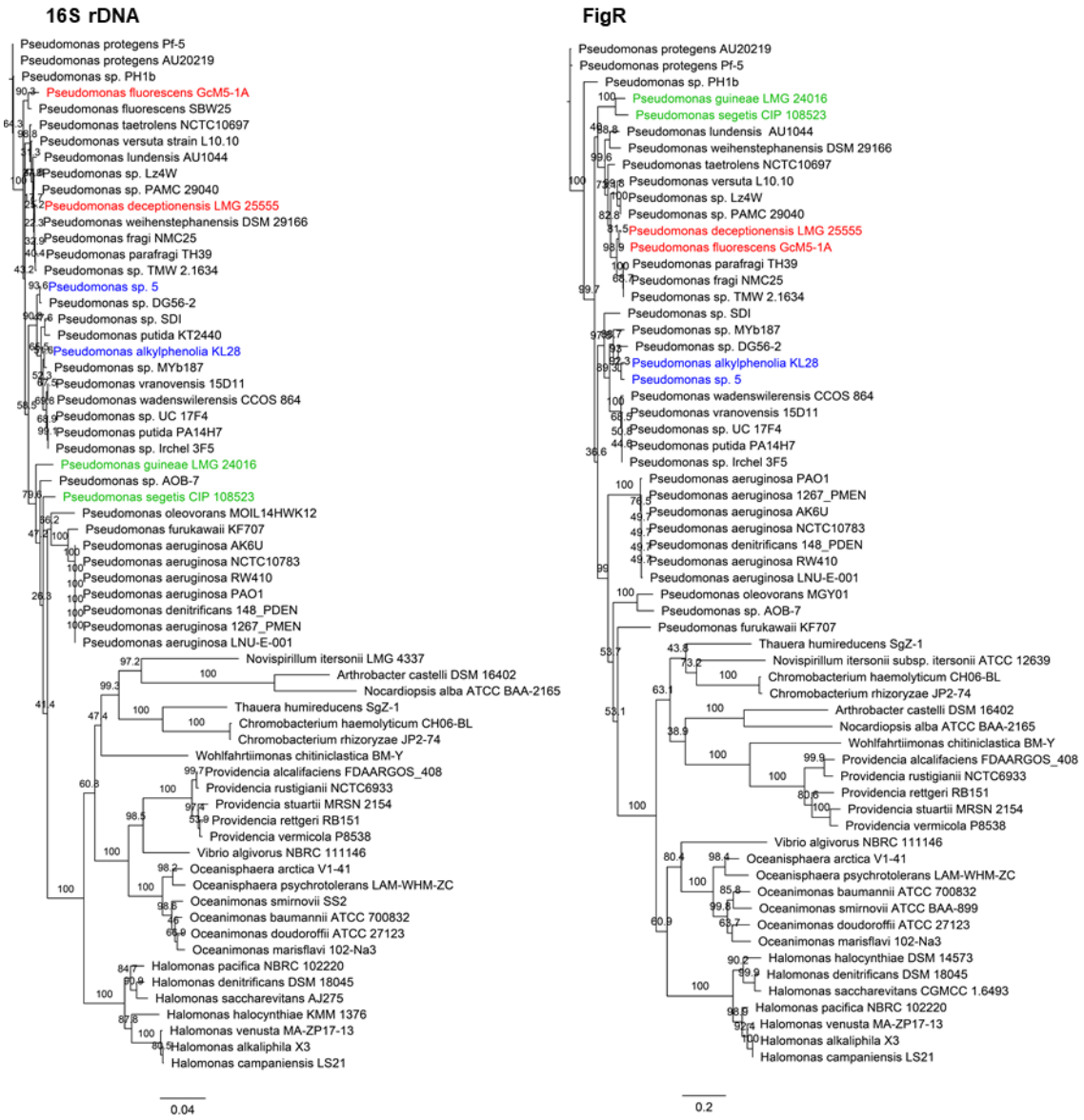

FIG 2.8 Neighbour-Joining consensus phylogenies of 16S rDNA and FigR protein.
Putative instances of HGT within *Pseudomonas* spp. are marked in identical colours on the 16S rDNA and protein trees. Branch support values shown above branches are based on bootstrapping (1000 replicates).

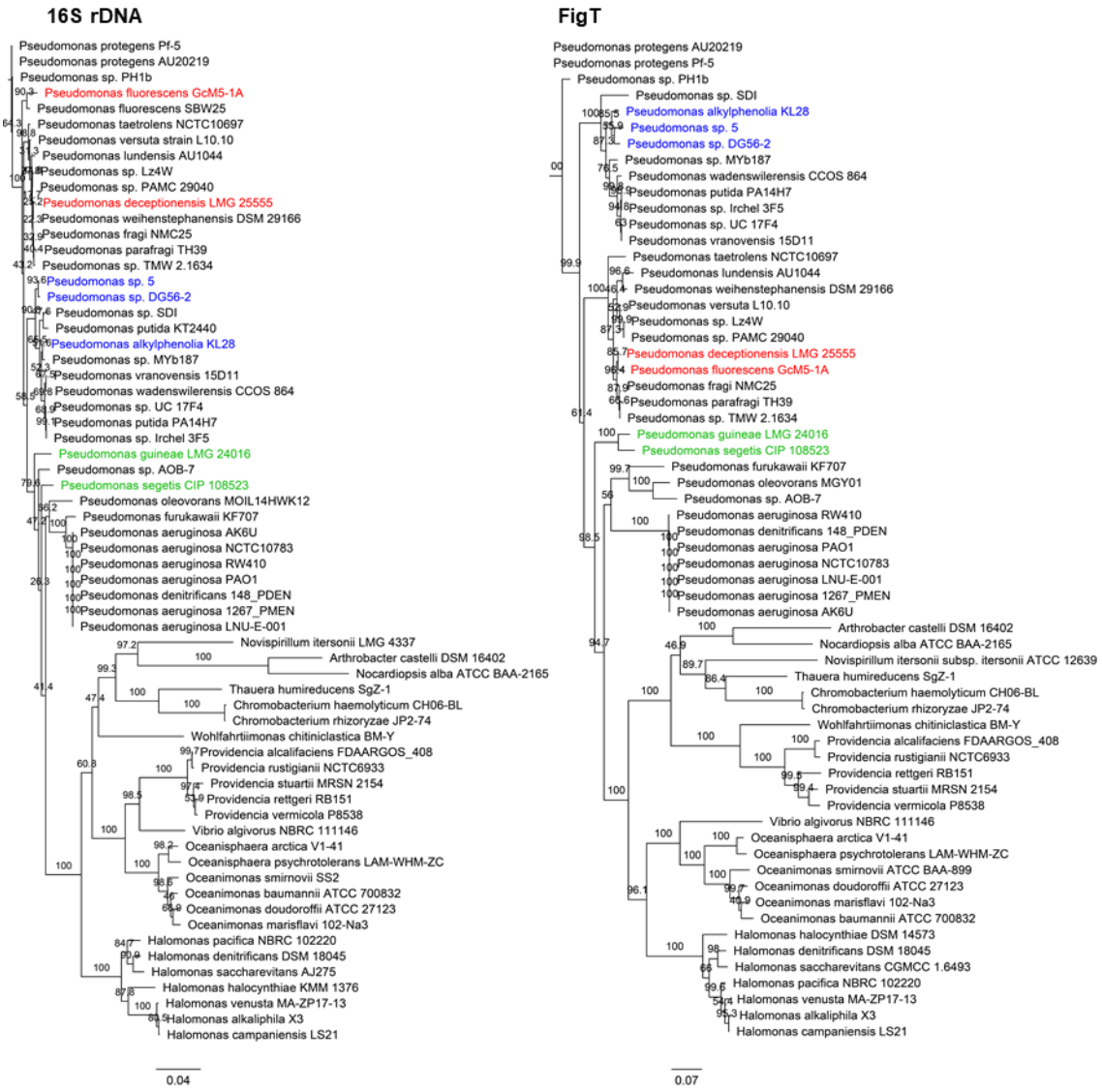

FIG 2.9 Neighbour-Joining consensus phylogenies of 16S rDNA and FigT protein.
Putative instances of HGT within *Pseudomonas* spp. are marked in identical colours on the 16S rDNA and protein trees. Branch support values shown above branches are based on bootstrapping (1000 replicates).

2.3.8.4 Anomalies in the *fig* genes

Previously, we identified four *P. aeruginosa* strains with anomalies in the *figA*, *figR*, and *figT* genes. In addition, we identified that *figR* from *P. lundensis* AU1044 contains multiple nucleotide deletions and insertions that cause a frame shift and stop codon resulting in a predicted truncated protein. The *figT* gene from *Halomonas denitrificans* DSM 18045 has a transition mutation (C → T) at position 943 resulting in a stop codon and predicted truncated protein. Also, *figT* from *Halomonas halocynthiae* DSM 14573 has a nucleotide (G) deletion at position 915 resulting in a frameshift and an immediate stop codon. Interestingly, partial sequences of *figR*, *figA*, and *figT* were identified in *Pseudomonas plecoglossicida* XSDHY-P. In this strain, C-terminus of FigR and FigA and N-terminus of FigT is found to be missing.

Similarly, four more strains belonging to this species (but with scaffold genome assembly) were also identified to possess partial sequences of *figR*, *figA*, and *figT* genes.

2.4 Discussion

Histidine catabolism in *Pseudomonas* spp. is widely known to follow a 5-step enzymatic pathway that breaks down intermediate FIGLU to glutamate in two successive enzymatic steps. In *P. aeruginosa* PAO1, the co-presence of an enzyme (FigA) that catalyses the direct conversion of FIGLU to glutamate led to a proposal that both 4 and 5-step histidine catabolic pathways co-exist (Gerth *et al.*, 2012, Marti-Arbona *et al.*, 2006). However, we identified a putative transporter (*figT*) in proximity to *figA* and its regulator *figR*. Significantly, this raised questions on the relevance of these genes in the uptake and utilization of FIGLU. In the present study, we demonstrated that *figT* encodes for a FIGLU-inducible FIGLU specific transporter in *P. aeruginosa* PAO1. The *figT* gene is co-transcribed with *figRA*, and *figRAT* operon exhibits a FIGLU-specific induction positively regulated by FigR. FIGLU utilization is subject to CCR regulation that targets FigT. Further, we determined that histidine is predominantly catabolized via the 5-step Hut pathway and flux through FigRAT accompanies a large fitness cost. Thus, we recommend that *figRAT* operon is dedicated for the uptake and utilization of FIGLU but not part of the 4-step histidine catabolic pathway as previously thought. The *figRAT* operon is highly conserved among *P. aeruginosa* strains and found in other members *Pseudomonas* spp. and Gammaproteobacteria. Phylogenetic analyses revealed transfer events within *Pseudomonas* spp. and indicate that *figRAT* is maintained and transferred as an operon. Further, we discovered for the first time that some *Pseudomonas* spp. possess *hut* operons for the catabolism of histidine via a 4-step enzymatic pathway like in enteric bacteria.

The ecological success of *P. aeruginosa* is largely attributed to metabolic versatility conferred by its large genome, which evolved through genetic expansion (Stover *et al.*, 2000). Functional redundancy appears to be common among *P. aeruginosa* strains (Mosquera-Rendon *et al.*, 2016, Colvin *et al.*, 2012, Recinos *et al.*, 2012). Functionally redundant enzymes/pathways could complicate studies of metabolic pathways, and consequently fail to acknowledge their biological relevance in metabolic diversity, as observed with the utilization of polyamines (Chou *et al.*, 2013, Yao *et al.*, 2011, Bandounas *et al.*, 2011). The functions of *figR* and *figA* in the degradation of FIGLU were previously described in the context of histidine catabolism (Marti-Arbona *et al.*, 2006, Gerth *et al.*, 2012). The genomic proximity of *figT* with *figA* and *figR* resembles an operon, where genes performing related functions are generally organized (Rocha, 2008). Consistently, our data revealed that deletion of *figT* gene in *P. aeruginosa* PAO1 abolished growth of this bacterium on FIGLU, while genetic complementation partially

restored growth. Also, this indicates that FigT is the only transporter for FIGLU uptake in *P. aeruginosa* PAO1. Taken together, the three genes comprise an entire catabolic pathway for the uptake and utilization of FIGLU. The fact that transfer of intact *figRAT* operon from *P. aeruginosa* PAO1 into *P. fluorescens* SBW25 conferred ability to grow on FIGLU, further, substantiates our claim. We know that FigR activates the expression of FigA and the two genes are predicted to form an operon (Gerth *et al.*, 2012). Significantly, analysis of *figT-lacZ* expression revealed that FigT expression is induced in response to FIGLU and this requires FigR. Further, a lack of promoter activity in the *figA-figT* intergenic region indicates that *figT* is co-transcribed with *figRA*.

FigT is computationally annotated as a sodium:glutamate symporter in the genome (Stover *et al.*, 2000, Winsor *et al.*, 2016), but is not involved in the transport of glutamate (Johnson *et al.*, 2008). A previous study reported that disruption of *figT* by transposon mutagenesis in *P. aeruginosa* PAO1 reduced growth on minimal salts agar medium containing N-acetyl-L-glutamic (NAG) acid as nitrogen source (Johnson *et al.*, 2008). However, our results show that deletion of *figT* in *P. aeruginosa* PAO1 did not impact growth on liquid minimal salts medium containing NAG acid as nitrogen source. Moreover, analysis of *figT-lacZ* expression revealed that NAG acid was not able to induce *figT* expression. Both our results implicate that *figT* is not involved in the utilization of NAG acid. A possible explanation for the differences is phenotypic diversity of the isolates (Chandler *et al.*, 2019), but the fact that *figT* forms an operon with *figRA* involved in the degradation of FIGLU augments confidence in our results.

In terms of regulation, the *figRAT* operon is subject to both positive and negative regulations at the transcriptional and translational levels, respectively. In the presence of FIGLU, FigR belonging to the IclR-family transcriptional regulators activates *figRAT* expression (Gerth *et al.*, 2012) from a predicted sigma-70 dependent promoter preceding *figR*. Using *in silico* analysis, two highly conserved inverted repeat sequences (TTCYCAYT N3 TGGGAA, and TTTCA N6 GRGAAA) that presumably constitutes the FigR binding site were identified in the *figR* promoter. The putative binding site is not present elsewhere in the *figRAT* operon indicating that *figR* is the only target for FigR. The predicted binding site sequence shows similarity with other members of the IclR-family transcriptional regulators: GenR (3-Hydroxybenzoate and Gentisate catabolism) and BaaR (Carboxylic acid oxidation) binding site sequences in *Corynebacterium* and *Brucella*, respectively (Chao & Zhou, 2013, Herrou *et al.*, 2018). Considering other members of the IclR-family acts as both activators and repressors (Guo & Houghton, 1999, Chao & Zhou, 2013), FigR may have dual functions. FigR may occupy the promoter region and represses *figRAT* expression in the absence of FIGLU. However, FIGLU-induced confirmational changes may turn FigR into an activator. This makes sense because our *in silico* data shows that FigR binding site sequence overlaps the putative

elements of the sigma-70 consensus sequence, typical of a repressor. Note that the 4 half-sites in the promoter may help co-ordinate this type of regulation, and we know from gene expression studies that FigR is required for the activation of *figRAT*. Further DNA binding studies are warranted for determining the mechanism of FigR interaction with the putative binding site and regulation of *figRAT* operon.

While FigR is the major regulator, our data shows that the *fig* operon is subject to carbon catabolite repression (CCR). CCR in *P. aeruginosa* is mediated by the complex interplay between CbrAB-CrcZ-Crc/Hfq regulators at the translational level that allows sequential utilization of preferred carbon sources. This is achieved by inhibiting translation of genes associated with the utilization of non-preferred carbon sources through the direct interaction of Crc/Hfq complex with CA-rich motifs (CAACAACAA) at the translation initiation region of mRNA (Sonnleitner *et al.*, 2009, Sonnleitner & Blasi, 2014, Rojo, 2010, Hernandez-Arranz *et al.*, 2013, Sonnleitner *et al.*, 2018). However, during the utilization of non-preferred carbon sources, the CbrAB two-component system (Nishijyo *et al.*, 2001) activates CrcZ (ncRNA) expression that sequesters Hfq proteins to relieve CCR (Sonnleitner *et al.*, 2012, Valentini *et al.*, 2014, Diaz-Perez *et al.*, 2018). In the *fig* operon, a 'CA' motif is present in the *figA-figT* intergenic region, and our EMSA data indicates that Hfq protein can bind to this region. Notably, FIGLU-induced expression of *figT* at the transcriptional level was strongly repressed in the presence of succinate (preferred carbon source), and wild-type *P. aeruginosa* PAO1 displayed a biphasic growth suggestive of succinate consumption prior to FIGLU. Moreover, deletion of *cbrB* resulted in a significant reduction in growth on FIGLU, while deletion of *crc* enhanced growth compared to the wild-type strain. Taken together, our results imply that FIGLU utilization is subject to CCR by targeting FigT transporter.

The targets of Crc/Hfq proteins are regulators, enzymes, and transporters involved in nutrient utilization. Previous studies show that CCR is exerted by Crc/Hfq targeting multiple genetic elements involved in nutrient utilization (Liu *et al.*, 2017, Wirebrand *et al.*, 2018, Hernandez-Arranz *et al.*, 2013) or the regulators (Sonnleitner *et al.*, 2017) or enzymes (Sonnleitner & Blasi, 2014). However, transporter by itself has not been previously reported as sole target mediating CCR. Multi-tier regulation by Crc/Hfq is generally thought to facilitate a strong CCR in the utilization of non-preferred carbon sources (Liu *et al.*, 2017, Hernandez-Arranz *et al.*, 2013). Contrarywise, FigT being the sole target of Crc/Hfq suggests that FIGLU utilization and *fig* operon are subjected to weak/intermediate CCR. This is consistent with the reduced growth of a *cbrB* deletion mutant of *P. aeruginosa* PAO1 on FIGLU, while a high CCR presumably abolishes growth (Liu *et al.*, 2017, Diaz-Perez *et al.*, 2018). Binding affinity for Hfq interaction with 'CA' motif (K_d=183.4 ± 7.1 nM) in the FigT transcript is also at least 3-fold lower than anthranilate regulator (*antR*) or aliphatic amidase (*amiE*) (Sonnleitner *et al.*, 2017, Sonnleitner

& Blasi, 2014), while admitting that they were determined using different procedures. A weak CCR on FIGLU utilization suggests that FIGLU may be a frequently encountered and good carbon source over other substrates as it is a single step away from glutamate. Indeed, it has been shown that several amino acids including histidine and glutamate are preferred over others in *P. putida* (Moreno *et al.*, 2009).

Nevertheless, a weak CCR on FIGLU utilization by targeting only FigT is still advantageous because of the presence of additional regulatory controls at both the transcriptional and translational level. CCR mediated inhibition of FigT translation lowers FIGLU uptake; consequently, reducing FIGLU-induced FigR activation of *figRAT* operon. This is evident from our data on succinate-induced repression of *figT* and glucose-induced repression of *figR* at the transcriptional level, albeit puzzling that glucose but not succinate repressed *figR* repression. Further, the predicted translational coupling of FigT with FigA in the absence of an RBS also reduces *figT* expression by at least 10-fold (Adhin & van Duin, 1990, Osterman *et al.*, 2013). Together, Crc/Hfq targeting only FigT may still be adequate to exert a tighter control over the expression of *fig* genes for the utilization of FIGLU in the presence of a more preferred carbon source.

Ammonium is a good nitrogen source for *P. aeruginosa* (Itoh *et al.*, 2007) and previous studies show that ammonium augments succinate-mediated catabolite repression (Collier *et al.*, 1996, Janssen *et al.*, 1982). In contrast, such an effect was not observed for *figT* expression or growth on FIGLU and FIGLU plus succinate supplemented with ammonium. Interestingly, ammonium enhanced *figT* expression and growth on FIGLU or FIGLU plus succinate.

The presence of HutFG (5-step histidine) pathway was disadvantageous for *P. aeruginosa* PAO1 in the uptake and utilization of FIGLU. Based on our growth data, exogeneous FIGLU cannot be catabolised via the HutFG pathway due to FIGLU being unable to induce *hutF* expression. One possible explanation for this is the accumulation of toxic Formyl glutamate (FG) produced from basal level HutF expression that is poorly broken down by an independently transcribed HutG enzyme. Despite the fitness costs associated with FIGLU utilization in the presence of HutFG pathway, *P. aeruginosa* PAO1 maintaining the *figRAT* operon indicates that FIGLU may be an important nutrient source.

Parallel analysis in *P. fluorescens* SBW25 produced a more pronounced effect for HutFG on exogeneous FIGLU utilization. The larger effect could be attributed to the differences in *hutF* expression caused by the presence of a Pntr site in *hutF* promoter of *P. fluorescens* SBW25. Consistently, *P. fluorescens* SBW25 exhibited a slower growth on FIGLU via the HutFG pathway. The precise function of the Pntr site in *hutF* promoter of *P. fluorescens* SBW25 has not been fully characterized but appears to be important for wild-type level expression of *hutF*

during growth on histidine (Chapter 4). Thus, it is predicted that Pntr site influences FIGLU utilization through HutFG pathway in *P. fluorescens* SBW25. Simultaneous activation of both HutFG and FigRAT pathways is likely disadvantageous and enhanced by toxicity from formyglutamate (produced through the HutFG pathway). *P. aeruginosa* PAO1 may have lost the Pntr site after acquiring *figRAT* operon for the better utilization of FIGLU via the FigRAT pathway.

Previously, the function of FigR and FigA in the degradation of FIGLU were correlated with 4-step pathway for histidine catabolism in *P. aeruginosa* PAO1 (Gerth *et al.*, 2012, Marti-Arbona *et al.*, 2006). However, the physiological inducer of *fig* genes and dominant enzymatic pathway utilized during histidine catabolism were not previously examined. Our results from the analysis of *figT-lacZ* expression in the wild-type and *hut* mutants of *P. fluorescens* SBW25 revealed that FIGLU is the direct inducer of *figRAT* operon. Histidine and urocanate can induce *figRAT* expression only by virtue of their conversion to FIGLU. These are significant observations because *hut* genes for histidine catabolism are induced by histidine or urocanate regardless of the 4-step or 5-step pathway utilized or organism (Chasin & Magasanik, 1968, Schlesinger *et al.*, 1965, Brill & Magasanik, 1969, Leidigh & Wheelis, 1973, Lessie & Neidhardt, 1967, Zhang & Rainey, 2007b). This includes *hut* pathway genes in *Corynebacterium* that was recently shown to possess a 4-step pathway positively regulated by HutR; also, an IclR family transcriptional regulator (Schroder *et al.*, 2012). In contrast to FigR, HutR in *Corynebacterium* is found in the *hut* locus with other *hut* enzymes. HutR shares little amino acid sequence identity (~ 25%) with FigR and was not identified in the FigR homolog search (top 500 hits). Also, HutR does not group closely with FigR homologs from *Pseudomonas* and other genus in the phylogeny (data not shown). These suggest that HutR (*Corynebacterium*) and FigR are distinct regulators belonging to the same family, and further validates renaming of *Pseudomonas hutR* (PA3174) to *figR* in this study. Moreover, our *in silico* analysis indicate that there is no cross-regulation between *figRAT* and *hut* operons in *P. aeruginosa* PAO1. Thus, our findings corroborate that *figRAT* operon is not linked to 4-step histidine catabolic pathway and not directly involved in the 5-step histidine catabolism.

Significantly, growth and fitness data comparing wild-type *P. aeruginosa* PAO1 and its derived *figA* and *hutFG* deletion mutants on histidine as carbon and nitrogen source (at 10 mM) indicate that HutFG pathway is preferred over FigRA. Although, the individual pathway mutants were less fit than wild-type, flux through FigA had a large fitness (SRC = -0.628 ± 0.029 day^{-1}) cost than HutFG (SRC = -0.169 ± 0.046 day^{-1}) relative to the wild-type. Several inconsistencies were noted here with a previous study (Gerth *et al.*, 2012) showing that (i) FigA pathway had a large fitness advantage over HutFG, and (ii) HutFG pathway had a large fitness disadvantage over wild type, at 20 mM histidine. At present we do not know if

concentration of histidine could explain such an effect. However, our data seems reasonable considering two aspects. First, HutF has a 20-fold higher affinity for FIGLU than FigA (Marti-Arbona *et al.*, 2006), which indicates that the intracellular concentrations of FIGLU must be high enough for breaking down FIGLU via FigA (Bender, 2012). In addition, urocanate is the physiological inducer of *hut* genes that ensures induction of HutF and HutG along or prior to production of FIGLU. Both together, minimises FIGLU accumulation and catabolism via FigA.

Parallel investigation in mutants of *P. fluorescens* SBW25 (*figRAT*) revealed that histidine catabolism through HutFG had a negligible fitness cost, but FigRAT pathway was equally fit as a strain possessing both FigRAT and HutFG pathways. While data tend to agree for the minor fitness costs associated with HutFG pathway, differences observed with FigA pathway between the two species is elusive.

A conclusive indication that HutFG pathway is predominantly utilized for histidine catabolism in the presence of *figRAT* operon was obtained from the comparison of *hutD* phenotypes of *P. fluorescens* SBW25 (*figRAT*) mutants. Growth and fitness data consistently revealed that mutation of *hutD* from strain possessing both FigRAT and HutFG pathways resulted in growth defects and a very large fitness cost on histidine. But such phenotypes were not observed with mutation of *hutD* in strain possessing only the FigRAT pathway. The slower growth and reduced fitness phenotypes of *hutD* is linked to histidine degradation via the 5-step (HutFG) pathway (Zhang & Rainey, 2007b). Although, we agree that FIGLU produced from histidine catabolism can induce *figRAT* expression in the presence of *hutFG* (revealed by *figT-lacZ* expression, Fig. 2.5), the catabolic flux is dominant via the HutFG pathway presumably due to HutF having high affinity and turnover of FIGLU (Marti-Arbona *et al.*, 2006).

The *figRAT* operon is highly conserved among *P. aeruginosa* strains and possibly a part of its core genome; indicated by its presence in all 190 completely genome sequenced strains (Winsor *et al.*, 2016). Homologs of *figRAT* are present in other *Pseudomonas* spp. and its distribution appears to be more widespread than previously thought (Gerth *et al.*, 2012). Some *Pseudomonas* spp. possess mutations in the *figR*, *figA*, and/or *figT* genes (Winsor et al., 2016), presumably, indicating genomic decay in response to niche adaptation (Winstanley *et al.*, 2016). The intact *figRAT* operon is also present in some members of g-proteobacteria and other genera. Phylogenetic analysis did not find any transfer events for *figRAT* between *Pseudomonas* spp. and these bacterial genera, however, transfer events within *Pseudomonas* spp. were observed. This may suggest that FIGLU is available in the diverse ecological niches shared by *Pseudomonas* spp. There is no evidence for genetic recombination from our phylogenetic study, indicating that the *figRAT* is maintained and transferred as an operon.

Further, we discovered *hut* locus containing *hutG4* (formimidoylglutamase) in *Pseudomonas* spp. This *hut* locus contains the entire set of *hut* genes for histidine catabolism via a 4-step enzymatic pathway as seen in the enteric bacteria. Interestingly, the 4-step histidine catabolic pathway is believed to be ancestral in *Pseudomonas* spp. (Itoh *et al.*, 2007, Bender, 2012) but was never identified before. Further studies may unravel events leading to the addition of HutF and HutG enzymes (5-step pathway). HutG4 and FigA are phylogenetically distinct and do not have a common ancestor. In both *Pseudomonas* and other bacterial genera, we found presence of *figRAT* in addition to *hutG4* (4-step *hut* pathway). Significantly, these findings clarify the role of *figRAT* in the uptake and utilization of FIGLU, and its non-involvement in histidine utilization via 4-or 5-step pathways.

In summary, the results of our present study indicate that *figT* encodes for a FIGLU specific transporter and forms an operon with *figRA*. We provide evidence that *figRAT* operon is dedicated to the direct utilization of FIGLU but not associated with 4-step histidine catabolism as previously thought. The *figRAT* operon is highly conserved in *P*. *aeruginosa* and homologs are clustered in the genomes of many *Pseudomonas* spp. This suggests that a number of *Pseudomonas* spp. are capable of utilizing FIGLU, and presumably FIGLU is a frequently encountered source of nutrient derived from eukaryotic hosts.

2.5 Materials and Methods

2.5.1 Bacterial strains, plasmids, and growth conditions

Strains and plasmids used in this work are shown in Table 2.6. *E*. *coli*, *P*. *aeruginosa* PAO1, and *P*. *fluorescens* SBW25 were routinely propagated in Luria-Bertani broth (LB). *E*. *coli* and *P*. *aeruginosa* were grown at 37°C, while *P*. *fluorescens* SBW25 was grown at 28°C. *Pseudomonas* were also grown in M9 minimal salts medium (MSM), which contained 47.8 mM Na_2HPO_4, 22 mM KH_2PO_4, 8.6 mM NaCl, 2 mM $MgSO_4$, supplemented with carbon and nitrogen sources at concentrations of 10 mM, unless specified otherwise. *E*. *coli* DH5$\alpha\lambda_{pir}$ was used for general cloning and triparental conjugation into both *P*. *aeruginosa* and *P*. *fluorescens* strains. When required, antibiotics were used at the following concentrations for *Escherichia coli* and *P*. *fluorescens* SBW25: 15 µg/ml tetracycline (Tc); 10 µg/ml gentamicin (Gm). For *P*. *aeruginosa* antibiotics were used at: 100 µg/ml Tc; 20 µg/ml Gm. Spectinomycin (Sp) and nitrofurantoin (Nf) were used at 100 µg/ml for *Escherichia coli*. X-gal (Melford) was used at concentrations of 60 µg/ml for blue/white screening of bacterial colonies. Succinate, histidine, urocanate, N-acetyl-L-Glutamic acid, and glutamate were purchased from Sigma, while FIGLU (N-formimino-L-glutamate) was custom synthesized at >95% purity by Dalton Pharma Services (Toronto, Canada).

Table 2.6 Strains and plasmids used in this study.

Strain or plasmid	Genotype or characteristics[b]	Reference/source
***P. aeruginosa* strains**[a]		
PAO1	Wild-type PAO1	Lab stock
PBR1023	PAO1::mini-Tn7T-*lacZ*, wild-type strain marked with *lacZ*	Gerth *et al.* (2012)
MU4A4-55	DUP *figT*::pUIC3, the *figT-lacZ* transcriptional fusion strain of wild-type PAO1	This work
MU46-9	PAO1 carrying pXY2::P_{figT}	Yunhao Liu, unpublished
MU46-18	PAO1 carrying mini-Tn7-Gm-*lacZ*::P_{figR}	Yunhao Liu, unpublished
MU59-96	P*hutF*$_{PAO1}$*-1* variant of PAO1	This work
MU52-86	Δ*figT*, PAO1 devoid of PA3176	This work
MU4A4-38	Δ*figT* carrying pME6010-*figT*	This work
MU57-63	Δ*figT* carrying pME6010	This work
PBR1026	Δ*figR*, PAO1 devoid of PA3174	Gerth *et al.* (2012)
MU4A4-64	Δ*figR* DUP *figT*::pUIC3, *figT-lacZ*	This work
MU4A4-48	Δ*hutF*, PAO1 devoid of PA5106	Monica Gerth, unpublished
MU4A4-47	Δ*hutG*, PAO1 devoid of PA5091	Monica Gerth, unpublished
PBR1021	Δ*hutF* Δ*hutG*, PAO1 devoid of PA5106 and PA5091	Gerth *et al.* (2012)
MU3U2-99	Δ*hutF* Δ*hutG*::mini-Tn7T-*lacZ*, *lacZ* marked strain	Monica Gerth, unpublished
PBR1020	Δ*figA*, PAO1 devoid of PA3175	Gerth *et al.* (2012)
PBR1024	Δ*figA*::mini-Tn7T-*lacZ*, *lacZ* marked strain	Gerth *et al.* (2012)
MU57-88	Δ*figA* carrying pME6010-*figT*	This work
MU3U3-9	Δ*figA* Δ*hutF*, PAO1 devoid of PA3175 and PA5106	Monica Gerth, unpublished
MU57-94	Δ*figA* Δ*hutF* carrying pME6010-*figT*	This work
MU43-92	Δ*crc*, PAO1 devoid of PA5332	Sonnleitner *et al.* (2009)
MU43-93	Δ*cbrB*, PAO1 devoid of PA4726	Sonnleitner *et al.* (2009)
MU46-21	Δ*crc* carrying mini-Tn7-Gm-*lacZ*::P_{figR}	Yunhao Liu, unpublished
***P. fluorescens* strains**[a]		
SBW25	Wild-type strain isolated from phyllosphere of sugar beet	Bailey *et al.* (1995)
SBW25-*lacZ*	SBW25 carrying *lacZ* marker in a phage locus	Zhang and Rainey (2007a)
MU58-32	SBW25-*lacZ* carrying mini-Tn7T-Gm-GW::*figRAT*	This work
MU43-79	SBW25 carrying mini-Tn7T-Gm-GW::*figRA*	Yunhao Liu, unpublished
MU36-55	SBW25 carrying mini-Tn7T-Gm-GW::*figRAT*	Xue-Xian Zhang, unpublished
MU56-45	DUP *figT*::pUIC3, *figT-lacZ* transcriptional fusion strain of MU36-55	This work
MU59-86	P*hutF*$_{SBW25}$*-1* variant of SBW25	This work
MU62-1	MU59-86 carrying mini-Tn7T-Gm-GW::*figRAT*	This work
MU35-45	SBW25 carrying pME6010-*figT*	Xue-Xian Zhang, unpublished
PBR806	Δ*hutD*, SBW25 devoid of PFLU0360	Zhang and Rainey (2007b)
MU56-22	Δ*hutD* carrying mini-Tn7T-Gm-GW::*figRAT*	This work
PBR803	Δ*hutH*$_2$, SBW25 devoid of PFLU0367	Zhang and Rainey (2007b)
MU56-10	Δ*hutH*$_2$ carrying mini-Tn7T-Gm-GW::*figRAT*	This work

MU56-48	DUP *figT*::pUIC3, *figT-lacZ* transcriptional fusion strain of MU56-10	This work
MU36-43	Δ*hutH*$_2$ Δ*hutU*, SBW25 devoid of PFLU0367 and PFLU0361	Xue-Xian Zhang, unpublished
MU58-53	Δ*hutH*$_2$ Δ*hutU* carrying mini-Tn7T-Gm-GW::*figRAT*	This work
MU58-73	DUP *figT*::pUIC3, *figT-lacZ* transcriptional fusion strain of MU58-53	This work
MU33-95	Δ*hutI*, SBW25 devoid of PFLU0369	Xue-Xian Zhang, unpublished
MU58-57	Δ*hutI* carrying mini-Tn7T-Gm-GW::*figRAT*	This work
MU58-63	DUP *figT*::pUIC3, *figT-lacZ* transcriptional fusion strain of MU58-57	This work
MU35-86	Δ*hutF*, SBW25 devoid of PFLU0358	Yunhao Liu, unpublished
MU36-57	Δ*hutF* carrying mini-Tn7T-Gm-GW::*figRAT*	Xue-Xian Zhang, unpublished
MU59-46	Δ*hutF* carrying pME6010-*figT*	This work
MU16-70	Δ*hutG*, SBW25 devoid of PFLU0370	Xue-Xian Zhang, unpublished
MU43-76	Δ*hutG* carrying mini-Tn7T-Gm-GW::*figRAT*	Yunhao Liu, unpublished
MU35-91	Δ*hutF* Δ*hutG*, SBW25 devoid of PFLU0358 and PFLU0370	Xue-Xian Zhang, unpublished
MU36-59	Δ*hutF* Δ*hutG* carrying mini-Tn7T-Gm-GW::*figRAT*	Xue-Xian Zhang, unpublished
MU36-50	Δ*hutF* Δ*hutG* Δ*hutD*, SBW25 devoid of PFLU0358, PFLU0370 and PFLU0360	Xue-Xian Zhang, unpublished
MU56-16	Δ*hutF* Δ*hutG* Δh*utD* carrying mini-Tn7T-Gm-GW::*figRAT*	This work
Plasmids		
pRK2013	Helper plasmid, Tra$^+$, Km^r	Ditta *et al.* (1980)
pUX-BF13	Helper plasmid for transposition of mini-Tn7 element, Mob$^+$, *ori*-R6K, Ap^r	Bao *et al.* (1991)
pCR8/GW/TOPO	Cloning vector, Sp^r	Invitrogen
pME6010	Broad-host-range cloning vector, Tc^r	Heeb *et al.* (2000)
pME6010-*figT*	Recombinant plasmid for *figT* complementation	Xue-Xian Zhang, unpublished
pUIC3	Integration vector with promoterless *lacZ*, Mob$^+$, *ori*-R6K, Tc^r	Rainey (1999)
pUIC3-135	pUIC3 containing *figT* deletion fragment	Xue-Xian Zhang, unpublished
pUIC3-145	pUIC3 containing *figT-lacZ* transcriptional fusion	Yunhao Liu, unpublished
pXY2	Mini-Tn7 vector for a *lacZ* translational fusion, Ap^r, Gm^r	Liu *et al.* (2014)
pXY2-P$_{figT}$	pXY2 containing the P$_{figT}$-*lacZ* translational fusion	Yunhao Liu, unpublished
pUC18-mini-Tn7T-Gm-GW	Mini-Tn7T; GW destination vector for gene insertion in Gm^s bacteria, Ap^r, Gm^r	Choi and Schweizer (2006)
pUC18-mini-Tn7T-Gm-GW::*figRAT*	Mini-Tn7T-Gm-GW containing *figRAT* for gene insertion	Xue-Xian Zhang, unpublished
pUC18-mini-Tn7T-Gm-GW::*figRA*	Mini-Tn7-Gm-GW vector containing *figRA* for gene insertion	Gerth *et al.* (2012)
pUC18-mini-Tn7T-Gm-*lacZ*	Mini-Tn7 vector for transcriptional fusion to promoterless *lacZ*, Ap^r, Gm^r	Choi and Schweizer (2006)
pUC18-mini-Tn7T-Gm-P$_{figR}$-*lacZ*	Mini-Tn7 vector containing *lacZ* fusion to P$_{figR}$ promoter	Gerth *et al.* (2012)

[a]The *figT-lacZ* fusion strains were constructed by cloning *figT* DNA fragment (~ 550bp) into pUIC3 vector and mobilization into desired genotypes by tri-parental mating. The fragments are integrated at the *fig* locus by insertion-duplication (DUP).

[b]Gm, gentamycin; Km, kanamycin; Sp, spectinomycin; Ap, Ampicillin; Tc, tetracycline.

2.5.2 Monitoring bacterial growth kinetics

P. aeruginosa or *P. fluorescens* strains from -80°C freezer stock were initially cultured overnight in LB broth to similar densities. Subsequently, overnight cultures were washed once in M9 salts and starved for 2 hours at 37°C (*P. aeruginosa*) or 28°C (*P. fluorescens*) to ensure that strains being compared were physiologically equal. The starved cells were diluted 1:100 times in 1 ml tested medium and 200 µl aliquots were transferred into a sterile clear 96-well microplate (Greiner Bio-One). Absorbance was measured at a wavelength of 450 nm using a Synergy 2 multi-detection microplate reader installed with Gen5 software (Bio-Tek). A_{450} readings were measured every 5 min following a 20 s shaking, for an incubation period of 24 to 72 hours (as required) at 37°C or 28°C. Data points every 2-hr and 4-hr are shown in growth plots for *P. aeruginosa* PAO1 and *P. fluorescens* SBW25 strains, respectively, unless specified otherwise. Growth rates were determined by fitting a logistic equation using the Growthcurver package in R (Sprouffske & Wagner, 2016).

2.5.3 Strain construction

Standard protocols were used for the isolation of plasmid DNAs, restriction endonuclease digestion, ligation, and PCR (Sambrook *et al.*, 1989). PCRs were performed using *Taq* DNA polymerase purchased from Invitrogen Ltd. (Auckland, New Zealand). Oligonucleotide primers were synthesized by Integrated DNA Technologies Inc. (Singapore) and are shown in Table 2.7. The pCR8™/GW/TOPO® (Invitrogen) cloning kit was used for cloning *Taq* polymerase amplified PCR products into pCR8 for verifying sequence identity (Macrogen, South Korea). The desired DNA fragments were sub-cloned into appropriate expression vectors and then introduced into *P. aeruginosa* or *P. fluorescens* strains by tri-parental mating or electroporation. Transformants were selected on LB agar (1.5%) plates supplemented with antibiotics and confirmed by PCR.

The unmarked *figT* deletion mutant was constructed by gene splicing by overlap extension (SOE) PCR (Horton *et al.*, 1989) in conjunction with a two-step allelic-exchange strategy using the suicide-integration vector pUIC3 (Rainey, 1999, Zhang & Rainey, 2007b). Briefly, two fragments (~600-bp) flanking the gene of interest were PCR amplified using oligonucleotide primers. The two fragments containing complementary sequences at their ends were then joined by a third PCR resulting in a ~1.2-kbp fragment. After verifying sequence identity, the *figT* deletion fragment was sub-cloned into pUIC3 (suicide vector containing promoterless *lacZ*) at the *Bgl*II site and introduced into *P. aeruginosa* PAO1 by tri-parental mating with the help of pRK2013. Integration of pUIC3 into the genome via a single homologous recombination event of the cloned DNA fragment was selected on LB agar plates supplemented with Tc, Nf (to counter select *E. coli* donor cells), and X-gal (for blue/white

screening). The double-cross over mutants that had lost the chromosomally integrated pUIC3-vector were selected by D-cycloserine enrichment process (Zhang & Rainey, 2007b). Of note that D-cycloserine was used at 1100 µg/ml for *P. aeruginosa* strains. Deletions were confirmed by PCR, sensitivity to Tc, and phenotypic analysis.

Site-directed mutagenesis by SOE-PCR in combination with the two-step allelic exchange strategy described above was used to construct the P_{hutF} Pntr site mutant strains of *P. aeruginosa* PAO1 and *P. fluorescens* SBW25. Briefly, P_{hutF} sequences from both *P. aeruginosa* PAO1 and *P. fluorescens* SBW25 were first aligned by built-in clustalW alignment feature in Geneious 9.0.5 (https://www.geneious.com). A 14-bp sequence encompassing the Pntr site in P_{hutF} from *P. fluorescens* SBW25 was exchanged with the corresponding region in P_{hutF} from *P. aeruginosa* PAO1; such that the nucleotides immediately flanking the exchanged region are identical in both species. The introduced mutations in P_{hutF} were further confirmed by sequencing the corresponding region and neither *hutF* nor *hutC* was disrupted.

Genetic complementation of *figT* was performed by cloning the PCR amplified-coding region of *figT* downstream of a constitutive kanamycin resistance promoter in pME6010 at the *Eco*RI site (Heeb *et al.*, 2000). The resulting plasmid was mobilized into *P. aeruginosa* Δ*figT* by tri-parental mating with the help of pRK2013. Transformants were selected on LB agar plates supplemented with Tc and Nf and were further confirmed by PCR. Additionally, this plasmid was also mobilized to other strains of *P. aeruginosa* PAO1 and *P. fluorescens* SBW25 pertaining to this study as indicated in the main text.

Complementation of *figRAT* operon was performed by cloning a PCR amplified 3.1 kb intact *figRAT* cassette (including *figR* promoter) into pUC18-mini-Tn7-Gm-GW by Gateway cloning strategy. The resulting plasmid was mobilized into *P. fluorescens* strains by electroporation with the help of pUX-BF13, where it is integrated into the neutral *attB* site. Transformants were selected on LB plates supplemented with Gm, and chromosomal integration downstream of *glmS* was confirmed by PCR. Complementation of *figRA* was performed similarly, with the exception that *figT* coding region was excluded from PCR amplification.

Table 2.7 Oligonucleotides used in this study.

Primer name	Sequence (5' - 3')[a]	Purpose
FigT-1new1	gagatCTGGCCGTTCGCCTACTGCT	Deletion fragment for *figT* mutant construction
FigT-2new1	cagcatgcGgatcCgttgacggaGTACGCACAGACGTGTCAGC	
FigT-3	tccgtcaacGgatcCgcatgctgCAACGCCTTCAGTTGAACCAT	
FigT-4	gagatCTCACCGAATGCTTGGCGCT	
FigT-SpeI-new2	gactaGTCGACAGCCTGGTCAACTGATC	Amplification of *figT* coding region for complementation
FigT-BgI2Hind3	gagatctaagcTTCAACTGAAGGCGTTGATGAACC	
FigT-BglII	gagATCTCCTGCTGCGCCTGCTGAC	Amplification of *figT* fragment for *figT-lacZ* fusion construction
FigT-BgI2Hind3	gagatctaagcTTCAACTGAAGGCGTTGATGAACC	
PfigT-SpeI	aactagtCTGGCCGTTCGCCTACTGCT	Amplification of *figT* promoter region for P_{figT}-*lacZ* translational fusion
PfigT-HindIII	aaagCTTCAATTGGCTGCCGAGGG	
FigR-SpeI-New1	gactagtAGGCCTTCGACGCCCAGTGATTC	Amplification of *figRAT* coding region for complementation
FigT-BgI2Hind3	gagatctaagcTTCAACTGAAGGCGTTGATGAACC	
SPntr-1	gagatctGGTGAAATCCTGCTGCAGGT	Pntr site mutant fragment for deleting Pntr site from the *hutF* promoter in *P. fluorescens* SBW25
SPntr-2	tcagctcacacgcagtcTGTGTTTATTTGTATATACA	
SPntr-3	acagactgcgtgtgagcTGATCATGTCCGCTTTCTTTG	
hutC-1	agatctGAGTGGAAGCACAGGCCCA	
PPntr-1	gagatctACGATCAGCGAGTGGAACAC	Pntr site mutant fragment for inserting Pntr site into the *hutF* promoter in *P. aeruginosa* PAO1
PPntr-2	tcaaggcaccccggtcgTGTTTTATTTGTATATACATATAC	
PPntr-3	acacgaccggggtgcctTGATTATGTCCGCAATTTTCG	
PPntr-4	gagatctGAAGCCTGCGTGACTGTAAAG	
pME6010-R	TCTGCGATTCCGACTCGTCC	Reverse primer for verifying inserts in pME6010
SBW25-Glms	CACCAAAGCTTTCACCACCCAA	Forward and reverse primer for verifying Tn7 integration in the chromosome
MLG049-PR	CAGCATAACTGGACTGATTTCAG	
FigT-P-1	AGCGACAATCGGCTGGAAGC	Confirm *figT-lacZ* integration at *figT* locus after pUIC3 integration
lacZ7	ATCTGCCAGTTTGAGGGGAC	

[a]Restriction sites are underlined; nucleotides in lower case (excluding RE sites) are manually incorporated complementary sequences between the primer pairs

2.5.4 Construction of *lacZ* fusions

The *figT-lacZ* transcriptional fusions were made by cloning a ~550-bp PCR amplified fragment of *figT* in front of promoterless *lacZ* on the integration vector pUIC3 at the *Bgl*II site. The resulting plasmid was mobilized into *P*. *aeruginosa* or *P*. *fluorescens* strains by tri-parental mating with the help of pRK2013. Integration of the plasmid into the chromosome via a single homologous recombination event of the cloned DNA fragment was selected on LB agar plates supplemented with Tc and Nf. Transformants were confirmed by PCR. Of note, this integration at the *figT* locus do not disrupt *figT* function and was confirmed by phenotypic assays.

P_{figT}-*lacZ* translation fusion was made by cloning a ~500-bp PCR amplified putative *figT* promoter in front of *lacZ* (in frame) on pXY2 (mini-Tn7 based vector) at the *Spe*I/*Hin*dIII site (Liu *et al.*, 2014). The resulting plasmid was introduced into *P*. *aeruginosa* PAO1 by electroporation with the help of pUX-BF13. Transformants were selected on LB plates supplemented with Gm and X-gal, and chromosomal integration of this plasmid at the neutral *attB* site was confirmed by PCR. Similarly, P_{figR}-*lacZ* transcriptional fusion (Gerth *et al.*, 2012) was introduced into *P*. *aeruginosa* PAO1 and its derived mutant Δ*crc* for studying the effect of CCR on *figRAT* expression.

2.5.5 β-galactosidase assay

β-galactosidase assays were performed to measure the expression of *lacZ* reporter fusions using 4-methylumbelliferyl-b-d-galactoside (4MUG) as the enzymatic substrate (Zhang *et al.*, 2006). *P*. *aeruginosa* or *P*. *fluorescens* strains from -80°C freezer stock were cultured overnight in LB broth. Cells were washed once in M9 salts and starved for 2 hours at 28°C (*P*. *fluorescens*) or 37°C (*P*. *aeruginosa*), to ensure that strains being compared were physiologically equal. The strains were inoculated into the tested media at ~0.1 A_{600} and were continued to grow for a period of 24 hours. β-galactosidase activity was determined at different time points by measuring the fluorescence emitted by 7-hydroxy-4-methylcoumarin (4MU) at 460 nm after excitation at 365 nm using a Synergy 2 multi-detection microplate reader (Bio-Tek). β-galactosidase activity was reported as 'μM 4MU min^{-1} $cell^{-1}$.

2.5.6 *In vitro* competitive fitness assays

Fitness of the genotypes in laboratory medium was measured by head-to-head competition experiments between two pairs of strains of interest. One of the competitors was marked with a functional copy of *lacZ* (Zhang & Rainey, 2007a, Gerth et al., 2012) to differentiate between the strains in direct competition. Overnight cultures of single clones from -80°C stocks grown in LB broth were washed once in M9 salts and starved for 2 hours. The strains in competitions were mixed at a 1:1 volumetric ratio and were diluted 1:1000 times in the tested media. Strains were competed for 24 hours at 28°C (*P*. *fluorescens*) or 37°C (*P*. *aeruginosa*). Of note, cultures were diluted 1:100 times in the tested medium when competitions were performed on 96-well microplates. The initial (at t=0) and final (at t=T) population densities (N_i) were determined by enumerating colonies on LB agar plates supplemented with X-gal that were used to calculate the Malthusian parameters (m_i) (Lenski, 1991), which is the average rate of increase: $m_i = \ln[N_i(T) / N_i(0)]$. Population Relative fitness was expressed in terms of the selection rate constant (SRC): difference in Malthusian parameters, resulting in a fitness of zero when the competitor and *lacZ* marked strain are equally fit.

2.5.7 Statistical methods

Graphical representation of data and statistical analyses were executed in Prism 7.0. Where appropriate, one-way ANOVA, two-way ANOVA, and student's t-test were utilized to compare and determine the statistical significance of the data. The results were considered statistically significant if the *P* value was lower than 0.05.

2.5.8 *In silico* analysis of *figRAT* homologs in *Pseudomonas* spp.

Diamond BLASTP search feature available within the Pseudomonas.com database (Winsor *et al.*, 2016) was utilized to search (accessed on 13 August 2019) for the homologs of FigA (*P*. *aeruginosa* PAO1) in *Pseudomonas* spp. E-value Cut-off= 1e-4, Sensitivity = default, Query Coverage = 20, and Identity Cut-off = 20, were chosen parameters for the query. The list of hits was exported and BLASTP (Expect value cutoff = 1e-4 and Word size = 2) was utilized to query for FigA (*P*. *aeruginosa* PAO1) homologs in each of the species in the list. The genomic locus was examined for the presence of FigR and FigT and to differentiate FigA from HutG4.

2.5.9 *In silico* prediction of FigR binding sites and cross-regulation of *fig* and *hut* operons

The genomic sequences of all *Pseudomonas* spp. possessing the homologs of *figRAT* were collected from Pseudomonas.com as gbk file (Winsor *et al.*, 2016). A 500-bp sequence encompassing the putative *figR* promoter region and first 30 nucleotides of *figR* coding region from 30 strains, representing 19 species and 11 unclassified species, were extracted using Geneious 9.0.5 (https://www.geneious.com). To determine the putative FigR binding sites, the *figR* promoter sequences were aligned using MUSCLE in-built feature in Geneious. Sequence logo of the predicted binding sites were constructed using WebLogo 3.0 (Crooks *et al.*, 2004).

MEME motif discovery program was used to generate a probability matrix for the putative FigR binding sites with 0-order model of sequences as the background model (Bailey & Elkan, 1994). This probability matrix was used to search for FigR binding sites in the *hut* operons utilizing FIMO (Grant *et al.*, 2011) with a *P*-value less than 10^{-3}. Similarly, a probability matrix for HutC binding site (Chapter 3) was used to scan for HutC binding sites in the *fig* operon.

2.5.10 Phylogenetic analyses

Amino acid sequences of the homologs of FigR, FigA, and FigT (*P*. *aeruginosa* PAO1) from *Pseudomonas* spp. were obtained from Pseudomonas.com database (Winsor *et al.*, 2016). Sequences that were unable to be retrieved for technical reasons were imported from NCBI RefSeq database. BlastP search feature available in the NCBI Reference Sequence Protein

(refseq_protein) database (Pruitt *et al.*, 2007, Sayers *et al.*, 2019) was utilized to query the homologs of FigR, FigA, and FigT from non-pseudomonas species. Alignment pairs were scored by BLOSUM62 matrix with word size 6 and a expect threshold of 10. The maximum target hits were increased to 500 to obtain a good representation of species from different genus. Protein sequences representing at least one species per genus was imported into Geneious 9.0.5 (https://www.geneious.com); of note, unclassified species were excluded. Frameshift in *figR, figA,* or *figT* gene was fixed by deleting nucleotide insertions and deletions to adjust the frame. The resulting sequences were translated in Geneious 9.0.5 and included in the analyses. The sequences were aligned in Geneious 9.0.5 using ClustalW (cost matrix – BLOSUM; Gap open cost – 10; Gap extend cost – 0.1; Free end gaps selected).

The 16S rDNA sequences of *Pseudomonas* spp. were obtained from Pseudomonas.com database. Sequences that were unable to be retrieved for technical reasons were obtained from the genome sequences deposited in NCBI. 16S rDNA sequences of non-*Pseudomonas* spp. were obtained from their genome sequences in NCBI. 16S rDNA sequences were partial or not available for some strains and these were replaced with 16S rDNA sequences from another strain belonging to the same species. The sequences were aligned in Geneious 9.05 using ClustalW (cost matrix – CLUSTALW; Gap open cost – 10; Gap extend cost – 0.1; Free end gaps selected).

The protein and nucleotide alignments were trimmed to remove overhangs from either ends prior to constructing phylogenetic trees. Concatenated FigRAT alignment was made by concatenating the individual alignments of FigR, FigA, and FigT using the built-in feature in Geneious 9.0.5. Neighbour-Joining consensus trees (1000 bootstrap replicates) based on Jukes-Cantor distance model were constructed in Geneious 9.0.5 using the built-in tree builder algorithm. The trees were analysed in Geneious 9.0.5 and the nodes/clusters highlighted using FigTree v1.4.4 (http://tree.bio.ed.ac.uk/software/figtree/).

2.6 Supplementary data

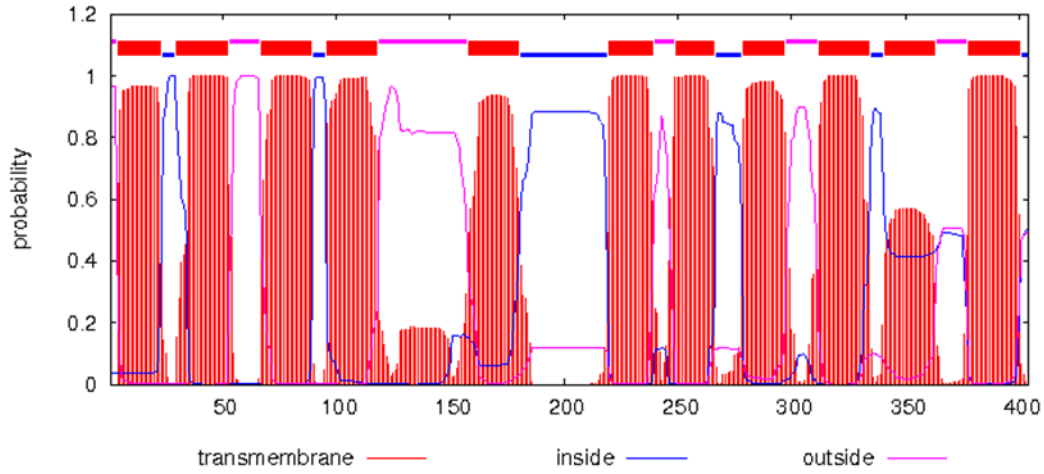

FIG S2.1 Prediction of transmembrane helices in FigT using TMHMM2.0.
The plot shows the posterior probabilities of inside/outside/TM helix. At the top of the plot (between 1 and 1.2) the N-best prediction is shown.

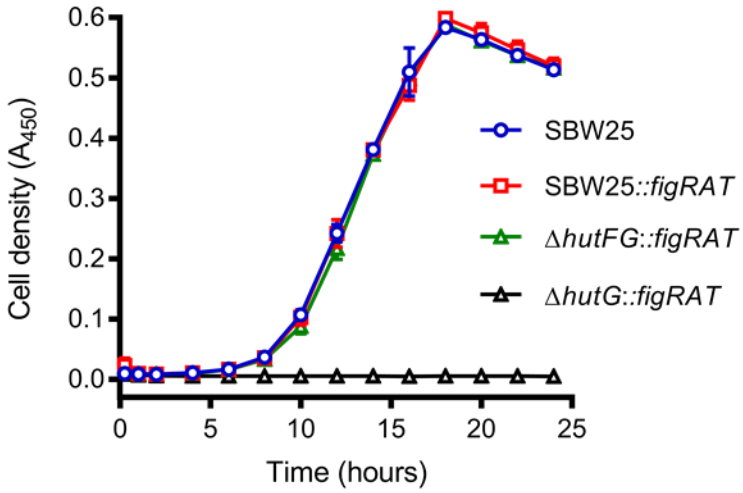

FIG S2.2 Effect of *figRAT* on histidine catabolism in *P. fluorescens* SBW25 determined by growth assay.
Growth dynamics of wild-type SBW25, MU36-55 (SBW25*::figRAT*), MU36-59 (Δ*hutF* Δ*hutG*::*figRAT*), and MU43-76 (Δ*hutG*::*figRAT*) on minimal salts medium containing histidine (10 mM) as the sole source of carbon and nitrogen. Data are means ± standard errors for 2 independent experiments (at least 4 cultures per experiment)**.** If not visible, error bars are contained within the symbol.

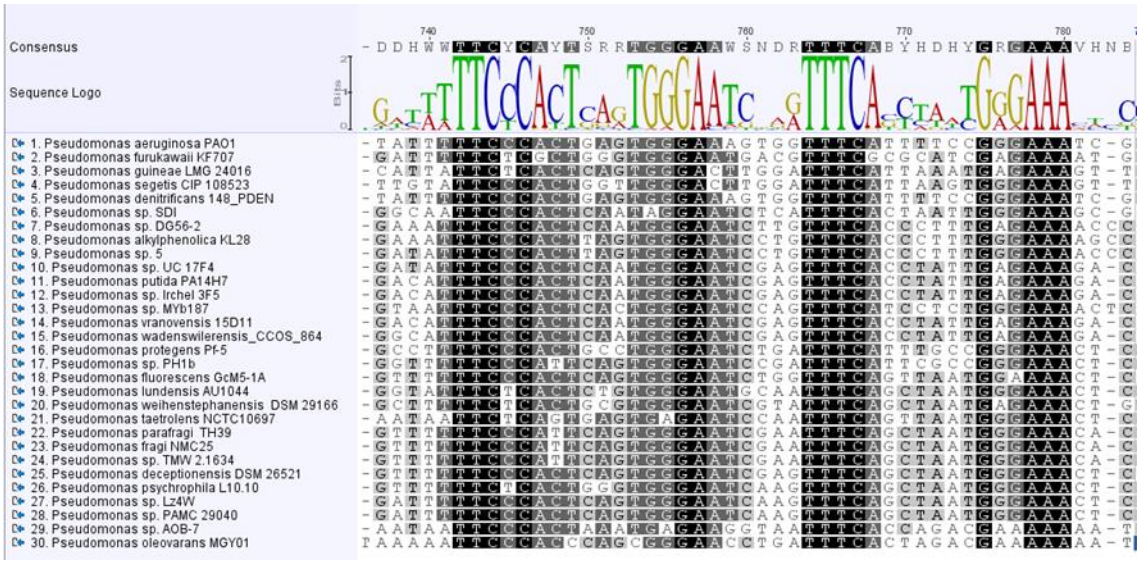

FIG S2.3 Sequence alignment of *figR* promoter from 30 *Pseudomonas* strains.
Nucleotides highlighted in black are 100% conserved. Consensus sequence was generated with a threshold of 90% nucleotide identity.

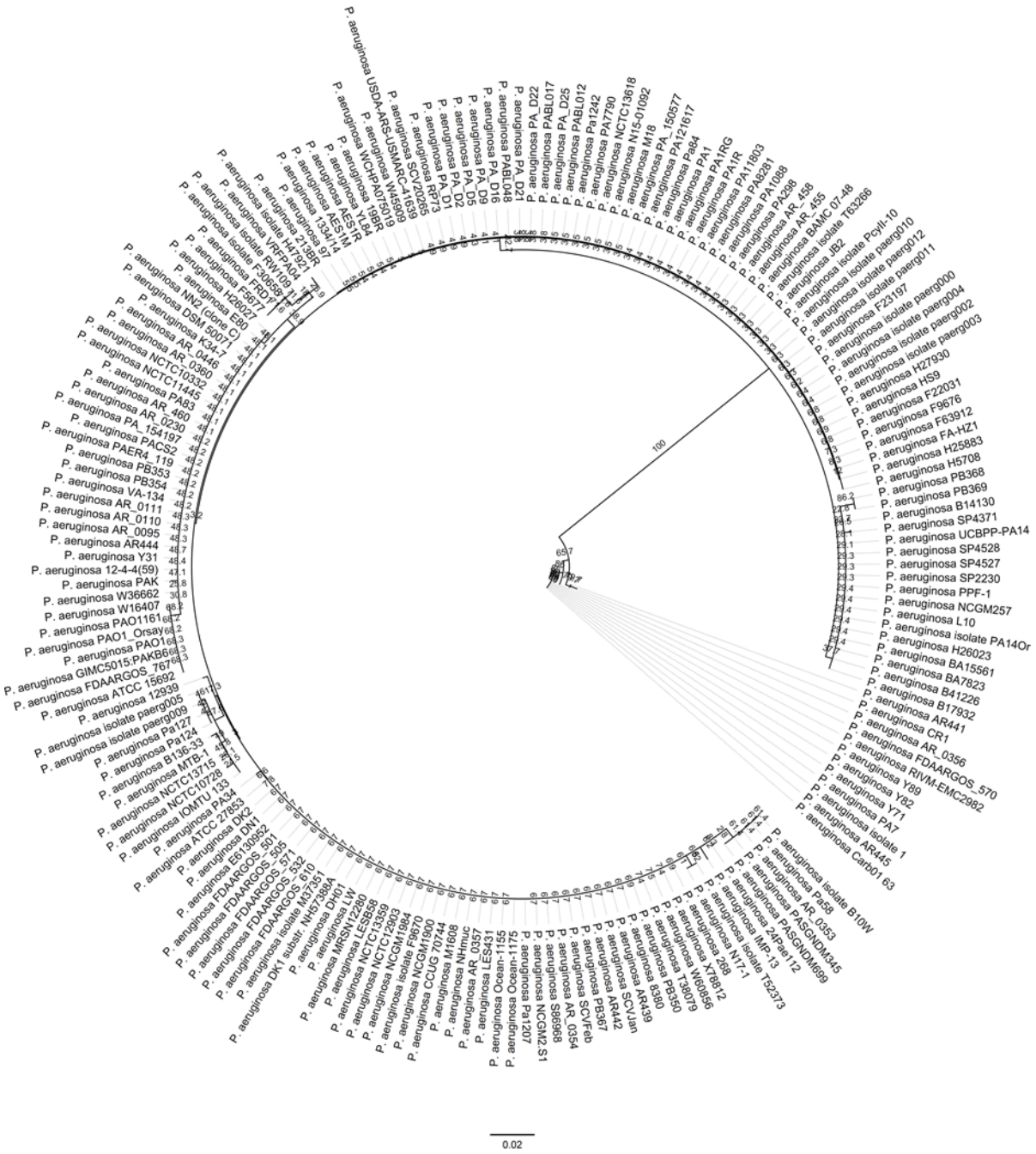

FIG S2.4 Neighbour-Joining consensus phylogeny for FigA protein from *P. aeruginosa*.
Tree was constructed from all completely genome sequenced *P. aeruginosa* strains available in the Pseudomonas.com database. Branch support values shown above branches are based on bootstrapping (1000 replicates).

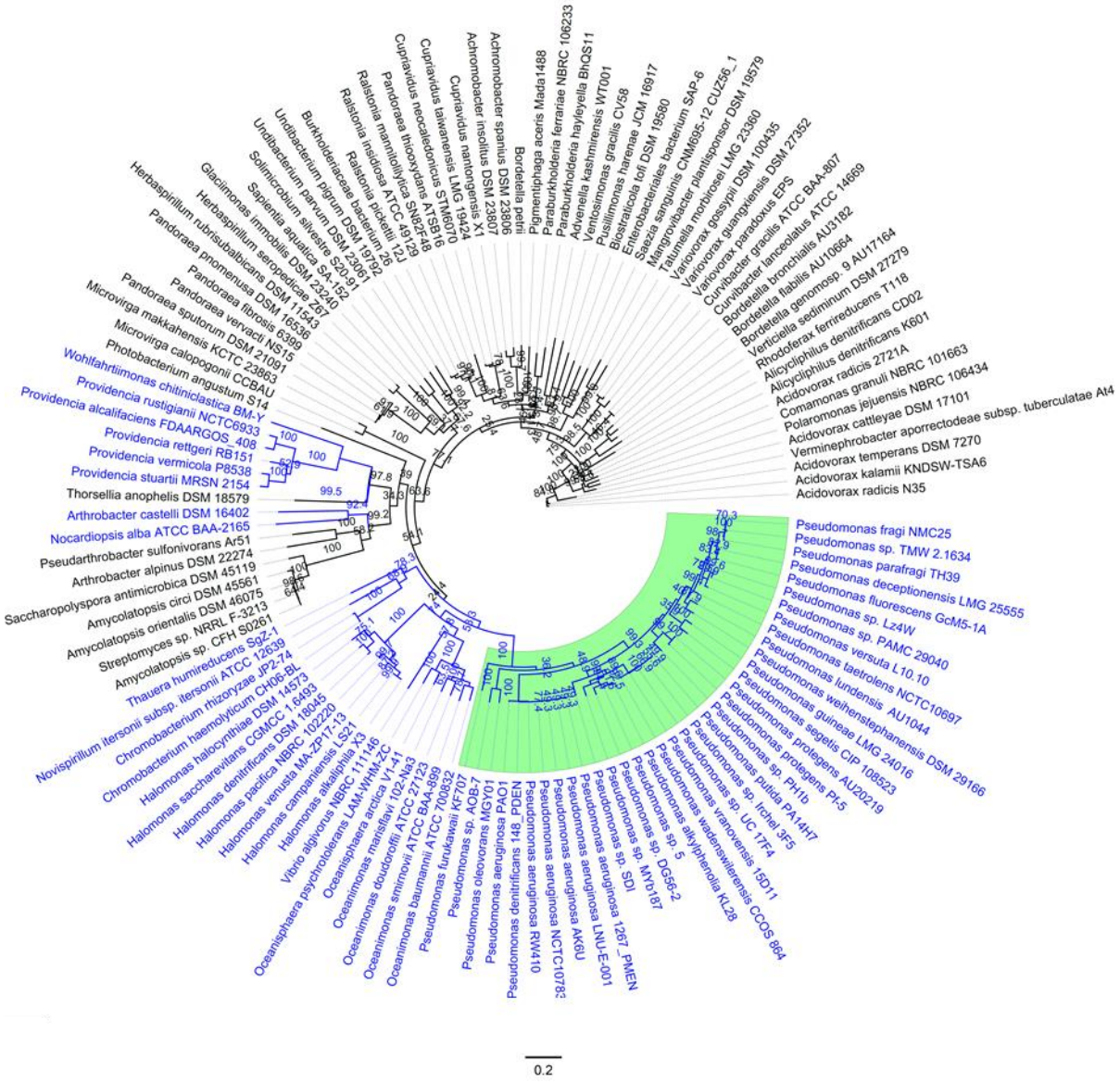

FIG S2.5 Neighbour-Joining consensus phylogeny for FigR protein constructed using amino acid sequences of the homologs identified in *Pseudomonas* spp. and non-*Pseudomonas* spp.
FigR homolog that co-exists with FigA and FigT are marked in blue. Clade of *Pseudomonas* spp. is highlighted in green. Branch support values shown above branches are based on bootstrapping (1000 replicates).

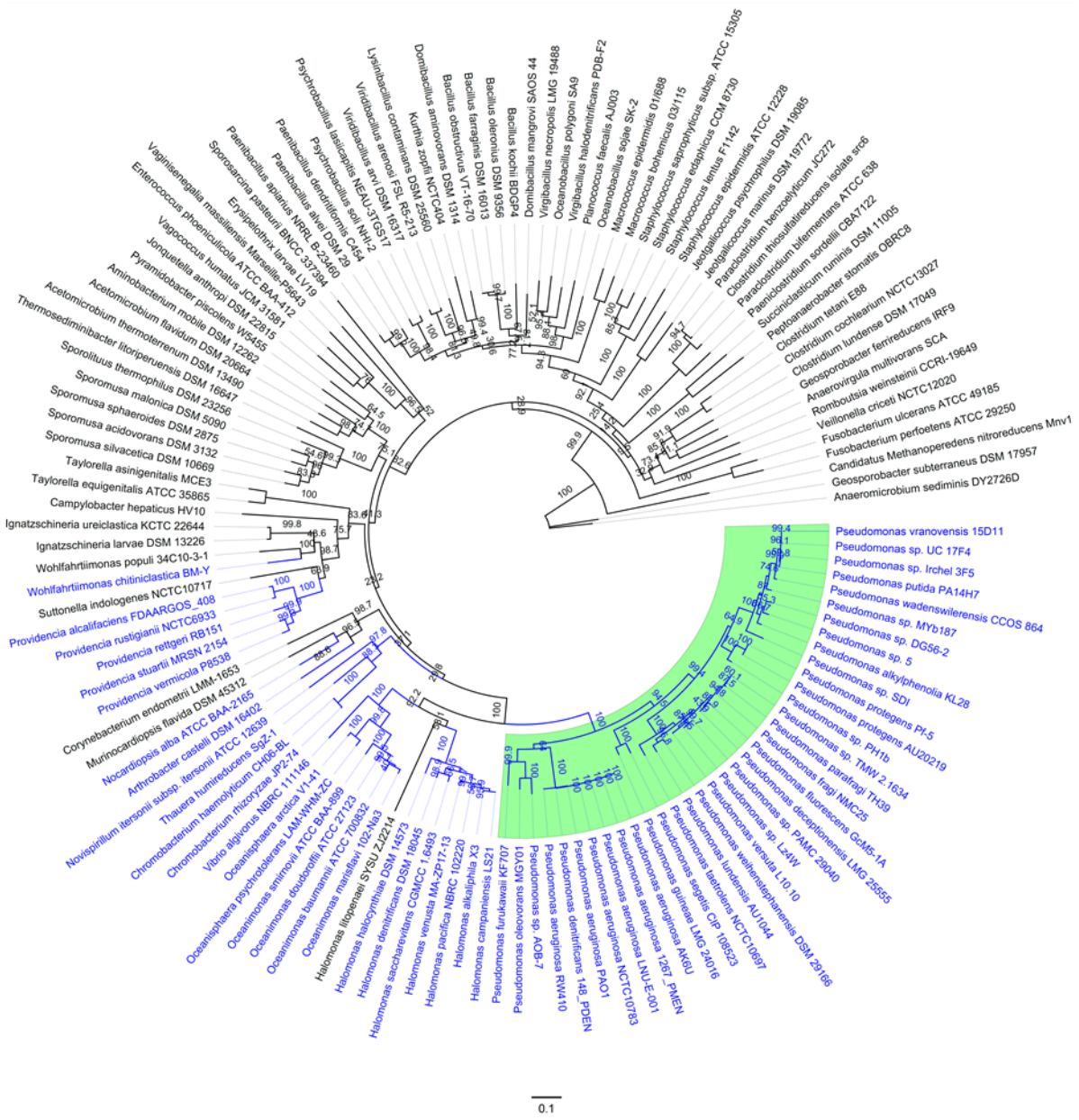

FIG S2.6 Neighbour-Joining consensus phylogeny for FigT protein constructed using amino acid sequences of the homologs identified in *Pseudomonas* spp. and non-*Pseudomonas* spp.
FigT homolog that co-exists with FigR and FigA are marked in blue. Clade of *Pseudomonas* spp. is highlighted in green. Branch support values shown above branches are based on bootstrapping (1000 replicates).

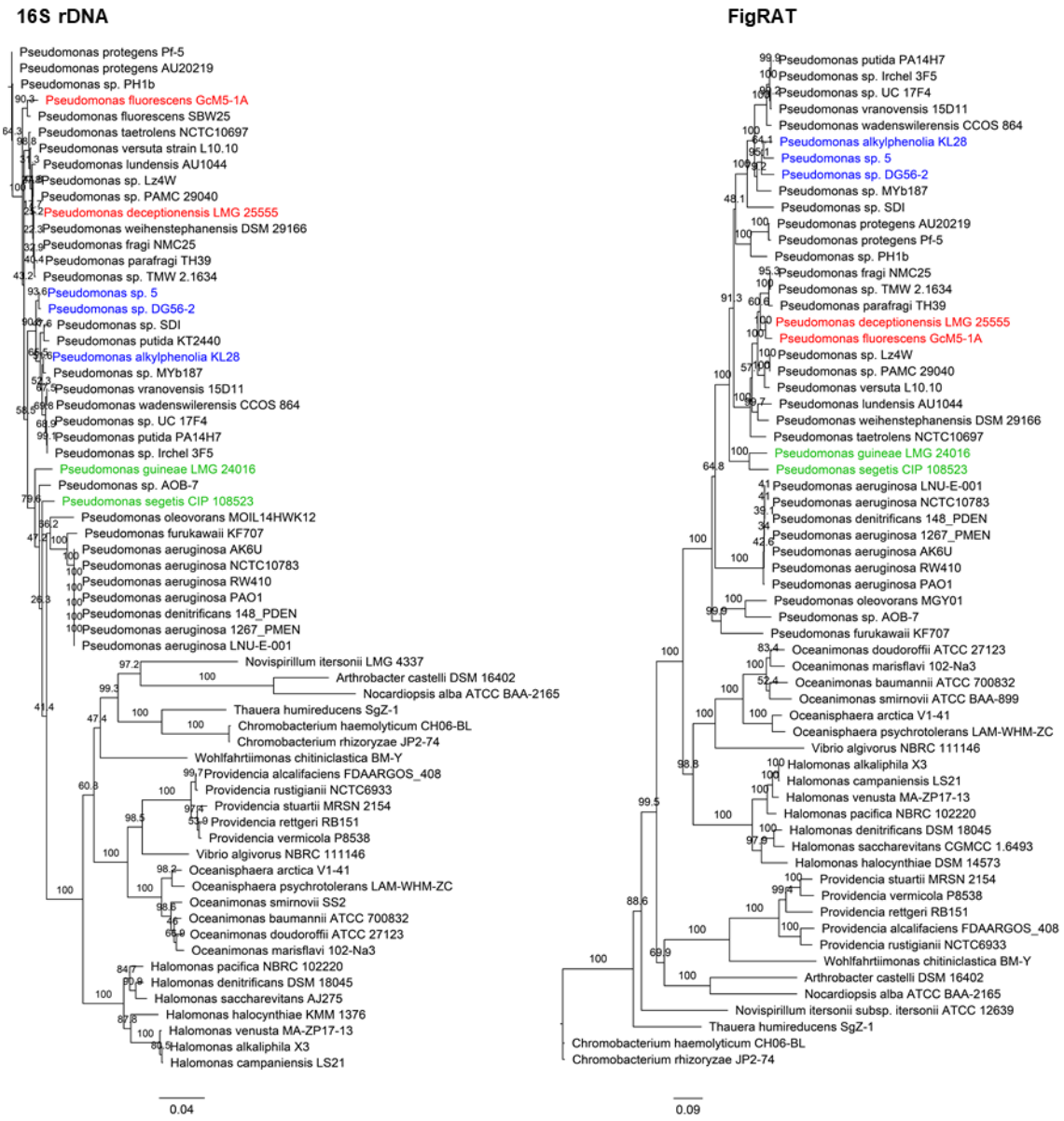

FIG S2.7 Neighbour-Joining consensus phylogenies of 16S rDNA and the concatenated FigR, FigA, and FigT proteins.
Putative instances of HGT within *Pseudomonas* spp. are marked in identical colours in the 16S rDNA and FigRAT trees. Branch support values shown above branches are based on bootstrapping (1000 replicates).

Table S2.1 Growth rate of *P. aeruginosa* PAO1 *hut* pathway mutants growing on FIGLU.

Strain (genotype)[1]	Growth rate (h^{-1})[2]
PAO1 (wild-type)	0.317 ± 0.023 (a)
MU4A4-48 (Δ*hutF*)	0.484 ± 0.019 (b)
PBR1021 (Δ*hutFG*)	0.513 ± 0.051 (b)
MU4A4-47 (Δ*hutG*)	0.317 ± 0.039 (a)

[1]Strains were grown in minimal salts medium containing FIGLU (10 mM) as the sole source of carbon and nitrogen.

[2]Data are means ± standard deviations of at least 9 replicate cultures pooled from 2-3 independent experiments. Growth rates with different letters are statistically different as determined by Tukey's test ($P < 0.05$).

Table S2.2 Growth rate of *P. fluorescens* SBW25 *hutD* mutants possessing HutFG and/or FigRAT pathways.

Strain (genotype)[1]	Growth rate (h^{-1})[2]
SBW25 (wild-type)	0.601 ± 0.023 (a)
PBR806 (Δ*hutD*)	0.474 ± 0.021 (b)
MU36-55 (SBW25::*figRAT*)	0.596 ± 0.025 (a)
MU56-22 (Δ*hutD*::*figRAT*)	0.479 ± 0.010 (bc)
MU36-59 (Δ*hutFG*::*figRAT*)	0.659 ± 0.032 (d)
MU56-16 (Δ*hutFGD*::*figRAT*)	0.628 ± 0.026 (ad)

[1]Strains were grown in minimal salts medium containing histidine (10 mM) as the sole source of carbon and nitrogen.

[2]Data are means ± standard deviations of 8 replicate cultures pooled from 2 independent experiments. Growth rates with different letters are statistically different as determined by Tukey's test ($P < 0.05$).

2.7 Statement of Contribution

The results of EMSA binding assay presented in Fig. 2.3A was performed by Dr Yunhao Liu, a previous doctoral student in Zhang lab.

This work involved 5 plasmids and 19 strains (unpublished) that were constructed by previous researchers (Dr Yunhao Liu, Dr Monica Gerth, and Dr Xue-Xian Zhang) prior to the start of this study. The specific details are provided in the list of bacterial strains and plasmids (Table 2.6).

Chapter 3

Global regulatory roles of HutC in the human pathogenic bacterium *Pseudomonas aeruginosa* PAO1

3.1 Abstract

HutC is a well-characterized transcriptional repressor that mediates substrate-specific expression of histidine utilization (*hut*) genes in Gram-negative bacteria, including *Pseudomonas*. However, recent progresses with a plant growth-promoting bacterium *P. fluorescens* SBW25 showed that HutC plays global regulatory roles beyond histidine catabolism. This work aims to extend our understanding to a closely related human opportunistic pathogen *P. aeruginosa* PAO1. An *in silico* analysis identified 172 putative HutC-target sites in the genome of *P. aeruginosa* PAO1 with a *P* value less than 10^{-4}. Next, six candidate genes were subject to experimental verification for HutC binding by means of gel shift assays (EMSA) and/or DNAse I footprinting assays. All six candidates, including aminoglycoside response regulator (Arr) for tobramycin-induced biofilm formation, fimbrial structures (CupA cluster), and FaoAB for catabolism of long chain fatty acids, were able to bind with purified $HutC_{his6}$ protein. Phenotypic analyses revealed that *hutC* is involved in biofilm formation, tobramycin-induced biofilm formation, cell motility, and pyoverdine production. Finally, we found that *hutC* deletion caused a reduced virulence in *P*. *aeruginosa* PAO1 using the *Caenorhabditis elegans* infection model. Together, our data suggest that HutC plays a significant role in global gene expression as a new virulence factor for *P. aeruginosa* PAO1.

3.2 Introduction

Pseudomonas aeruginosa is an important opportunistic pathogen commonly associated with nosocomial infections. It is responsible for causing a wide spectrum of infections, particularly burn wound infections, skin and soft-tissue infections, ventilator-associated pneumonia, and chronic lung infections in cystic fibrosis (CF) patients (Glik *et al.*, 2018, Koulenti *et al.*, 2009, Panagea *et al.*, 2005). *P. aeruginosa* is the common cause of morbidity and mortality in CF patients due to accompanying respiratory failure (Winstanley *et al.*, 2016). It is also capable of infecting diverse hosts, including plants, insects, nematodes, amoeba, and zebra fish among others (Rahme *et al.*, 2000, Tan *et al.*, 1999, Miyata *et al.*, 2003, Clatworthy *et al.*, 2009). *P. aeruginosa* thrives in diverse environmental habitats and are isolated from rivers, oceans, crude oil, and pharmaceutical products (Marin *et al.*, 2003, Pirnay *et al.*, 2005, Khan *et al.*, 2007, Weiser *et al.*, 2019). Ubiquity is a striking feature of this bacterium largely associated with its metabolic flexibility, conferred by its large and expanding genome (Stover *et al.*, 2000, Silby *et al.*, 2011).

P. aeruginosa contains a large repertoire of virulence factors that help in establishing infection and facilitating transition from acute to chronic infections by subverting host immune responses. Briefly, flagella and type IV pili help in moving towards host and establishing initial cell contact (Balasubramanian *et al.*, 2013). The T3SS injects toxins directly into the host cells, leading to cytoskeletal rearrangements and rapid cell death (Hauser, 2009). Pyoverdine and pyochelin are two siderophores produced to scavenge iron required for their proliferation (Gellatly & Hancock, 2013). *P. aeruginosa* establishes chronic infections by forming biofilms that contribute to increased antibiotic resistance and persistent infections (Hall & Mah, 2017). They are intrinsically resistant to many antibiotics and possess multidrug efflux systems making it often difficult to treat *P. aeruginosa* infections (Lister *et al.*, 2009). The regulatory mechanisms associated with the expression of virulence factors are complex and involve both local and global regulators that act at multiple levels (Balasubramanian *et al.*, 2013).

Bacteria require to quickly adapt metabolic pathways and co-ordinate the expression of virulence factors for the successful colonization of eukaryotic hosts. Acquisition of nutrients is the primary basis for bacterial association with eukaryotic hosts, hence nutrients can be considered as Host Associated Molecular Patterns (HAMPs) that act as signals eliciting bacterial infection (Galletti *et al.*, 2009, Rohmer *et al.*, 2011, Zhang *et al.*, 2014). Consistently, several studies show that defects in the utilization of certain nutrients resulted in reduced or loss of pathogenicity in many bacteria, including *Salmonella* Typhimurium, *Legionella pneumophila*, *Vibrio cholera*, and *Streptococcus pyogenes* (Sauer *et al.*, 2005, Almagro-Moreno & Boyd, 2009, Cusumano *et al.*, 2014, Eisenreich *et al.*, 2015). In *P. aeruginosa*,

defects in amino acid catabolism including alanine, tryptophan, and histidine correlated with reduced virulence (Boulette *et al.*, 2009, Shen *et al.*, 2008, Rietsch *et al.*, 2004). However, the underlying mechanisms modulating metabolism and virulence remain largely unexplored. A deeper understanding of the metabolic pathways and mechanisms of interdependence on virulence can reveal novel therapeutic targets.

Histidine is an expensive amino acid and a good nutrient that can serve as a source of carbon, nitrogen, and energy for many bacteria, including *P. aeruginosa* (Itoh et al., 2007, Bender, 2012). In *P. aeruginosa* PAO1, the excessive histidine uptake and utilization caused a significant reduction in T3SS mediated cytotoxicity, where the expression of exoenzyme S was abolished and the strain was unable to lyse macrophages (Rietsch *et al.*, 2004). Dysregulation of histidine utilization (*hut*) genes during *in vivo* growth in model organisms and defects in virulence phenotypes have also been reported in other human and plant pathogens (Chouikha *et al.*, 2019, Cabral *et al.*, 2011, Lonergan *et al.*, 2020, Liang *et al.*, 2018). While serving as a nutrient, histidine may send signals triggering bacterial infection. Our laboratory proposed that urocanate accumulated in the mammalian tissues such as skin acts as a signalling molecule eliciting *P. aeruginosa* infections via interactions with the HutC regulator (Zhang *et al.*, 2014). Urocanate is produced by the deamination of histidine, catalysed by histidase (HutH) enzyme (Fig. 1.1, Chapter 1). Human skin lacks urocanase (HutU) activity, which is required for the subsequent degradation of urocanate. Consequently, urocanate accumulates in the skin and functions as natural sunscreen (Gibbs & Norval, 2011). HutC belongs to the second largest sub-family of the GntR family of transcriptional regulators, which possess a winged helix-turn-helix DNA binding domain at the N-terminus and substrate binding domain at the C-terminus (Suvorova *et al.*, 2015). HutC functions as a transcriptional repressor of *hut* genes by binding to their promoter regions. However, this repression is relieved by the interaction of urocanate with HutC, inducing a conformational change and causing its dissociation from the promoter regions (Bender, 2012, Naren & Zhang, 2020). Presumably, urocanate and HutC function analogous to a one-component system, where HutC modulates the expression of both metabolic and virulence factors in response to urocanate.

In a recent study from our laboratory in *P. fluorescens* SBW25 (a plant growth-promoting bacterium), HutC was found to possess a governor role in the regulation of *ntrBC*, a global regulator of cellular nitrogen metabolism (Naren & Zhang, 2021). HutC represses expression of *plcC* genes for phosphatidylcholine catabolism, and RNA-seq data showed differential regulation of genes associated with T3SS, T6SS, iron uptake, and pyoverdine synthesis among others (Naren & Zhang, 2020). A direct role for *hutC* in the expression of virulence determinants was established in the zoonotic pathogen *Brucella abortus*, where HutC

regulates *btaE* gene and *virB* operon encoding for adhesin and type IV secretion system, respectively (Sieira *et al.*, 2017, Sieira *et al.*, 2010). Further, *hutC* was associated with biofilm formation in *Yersinia pseudotuberculosis* (Joshua et al., 2015). Interestingly, *P*. *aeruginosa* PAK carrying a transposon insertion in *hutC* was defective in swimming and swarming motilities (Yeung *et al.*, 2009). Taken together, we hypothesized that in addition to the regulation of *hut* genes, HutC may play a global regulatory role in *P*. *aeruginosa*.

In the present study, utilizing *in silico* analysis we identified novel HutC-target sites in the genome of *P*. *aeruginosa* PAO1. Selected candidates were subjected to EMSA analysis and examined their binding affinities for HutC in relation to *hut* promoters. Further phenotypic analyses revealed that *hutC* plays a key role in biofilm formation, tobramycin-induced biofilm formation, motility (swarming, twitching, and swimming), and pyoverdine synthesis. Significantly, we found that mutation of *hutC* resulted in reduced killing of *C*. *elegans* by *P*. *aeruginosa* PAO1. Together, our data support a global regulatory role for HutC in *P*. *aeruginosa* PAO1 that contributes to the successful colonization of eukaryotic hosts and a potential therapeutic target.

3.3 Results

3.3.1 *In silico* prediction of novel HutC-regulated candidate genes in *P. aeruginosa* PAO1

HutC-binding sites on *hut* promoters were characterized in *P*. *fluorescens* SBW25 in our laboratory. The HutC-binding site sequence comprises of an 8-bp inverted repeat sequence, TGTA-N2-TACA, designated as the Phut site. To predict the novel HutC-regulated candidate genes in *P*. *aeruginosa* PAO1, we searched for similar sequences in the genome using a probability matrix of the HutC-binding site consensus sequence.

Briefly, promoter sequences of *hutU* and *hutFC* from 12 *Pseudomonas* species were put through MEME motif discovery program to generate a motif encompassing the Phut site and corresponding probability matrix (Fig. S3.1). Subsequently, the probability matrix of the motif was used to scan the genome of *P*. *aeruginosa* PAO1 utilizing FIMO to predict novel HutC-regulated candidate genes. FIMO identified 172 motif occurrences (HutC-target sites) with a *P* value less than 0.0001 (Table S3.1). This *P* value was chosen based on a trial-and-error process, which identified HutC binding sites in both *hutU* and *hutFC* promoters. In addition to *hut* promoters, motifs displaying similarity with the Phut site were identified in the regulatory regions of genes linked to biofilm, cell motility, pyoverdine synthesis, fatty acid catabolism, and nutrient metabolism. For further analysis, we chose 6 candidates (Table 3.1) of our

interest: that are linked to virulence traits, have target sites located within 400-bp upstream of the coding region (regulatory sequences), and displaying strong similarity with the HutC-binding palindromic sequence.

Table 3.1 HutC-target sites confirmed by *in vitro* DNA-Protein binding assays.

Site sequence	Location[a]	Locus Tag	Gene product information
TGCTTGTATTTTCAAC		PA2819	Hypothetical protein
		PA2818	Arr, aminoglycoside response regulator
TCCTTGTGCGTACAGG		PA2780	BsWR, bacterial swarming regulator
		PA2781	Hypothetical protein (biofilm)
AAGCTTGAACTTACACA		PA3015	Hypothetical protein
		PA3014	FaoA, fatty-acid oxidation complex alpha-subunit
ATAGTCGGAAATACAAG		PA2128	CupA1, fimbrial subunit
		PA2127	CgrA, cupA gene regulator A
TGCATGTCTGGACAAA		PA1293	Hypothetical protein
		PA1292	probable 3-mercaptopyruvate sulfurtransferase
CCCTAGTATATAGAAG		PA0762	AlgU, alginate biosynthesis
		PA0761	NadB, L-aspartate oxidase

[a]HutC-target site (filled circle) is shown together with genes located in the immediate vicinity of *P. aeruginosa* PAO1 genome (Stover *et al.*, 2000, Winsor *et al.*, 2016).

Intriguingly, in our *in silico* prediction for HutC-target sites, we found that the inverted repeat sequence (Phut site sequence) is fully conserved only in the *hut* promoters and 3 other novel targets (Table S3.1). The dissimilarities with the inverted repeat sequence may contribute significantly to the binding affinity of HutC with the target sites. Therefore, we predicted that HutC binds with high affinity to *hut* promoters and low affinity to target sites possessing imperfect inverted repeat sequence. Subsequently, we first examined the molecular interactions between HutC and *hutU* promoter (P_{hutU}) in *P. aeruginosa* PAO1. The interaction between HutC and *hutF* promoter is detailed in Chapter 4.

3.3.2 Molecular interactions between HutC and P_{hutU}

EMSA was performed using purified $HutC_{his6}$ and a 191-bp biotinylated P_{hutU}-191 DNA probe to examine the molecular interactions between HutC and P_{hutU} and determine the binding affinity of this interaction. As expected, a single unshifted band was observed in lane 1 without $HutC_{his6}$, while a $HutC_{his6}$ concentration dependent shift in P_{hutU}-191 DNA probe was observed in lanes 2-9 (Fig. 3.1B). This interaction resulted in four Protein-DNA complexes (shifted

bands), ‘a’, ‘b’, ‘c’, and ‘d’, in the order of low to high molecular weights. We can infer that with increasing concentrations of $HutC_{his6}$, complex ‘a’ is gradually transformed to higher order complexes (‘b’ → ‘c’ → ‘d’) resulting from $HutC_{his6}$ oligomerization with P_{hutU}-191 DNA probe. Note that the complex ‘d’ was fully abolished and complex ‘c’ was near eliminated by the addition of an unlabelled competitor probe, indicating that this interaction is specific.

A previous study from our laboratory also reported the formation of four shifted complexes during HutC interaction with P_{hutU} in *P. fluorescens* SBW25. The four complexes where further characterized and was found to be a monomer, dimer, timer, and tetramer (Naren & Zhang, 2020). Taken together, we predict that the four complexes formed from $HutC_{his6}$ interaction with P_{hutU}-191 correspond to monomer, dimer, trimer, and tetramer, suggesting the mechanism of HutC interaction with *hutU* promoter is similar in both species. We next determined the binding affinity of $HutC_{his6}$ interacting with P_{hutU}-191 from the EMSA (Fig. 3.1B) by estimating the apparent dissociation constant (K_d). K_d was obtained by plotting the fractions of $HutC_{his6}$-P_{hutU}-191 complex against $HutC_{his6}$ concentrations (Fig. 3.1C). The K_d of this interaction was found to be 250 ± 13.09 nM.

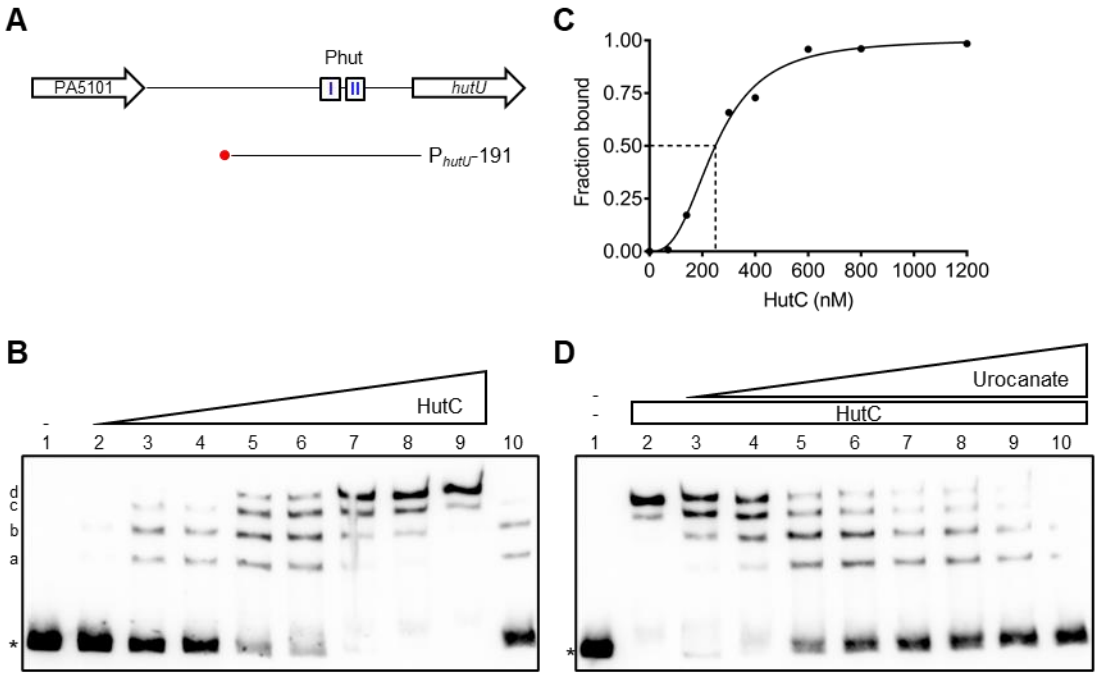

FIG 3.1 EMSA analysis of $HutC_{his6}$ interaction with P_{hutU}-191 DNA and the effect of urocanate.
(A) Schematic representation of the genetic loci of *hutU* and biotin labelled (red circle) DNA probe used for EMSA. The putative Phut half-sites (Phut-I and Phut-II) are marked in blue.
(B) $HutC_{his6}$ was added at increasing concentrations of 0, 70, 140, 200, 300, 400, 600, 800, and 1200 nM in lanes 1 to 9. Lane 10 contains 800 nM of $HutC_{his6}$ and x75 molar excess unlabelled specific competitor. The four shifted complexes are denoted by a, b, c, and d.
(C) Estimation of dissociation constant (K_d) from **(B)**
(D) The concentration of $HutC_{his6}$ was held constant at 800 nM and increasing concentrations of urocanate were added at 0, 0.05, 0.1, 0.2, 0.3, 0.4, 0.6, 1.0, and 1.5 mM in lanes 2-10 respectively.
Asterisks denote free probe. The biotin labelled P_{hutU}-191 DNA probe was used at 20 nM in the EMSAs.

Urocanate is the known physiological inducer of *hut* genes that activates *hut* expression. We next investigated the effect of urocanate on $HutC_{his6}$ interaction with P_{hutU}-191 DNA probe by EMSA (Fig. 3.1D). $HutC_{his6}$ concentration was fixed at 800 nM and varied urocanate concentrations from 0 to 1.5 mM (lanes 2-10). We observed a urocanate concentration dependent dissociation of the shifted $HutC_{his6}$-P_{hutU}-191 complexes. A gradual transformation of complex 'd' to lower molecular weight complexes ('c' → 'b → 'a') was observed with increasing concentrations of urocanate. Indeed, this is a consequence of the gradual dissociation of $HutC_{his6}$ from the higher molecular weight Protein-DNA complexes. This reverse phenomenon fully agrees with our inference on the binding pattern of $HutC_{his6}$ with P_{hutU}-191 ('a' → b' → 'c' → 'd'). The shifted bands were nearly eliminated at urocanate concentrations of 1.5 mM (lane 10), indicating a near complete dissociation of $HutC_{his6}$ from P_{hutU}-191 probe.

Consistent with our prediction, $HutC_{his6}$ binds to *hutU* promoter with very high binding affinity requiring urocanate in millimolar concentrations for absolute dissociation of this interaction.

3.3.3 Determining the HutC-binding sequences in P_{hutU}

To determine the specific HutC-binding site sequences in P_{hutU}, we performed DNAse I footprinting assay using purified $HutC_{his6}$ and a 191-bp biotinylated P_{hutU}-191 DNA probe (used for EMSA). We observed that a 51-bp region containing the Phut site was protected from DNAse I digestion (Fig. 3.2A). The longer protected region is consistent with the multiple shifted bands observed in the EMSA (Fig. 3.1B) as consequence of protein oligomerization with the DNA. The protected region overlaps putative elements of the sigma-54 consensus sequence (Fig. 3.2B). This finding is in favour of the repressor role of HutC in *hut* gene expression by acting as a roadblock for RNA polymerase during transcription.

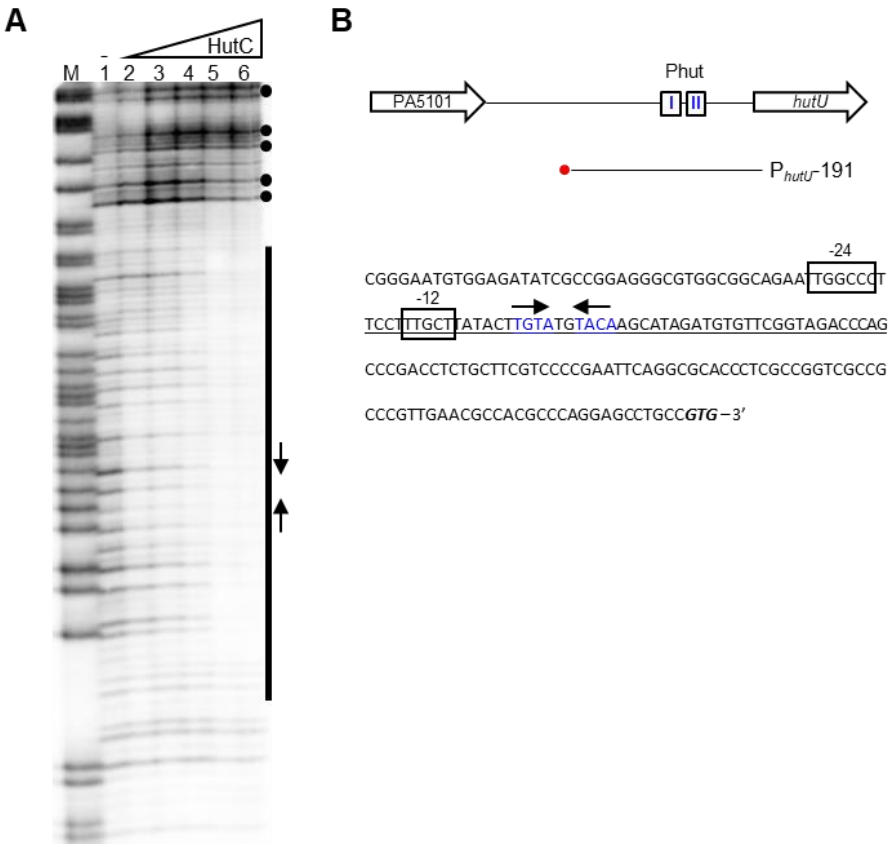

FIG 3.2 Identification of HutC binding sequences in P_{hutU}.
(A) DNAse I footprinting was performed using $HutC_{his6}$ and biotin labelled P_{hutU}-191 DNA probe. Lane M, G+A marker; lanes 1-6, $HutC_{his6}$ added at increasing concentrations (0, 0.5, 1.0, 2.0, 4.0, and 6.0 µM). The HutC-protected region, Phut sites, and hypersensitive DNAse I cleavage sites are shown in black bar, inverted arrows, and filled circles, respectively.
(B) Schematic representation of the genetic loci of *hutU* and biotin labelled (red circle) DNA probe used for DNAse I footprinting assay. The Phut half-sites (Phut-I and Phut-II) are marked in blue. The sequences below correspond to the promoter region of *hutU* used for DNAse I footprinting. $HutC_{his6}$ protected region is underlined, Phut half-sites are shown by inverted arrows, and predicted sigma-54 elements (-24 and -12 sites) of the promoter are boxed.

3.3.4 Experimental verification of the novel HutC-target sites in *P. aeruginosa* PAO1

In vitro Protein-DNA binding assays were performed to examine if HutC can bind to the six candidates (Table 3.1) predicted *in silico*. The target sites for this study were selected based on proximity of the predicted Phut sites to the genes linked to virulence traits of our interest and similarity with the HutC-binding site inverted repeat sequence (TGTA-N2-TACA).

3.3.4.1 Molecular interactions between HutC and P_{arr}

First, we tested if HutC can bind to the predicted putative Phut site in the promoter region of *arr* (aminoglycoside response regulator) gene. Arr is required for tobramycin induced biofilm formation in *P. aeruginosa* PAO1 (Hoffman *et al.*, 2005).

EMSA was performed to examine the molecular interaction between purified $HutC_{his6}$ and a 246-bp biotinylated P_{arr}-246 DNA probe. As expected, a single unshifted band (free probe) was observed in lane 1 without $HutC_{his6}$, while a $HutC_{his6}$ concentration dependent shift in P_{arr}-246 DNA probe was observed in other lanes (Fig. 3.3B). We next determined the binding affinity of this interaction from the EMSA (Fig. 3.3B) by estimating the apparent dissociation constant (K_d). The K_d of this interaction was found to be 5.68 µM (Fig. 3.3C), indicating a relatively weaker interaction when compared with promoters of *hutU* (250 ± 13.09 nM) and *hutFC* (1.34 ± 0.11 µM, Chapter 4).

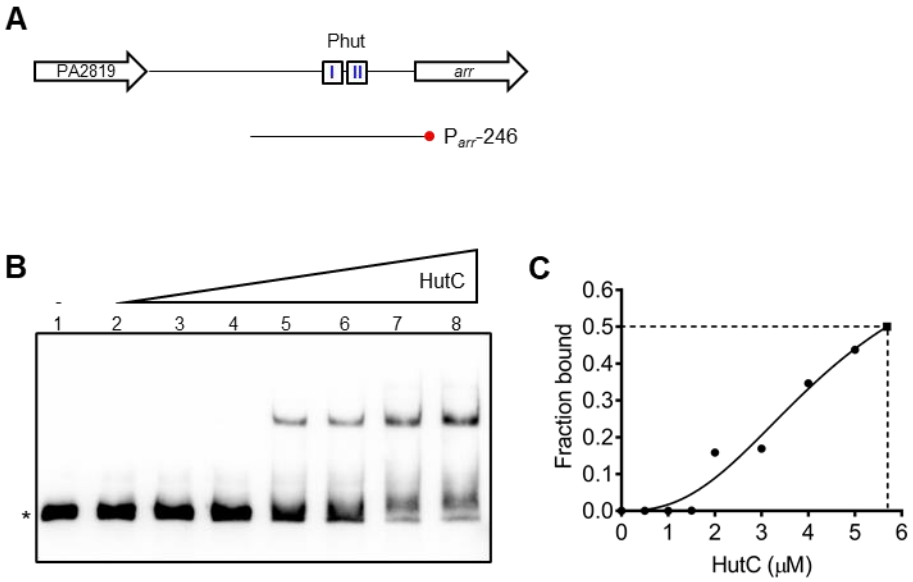

FIG 3.3 EMSA analysis of $HutC_{his6}$ interaction with P_{arr}-246 DNA.
(A) Schematic representation of the genetic loci of *arr* and biotin labelled (red circle) DNA probe used for EMSA. The putative Phut half-sites (Phut-I and Phut-II) are marked in blue.
(B) $HutC_{his6}$ was added at increasing concentrations of 0, 0.5, 1.0, 1.5, 2.0, 3.0, 4.0, and 5.0 μM in lanes 1 to 8.
(C) Estimation of dissociation constant (K_d) from (B). K_d was obtained by extrapolating (filled square) the line of best fit by a limited distance beyond the data points.
Asterisk denotes free probe. The biotin labelled P_{arr}-246 DNA probe was used at 20 nM in the EMSA.

3.3.4.2 Determining the HutC-binding site sequences in P_{arr}

DNAse I footprinting was performed to determine the HutC-binding site sequences in P_{arr}. We observed that $HutC_{his6}$ protected a 30-bp region in the P_{arr}-246 DNA probe from DNAse I digestion (Fig. 3.4A). A shorter protected region is consistent with the single shifted band in the EMSA (Fig. 3.3B), suggesting a lower order oligomerization of protein with the DNA compared to P_{hutU}. Indeed, this 30-bp region encompasses the *in silico* predicted HutC- binding site, suggesting that this interaction is specific and determined by Phut site. Moreover, the $HutC_{his6}$ protected region also overlaps the putative elements of the sigma-70 consensus site sequence (Fig. 3.4B). Promoter prediction was executed in SAPPHIRE (Coppens & Lavigne, 2020) and SoftBerry, where both programs identified similar sites.

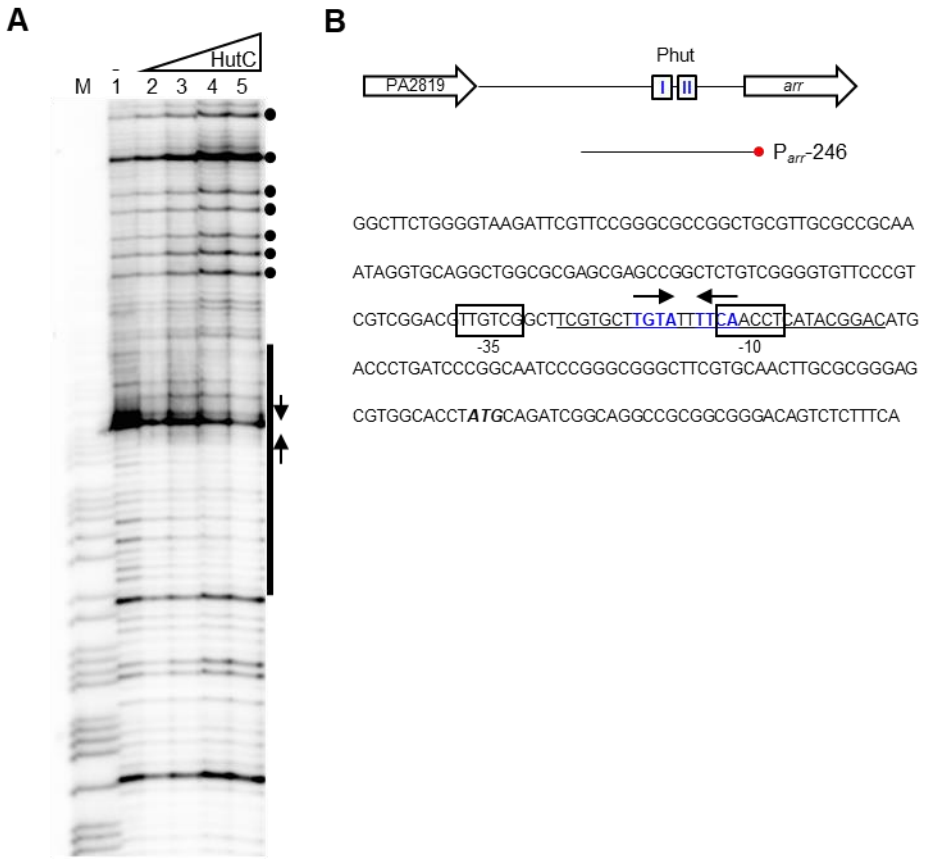

FIG 3.4 Identification of HutC binding site sequences in P_{arr}.
(A) DNAse I footprinting was performed using $HutC_{his6}$ and biotin labelled P_{arr}-246 DNA probe. Lane M, G+A marker; lanes 1-5, $HutC_{his6}$ added at increasing concentrations (0, 1.0, 2.0, 3.0, and 5.0 µM). The HutC-protected region, Phut half-sites, and hypersensitive DNAse I cleavage sites are shown by black bar, inverted arrows, and filled circles, respectively.
(B) Schematic representation of the genetic loci of *arr* and biotin labelled (red circle) DNA probe used for DNAse I footprinting assay. The Phut half-sites (Phut-I and Phut-II) are marked in blue. The sequences below correspond to the promoter region of *arr*, used for DNAse I footprinting. $HutC_{his6}$ protected region is underlined, Phut half-sites are shown by inverted arrows, and predicted sigma-70 elements (-35 and -10 sites) of the promoter are boxed.

3.3.4.3 Molecular interaction between HutC and four other candidates in *P. aeruginosa* PAO1

In silico analysis identified putative Phut sites in the promoter regions of *faoAB*; *cupA1* and *cgrA*; *nadB* and *algU*; and PA1292. Additionally, a Phut site was identified in the 3' end of the CDS of *bsWR* and a few nucleotides upstream of the CDS of PA2781 (Fig. 3.5A). To determine if $HutC_{his6}$ can interact with the above target sites, EMSA was performed using purified $HutC_{his6}$ and biotinylated DNA probes encompassing the putative Phut sites. Intriguingly, we observed that $HutC_{his6}$ was able to bind with all five candidates (Fig. 3.5B-F). Indeed, a $HutC_{his6}$ concentration dependent shift in the biotin labelled DNA probe was observed with all the candidates.

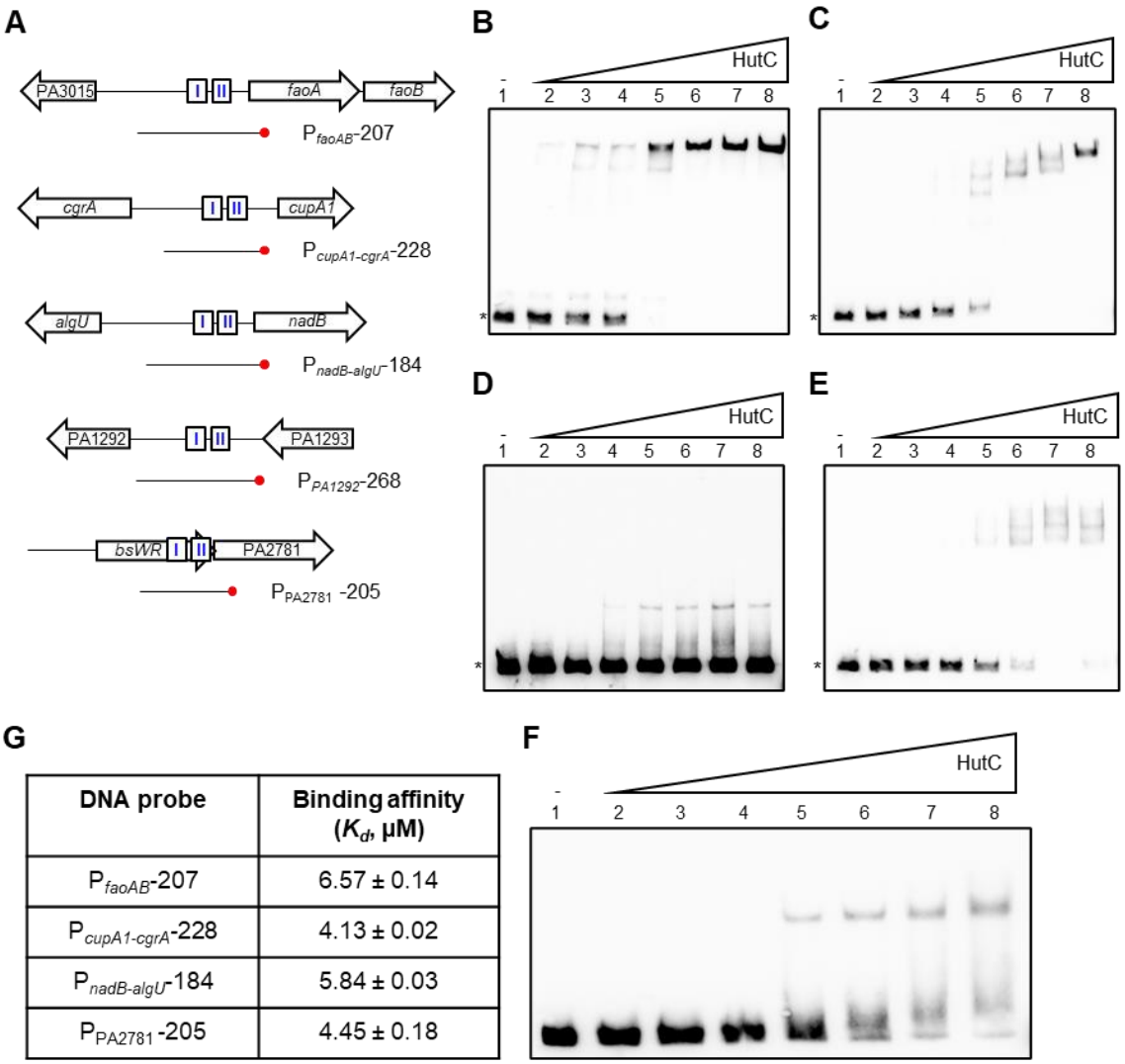

G

DNA probe	Binding affinity (K_d, µM)
P_{faoAB}-207	6.57 ± 0.14
$P_{cupA1\text{-}cgrA}$-228	4.13 ± 0.02
$P_{nadB\text{-}algU}$-184	5.84 ± 0.03
P_{PA2781}-205	4.45 ± 0.18

FIG 3.5 EMSA analyses of $HutC_{his6}$ interaction with chosen candidates from *in silico* prediction.
(A) Schematic representation of the genetic loci of HutC-target sites and biotin labelled (red circle) DNA probe used for EMSA. The putative Phut half-sites (Phut-I and Phut-II) are marked in blue.
(B) $HutC_{his6}$ interaction with P_{faoAB}-207 DNA. $HutC_{his6}$ was added at increasing concentrations of 0, 4, 5, 6, 8, 10, 12, and 15 µM in lanes 1 to 8.
(C) $HutC_{his6}$ interaction with $P_{cupA1\text{-}cgrA}$-228 DNA. $HutC_{his6}$ was added at increasing concentrations of 0, 1, 2, 3, 4, 6, 7.5, and 12 µM in lanes 1 to 8.
(D) $HutC_{his6}$ interaction with P_{PA1292}-268 DNA. $HutC_{his6}$ was added at increasing concentrations of 0, 0.5, 1, 2, 2.5, 3, 3.5, and 4 µM in lanes 1 to 8.
(E) $HutC_{his6}$ interaction with $P_{nadB\text{-}algU}$-184 DNA. $HutC_{his6}$ was added at increasing concentrations of 0, 1, 2, 3, 4, 6, 7.57, and 10 µM in lanes 1 to 8.
(F) $HutC_{his6}$ interaction with P_{PA2781} -205 DNA. $HutC_{his6}$ was added at increasing concentrations of 0, 0.5, 1, 1.5, 2, 3, 4, and 5 µM in lanes 1 to 8.
(G) Dissociation constant (K_d) of $HutC_{his6}$ interacting with the candidates estimated from (B, C, E, and F). Asterisks denote free probe. The biotin labelled DNA probe was used at 20 nM in the EMSAs.

Next, binding affinity (K_d) of these interactions were estimated from the EMSA (Fig. 3.5G). K_d values for P_{faoAB}-207, $P_{cupA1\text{-}cgrA}$-228, $P_{nadB\text{-}algU}$-184, and P_{PA2781} -205 were found to be 6.57 ± 0.14, 4.13 ± 0.02, 5.84 ± 0.03, and 4.45 ± 0.18 µM, respectively. The K_d of the candidates are at least 16-fold higher than *hutU* promoter (250 ± 13.09 nM) and 3-fold higher than *hutFC*

(1.34 ± 0.11 µM) promoter, indicating a relatively lower binding affinity for $HutC_{his6}$ with the candidates compared to *hut* promoters.

Indeed, our EMSA results showing that HutC can recognize and bind to the regulatory region of these candidates is consistent with our hypothesis that HutC plays a global regulatory role beyond histidine catabolism. The *faoA* and *faoB* genes form an operon and encode for alpha and beta subunits of the fatty acid oxidation complex, associated with the catabolism of long chain fatty acids in *P*. *aeruginosa* PAO1 (Kang *et al.*, 2010, Turner *et al.*, 2014). The *cupA1* gene is part of the *cupA* gene cluster that encodes for components of fimbrial structure, essential to form biofilms on abiotic surfaces. The divergently transcribed *cgrA* encodes a regulator essential for the phase-variable expression of *cupA* genes under anaerobic conditions (Vallet-Gely *et al.*, 2007). The divergently transcribed genes *algU* and *nadB* encode for enzymes involved in alginate biosynthesis and aspartate metabolism, respectively (Winsor *et al.*, 2016). PA1292 encodes a probable 3-mercaptopyruvate sulfurtransferase enzyme. It possesses a Rhodanese-like domain associated with cyanide detoxification (Shatalin *et al.*, 2011). The *bsWR* gene and PA2781 are co-transcribed and associated with regulating swarming motility and biofilms, respectively (Wang *et al.*, 2014).

3.3.5 Characterization of *hutC* associated phenotypes in *P. aeruginosa* PAO1

In the light of our *in vitro* data combined with *in silico* prediction emphasizing the association of *hutC* with the regulation of virulence genes prompted us to investigate the phenotypic effects of *hutC* in biofilm formation, antibiotic-induced biofilm formation, motility, pyoverdine production, and virulence towards *Caenorhabditis elegans* (*C*. *elegans*).

3.3.5.1 Effect of *hutC* in tobramycin-induced biofilm formation in *P. aeruginosa* PAO1

Having identified above that HutC can bind to the regulatory regions of *aminoglycoside response regulator* (*arr*) gene (Fig. 3.3 and 3.4), persuaded us to investigate the phenotypic effect of *hutC* in tobramycin-induced biofilm formation and explore the regulatory mechanism.

3.3.5.1.1 Phenotypic effects of tobramycin in *P. aeruginosa* PAO1

To determine the effects of tobramycin on planktonic growth and biofilm formation, wild-type *P*. *aeruginosa* PAO1 (MPAO1) was exposed to increasing concentrations of tobramycin. As expected, a dose-dependent inhibition of growth was observed with increasing concentrations of tobramycin (Fig. 3.6A). Tobramycin at 2.5 µg/ml (MIC) was found to completely inhibit the growth of planktonic cells. We next quantified biofilm formed by MPAO1 when exposed to sub-inhibitory tobramycin concentrations of 0 to 1.0 µg/ml (i.e., <2 times of MIC). A >2-fold induction in biofilm was observed when cells were exposed to tobramycin concentrations

between 0.3 and 1.0 µg/ml (Fig. 3.6B). Interestingly, tobramycin concentrations at which planktonic mass were significantly reduced displayed a stronger induction in biofilm (Fig. 3.6C). Indeed, this was observed at tobramycin concentrations as high as 1.0 µg/ml, where planktonic mass reduced by more than 5-fold. This suggests that biofilm induction is an alternative strategy to tackle antibiotic mediated inhibition of planktonic growth.

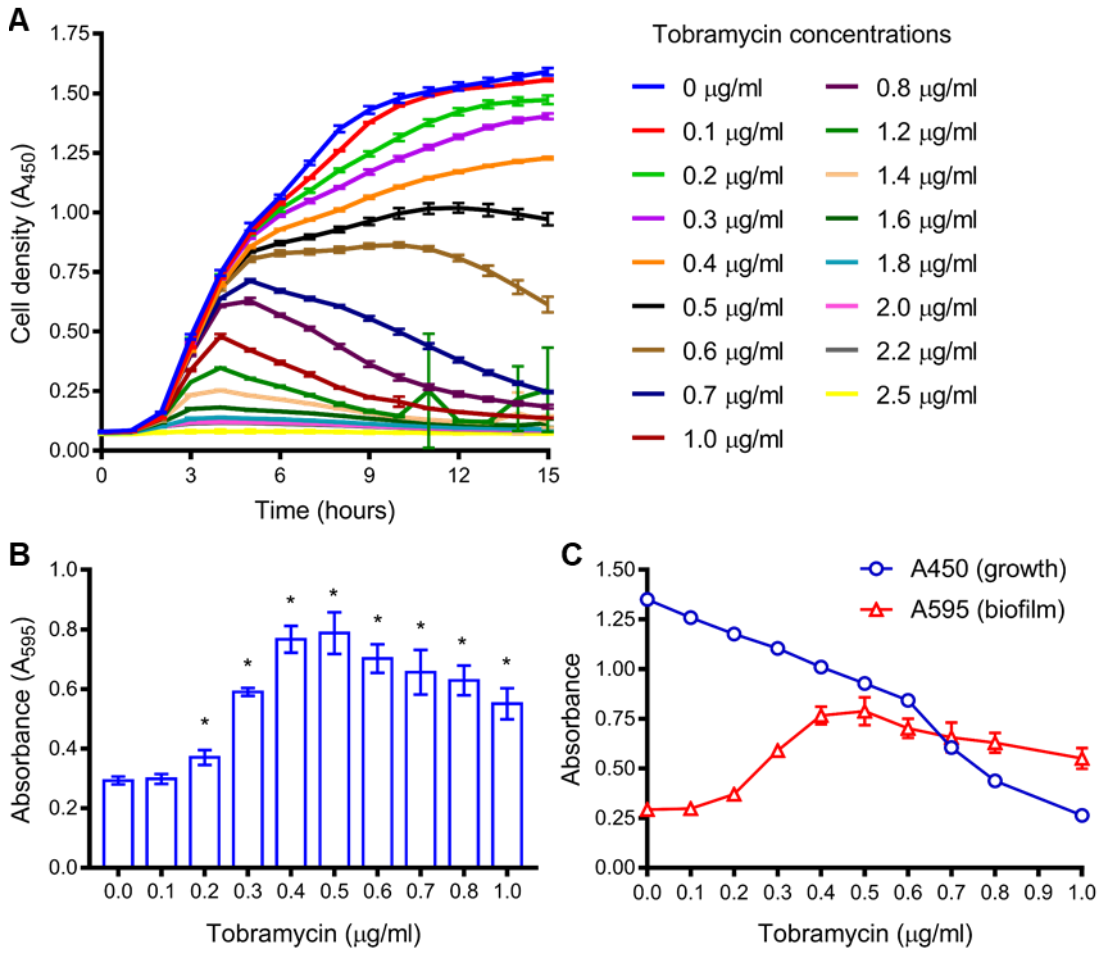

FIG 3.6 Phenotypic effects of tobramycin on wild-type *P. aeruginosa* PAO1 (MPAO1).
(A) Growth inhibitory effect of varying concentrations of tobramycin. Data are means ± standard errors of 4 independent continuously shaken cultures.
(B) Sub-inhibitory concentrations of tobramycin induce biofilm formation (after 8 hours of static growth). A similar pattern in biofilm induction was observed in at least 5 independent experiments (data not shown). Data are means ± standard deviations of 8 replicate cultures from a single experiment. Asterisks denote statistical significance determined by student's t-test ($P < 0.0001$, compared with control: unexposed to tobramycin).
(C) Biofilm induction is stronger at tobramycin concentrations that significantly inhibit planktonic growth. Data inferred from (A) and (B) at 8 hours after inoculation.
Cells were grown in LB medium supplemented with tobramycin at concentrations indicated in the figure. Growth was measured at 450 nm, and biofilm was quantified at 595 nm.

In a previous study (Hoffman *et al.*, 2005), biofilm induction in response to sub-inhibitory concentrations of tobramycin was attributed to *arr* gene, which encodes a c-di-GMP phosphodiesterase. *P. aeruginosa* PAO1 carrying a mutation in *arr* was found to be incapable

of inducing biofilm in response to tobramycin (Hoffman *et al.*, 2005). This is, however, in contradiction with the current literature because c-di-GMP is required for biofilm formation and expression of c-di-GMP phosphodiesterases are linked to a reduction in biofilm formation (Hall & Lee, 2018). In view of the significance of the present study, first we tested the role of *arr* in tobramycin-induced biofilm formation. However, in compliance with the current understanding of the role of c-di-GMP in biofilm formation, we hypothesized that mutation of *arr* induces a stronger induction in biofilm.

3.3.5.1.2 Role of *arr* in tobramycin-induced biofilm formation in *P. aeruginosa* PAO1

To test the predicted role of *arr* in tobramycin-induced biofilm formation, both wild-type *P. aeruginosa* PAO1 (MPAO1) and a transposon insertion mutant of *arr* (MU61-32) were exposed to sub-inhibitory concentrations of tobramycin (0.2-2.0 µg/ml). Biofilms were quantified after 8 hours of static growth in a 96-well microtiter plate.

Note, biofilm data shown in Fig 3.7B and 3.7D are from an experiment carried out by an undergraduate student, Sara Hammouda, in our laboratory. I trained Sara Hammouda to perform biofilm assays and the data was generated under my supervision and assistance in the laboratory.

In the absence of tobramycin, MU61-32 (*arr*::ISphoA/hah) formed slightly higher biofilm compared to MPAO1. Consistent as above, sub-inhibitory concentrations of tobramycin induced biofilm formation in MPAO1. However, in contradiction to the previously reported phenotype for *arr*, we observed a stronger biofilm induction for the mutant MU61-32 (*arr*::ISphoA/hah) in response to tobramycin. MU61-32 also formed much higher biofilm than MPAO1 when exposed to sub-inhibitory concentrations of tobramycin (Fig. 3.7B). Consistent with microtiter plate experiments, we observed a similar pattern in biofilm formed on glass test tubes (Fig. 3.7C). The mutant MU61-32 (*arr*::ISphoA/hah) formed slightly higher biofilm than MPAO1 in the absence of tobramycin on glass test tubes. Biofilm was induced in both MPAO1 and MU61-32 (*arr*::ISphoA/hah) in response to tobramycin. The mutant MU61-32 (*arr*::ISphoA/hah) also formed higher biofilm than MPAO1, significantly between tobramycin at 0.4 and 1.0 µg/ml (Fig. 3.7C).

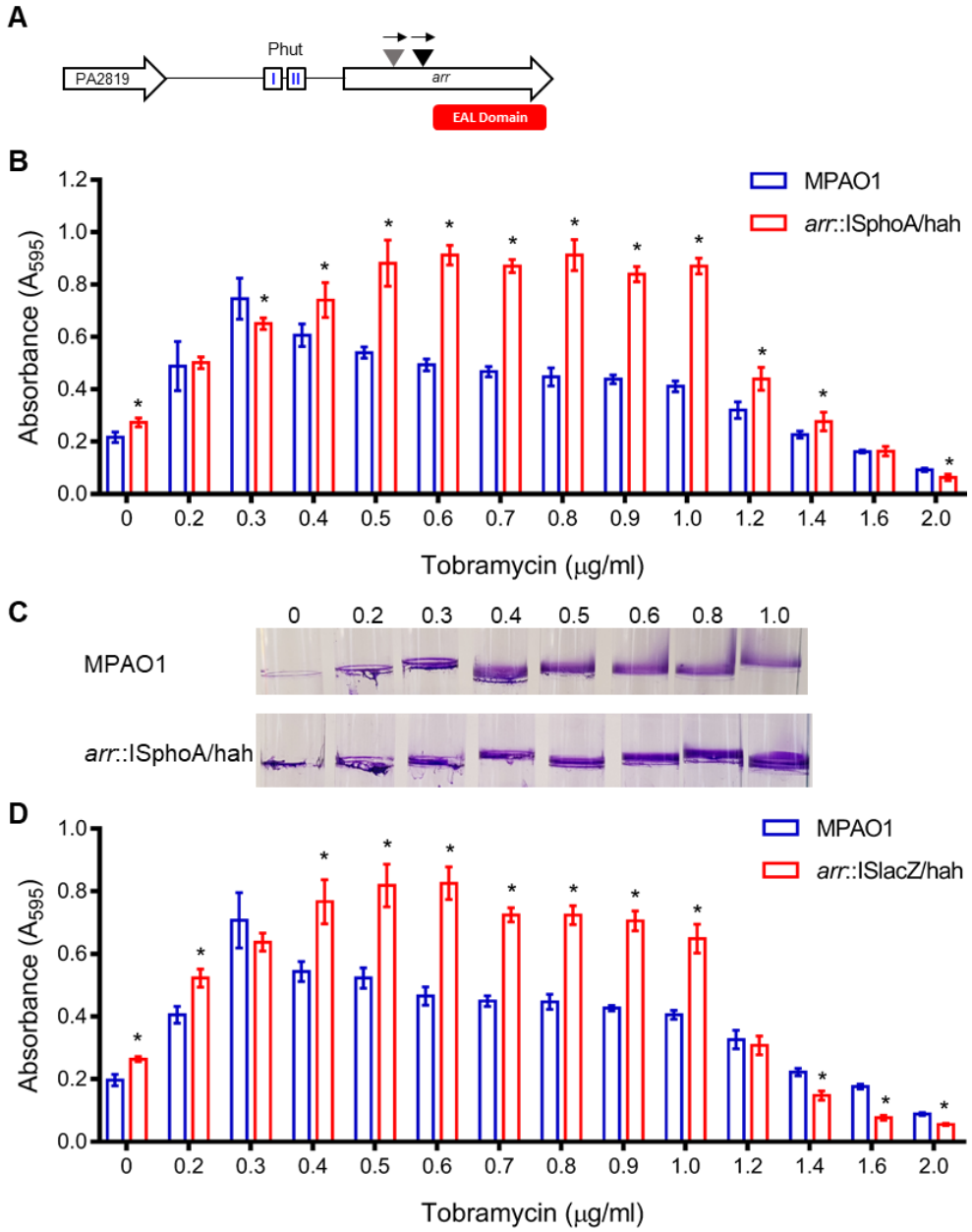

FIG 3.7 Biofilm phenotype of *P. aeruginosa* PAO1 *arr* mutants in response to sub-inhibitory concentrations of tobramycin.
(A) Schematic representation of the genetic loci of *arr* gene. HutC binding site is marked in blue (Phut-I and Phut-II). Black and grey inverted triangles denote location of insertion of transposons ISphoA/hah and ISlacZ/hah in strains MU61-32 and MU61-33, respectively. Black arrow above the triangles represents direction of transposon. NCBI predicted phosphodiesterase domain (EAL) is shown in red.
(B) Biofilm profiles of MPAO1 (wild type) and MU61-32 (*arr*::ISphoA/hah) on microtiter plates (after 8 hours static growth).
(C) Crystal-violet stain of the biofilm (at the air-liquid interface) formed by MPAO1 and MU61-32 (ISphoA/hah) on glass test tubes (after 24 hours static growth). Representative image of 4 replicates.
(D) Biofilm profiles of MPAO1 and MU61-33 (*arr*::ISlacZ/hah) on microtiter plates (after 8 hours static growth).
A similar pattern (B & D) in biofilm induction was observed for MPAO1 and both *arr* mutants (MU61-32 and MU61-33) in at least two independent experiments (data not shown). Data shown are means ± standard deviations of 8 replicate cultures from a single experiment. Asterisks denote statistical significance of biofilm formed by mutant compared to wild type, determined by multiple t-test ($P < 0.05$). Cells were grown in LB medium supplemented with tobramycin at concentrations indicated in the figure.

Indeed, these results were surprising, and prompted us to test another *arr* transposon mutant (MU62-33) to confirm the results. Significantly, we observed that MU62-33 (*arr*::ISlacZ/hah) formed a slightly higher biofilm compared to MPAO1 in the absence of tobramycin. Biofilm was strongly induced, and MU62-33 formed higher biofilm than MPAO1 when exposed to tobramycin in microtiter plate experiments. Locations of the transposon insertion in *arr* gene and the predicted phosphodiesterase (EAL) domain is shown in Fig. 3.7A. The results were indeed consistent with both the *arr* transposon mutants; MU62-32 and MU62-33. Thus, we conclude that mutation of *arr* results in an enhanced biofilm phenotype when exposed to sub-inhibitory concentrations of tobramycin, which fully agrees with our hypothesis and is consistent with the role of c-di-GMP in biofilm formation.

Having identified a phenotype for the *arr* mutant, we next examined the effect of *hutC* in tobramycin-induced biofilm formation.

3.3.5.1.3 Role of *hutC* in tobramycin-induced biofilm formation in *P. aeruginosa* PAO1

Considering that HutC binds to the predicted promoter region of *arr* (Fig. 3.4), HutC is likely to function as a repressor of *arr* gene. Hence, we hypothesized that loss of HutC enhances *arr* expression and forms reduced biofilm in response to sub-inhibitory concentrations of tobramycin.

To test the predicted role of HutC in tobramycin-induced biofilm formation, both wild type (MPAO1) and *hutC* deletion mutant (MU61-68) were grown in the presence of tobramycin at concentrations in the range of 0 to 0.6 µg/ml. The maximum biofilm induction was observed at 0.6 µg/ml (Fig. 3.7B & D); therefore, we chose to test tobramycin concentrations between 0 and 0.6 µg/ml. Intriguingly, we observed that MU61-68 (Δ*hutC*) formed higher biofilm than MPAO1 in the absence of tobramycin (Fig. 3.8A). Consistent with our expectation, an induction in biofilm was observed for MPAO1 in the presence of tobramycin. However, MU61-68 (Δ*hutC*) showed a stronger induction in biofilm and formed significantly higher biofilm than MPAO1 in the presence of sub-inhibitory concentrations of tobramycin (Fig. 3.8). The results were confirmed with another independent *hutC* deletion mutant strain (MU61-69), which also showed a similar pattern in biofilm formation as MU61-68 (Δ*hutC*) (Fig. S3.2).

First, our finding here that *hutC* mutant formed higher biofilm than wild type suggests a biofilm suppressor role for *hutC*, potentially regulating planktonic-biofilm switch. Our next observation that mutation of *hutC* enhanced tobramycin-induced biofilm formation is consistent with the biofilm profile of *arr* mutant (Fig. 3.7), suggesting that HutC regulates *arr* gene expression.

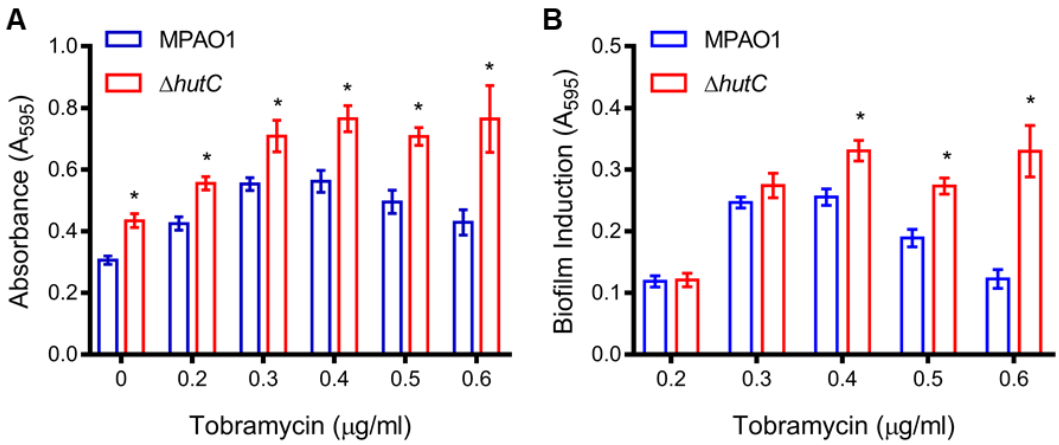

FIG 3.8 Role of *hutC* in tobramycin-induced biofilm formation in *P. aeruginosa* PAO1.
(A) Biofilm profiles of MPAO1 (wild type) and MU61-68 (Δ*hutC*) in the presence of sub-inhibitory concentrations of tobramycin. Data are means ± standard deviations of 8 replicate cultures.
(B) Amount of biofilm induced at each concentration of tobramycin with respect to biofilm formed in the absence of tobramycin by MPAO1 and MU61-68 (Δ*hutC*). Data obtained from (A) by extracting the amount of biofilm formed at zero tobramycin concentration. Error bars represent standard error of the means.
Cells were grown statically in microtiter plates for 8 hours in LB medium supplemented with tobramycin at concentrations indicated in the figure. Asterisks denote statistical significance of biofilm formed by mutant compared to wild type at same tobramycin concentrations; determined by multiple t-test ($P < 0.05$).

3.3.5.2 Screening for biofilm phenotypes of genes targeted by HutC in *P. aeruginosa* PAO1

Our *in silico* prediction for novel HutC-regulated candidate genes identified HutC-target sites in the vicinities of regulatory regions of genes whose functions have not been established (Table S3.1). We utilized reverse genetics approach to determine if they are associated with biofilm formation. First, we examined 8 mutant strains of *P. aeruginosa*, possessing transposon insertions in genes of our interest, for their ability to form biofilms compared to wild type (MPAO1). The location of transposon insertions in the genes are shown in Fig. 3.9A.

Note, biofilm data shown in Fig 3.9B is from an experiment carried out by Sara Hammouda, my trainee in our laboratory.

We observed that biofilm was significantly enhanced in 6 of the 8 mutant strains, while one mutant formed lower biofilm compared to MPAO1 (Fig. 3.9B). MU61-42 (PA2359::IS) formed similar amount of biofilm as MPAO1, indicating that PA2359 is not associated with biofilm formation. A recent study has assigned PA2359 a role in the utilization of DMSO as a sulfur source (Lundgren *et al.*, 2019). Biofilm formed by MU61-52 (PA4574::IS) was reduced by at least 70% compared to the MPAO1. PA4574 encodes a conserved hypothetical protein. The expression of PA4574 was found upregulated by 9-fold in response to azithromycin while *hutC* was downregulated by 5-fold (Ding *et al.*, 2018), suggesting a role in biofilm response to antibiotic.

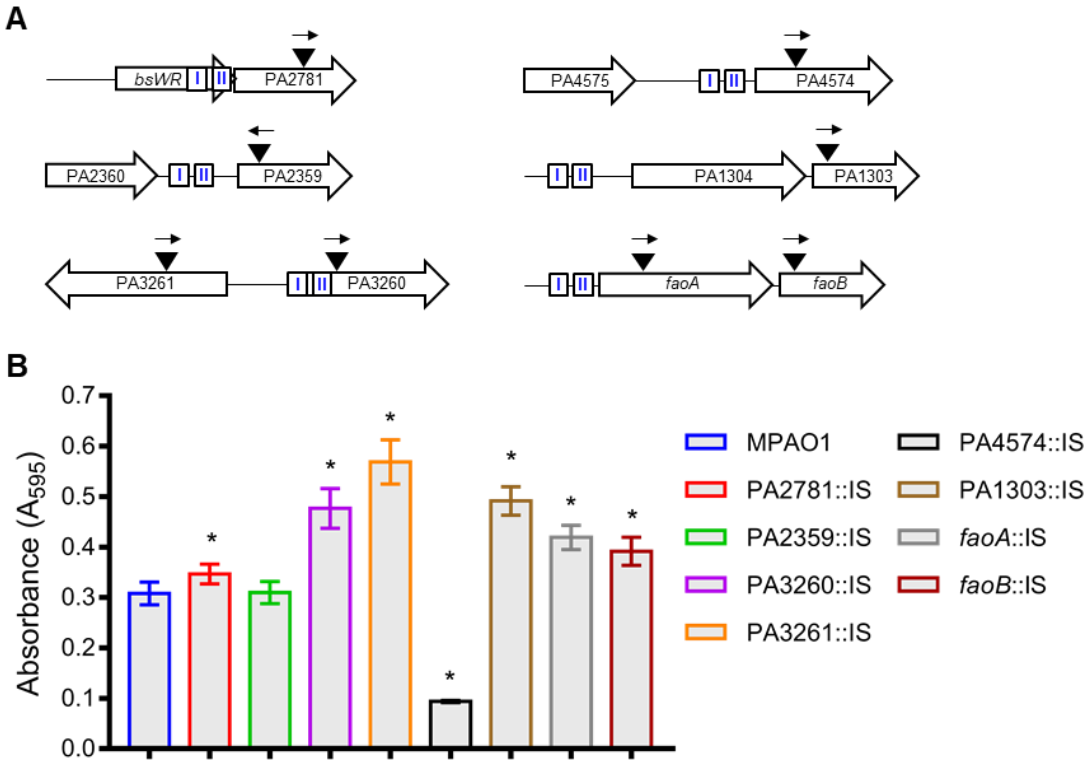

FIG 3.9 Biofilm phenotype of genes predicted to be targeted by HutC.
(A) Schematic representation of the genetic loci of HutC target sites. Putative HutC-binding sites are marked in blue, where I and II represent the two half-sites. Black inverted triangles denote locations of transposon insertions in the genes. Black arrows above the triangles represent direction of transposon.
(B) Biofilm phenotypes of MPAO1 and mutants carrying transposon insertions in the genes shown in (A). MPAO1, wild type; MU61-38, PA2781::IS*phoA*/hah; MU61-42, PA2359::IS*phoA*/hah; MU61-49, PA3260::IS*lacZ*/hah; MU61-50, PA3261::IS*lacZ*/hah; MU61-52, PA4574::IS*lacZ*/hah; MU61-53, PA1303::IS*phoA*/hah; MU61-34, *faoA*::IS*lacZ*/hah; MU61-36, *faoB*::IS*lacZ*/hah. Cells were grown statically for 16 hours in microtiter plates in LB medium. Similar pattern was also observed after 24 hours growth (data not shown). Data are means ± standard deviations of 8 replicate cultures. Asterisks denote statistical significance of biofilm formed by mutant compared to wild type; determined by Dunnett's multiple comparison test ($P < 0.05$).

We observed that mutants of PA3260 (strain MU61-49) and PA3261 (strain MU61-50) formed at least 50% and 80% more biofilm than MPAO1, suggesting a biofilm suppressor role for these genes. PA3260 and PA3261 are divergently transcribed genes with putative HutC-binding site overlapping the 5' end of PA3260. PA3261 encodes a hypothetical protein, while PA3260 is predicted to encode a transcriptional regulator containing a Xenobiotic Response Element family helix-turn-helix domain. PA3260 also forms an operon with two other genes of unknown function. We observed that MU61-53 (PA1303::IS) produced at least 50% more biofilm than wild type. PA1303 forms an operon with PA1304 and encodes for a signal peptidase that has been linked to the suppression of virulence phenotypes (Waite *et al.*, 2012). Interestingly, transposon insertions in *faoA* (strain MU61-34) and *faoB* (strain MU61-36) genes also enhanced biofilm formation by at least 35% and 26% compared to wild type. Both *faoA* and *faoB* genes are associated with the utilization of long chain fatty acids. A slightly higher biofilm was also formed by mutant MU61-38, which carries a transposon insertion in PA2781.

PA2781 encodes a hypothetical protein and forms an operon with *bsWR* (bacterial swarming regulator).

Our data indicate that genes in the vicinities of putative HutC-target sites have functions in both enhancing and suppressing biofilm formation. Together, with the observation that mutation of *hutC* enhanced biofilm (Fig. 3.8A) formation suggest that HutC may regulate planktonic-biofilm switch by targeting these genes. This warrants further biochemical and gene expression studies to determine the regulatory network of *hutC* in biofilm formation.

3.3.5.3 Role of *hutC* in determining the motility phenotypes of *P. aeruginosa* PAO1

Motility is considered as an important virulence trait of *P. aeruginosa*. Having identified that *hutC* plays a role in biofilm formation prompted us to further investigate the effect of *hutC* on swarming, swimming, and twitching forms of motility phenotypes.

We first examined the role of *hutC* in swarming motility by comparing the swarm areas of wild type (MPAO1) and its derived *hutC* deletion mutant (strain MU61-68) on 0.5% nutrient broth agar supplemented with glucose. Interestingly, we observed a hyperswarming phenotype for *hutC* mutant (Fig. 3.10A). The *hutC* mutant swarmed at least twice more area than wild type. Subsequently, we supplemented the medium with histidine or urocanate to test their effect on the swarming phenotype. In the presence of histidine, swarming area was significantly reduced in the *hutC* mutant compared to the wild type. Wild-type strain had no significant effect on swarming in the presence or absence of histidine (Fig. 3.10B). The differences in the swarming phenotypes of *hutC* mutant suggest a role for *hutC* in the nutrient dependent regulation of swarming motility. Interestingly, addition of urocanate was found to have an inhibitory effect on swarming in both wild type and *hutC* mutant (Fig. 3.10B). However, the *hutC* mutant was able to form slightly larger colony than wild type.

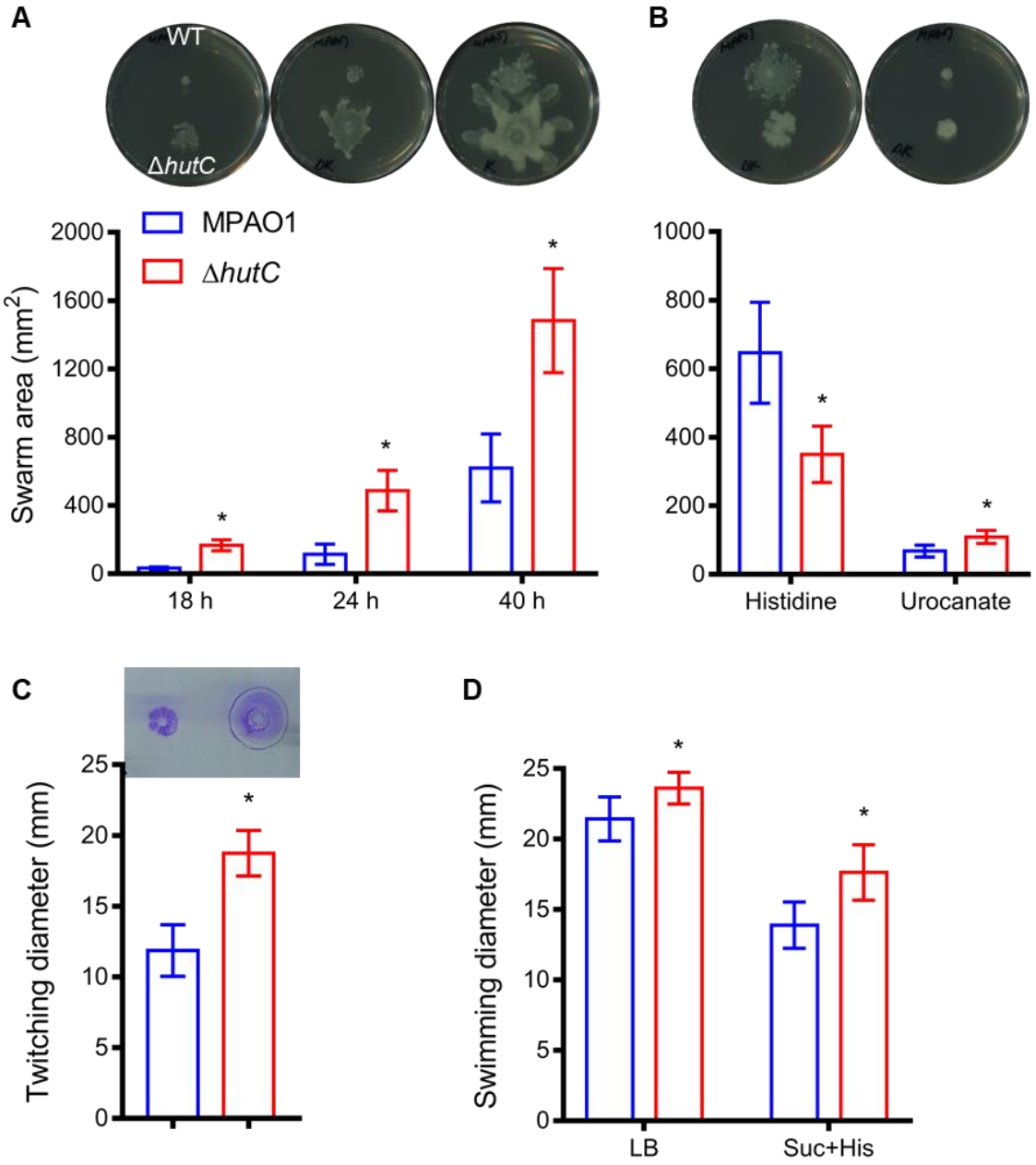

FIG 3.10 Role of HutC in *P. aeruginosa* PAO1 motility.
(A) Hyperswarming phenotype of *hutC* mutant (MU61-68) on 0.5% nutrient broth agar supplemented with 28 mM glucose observed between 18 to 40 hours post-inoculation. MPAO1, wildtype. Data are means ± standard deviations of 6 replicates. A representative image at each time point is shown above the bars. Data are representative of two independent experiments and two independently constructed *hutC* mutants.
(B) Effect of histidine and urocanate on swarming motilities of wild type (MPAO1) and *hutC* mutant (MU61-68). Cells were inoculated onto 0.5% nutrient broth agar containing 28 mM glucose supplemented with histidine or urocanate at 5 mM and grown for 40 hours. Data are means ± standard deviations of 6 replicates; a representative image is shown above the bars.
(C) Twitching phenotype of wild type (MPAO1) and *hutC* mutant on 1% LB agar. Data are means ± standard deviations of 9 replicates (includes 2 biologically independent *hutC* mutants: strains MU61-68 and MU61-69). A representative image of twitching zone stained with 0.1% crystal violet is shown above the bars.
(D) Swimming phenotype of wild type (MPAO1) and *hutC* mutant (MU61-68) on 0.25% LB agar (16 hours growth) and minimal salts agar medium containing succinate and histidine (24 hours growth). Data are means ± standard deviations of at least 6 replicates.
Asterisks denote statistical significance between the means of wild type and mutant; determined by unpaired t-test ($P < 0.05$).

We next examined the effect of *hutC* on twitching motility phenotype in *P*. *aeruginosa* PAO1 by comparing the diameters of twitching zones in wild type and its derived *hutC* deletion mutant. Interestingly, the *hutC* mutant was found to twitch a larger zone compared to wild type (Fig. 3.10C). Further, the effect of *hutC* in swimming motility was tested by comparing the swim diameters of wild type and its derived *hutC* deletion mutant on LB and minimal salts medium containing succinate and histidine. Under both conditions, a slightly enhanced swimming motility for *hutC* mutant was observed compared to the wild type.

3.3.5.4 Role of *hutC* in pyoverdine production in *P*. *aeruginosa* PAO1

In our *in silico* analysis, HutC-target sites were predicted in the regulatory region of genes associated with pyoverdine transport and biosynthesis (Table S3.1). This suggested that *hutC* may have a role in pyoverdine production. We took advantage of the fluorescence property of pyoverdine to investigate the effect of *hutC* in their production.

To determine the role of *hutC* in pyoverdine synthesis, we quantified pyoverdine produced by wild type (MPAO1) and its derived *hutC* deletion mutant (MU61-68) during growth on iron-depleted King's B (KB) medium. Intriguingly, we observed that *hutC* mutant (MU61-68) produced significantly lower pyoverdine compared to MPAO1 over a 48-hr growth period (Fig. 3.11A). Indeed, both strains grew similarly in KB medium (Fig. 3.11B), excluding the possibility of growth differences contributing to the observed phenotype. This indicates that *hutC* is required for the optimal production of pyoverdine in *P*. *aeruginosa* PAO1.

In a separate experiment, we observed that pyoverdine produced by wild-type *P*. *aeruginosa* PAO1 (MU62-14) was significantly reduced in a medium containing urocanate. We hypothesized that urocanate has an inhibitory effect on pyoverdine production potentially through its interaction with HutC regulator. To test this, MU62-14 (wild type) was grown in minimal salts medium containing succinate and NH_4Cl supplemented with increasing concentrations of urocanate. Pyoverdine was quantified by measuring fluorescence after 16 hours of growth. Indeed, a urocanate concentration dependent reduction in pyoverdine production was observed. At 20 mM of urocanate, pyoverdine production was nearly abolished (Fig. 3.11C). The results are consistent with our expectation, warranting further molecular investigation into the mechanism of HutC regulation of pyoverdine linked genes.

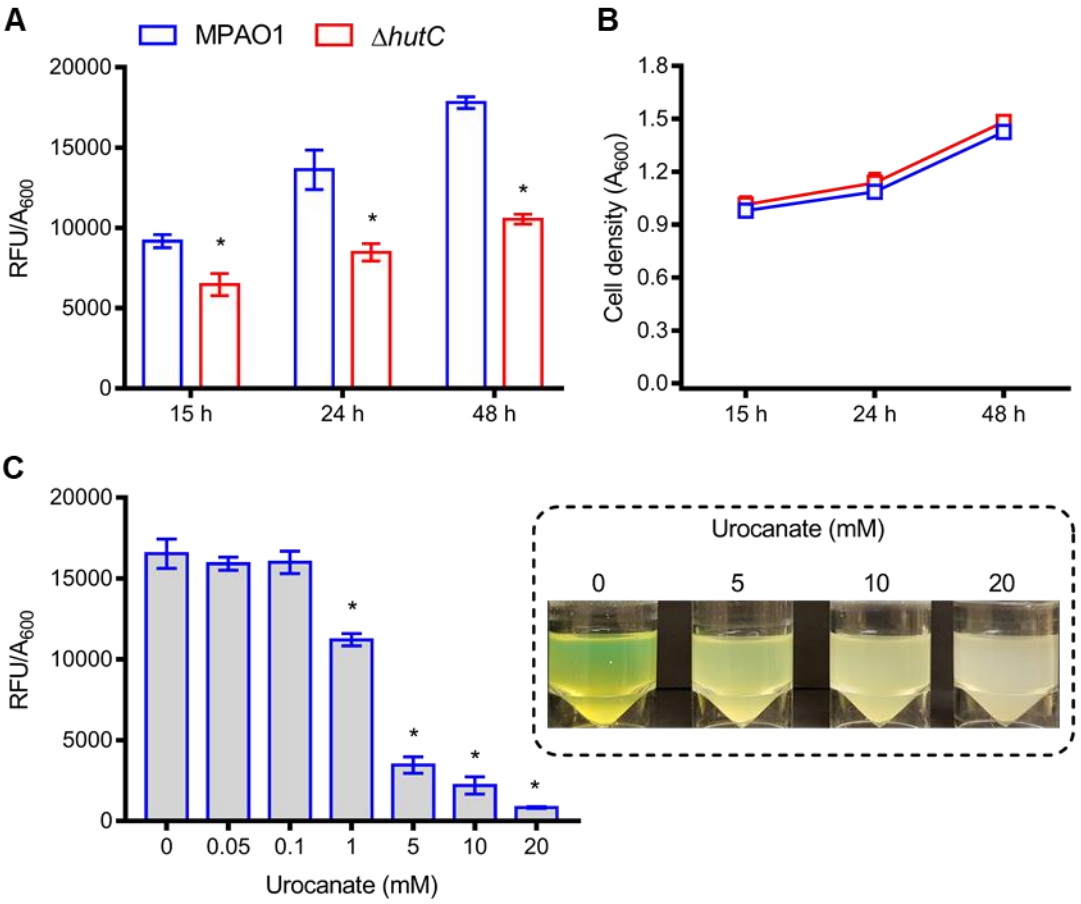

FIG 3.11 Effects of *hutC* and urocanate on pyoverdine production in *P*. *aeruginosa* PAO1.
(A) Pyoverdine produced by wild type (MPAO1) and *hutC* deletion mutant (MU61-68); quantified in relative fluorescence units (RFU) and normalized to cell density (A_{600}). Data are means ± standard deviations of 4 independent cultures. Cells were grown in KB medium. Asterisks denote statistical significance of the means between wild type and mutant; determined by t-test ($P < 0.001$).
(B) Cell density of the strains at the time of pyoverdine quantification (A).
(C) Inhibitory effect of urocanate on pyoverdine synthesis in wild-type *P*. *aeruginosa* PAO1 (MU62-14). Cells were grown for 16 hours in minimal salts medium containing succinate (20 mM) and NH_4Cl supplemented with increasing concentrations of urocanate, as indicated in the figure. The yellow pigment (pyoverdine) was significantly lowered in response to high concentrations of urocanate. Data are means ± standard deviations of 4 independent cultures. Asterisks denote statistical significance of the means when compared to zero urocanate and was determined by Dunnett's multiple comparison test ($P < 0.05$).

3.3.5.5 *Caenorhabditis elegans* killing assay

Having shown above that *hutC* plays a significant role in biofilm formation, cell motility, and pyoverdine production, we next evaluated the virulence potential of *P*. *aeruginosa* PAO1 *hutC* mutant towards *C*. *elegans* in fast killing assays.

To determine this, we transferred L4 stage worms on to PGS agar plates containing a lawn of bacteria and counted the number of worms that survived exposure to wild-type PAO1, *hutC* deletion mutant, and a non-pathogenic strain of *Escherichia coli* (control) over 4 to 24 hours. We observed that 72.2 ± 16.7% [Mean ± SD] of *C*. *elegans* were killed by wild-type PAO1 in 4 hours, while only 23.5 ± 13% of the worms were killed by *hutC* mutant (Fig. 3.12). However,

the *hutC* mutant was able to kill 59.6 ± 10.3% of *C*. *elegans* after 24 hours exposure (data not shown). As expected, 100% of the worms survived exposure to a non-pathogenic *Escherichia coli* HB101 strain.

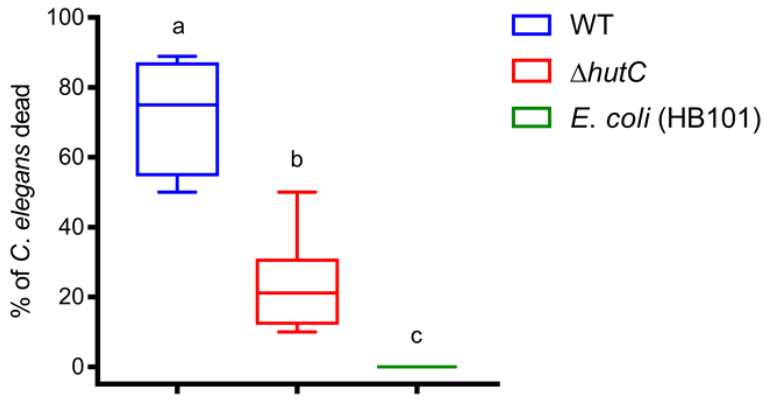

FIG 3.12 Effect of *hutC* in the killing of *C*. *elegans* by *P*. *aeruginosa* PAO1. Results are shown in standard box-and-whisker plots showing minima and maxima of the percentage of *C*. *elegans* killed by wild type PAO1 (MU62-14), two independently constructed *hutC* deletion mutants (MU57-46 and MU4A4-84), and non-pathogenic *Escherichia coli* HB101 (MU62-97) following 4 hours exposure. Data are from 4 independent replicate plates per strain. Different letters indicate significant differences determined by Tukey's test ($P < 0.05$).

The significant reduction in killing of *C*. *elegans* by *hutC* mutant observed at short exposure time (~ 4 hours) indicates that *hutC* is required for the fast killing of *C*. *elegans*. Thus, our data strongly suggests the involvement of *hutC* in regulating virulence factors beyond biofilm formation and motility.

3.4 Discussion

Signals and mechanisms associated with host-perception by pathogens is an exciting area of research that has the potential to identify novel therapeutic targets. Host-derived signals are sensed by bacterial two-component systems involving membrane-bound histidine sensor kinases (HKs) that undergo phosphorylation to activate response regulators (RRs) such as transcription factors for the regulation of gene expression. A typical example is the FusKR two-component system in Enterohemorrhagic *E. coli* where FusK (HK) senses mucosal sugar fucose and undergoes phosphorylation to activate FusR (RR), which regulates the expression of T3SS, adhesins, and effectors required for attachment to the enterocytes (Cameron & Sperandio, 2015). Considering bacterial association with eukaryotes are primarily driven by nutrients, our laboratory previously proposed that urocanate accumulated in human tissues such as skin has the potential to elicit *P*. *aeruginosa* infection by modulating HutC regulator (Zhang *et al.*, 2014). In an attempt to dissect the mechanism, here, we investigated the global

regulatory role of HutC in *P*. *aeruginosa* PAO1 with a focus on virulence traits. Utilizing an *in silico* approach, we identified 172 novel HutC-target sites in the genome. Six selected HutC-target sites were found to interact with purified HutC protein by means of EMSA and/or DNAse I footprinting assay(s). Further phenotypic analyses confirmed that *hutC* is involved in biofilm formation, tobramycin-induced biofilm formation, cell motility, and pyoverdine production. Significantly, we found that mutation of *hutC* resulted in reduced killing of *C*. *elegans* by *P*. *aeruginosa* PAO1.

Genome-wide *in silico* sequence analysis for the putative HutC-binding sites revealed that the inverted sequence (TGTA-N2-TACA) is fully conserved only in the *hut* promoters and 3 other novel targets. In contrast, the remaining targets differed in at least one nucleotide forming an imperfect inverted repeat sequence. Significantly, this altered binding affinities for HutC with the novel target sites. Our EMSAs revealed that HutC binds to *hut* promoters with relatively high affinity, while a lower affinity was observed for novel target sites examined in this study. Similarly, differences in HutC-binding affinities for *hut* and *virB* promoters (also possesses an imperfect inverted repeat sequence) was reported in *Brucella abortus* (Sieira et al., 2010). A general assumption is that global regulators bind to less specific sites with low affinities, while local regulators bind to specific sites with high affinities (Balleza *et al.*, 2009, Lozada-Chavez *et al.*, 2008). In this regard, HutC functions as a local regulator for histidine catabolism and appears to be a global regulator modulating the expression of other genes in *P*. *aeruginosa* PAO1. A typical example of a global regulator with varying binding affinities (20 to 400-fold) towards its regulon is Lrp (leucine-responsive regulatory protein), widely studied in many organisms (Cui *et al.*, 1995, Friedberg *et al.*, 2001, Peterson *et al.*, 2007, Baek *et al.*, 2009). Lrp has dual functions in activating and repressing gene expressions (Brinkman *et al.*, 2003). Beyond *hut* repression, HutC is also reported to function as a co-activator and governor by binding to low-affinity sites in *Brucella abortus* (Sieira *et al.*, 2010) and *P*. *fluorescens* SBW25 (Naren & Zhang, 2020), respectively. Thus, the low-affinity sites identified in our study suggest multiple regulatory effect of HutC in *P*. *aeruginosa* PAO1.

Based on HutC-binding affinities, we predict a hierarchical order of regulation between *hut* promoters and other targets. The high affinity of HutC towards *hut* promoters indicates that a low amount of protein is sufficient to repress *hut* gene expression, and this may be achieved from basal level expression of *hutC*. However, a lower affinity of HutC towards other targets suggests that higher amount of protein is required for modulating the expression of these targets. High amount of HutC can be formed by inducing *hut* pathway in response to histidine/urocanate. Significantly, human skin contains high concentrations of urocanate, in the range of 0.3-8.9 mM (Hug *et al.*, 1999, Snellman *et al.*, 1999), that can drive *hut* pathway and consequently increase HutC concentration. This fits in well with the previous observation

that increased histidine utilization resulted in a significant reduction in T3SS mediated cytotoxicity (Rietsch *et al.*, 2004). However, an interesting paradox is despite of the fact that histidine is present at low amounts (~4 µM) on plant surfaces, mutation of *hutC* had global effects on *P. fluorescens* SBW25 colonization on plants (Zhang *et al.*, 2006, Naren & Zhang, 2020). Therefore, it is also possible that the intracellular levels of HutC is maintained at high levels, allowing to occupy binding sites of its various targets. Considering HutC possesses lower affinity towards its target sites, smaller amount of urocanate is likely sufficient to alter this interaction. Global regulators are typically expressed at higher levels (Lozada-Chavez *et al.*, 2008); for instance, Lrp protein maintains 3000 dimers in each *E. coli* cell (D'Ari *et al.*, 1993). Further studies are required to understand if urocanate is merely a signal or driver of the *hut* pathway that helps in adapting to host environment through interaction with HutC.

Examination of phenotypes of *hutC* deletion mutant revealed that *hutC* plays a significant role in the regulation of biofilm formation. Biofilms are bacterial communities formed by the aggregation of microbial cells in a self-produced matrix comprising of exopolysaccharides, proteins, lipoproteins, lipids, and nucleic acids (Balasubramanian *et al.*, 2013, Flemming & Wingender, 2010). Biofilm formation generally indicates transition to life-long chronic infection and are associated with poor prognosis particularly in CF patients. This is due to the poor penetration of antibiotics and host defences through the matrix in which the microbial cells are embedded (Hoiby *et al.*, 2010, Lund-Palau *et al.*, 2016). Biofilms can also be formed on abiotic surfaces. The regulatory mechanisms involved in biofilm formation is complex and includes QS system, c-di-GMP signalling, and small RNAs (Balasubramanian *et al.*, 2013). Significantly, we found that mutation of *hutC* enhanced biofilm in *P. aeruginosa* PAO1, suggesting a biofilm suppressor role for *hutC*. Some suggested that histidine degradation contributes to biofilm formation via the production of extracellular DNA (eDNA) from purine and pyrimidine synthesis (Cabral *et al.*, 2011). However, in this study we found that HutC can directly interact with the regulatory region of genes associated with biofilm formation (Fig. 3.5). Further, mutation of some of the putative targets of HutC whose functions have not been previously characterized also displayed a phenotype similar to that of *hutC* mutant (Fig. 3.9). Thus, our data suggest a more direct role for *hutC* in biofilm formation, presumably by regulating these candidates.

More importantly, we found that *hutC* plays a key role in tobramycin-induced biofilm formation by targeting *aminoglycoside response regulator* (*arr*) gene. Tobramycin is an aminoglycoside antibiotic generally used to treat *P. aeruginosa* infections (Mogayzel *et al.*, 2014). Interestingly, *P. aeruginosa* have evolved mechanisms to sense sub-inhibitory concentrations of tobramycin that act as signals inducing high levels of biofilm. In PAO1, this is mediated by Arr, a c-di-GMP phosphodiesterase, by regulating the intracellular levels of c-di-GMP (Hoffman *et al.*, 2005,

Kulasakara *et al.*, 2006). Although, a previous study indicated that *arr* gene is required for tobramycin-induced biofilm formation (Hoffman *et al.*, 2005), we found that mutation of *arr* resulted in a stronger biofilm induction than wild-type strain. It is known that high levels of intracellular c-di-GMP enhances biofilm formation, while low levels are associated with biofilm dispersion. The role of c-di-GMP phosphodiesterases is to lower the intracellular pools of c-di-GMP (Hall & Lee, 2018), hence our results seem consistent. Our EMSA and DNAse I analyses revealed that HutC can bind to the *in silico* predicted target site in the putative promoter region of *arr*. Further phenotypic analysis revealed that mutation of *hutC* strongly induced biofilm in *P*. *aeruginosa* PAO1 and formed higher levels of biofilm than wild-type strain. Thus, our data consistently indicate that *hutC* has a suppressor role in biofilm formation. Considering that both *hutC* and *arr* mutants displayed enhanced abilities to form biofilms relative to wild-type during exposure to sub-inhibitory concentrations of tobramycin suggest that HutC likely functions as a transcriptional activator of *arr* gene expression. In the *hutC* mutant, the expression of *arr* is likely maintained at basal levels resulting in increased cellular pools of c-di-GMP; consequently, forming hyperbiofilms. Further gene expression studies and monitoring of the intracellular levels of c-di-GMP are in progress to test our prediction that HutC activates the expression of *arr* in response to tobramycin.

Besides biofilm formation, *hutC* appears to have regulatory role in swarming, swimming, and twitching forms of motilities in *P*. *aeruginosa* PAO1. We observed that mutation of *hutC* contributed to a hyperswarming phenotype in nutrient broth agar medium supplemented with glucose, while the wild type exhibited a limited swarming motility. Under similar conditions, a *bsWR* (HutC candidate) mutant also exhibited a hyperswarming motility while wild type exhibited limited swarming (Wang *et al.*, 2014). Note that HutC was also able to bind to the *in silico* predicted HutC-target site in *bsWR*, presumably suggesting that HutC may regulate *bsWR*-PA2781 operon. Moreover, HutC target-sites have been identified in or near the genes such as PA3817, PA1431 (*rsaL*), PA2622 (*cspD*), and PA4725 (*cbrA*) associated with swarming motilities in *P*. *aeruginosa* strains PAO1 and PAK (Overhage *et al.*, 2008, Yeung *et al.*, 2009) and need to be further investigated. In *P*. *aeruginosa* strain PAK, a transposon insertion in *hutC* resulted in a defect in swarming motility (reduced swarming) (Yeung *et al.*, 2009). This is in contrast with the hyperswarming phenotype of PAO1 *hutC* deletion mutant observed in this study. Strain specific regulation could be a possible explanation for the differences. However, swarming ability and pattern are also determined by other factors such as nutrients in the medium (Rashid & Kornberg, 2000, Kohler *et al.*, 2000, Kollaran *et al.*, 2019, Overhage *et al.*, 2008); consistently we observed that addition of histidine resultant in a defect in swarming motility for the *hutC* mutant, while urocanate had an inhibitory effect for both wild type and *hutC* mutant. Therefore, whether (i) HutC is an essential regulator such as involved

in flagellar synthesis/rhamnolipid production for swarming, (ii) only a nutrient-dependent regulator, or (iii) strain-dependent needs to be further established.

Furthermore, we found that *P. aeruginosa* PAO1 *hutC* mutant exhibited a hypertwitching phenotype and enhanced swimming relative to the wild type in our study. Since twitching and swimming motilities are dependent on type IV pili and flagellum, respectively, HutC may have a direct or indirect effect on the regulation of these motility appendages. Interestingly, in *Yersinia pseudotuberculosis*, mutation of *hutC* also resulted in enhanced swimming motility where HutC negatively regulated the flagellar motility regulator encoding *flhDC* operon (Joshua *et al.*, 2015). However, in contrast, transposon insertion in *hutC* of *P. aeruginosa* strain PAK resulted in a minor defect in swimming (reduced swimming) but had no effect on twitching motility (Yeung *et al.*, 2009). The differences observed in all forms of motilities between the *hutC* mutants of *P. aeruginosa* strains PAO1 (this study) and PAK (Yeung *et al.*, 2009) is rather surprising and need to be further explored. Generally, motility and biofilm show an inverse relation, where both works in tandem facilitating movement of bacterial populations to a suitable surface, attachment, promoting surface-associated growth, and dispersion (Kazmierczak *et al.*, 2015). However, enhancement of biofilm and motility phenotypes in the *hutC* mutant in our study could be caused by hyperflagellation (Rashid & Kornberg, 2000, Kohler *et al.*, 2000) of the cells that needs to be further explored.

Iron is an important transition metal, for both prokaryotes and eukaryotes, required for various biological processes. Iron restriction is a strategy evolved by most eukaryotes for reducing iron availability to invading pathogens to limit infection (Meyer *et al.*, 1996). However, pathogens have evolved mechanisms to derive iron from the host by producing siderophores (iron-chelators). Pyoverdine is an important siderophore produced by *P. aeruginosa* to scavenge iron from transferrin or ferroprotein from the host (Kirienko *et al.*, 2013, Kirienko *et al.*, 2015, Kang *et al.*, 2018). Besides scavenging iron, interaction of pyoverdine bound iron complex with the FpvA receptor (present in the outer membrane) triggers the activation of PvdS, an alternate sigma factor, that further amplifies pyoverdine synthesis and expression of virulence factors such as exotoxin A and protease PrpL (Lamont *et al.*, 2002). Pyoverdine production correlated with enhanced virulence of strains PAO1, PAK (hypervirulent) and clinical isolates toward *C. elegans* and murine models (Meyer *et al.*, 1996, Takase *et al.*, 2000) (Minandri *et al.*, 2016, Kirienko *et al.*, 2013, Kang *et al.*, 2018, Kang *et al.*, 2019). Pyoverdine is, therefore, considered as an important virulence factor and was proposed as a potential therapeutic target; because inhibition of pyoverdine significantly impaired *P. aeruginosa* pathogenesis (Kirienko *et al.*, 2016, Kaneko *et al.*, 2007, Kang *et al.*, 2019). Significantly, we observed that *hutC* mutant produced lower pyoverdine compared to wild type, suggesting that HutC may be involved in the regulation pyoverdine synthesis, secretion, or recycling through

outer membrane receptors. Interestingly, regulatory regions of a secondary receptor, FpvB, transporting iron bound pyoverdine into the cell contains a putative HutC-target site, predicted *in silico*. We also observed that urocanate exhibited an inhibitory effect on pyoverdine production in the wild-type strain. This finding is exciting from a therapeutic perspective and needs to study in detail. Moreover, *hutC* was also required for full *P*. *aeruginosa* PAO1 virulence against *C*. *elegans* in fast killing assays. The defect in killing of *C*. *elegans* by *hutC* mutant could be related to pyoverdine synthesis or associated with the secretion of diffusible toxins, such as cyanide and phenazines, that kill worms faster even in the presence of exudates of *P*. *aeruginosa* (Mahajan-Miklos *et al.*, 1999, Cezairliyan *et al.*, 2013, Gallagher & Manoil, 2001).

In this preliminary study, we identified that *hutC* has a global control on factors mediating host-adaptation in *P*. *aeruginosa* PAO1. Antibiotic resistant infections are a major concern at present. Novel treatment strategies such as developing drugs targeting *P*. *aeruginosa* virulence factors have been previously proposed; some including anti-biofilm therapies are in already progress (Maurice *et al.*, 2018). In this respect, *hutC* could be a potential therapeutic target. Thus, further studies are warranted to examine the molecular mechanism and clinical significance of *hutC* in determining *P*. *aeruginosa* virulence towards host.

3.5 Materials and Methods

3.5.1 Strains, plasmids, and growth conditions

Bacterial strains and plasmids used in this work are shown in Table 3.2. The MPAO1 strain and transposon-insertion mutants were obtained from Manoil Lab (Jacobs *et al.*, 2003, Held *et al.*, 2012). Wild type N2 *C*. *elegans* and *E*. *coli* HB101 were obtained from Prof. Russell Grant Snell (Young *et al.*, 2018). *C*. *elegans* was maintained in Nematode Growth Medium (NGM) between 20-23°C. *E*. *coli* and *P*. *aeruginosa* PAO1 were routinely propagated in Luria-Bertani broth (1% Tryptone, 0.5% Yeast extract, and 1% NaCl) at 37°C. *E*. *coli* DH5$\alpha\lambda_{pir}$ was used for general cloning and triparental conjugation into *P*. *aeruginosa* PAO1. When required, antibiotics were used at the following concentrations for *E*. *coli*: 15 µg/ml tetracycline (Tc); 10 µg/ml gentamicin (Gm). For *P*. *aeruginosa* PAO1, antibiotics were used at: 100 µg/ml Tc; 20 µg/ml Gm. Spectinomycin (Sp) and nitrofurantoin (Nf) were used at 100 µg/ml for *Escherichia coli* and *P*. *aeruginosa* PAO1, respectively. X-gal (Melford) was used at concentrations of 60 µg/ml for blue/white screening of bacterial colonies. Succinate, histidine, and urocanate were purchased from Sigma. Tryptone and Yeast extract were purchased from Acumedia and Oxoid, respectively.

Table 3.2 Strains and plasmids used in this study.

Strain or plasmid	Genotype or characteristics[a]	Reference or source
E. coli		
MU4A4-53	BL21-GOLD (DE3) carrying *hutC* expression vector	Monica Gerth, unpublished
***P. aeruginosa* PAO1**		
MPAO1	Wild-type strain	Held *et al.* (2012)
MU61-68	Δ*hutC*, MPAO1 devoid of PA5105	This work
MU61-69	Δ*hutC*, MPAO1 devoid of PA5105	This work
MU61-32	*arr*::IS*phoA*/hah, MPAO1 carrying transposon insertion in PA2818 at nucleotide 688	Held *et al.* (2012)
MU61-33	*arr*::IS*lacZ*/hah, MPAO1 carrying transposon insertion in PA2818 at nucleotide 672	Held *et al.* (2012)
MU61-38	PA2781::IS*phoA*/hah, MPAO1 carrying transposon insertion in PA2781 at nucleotide 227	Held *et al.* (2012)
MU61-42	PA2359::IS*phoA*/hah, MPAO1 carrying transposon insertion in PA2359 at nucleotide 53	Held *et al.* (2012)
MU61-49	PA3260::IS*lacZ*/hah, MPAO1 carrying transposon insertion in PA3260 at nucleotide 55	Held *et al.* (2012)
MU61-50	PA3261::IS*lacZ*/hah, MPAO1 carrying transposon insertion in PA3261 at nucleotide 257	Held *et al.* (2012)
MU61-52	PA4574::IS*lacZ*/hah, MPAO1 carrying transposon insertion in PA4574 at nucleotide 141	Held *et al.* (2012)
MU61-53	PA1303::IS*phoA*/hah, MPAO1 carrying transposon insertion in PA1303 at nucleotide 82	Held *et al.* (2012)
MU61-34	*faoA*::IS*lacZ*/hah, MPAO1 carrying transposon insertion in PA3014 at nucleotide 578	Held *et al.* (2012)
MU61-36	*faoB*::IS*lacZ*/hah, MPAO1 carrying transposon insertion in PA3013 at nucleotide 191	Held *et al.* (2012)
MU62-14	Wild-type strain	Lab stock
MU57-46	Δ*hutC*, MU62-14 devoid of PA5105	This work
MU4A4-84	Δ*hutC*, PAO1 devoid of PA5105	Lab stock; Monica Gerth, unpublished
Plasmid		
pRK2013	Helper plasmid, Tra^+, Km^r	Ditta *et al.* (1980)
pUIC3	Integration vector with promoterless *lacZ*, Mob^+, *ori*-R6K, Tc^r	Rainey (1999)
pCR8/GW/TOPO	Cloning vector, Sp^r	Invitrogen
pCR8-Δ*hutC*	Recombinant plasmid containing *hutC* deletion fragment, Tc^r	This work
pUIC3-Δ*hutC*	Recombinant plasmid containing *hutC* deletion fragment, Tc^r	This work
pET14b-*hutC*	pET14b expression vector carrying *hutC* from PAO1, Ap^r	Monica Gerth, unpublished

[a]Gm, gentamycin; Km, kanamycin; Sp, spectinomycin; Ap, Ampicillin; Tc, tetracycline.

3.5.2 Monitoring bacterial growth kinetics

P. aeruginosa PAO1 from -80°C freezer stock was cultured overnight in LB broth. Subsequently, cultures were washed once in M9 salts and starved for 2 hours at 37°C. The starved cells were diluted 1:100 times in 1 ml LB medium supplemented with tobramycin (Sigma) and 200 µl aliquots were transferred into a sterile clear 96-well microplate (Greiner

Bio-One). Absorbance was measured at a wavelength of 450 nm using a Synergy 2 multi-detection microplate reader installed with Gen5 software (Bio-Tek). A_{450} readings were measured every 5 min during incubation (with continuous medium shaking) for 24 hours at 37°C. Hourly data points are shown in the figure for clarity.

3.5.3 Strain construction

Standard protocols were used for the isolation of plasmid DNAs, restriction endonuclease digestion, ligation, and PCR (Sambrook *et al.*, 1989). PCRs were performed using *Taq* DNA polymerase purchased from Invitrogen Ltd. (Auckland, New Zealand). Oligonucleotide primers were synthesized by Integrated DNA Technologies Inc. (Singapore) and are shown in Table 3.3. The pCR8™/GW/TOPO® (Invitrogen) cloning kit was used for cloning *Taq* polymerase amplified PCR products into pCR8 for verifying sequence identity (Macrogen, South Korea).

The unmarked *hutC* deletion mutant was constructed by gene splicing by overlap extension (SOE) PCR (Horton *et al.*, 1989) in conjunction with a two-step allelic-exchange strategy using the suicide-integration vector pUIC3 (Rainey, 1999, Zhang & Rainey, 2007b). Briefly, two fragments (~600-bp) flanking *hutC* gene were PCR amplified using oligonucleotide primers. The two fragments containing complementary sequences at their ends were then joined by a third PCR resulting in a ~1.2-kbp fragment. After verifying sequence identity, the *hutC* deletion fragment was sub-cloned into pUIC3 (suicide vector containing promoterless *lacZ*) at the *Bgl*II site and introduced into *P. aeruginosa* PAO1 by tri-parental mating with the help of pRK2013. Integration of pUIC3 into the genome via a single homologous recombination event of the cloned DNA fragment was selected on LB agar plate supplemented with Tc, Nf (to counter select *E. coli* donor cells), and X-gal (for blue/white screening). The double-cross over mutants that had lost the chromosomally integrated pUIC3-vector were selected by D-cycloserine enrichment process (Zhang & Rainey, 2007b). Of note, D-cycloserine was used at 1100µg/ml. The *hutC* gene deletion was confirmed by PCR, sensitivity to Tc, and examining *hutU* promoter activity.

Table 3.3 Oligonucleotides used in this study.

Primer name[a]	Sequence (5' - 3')[b]	Purpose
HutC-del-F1 (BglII)	cagatctATGCGCAGGGAAAGTTCGGC	*hutC* deletion fragment for mutant construction
HutC-del-R1	ccagacggtgTACCTCGCCGAGTTGCGAG	
HutC del-F2	cggcgaggtaCACCGTCTGGAAGGACGTT	
HutC-del-R2 (BglII)	gagatctTACCCTTTCGGTGTAGACGC	
MLG036-PF	ggaattccataTGACGTCCTCTTCCTCCGA	Amplify *hutC* coding region for cloning into pET14b vector at NdeI and BamHI restriction sites. To express and purify his_6 tagged HutC protein for *in vitro* assays.
MLG037-PR	ctggatccTCATGAGCTGAAACGTCCTTCC	
Arr-1-BglII	cagatCTGCTCGTCCTGGTCTCCTT	Primers used to confirm *arr* gene was disrupted by transposon insertion
Arr-4-BglII	gagatCTCCTACCTCGAGCACCACCT	
PhutU-bio1	CGGGAATGTGGAGATATCG	Amplify *hutU* promoter region for EMSA and DNAse I footprinting assays
MLG093-PR	cacaagcttCGGGGTGGTCACGGCAGGCTCCTG	
KSJ-111-F-Bio	TGAAAGAGACTGTCCCGCCG	Amplify *arr* promoter region for EMSA and DNAse I footprinting assays
KSJ-012-R	GGCTTCTGGGGTAAGATTCG	
KSJ-009-F	CTCATCCTCAAGGTGTCCAG	Amplify intergenic region between *bsWR* and PA2781 for EMSA
KSJ-010-R-Bio	TACTGCTCCGGATGCGTGTC	
foaA-1	GCGCAGGCCTCGACAATAGA	Amplify *faoAB* promoter region for EMSA
foaA-2-Bio	TCAACTCGACGATGCCGC	
CupA-1-Bio	CGTTCGAGTACCCGCCATTC	Amplify region between *cupA* and *cgrA* genes for EMSA
CupA-2	CAGGGAAGTGCATACTCCAAC	
AlgU-F-Bio	GCTGCCGATGACCAGTACAT	Amplify region between *algU* and *nadB* genes for EMSA
AlgU-R	GTTCCAGCACTACATCGCC	

[a]Bio – biotin labelled

[b]Restriction sites are underlined; nucleotides in lower case (excluding RE sites) are manually incorporated complementary sequences between the primer pairs

3.5.4 *In silico* prediction of novel HutC-regulated candidate genes

Probability matrix of the motif encompassing the HutC binding palindromic sequence was generated using MEME motif discovery program (Bailey *et al.*, 2009) by inputting a 64-bp sequence of the promoter regions of *hutU* and *hutFC*. The promoter regions were extracted from the genomes of 40 *Pseudomonas* strains (NCBI) representing 12 species. The conserved

motif and corresponding probability matrix were generated using the following parameters - motif discovery mode: classic mode; site distribution: zero or one occurrence per sequence; background model: 0-order model of sequences; and motif width (minimum-maximum): 10-16. Probability matrix of the conserved motif with highest negative E-value and that contains the HutC binding palindromic sequence was chosen for subsequent analysis.

The HutC-target sites were predicted utilizing FIMO (Grant *et al.*, 2011), an inbuilt feature of the MEME package. FIMO scans for motif occurrences based on probability matrix. The probability matrix of the conserved motif was used to scan the genome of *P*. *aeruginosa* PAO1 for similar motif occurrences (target sites), with a *P* value less than 0.0001. The target sites identified were then examined manually to determine similarity with the HutC binding palindromic sequence (TGTA-N2-TACA) and locate their position in the genome with respect to neighbouring genes.

3.5.5 Purification of $HutC_{his6}$ proteins from *P. aeruginosa* PAO1

Cloning of *hutC* gene from *P*. *aeruginosa* PAO1 into the expression vector pET14b was performed by Dr Monica Gerth. The final construct in *E*. *coli* BL21(DE3) was available for protein expression and purification at the start of this study.

Briefly, the HutC-coding region was PCR amplified from the genomic DNA and cloned into pET14b vector at the NdeI and BamHI restriction sites, which will incorporate 6XHis affinity tags to the N-terminus of HutC when expressed. The recombinant plasmid was subsequently transformed into *E*. *coli* BL21(DE3) and $HutC_{his6}$ protein expression was induced by addition of 1 mM IPTG. The protein was purified using TALON metal affinity resin (Clontech Laboratories Inc.) (Fig. S3.3).

3.5.6 Electrophoretic Mobility Shift Assays (EMSAs) and dissociation constant (K_d)

EMSA. Biotin end-labeled probe DNAs were synthesised by PCR with a biotinylated primer using genomic DNA as template. Binding reactions (20 µl) were carried out by incubating $HutC_{his6}$ with probe DNA (20 nM) for at least 30 min at 23°C in a buffer (pH 7.5) containing 10 mM HEPES, 5 mM $MgCl_2$, 50 mM KCl, 1 mM dithiothreitol, and 1 µg salmon sperm DNA. The samples were subjected to electrophoresis on a 5% polyacrylamide gel at 120 V in 0.5XTBE buffer. The electrophoresis was carried out in a cold space to maintain temperatures ~4°C. Subsequently, DNA from the gel were electrophoretically transferred to a nitrocellulose membrane (Sigma Aldrich) at 80 V for 1 hour in 0.5% TBE (maintaining low temperatures) and fixed by oven baking at 80°C for 30 min. The immobilized biotin labeled DNA on the membrane was detected using the Chemiluminescent Nucleic Acid Detection kit (ThermoFisher) as per

the manufacturer's instructions. The images were photographed with a LAS-4000 luminescent imager installed with ImageQuant LAS 4000 software (Fujifilm) and further analysed in ImageJ program.

Dissociation constant (K_d). Relative amounts of free probe DNA and Protein-DNA complex were quantified from the EMSA gel as band intensities using the ImageJ program. Fractions of Protein-DNA complex were plotted against protein concentrations using a non-linear regression model, specific binding with hill slope, in Prism. K_d was estimated from the curve; representing protein concentration required to bind 50% of the probe DNA.

3.5.7 DNAse I footprinting analysis

Biotin end-labeled probe DNAs prepared for EMSAs were also used for DNAse I footprinting assays. Binding reactions were carried out by incubating 2 µM DNA probe with $HutC_{his6}$ protein for at least 30 min at 23°C in a 50 µl reaction buffer (containing 10 mM HEPES, 5 mM $MgCl_2$, 50 mM KCl, 1 mM dithiothreitol, and 1 µg salmon sperm DNA; pH 7.5). Subsequently, 50 µl of the co-factor solution (5 mM $CaCl_2$ and 10 mM $MgCl_2$) was added to the reaction with gentle mixing. The reaction was treated with 0.02 unit of DNAse I for 6 min and digestion was terminated immediately by adding 100 µl of DNAse I stop solution [200 mM NaCl, 20 mM EDTA (pH 8), and 1% SDS]. The digested DNA fragments were purified and extracted by 1:1 phenol:chloroform treatment and ethanol precipitation at -80°C for an hour. Air-dried pellets were re-suspended in 8 µl of loading dye (95% formamide, 0.05% bromophenol blue, and 20 mM EDTA), heat denatured at 90°C for 15 min, and subjected to electrophoresis in a 6% urea-polyacrylamide sequencing gel (21 x 40 cm) in 1X TBE buffer, using the Sequi-Gen GT system (Bio-Rad Laboratories Pty). The DNAs were transferred to a nitrocellulose membrane by contact blotting (performed overnight) and heat immobilized by oven-baking at 80°C for 30 min. The DNA fragments were detected using the Chemiluminescent Nucleic Acid Detection kit (ThermoFisher) as per the manufacturer's instructions. The images were photographed with a LAS-4000 luminescent imager installed with ImageQuant LAS 4000 software (Fujifilm) and further analysed in ImageJ program. A G+A marker synthesized from chemical sequencing reaction was included in the assay to help determine the footprinting site sequence.

3.5.8 Biofilm assays

Biofilm assays were performed as previously described (O'Toole, 2011). Briefly, *P. aeruginosa* PAO1 strains were cultured overnight (~22 hours) in LB broth to similar densities. Bacterial cells were diluted 1:100 times in fresh LB broth supplemented with tobramycin. To assay biofilm formation in microplates, 200 µl aliquots were transferred into a sterile clear 96-well

microplate (Greiner Bio-One). To assay biofilm formation on glass surface, 3 ml was transferred into 13 mm glass test tubes. Biofilms were then allowed to develop for 8 hours in microplates and 24 hours in glass test tubes at 37°C without shaking. Biofilms were stained by pouring off the culture, washing 2-3 times with double distilled water, and staining with 0.1% crystal violet (CV) dye for at least 15 min in room temperature. Excess CV dye was removed by washing 3-4 times in double distilled water. Biofilms formed at the air-liquid interface were dissolved in 30% acetic acid and quantified by measuring absorbance at 595 nm in Synergy 2 multi-detection microplate reader installed with Gen5 software (Bio-Tek).

3.5.9 Motility assays

Protocol for motility assays were adapted from previous studies (Rashid & Kornberg, 2000, Patriquin *et al.*, 2008) with minor amendments. Inoculum for motility assays were prepared from bacterial cultures grown overnight (~24 hours) on 0.3% LB agar at 37°C. Cells for inoculating motility pates were obtained by gently touching the colony surface using a sharp pointed plastic needle. Agar plates for assessing motility were dried overnight at room temperature (20-21°C) prior to the experiment.

Swimming assay. Swimming was examined on 0.25% LB agar [1% Tryptone (Difco), 0.5% Yeast extract (Oxoid), 1% NaCl, and agar (Oxoid)] and M9 salts (47.8 mM Na_2HPO_4, 22 mM KH_2PO_4, 8.6 mM NaCl, and 2 mM $MgSO_4$) agar medium containing succinate (20 mM) and histidine (5 mM). Swim plates were inoculated by gently stabbing into the agar with a sharp pointed plastic needle. Plates were incubated upright at 30°C for 16-24 hours. Swimming was scored quantitatively by measuring diameter of the colony using ImageJ program.

Swarming assay. Swarming was examined on 0.5% Nutrient broth agar [Nutrient broth (Difco) and agar (Oxoid)] supplemented with 28 mM glucose. Swarm plates were inoculated by gently stabbing into the agar with a sharp pointed plastic needle. Plates were incubated upright at 30°C for 18-40 hours. Swarming was scored quantitatively by measuring area of the expanding colony using ImageJ program (Morales-Soto *et al.*, 2015).

Twitching assay. Twitching was examined on 1% LB agar [1% Tryptone (Difco), 0.5% Yeast extract (Oxoid), 1% NaCl, and agar (Oxoid)]. Twitch plates were inoculated by stabbing agar all the way down to the agar-plastic interface with a sharp pointed plastic needle. Plates were incubated facedown at 37°C for 48 hours, followed by an additional 24 hours at room temperature (~21-23°C). Agar was carefully removed with the help of a scalpel and the plates were stained with 0.1% CV dye for 15-30 min at room temperature. Excess CV dye was poured off and the plates were washed 2-3 times with double distilled water prior to taking

photographs. Twitching was scored quantitatively by measuring diameter of the colony using ImageJ program.

3.5.10 Pyoverdine quantification

Pyoverdine production was estimated as described previously (Zhang & Rainey, 2013). Briefly, *P. aeruginosa* PAO1 test strains were cultured overnight (~22 hours) in LB broth to similar densities. Cells were washed twice in M9 salts medium and starved for 2 hours at 37°C. Bacterial cells were diluted 1:1000 times in fresh 5 ml King's B broth [10 g/L glycerol, 20 g/L proteose peptone (Difco), 1.5 g/L $MgCl_2$, and 1.5 g/L K_2HPO_4] or M9 salts (47.8 mM Na_2HPO_4, 22 mM KH_2PO_4, 8.6 mM NaCl, and 2 mM $MgSO_4$) broth containing succinate (20 mM) and NH_4Cl supplemented with urocanate (0-20 mM). Cultures were incubated at 37°C with shaking for 15-48 hours. A_{600} (growth) was measured using Synergy 2 multi-detection microplate reader installed with Gen5 software (Bio-Tek). Cultures were centrifuged at 13000 rpm for a minute and fluorescence (RFU) of the supernatant at 460 nm with an excitation wavelength of 360 nm was measured using Synergy 2 multi-detection microplate reader. Data are presented as RFU normalized to A_{600}.

3.5.11 *C. elegans* killing assay

C. elegans synchronization. *C. elegans* was maintained in NGM [2.5 g Bacto-Peptone, 3 g NaCl, 17 g agar, 1 ml of 1M $MgSO_4$, 25 ml of 1M KH_2PO_4, 1 ml of $CaCl_2$, and 1 ml of cholesterol (sigma); all per litre] agar plates containing *E. coli* HB101 (food source), between 20-23°C. Synchronization of worms were carried out as previously described (Porta-de-la-Riva *et al.*, 2012). Briefly, adult worms carrying eggs were collected from NGM plates by washing with M9 buffer. The worms were pelleted by centrifuging at 400g for 2 min at room temperature and washed 3 times to reduce *E. coli* HB101 contamination. Eggs were collected by exposing worms to bleaching solution [by mixing 0.5 ml of 5 N NaOH, 1 ml of 5% bleach, and 3.5 ml of double distilled H_2O] for a maximum of 5 min. Excess bleaching solution was removed by washing eggs at least 4 times in M9 buffer. Eggs were allowed to hatch (L1 stage) by overnight incubation in M9 buffer at 20°C with gentle shaking. L1 stage worms were seeded on to NGM plates containing a lawn of *E. coli* HB101 and incubated for 36-40 hours at 20°C to reach L4 stage.

Virulence assay. The protocol was adapted from a previous study with the following amendments (Tan *et al.*, 1999). Briefly, *P. aeruginosa* PAO1 and *E. coli* HB101 control strains were cultured overnight (~22 hours) in LB broth to similar densities. 30 µl of the culture was spread (covering the entire surface) on a 30 mm diameter PGS [1% Bacto-Peptone, 1% NaCl,

1% glucose, 0.15 M sorbitol, and 1.7% agar] agar plate and incubated at 37°C for 16 hours. The plates with bacterial lawn were allowed to cool down to room temperature, and each plate was seeded with 10 L4 stage worms using a platinum wire. Plates were incubated at 25°C, and both live and dead worms were counted at 4 and 24 hours. Worms that did not respond to touch for ~15 s were counted as dead and those missing (hiding around the corners of plates) were excluded from the analysis.

3.5.12 Statistical analysis

Graphical representation of data and statistical analyses were executed in Prism 7.0. The results were considered statistically significant if the *P* value was lower than 0.05.

3.6 Supplementary data

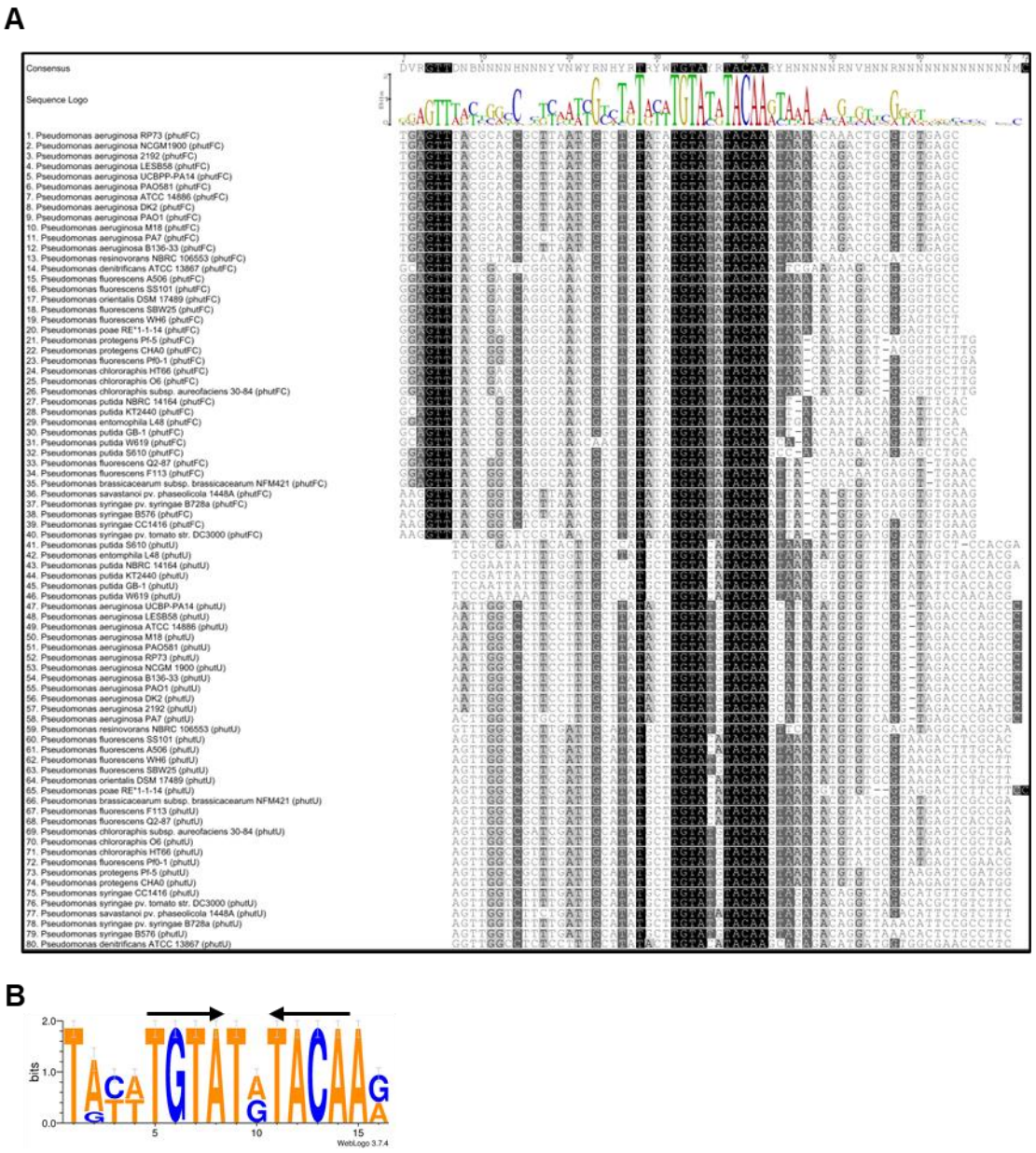

FIG S3.1 Sequence alignment of *hutU* and *hutFC* promoter sequences **(A)** and sequence logo of MEME generated motifs utilized for predicting HutC regulated candidate genes from the alignment **(B)**.
Inverted arrows denote the 8-bp palindromic HutC binding consensus sequence (TGTA-N2-TACA). Sequence logo was created in WebLogo 3. The sequences were aligned in geneious 9.0.5 and identical nucleotides in the alignment are highlighted in black.

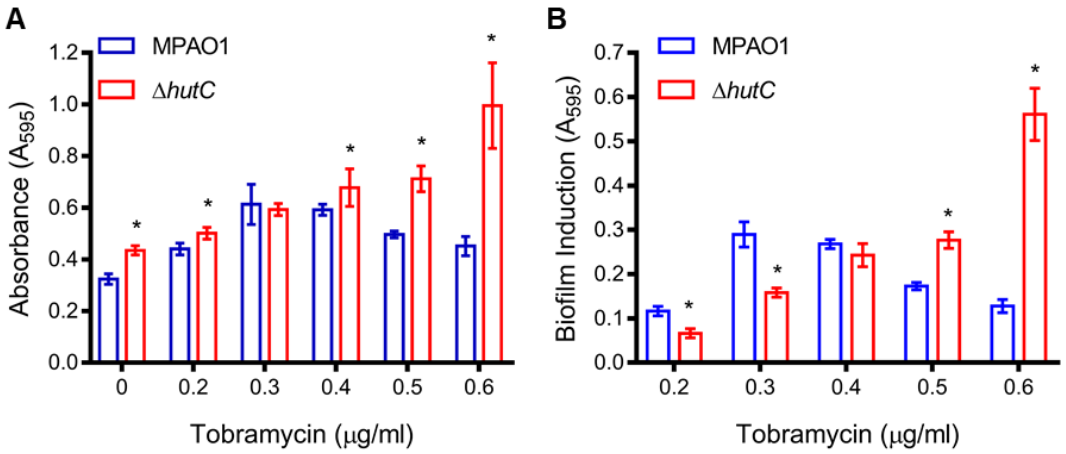

FIG S3.2 Role of *hutC* in tobramycin-induced biofilm formation in *P. aeruginosa* PAO1.
(A) Biofilm profiles MPAO1 (wild type) and MU61-69 (*hutC* deletion mutant) in the presence of sub-inhibitory concentrations of tobramycin. Data are means ± standard deviations of 8 replicate cultures. **(B)** Amount of biofilm induced at each tobramycin concentration with respect to biofilm formed in the absence of tobramycin by MPAO1 and MU61-69. Data obtained from (A) by extracting the amount of biofilm formed at zero tobramycin concentration from all points. Error bars represent standard error of the means.
Cells were grown statically in microtiter plates for 8 hours in LB medium supplemented with tobramycin at concentrations indicated in the figure. Asterisks denote statistical significance of biofilm formed by mutant compared to wild type at same tobramycin concentration; determined by student's t-test ($P < 0.05$).

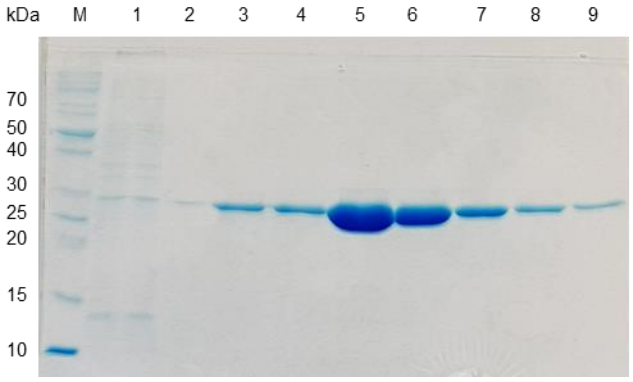

FIG S3.3 SDS-PAGE analysis of purified $HutC_{his6}$ protein from *P. aeruginosa* PAO1.
Lane M, Protein Ladder (Thermo Scientific); Lane 1, a small volume of total protein from lysate; Lane 2 & 3, flow-through fractions from wash steps with 5 mM and 70 mM imidazole, respectively; Lanes 4-9, elution fractions of $HutC_{his6}$ washed with 200 mM imidazole. Estimated molecular weight of HutC protein in 27.8 kDa.

Table S3.1 *In silico* predicted HutC-binding sites in *P. aeruginosa* PAO1.

Motifs[1]	Motif Location[3]		*P* value	Locus tag and gene/protein information
	Start	End		
TACT**TGTA**TG**TACA**AG[2]	5744858	5744873	3.89E-10	PA5100: *hutU*
AGCT**T**C**TA**TA**TACA**AG	1757703	1757718	1.26E-06	PA1613: hypothetical protein; PA1612: hypothetical protein; PA1614: glycerol-3-phosphate dehydrogenase, biosynthetic
GGCTG**GTA**GG**TACA**AG	5629913	5629928	5.42E-06	PA5011: *waaC*, heptosyltransferase I; PA5010: *waaG*, UDP-glucose:(heptosyl) LPS alpha 1,3-glucosyltransferase
TGCC**TGT**GTG**T**C**CA**AG	4198908	4198923	6.31E-06	PA3747: conserved hypothetical protein; PA3748: conserved hypothetical protein; PA3746: *ffh*, signal recognition particle protein
TGCT**TGTA**TT**T**T**CA**AC[2]	3173249	3173264	9.03E-06	PA2818: *arr,* aminoglycoside response regulator
TACGG**GTA**TA**TACA**CG	1396746	1396761	1.04E-05	PA1285: probable transcriptional regulator; PA1284: acyl-coA dehydrogenase; PA1286: probable major facilitator superfamily (MFS) transporter
TATA**TGTA**TA**TACA**AA[2]	5749411	5749426	1.32E-05	PA5106: *hutFC* PA5105: *hutC*
TGTT**TT**TGTA**TACA**AG	537923	537938	1.71E-05	PA0476: permease
TCCT**TGT**GCG**TACA**GG[2]	3138168	3138183	1.80E-05	PA2781: hypothetical protein; PA2780: *bsWR*, bacterial swarming regulator
TCCT**TGTA**AGC**ACA**AA	2549639	2549654	1.94E-05	PA2311: hypothetical proten; PA2310: hypothetical protein
TTGT**TGTA**GG**T**G**CA**AG	2766998	2767013	1.96E-05	PA2462: probable haemagglutinin
TCCT**TGT**GTG**T**G**CA**AC	3930462	3930477	2.04E-05	PA3514: probable ATP-binding component of ABC transporter
AACT**TG**A**A**TG**T**G**CA**GG	5928562	5928577	2.27E-05	PA5265: hypothetical protein
GACA**TG**A**A**TG**T**C**CA**AG	3648054	3648069	2.35E-05	PA3260: probable transcriptional regulator; PA3261: hypothetical protein

TACAG**GTA**TGA**ACA**TG	3549787	3549802	2.38E-05	PA3162: *rspA*, 30S ribosomal subunit
TACGG**G**C**A**TG**TACA**GG	2084259	2084274	2.49E-05	PA1910: *femA*, ferric mycobactin receptor
GACC**TGT**GTG**T**G**CA**AG	5355312	5355327	2.49E-05	PA4769: probable transcriptional regulator?; PA4770: *lldP*, lactate permease
TACG**TG**G**A**TG**T**G**CA**TG	4499829	4499844	2.53E-05	PA4020: *mpl*, UDP-N-acetylmuramate: L-alanyl-gamma-D-glutamyl-meso-diaminopimelate ligase
TACTG**GTA**GG**T**G**CA**TG	5172764	5172779	2.53E-05	PA4613: *katB,* catalase
CACCG**GTA**TGA**ACA**AG	6136787	6136802	2.58E-05	PA5447: *wbpZ*, lipopolysaccharide biosynthetic process
CACC**TG**G**A**TG**TACA**GG	5170863	5170878	2.67E-05	PA4613: *katB*, catalase; PA4612: hypothetical protein
TTTT**TGT**TTT**TACA**AG	3685174	3685189	2.74E-05	PA3291: *til1*; PA3292: hypothetical protein
CACC**TG**CCTG**TACA**AG	657340	657355	2.81E-05	PA0596: aminoglycoside phophotransferase?; PA0597: nucleotidyl transferase; PA0595: *ostA*, LPS assembly protein?
TAGA**TGT**GTG**TACA**GG	1985456	1985471	2.94E-05	PA1827: probable short chain-dehydrogenase, fatty acid metabolism?
TACT**TGTA**GG**T**G**CA**GC	2289653	2289668	3.35E-05	PA2080: *kynU*, kynureninase, Tryptophan metabolism; PA2079: probable amino acid permease
TAATG**G**CCTG**TACA**AG	3122777	3122792	3.54E-05	PA2763: hypothetical protein
TACA**T**CG**A**TG**T**T**CA**AG	5174644	5174659	3.67E-05	PA4616: encoding C4-dicarboxylate binding protein; PA4617: encoding a hypothetical protein?
GACG**TG**C**A**TG**TACA**AC	4840089	4840104	3.75E-05	PA4311: encoding glycoside hydrolase; PA4312: hypothetical proein
AACT**TG**C**A**TG**T**C**CA**AC	5182260	5182275	3.90E-05	PA4621: probable oxidoreductase; PA4622: probable major facilitator superfamily (MFS) transporter
TACT**TG**C**A**TGA**A**TTAG	3683857	3683872	4.03E-05	PA3290: *tle1*, hydrolase?
TACTG**GTA**TG**T**TTCAG	259666	259681	4.15E-05	PA0230: *pcaB*, 3-carboxy-cis, cis-muconate cycloisomerase
TACT**TGTA**CG**T**T**C**CAT	654607	654622	4.22E-05	PA0595: *ostA*, LPS assembly protein? PA0594: *surA*, peptidyl-prolyl cis-trans isomerase

TACA**T**TT**TA**TGA**A**G**A**AG	1246585	1246600	4.49E-05	
CGCA**TG**A**A**TGA**ACA**AG	1416960	1416975	4.56E-05	PA1305: hypothetical protein (MFS?); PA1304: probable oligopeptidase
TGCT**TG**CGAGA**ACA**AG	1103989	1104004	4.73E-05	PA1019: *mucK*, cis,cis-muconate transporter
TGCT**TG**ATTGA**ACA**GG	237162	237177	4.83E-05	PA0208: *mdcA*, malonate decarboxylase alpha subunit
TGCTG**G**G**A**TGA**AC**CAG	4766004	4766019	4.93E-05	PA4261: *rplW*, 50S ribosomal protein L23; PA4260: *rpiB*, 50S ribosomal protein L2
TACT**T**C**TA**TG**T**GA**A**CG	5550895	5550910	4.93E-05	PA4946: *mutL*, DNA mismatch repair protein
TGCCG**G**G**A**TGA**ACA**AG	403990	404005	4.93E-05	PA0360: hypothetical protein
CGCTG**G**A**A**TG**TACA**GG	4961313	4961328	4.93E-05	PA4427: *sspB*, stringent starvation protein C
TGCT**TGT**GGG**T**C**CA**GG	6168711	6168726	5.15E-05	PA5476: *citA*, citrate transporter
TACT**T**C**TA**TCC**ACA**GG	3561017	3561032	5.23E-05	PA3170: N-ethylammeline chlorohydrolase; PA3171: *ubiG*, 3-demethylubiquinone-9 3-methyltransferase
AGCTC**G**G**A**TG**TAC**TAG	4101948	4101963	5.42E-05	PA3660: sodium/hydrogen antiporter; PA3661: hypothetical protein
TGCC**TG**C**A**GG**TACA**GG	753190	753205	5.51E-05	PA0690: *pdtA*, phosphate depletion regulated TPS partner A
TGCC**TG**GCTGG**ACA**AG	3058190	3058205	5.51E-05	PA2704: probable transcriptional regulator
GGCC**TGTA**CG**TACA**GG	4371161	4371176	5.51E-05	PA3901: *fecA*, Fe(III) dicitrate transport protein
CGCC**TG**C**A**AG**TACA**AG	4274816	4274831	5.63E-05	PA3818: *suhB*, extragenic supprerssor protein; PA3817: probable methyltransferase
TGCTC**G**C**A**TGAT**CA**AG	3543504	3543519	5.68E-05	PA3158: *wbpB*, UDP-2-acetamido-2-deoxy-d-glucuronic acid 3-dehydrogenase; PA3157: probable acetyltransferase
TGCCG**GT**CTG**TAC**CAG	4050611	4050626	5.70E-05	PA3615: hypothetical protein
GGCT**TG**C**A**TG**T**C**CA**TG	1429003	1429018	5.74E-05	PA1317: *cyoA*, cytochrome o ubiquinol oxidase subunit II; PA1318: *cyoB*, cytochrome o ubiquinol oxidase subunit I
CGCC**TG**C**A**TG**T**C**CA**AG	4123169	4123184	5.79E-05	PA3680: rRNA small subunit methyltransferase J
CGCC**TGTA**TG**T**C**CA**CG	3802221	3802236	5.79E-05	PA3396: *nosL*, putative nitrous oxide reductase protein

TATT**TA**T**A**TG**T**GA**A**AG	4820039	4820054	5.91E-05	PA4295: *fppA*, Fip prepilin peptidase A; PA4294: hypothetical protein; PA4296: *pprB* -two-component response regulator
AGCTG**GTA**TCG**ACA**AG	3541132	3541147	6.00E-05	PA3157: probable acetyltransferase; PA3156: *wbpD*, UDP-2-acetamido-3-amino-2,3-dideoxy-d-glucuronic acid N-acetyltransferase
TGCA**TGT**CTGG**ACA**AA[2]	1404013	1404028	6.09E-05	PA1292: probable 3-mercaptopyruvate sulfurtransferase
GGAA**TG**C**A**TG**TACA**AG	4095558	4095573	6.09E-05	PA3657: *map*, methionine aminopeptidase; PA3658: *glnD*, protein-PII uridylyltransferase; PA3656: *rpsB*, 30S ribosomal protein S2
TGAA**TGTA**TGGT**CA**AG	1483097	1483112	6.16E-05	PA1369: hypothetical protein; PA1368: hypothetical protein
GGCT**TG**C**A**TGA**A**G**A**AG	517382	517397	6.25E-05	PA0458: probable major facilitator superfamily (MFS) transporter; PA0459: probable ClpA/B protease ATP binding subunit
AGCT**TGTA**GG**T**G**CA**AT	3343461	3343476	6.33E-05	PA2985: hypothetical protein; PA2984: hypothetical protein
TGCGG**GTA**TGC**A**G**A**AG	4625069	4625084	6.41E-05	PA4135: probable transcriptional regulator?
TGGTG**G**G**A**TG**TACA**TG	3325385	3325400	6.51E-05	PA2966: *acpP*, acylcarrier protein; PA2967: *fabG*, 3-oxoacyl-[acyl-carrier-protein] reductase
TGCT**TG**CGGC**TACA**AG	4756156	4756171	6.51E-05	PA4239: *rpsD*, 30S ribosomal protein S4; PA4240: *rpsK*, 30S ribosomal protein S11
TGTG**TGTA**TG**T**G**CA**GG	5122395	5122410	6.51E-05	PA4574: membrane protein
TGCC**TG**C**A**TGG**A**A**A**AG	995110	995125	6.61E-05	PA0911: *alpE*
TGCC**TG**A**A**TCC**ACA**AG	174721	174736	6.73E-05	PA0153: *pcaH*, protocatechuate 3,4-dioxygenase, beta subunit
TGAT**TG**CCTG**T**T**CA**AG	3406738	3406753	7.02E-05	PA3044: *rocsS2*, two component sensor
TGCT**T**TCCTG**TACA**GG	1515487	1515502	7.14E-05	PA1393: *cysC*, adenosine 5'-phosphosulfate (APS) kinase
TGCTCC**T**TTGG**ACA**AG	2824541	2824556	7.14E-05	PA2505: *opdT*, tyrosine porin OpdT
TGCT**TGT**CTG**T**CTGAG	3752459	3752474	7.14E-05	PA3340: hypothetical protein; PA3341: probable transcriptional regulator

TGCT**TGTA**CG**C**A**TA**CG	724610	724625	7.23E-05	PA4280.2: 23SrRNA
TGCT**TGTA**CG**C**A**TA**CG	4791203	4791218	7.23E-05	PA4690.2: 23SrRNA
TGCT**TGTA**CG**C**A**TA**CG	5266731	5266746	7.23E-05	PA5369.2: 23SrRNA
TGCT**TGTA**CG**C**A**TA**CG	6042215	6042230	7.23E-05	PA0668.4: 23SrRNA
TGGT**TGTA**AG**TACA**GA	1485968	1485983	7.29E-05	
TGCTA**GT**GTG**TA**A**A**AC	3546997	3547012	7.41E-05	PA3160: *wzz*, o-antigen chain length regulator
TGCT**TGTA**TC**T**CA**A**GG	417508	417523	7.57E-05	PA0372: zinc protease; PA0373: *ftsY*, signal recognition particle receptor
TGCACC**TA**TG**TACA**AT	5672231	5672246	8.09E-05	PA5036: *gltB*, glutamate synthase large chain precursor
CGGT**T**TC**A**TG**TACA**AG	5426167	5426182	8.17E-05	PA4835: *cntM*; PA4834: *cntI*, putative nicotianamine synthase
TGCT**TG**A**A**TT**TA**A**A**AA	1245777	1245792	8.29E-05	PA1151: *imm2*, pyocin S2 immunity protein
TGCT**T**A**TA**AC**TA**T**A**AG	1692716	1692731	8.35E-05	PA1554: *ccoN1*, cytochrome c oxidase, Cbb3-type
TGTC**TGTA**TG**TA**A**A**AA	1400645	1400660	8.40E-05	PA1288: probable outer membrane protein precursor, long chain fatty acid transporter?
TGGT**TGTA**TG**TA**G**A**TC	3542886	3542901	8.47E-05	PA3158: *wbpB*, UDP-2-acetamido-2-deoxy-d-glucuronic acid 3-dehydrogenase; PA3157: probable acetyltransferase
TCCG**T**AG**A**TA**TACAA**G	3683450	3683465	8.80E-05	PA3290: *tle1*, hydrolase?
CCCTA**GTA**TA**TA**G**A**AG[2]	830916	830931	8.87E-05	PA0761: *nadB*, L-aspartate oxidase; PA0762: *algU*, Alginate biosynthesis
TCCT**T**A**TA**TAA**A**G**A**AG	3329662	3329677	9.15E-05	
TACT**TG**A**A**AAC**AC**CAG	6090728	6090743	9.40E-05	PA5412: hypothetical protein
TACG**TG**G**A**TA**T**G**CA**TG	3450837	3450852	9.44E-05	PA3077: *cprR*, two-component response regulator
TCCT**T**C**TA**TA**T**G**CA**AT	2473522	2473537	9.55E-05	PA2247: *bkdA1*, 2-oxoisovalerate dehydrogenase (alpha subunit); PA2246: *bkdR*, transcriptional regulator
TACGG**GTA**TA**TAC**CCG	1397225	1397240	9.60E-05	PA1286: major facilitator superfamily transporter
AAGCT**TG**A**A**CT**TACA**CA[2]	3377524	3377540	5.43E-05	PA3014: *faoA*, fatty-acid oxidation complex alpha-subunit; PA3015: hypothetical protein

ATAGTC**GG**A**A**T**TACA**AG[2]	2343116	2343132	7.79E-05	PA2128: *cupA1*, fimbrial subunit
TATTG**GTA**TAG**AC**CAG	597683	597698	3.63E-05	PA0538: *dsbB*, disulfide bond formation protein; PA0539: hypothetical protein
GACA**TGTA**TA**TA**T**A**CG	5897294	5897309	3.88E-05	PA5238: o-antigen acetylase; PA5237: conserved hypothetical protein
TATT**TG**C**A**TT**TA**A**A**AA	2905126	2905141	3.95E-05	PA2569: hypothetical protein
TCTT**TG**G**A**TAG**ACA**AA	5747948	5747963	4.81E-05	PA5103: *puuR,* ABC transporter substrate binding protein
CACT**TGT**CTAG**ACA**AA	3788175	3788190	4.95E-05	PA3381: GntR family transcriptional regulator
TACA**TG**GTTA**TTCA**AA	699967	699982	5.12E-05	PA0643: hypothetical protein; PA0644: hypothetical protein
CATT**T**C**TA**TA**TA**G**A**AG	1558933	1558948	5.37E-05	PA1431: *rsaL*, regulatory protein; PA1432: *lasI*
TACT**T**A**TA**AA**TA**A**A**AA	5820495	5820510	6.26E-05	PA5170: *arcD*, arginine ornithine antiporter
TATT**T**A**TA**TA**TT**C**G**AA	2607095	2607110	6.49E-05	PA2359: *sfa3*, probable transcriptional regulator
TATA**T**TC**A**GA**TACA**AA	213605	213620	6.68E-05	PA0187: hypothetical protein
TGTA**TG**A**A**TG**TACA**GT	2516349	2516364	6.86E-05	PA2288: hypothetical protein
TGTA**TGTA**AA**TACA**GT	732791	732806	7.09E-05	PA0672: *hemO*; heme oxygenase PA0671: hypothetical protein
TGCA**TGT**GTA**T**G**C**CAG	5894399	5894414	7.49E-05	PA5236: probable aromatic hydrocarbon reductase
TGCC**T**T**T**GTA**TACA**AA	1652031	1652046	7.68E-05	PA1520: GntR family transcriptional regulator; PA1519: probable transporter
TGAT**TGTA**TAC**A**T**A**AA	4387175	4387190	8.25E-05	PA3918: *moaC*, molybdopterin biosynthetic protein C
TGTA**T**T**T**TTA**TACA**GG	514572	514587	8.79E-05	PA0456: cold-shock protein; PA0455: *dbpA*, RNA helicase
TGTA**TGTA**AA**T**GT**A**AA	4663738	4663753	9.92E-05	PA4167: oxidoreductase; PA4168: *fpvB*, second ferric pyoverdine receptor
TGTT**TGTA**TAC**A**A**A**CA	1746114	1746129	9.94E-05	PA1602: probable oxidoreducatse

TACA**TG**A**A**TGAT**CA**AA	559489	559504	4.24E-05	PA0500: *bioB*, biotin synthase; PA0499: probable pilin assembly chaperone protein
CTGTATA**TG**G**A**TAC**A**GTA	81078	81095	4.63E-06	PA0069: conserved hypothetical protein
CAGGATA**TG**A**A**TT**TAC**CA	5601089	5601106	1.00E-05	PA4986: probable oxidoreductase; PA4985: hypothetical protein
CTGTTAAG**GT**CTA**TG**C**A**A	3852568	3852585	1.13E-05	PA3446: NADPH dependent reductase; PA3445: hypothetical protein
CGGGGTA**TGTA**TA**TAC**CC	1073918	1073935	1.18E-05	PA0993: *cupC2*, pili and flagellar chaperone
CTGGTTA**TG**GGCA**TACA**A	4936915	4936932	1.24E-05	PA4405: hypothetical protein; PA4403: *secA,* secretory protein
CTGTTTC**TG**G**A**TC**TACA**G	4360251	4360268	1.48E-05	PA3893: conserved hypothetical protein
CTGCCCA**TG**G**A**TA**TACA**C	4612428	4612445	1.57E-05	PA4124: *hpcB*, homoprotocatechuate 2,3-dioxygenase; PA4123: *hpcC*, 5-carboxy-2-hydroxymuconate semialdehyde dehydrogenase
AAGAATA**TGT**CTA**TT**C**A**A	883205	883222	2.13E-05	PA0805: hypothetical protein; PA0806: hypothetical protein
CAGTATA**TT**T**C**GAG**ACA**A	3772701	3772718	2.69E-05	PA3361: *lecB*, fucose-binding lectin PA-IIL, biofilm and cell movement; PA3360: probable secretion protein
CTGTATAA**GTA**GAC**A**GTA	4052648	4052665	2.69E-05	PA3617: *recA*; PA3619: hypothetical protein
CTCGATC**TGT**CTC**TACA**A	5392120	5392137	3.78E-05	PA4806: probable transcriptional regulator; PA4805: probable class III aminotransferase
GTGTATAAA**TA**TCC**ACA**A	2228861	2228878	4.50E-05	PA2037: hypothetical protein
ATGTATT**TGTA**TAG**A**T**A**T	5225915	5225932	5.39E-05	PA4658: hypothetical protein
CTCTTTA**T**C**TA**AA**TA**A**A**A	1284353	1284370	5.97E-05	PA1182: probable transcriptional regulator; PA1183: *dctA*, C4-dicarboxylate transport protein
CTGTGAG**TG**A**A**GA**T**G**CA**A	6247728	6247745	6.20E-05	PA5552: *glmU*, glucosamine-1-phosphate acetyltransferase/N-acetylglucosamine-1-phosphate uridyltransferase

CAGTATT**TG**A**A**AAAG**CA**A	2761622	2761639	6.21E-05	PA2461: hypothetical protein
CGGAAGA**TG**GCTAA**ACA**A	5069048	5069065	6.35E-05	PA4526: *pilB*, type 4 fimbrial biogenesis protein PilB
CTGGAAG**TG**G**A**TA**TCCA**G	4888917	4888934	6.50E-05	PA4360a: hypothetical protein
CTGGATC**TG**GCAAA**ACA**A	501082	501099	6.74E-05	PA4797: probable transposase
CTGACTC**TGGA**AA**TACA**G	5003763	5003780	6.74E-05	PA4474: *tldD*, protease
CAGTATC**TG**C**A**AGG**ACA**A	5220234	5220251	6.74E-05	PA4653: *cupE6*, adhesin-like protein
CTGGAAA**TG**A**A**TA**TCC**TG	4273643	4273660	6.89E-05	PA3816: *cysE*, O-acetylserine synthase; PA3817: probable methyltransferase; PA3818: *suhB*, extragenic supprerssor protein
CTGTACA**TG**A**A**GG**TGCA**C	4169578	4169595	7.07E-05	PA3724: *lasB*, elastase; PA3723: probable FMN oxidoreductase
CTGCAGA**TG**A**A**CAG**ACG**A	5562432	5562449	7.07E-05	PA4957: *psd*, phosphatidylserine decarboxylase
CCGTGGC**TG**A**A**TA**TGCA**A	1058947	1058964	7.07E-05	PA0975: probable radical activating enzyme; PA0976: hypothetical protein
CTGAAGC**TGTA**CG**TACA**G	1738442	1738459	7.07E-05	PA1596: *htpG*, heat shock protein; PA1597: hypothetical protein
CTGTACA**TG**A**A**GGG**ACC**A	2654275	2654292	7.07E-05	PA2397: *pvdE*, pyoverdine biosynthesis protein; PA2398: *fpvA*, ferripyoverdine receptor
CTGGATA**TG**G**A**AACC**CA**G	3679970	3679987	7.07E-05	PA3286: beta-acetoacetyl-acyl carrier protein synthase; PA3287: hypothetical protein
CCGCGCAA**G**A**A**TA**TACA**A	1980983	1981000	7.44E-05	PA1822: *fimL*, hypothetical protein
CGGTAGA**TGTA**CA**TGC**CG	5303847	5303864	7.44E-05	PA4725: *cbrA*; PA4724.1: conserved hypothetical protein
CTGCAGGC**G**G**A**TA**TACA**G	5960101	5960118	7.44E-05	PA5294: putative multidrug efflux pump; PA5293: transcriptional regulator
CTGGAGG**TG**C**A**CA**TACA**G	2027429	2027446	7.44E-05	PA1866: ATP dependent DNA helicase
CGGTATCG**GTA**TAGG**C**CA	5054512	5054529	7.44E-05	PA4515: hydroxylase; PA4514: *piuA*, probable outer membrane receptor for iron transport
CTGGATC**TG**G**A**TGGT**CA**A	3759625	3759642	7.65E-05	PA3347: *hsbA*, biofilm anti-anti-sigma factor
CTGAAGA**TG**CGCA**TCCA**A	1721288	1721305	7.88E-05	PA1582: *sdhD*, encoding succinate dehydrogenase D subunit

CTGGTGGG**GT**TTA**TACA**A	2762064	2762081	7.88E-05	PA2461: hypothetical protein
CTGAACC**TG**G**A**TA**T**C**CA**G	509367	509384	7.88E-05	PA0452: probable stomatin-like protein; PA0451a: amino acid ABC transporter substrate binding protein
CTGGAAAG**G**C**A**CA**TACA**C	795731	795748	7.88E-05	PA0727: Pf replication initiator protein PA0728: probable bacteriophage integrase
CAGCACA**TG**G**A**TC**T**G**CA**A	2549213	2549230	7.88E-05	PA2310: taurine metabolism?; PA2311: hypothetical protein; PA2309: hypothetical protein
CCGAGTA**TG**C**A**TGC**ACA**A	4783725	4783742	7.88E-05	PA4275: *nusG*, transcription-antitermination protein; PA4274: 50S ribosomal protein L11
CGGAATA**TG**C**A**TA**T**T**C**CG	2312407	2312424	8.14E-05	PA2101: hypothetical protein; PA2100: probable transcriptional regulator
CTGGAAA**TGTA**AT**T**T**CA**T	2843707	2843724	8.14E-05	PA2523: *czcR*, two component response regulator; PA2522: *czcC*, outer membrane protein precursor
CTGAGTA**TGTA**CCGT**CA**A	2964727	2964744	8.14E-05	PA2621: *clpS*, biofilm related gene; PA2620: *clpA*, ATP-binding protease component; PA2622: *cspD*, encoding cold-shock protein
CTGCGTC**TG**G**A**TG**TAC**CA	1276651	1276668	8.36E-05	PA1176: *napF*, ferredoxin protein; PA1177: *napE*, periplasmic nitrate reductase protein; PA1178: *orpH*, PhoP/Q and low Mg2+ inducible outer membrane protein H1 precursor
CTGTACA**TG**GGCC**T**G**CA**A	1769581	1769598	8.36E-05	PA1626: probable major facilitator superfamily transporter
CGGCATGC**GTA**TC**TAC**GA	4380756	4380773	8.36E-05	PA3910: *eddA*, extracellular DNA degradation protein; PA3909: *eddB*, extracellular DNA degradation protein
CTGTACC**TGT**GGC**T**G**CA**A	4723280	4723297	8.36E-05	PA4219: *ampO*; PA4218: *ampP*, regulation of beta-lactamase activity
CTGTAGAG**GTA**GTCC**CA**A	5352392	5352409	8.56E-05	PA4764: *fur*, ferric uptake regulation protein; PA4765: *omlA*, outer membrane lipoprotein precursor
CTGGATC**TG**G**A**TG**TTCA**C	6038962	6038979	8.56E-05	PA5369: *pstS*, phosphate ABC transporter, periplasmic phosphate-binding protein

CTGGCCA**TG**ACTAC**ACA**A	4252998	4253015	8.73E-05	PA3793: hypothetical protein; PA3795: probable oxidoreductase
CAGTATTC**GTA**CA**TC****CA**G	1294152	1294169	8.93E-05	PA1193: hypothetical protein; PA1191: hypothetical protein
CTGCACA**TGT**TCAAG**CA**A	1779871	1779888	8.93E-05	PA1635: *kdpC*, potassium transporting ATPase, C chain
CTGTATTC**GA****A**TA**TC****C**GT	2555567	2555584	9.12E-05	PA2317: probable oxidoreductase; PA2318: hypothetical protein
CCGTCCA**TGT**CGA**TG****CA**A	4301478	4301495	9.12E-05	PA3839: probable sodium:sulfate symporter; PA3840: conserved hypothetical protein
CTGTCGA**TG**CCTA**TC****C**GA	5924360	5924377	9.12E-05	PA5262: *fims*, cell motility; PA5263: *argH*, argininosuccinate lyase
CTGTTCG**TG****G****A**TA**TC****CA**C	3689962	3689979	9.32E-05	PA3295: probable HIT family protein; PA3296: *phoA*, alkaline phosphatase
CTGGATTC**GTA**CA**TC****CA**G	1885705	1885722	9.32E-05	PA1742: *pauD2*, glutamine amidotransferase class I; PA1741: hypothetical protein
CTGCTTA**TGTA**TTGG**CA**C	5308573	5308590	9.44E-05	PA4726.11: *crcZ*, ncRNA
CTGTCCA**TGTA**TCAC**C**TA	2004325	2004342	9.57E-05	PA1844: *tse1*; PA1843: *metH*, methionine synthase; PA1846: *cti*, cis/trans isomerase
CGGAATA**TG****G****A**AAG**A**A**A**A	3937412	3937429	9.57E-05	PA3519: hypothetical protein; PA3520: putative periplasmic substrate binding protein
CTGCTTCC**G**C**A**TG**TACA**A	3207627	3207644	9.84E-05	PA2854: putative L,D-transpeptidase
CAGAATA**TG****G****A**TA**T**GGGA	3803461	3803478	9.84E-05	PA3397: *fprA*, heme catabolic process?; PA3398: probable transcriptional regulator

[1]half-sites corresponding to the HutC-binding consensus sequence (**TGTA**-N2-**TACA**) are underlined and identical nucleotides are shown in boldface.

[2]candidates subjected to EMSA analysis

[3]motif location in the genome

3.7 Statement of Contribution

Cloning of *hutC* gene into the protein expression vector was carried out by a previous researcher, Dr Monica Gerth, and was available at the beginning of my PhD study in Zhang lab. This work also involved the use of a *hutC* mutant strain constructed by Dr Monica Gerth. The specific details are provided in the list of bacterial strains and plasmids (Table 3.2).

I trained an undergraduate student, Sara Hammouda, who performed assays for biofilm data shown in Fig. 3.7B, 3.7D, and 3.9B, under my supervision.

Chapter 4

Dissecting the regulatory role of HutC on *hutF* expression in *Pseudomonas*

4.1 Abstract

The HutC transcription factor negatively regulates the expression of histidine utilization (*hut*) genes in *Pseudomonas* in response to the presence of histidine or urocanate in the medium. The detailed regulatory mechanisms have been studied in a model organism of *P. fluorescens* SBW25 in regard to the expression of *hutU* promoter (P_{hutU}). HutC recognizes a highly conserved Phut site (TGTA-N2-TACA); and surprisingly, it also recognizes a distinct Pntr site (GCACCA-N3-TGGTGC) that shows little sequence similarity with the Phut site. The role of HutC targeting the Pntr site in the *ntrBC* promoter has been functionally characterized (Naren and Zhang, 2021). In this work, we focused on the role of HutC in regulating the *hutF* promoter activities in two model *Pseudomonas* strains: *P. fluorescens* SBW25 and *P. aeruginosa* PAO1. Results of protein-DNA interaction assays (EMSA and DNase I footprinting) led to a surprising finding that the P_{hutF} promoter of *P. fluorescens* SBW25 contains two distinct HutC-binding sites (Phut and Pntr), whereas the *P. aeruginosa* P_{hutF} promoter harbours only the Phut site. Next, we performed functional analysis of this newly identified Pntr site in terms of bacterial growth on histidine. Results showed that the Pntr site was required for histidine utilization in *P. fluorescens* SBW25 but produced negligible effects in *P. aeruginosa* PAO1. Together, our data provide valuable empirical evidence for HutC functioning as a unique transcriptional factor that can recognize two distinct DNA binding motifs.

4.2 Introduction

HutC has long been known as a transcriptional repressor of histidine utilization (*hut*) genes in *Pseudomonas* and some enteric bacteria (Smith & Magasanik, 1971a, Consevage *et al.*, 1985, Hu *et al.*, 1989, Allison & Phillips, 1990, Schwacha & Bender, 1990, Zhang & Rainey, 2007b, Yuji, 2010). HutC belongs to the second largest sub-family of the GntR family of transcriptional regulators. GntR family transcriptional regulators possess a winged helix-turn-helix DNA binding domain at the N-terminus and substrate binding domain at the C-terminus (Gorelik *et al.*, 2006, Suvorova *et al.*, 2015). The expression of *hut* genes is tightly regulated to prevent toxicity from the accumulation of various intermediates during histidine catabolism. It is known that in the absence of histidine and urocanate (inducers), HutC occupies the promoter regions of *hut* transcriptional units repressing *hut* gene expression. However, inducer mediated confirmational change is thought to dissociate HutC from the promoter regions; consequently, relieving repression on the expression of *hut* genes (Itoh *et al.*, 2007, Bender, 2012).

Genetic studies on the characterisation of histidine utilization genes and regulatory mechanisms date to the 1950s (Itoh *et al.*, 2007, Bender, 2012). Previous studies on the interaction of HutC with *hut* transcriptional units could not elucidate a precise mode of action of HutC on *hut* promoters due to the unavailability of highly purified HutC proteins or clear knowledge on the specific HutC-binding site sequences (Hagen & Magasanik, 1973, Hu *et al.*, 1989). However, a recent study from our laboratory utilizing highly purified HutC protein updated our knowledge on the mode of action of HutC with *hutU* promoter in *Pseudomonas fluorescens* SBW25 (Naren & Zhang, 2020). HutC recognizes a palindromic sequence (TGTA-N2-TACA) in the *hutU* promoter and binds each half-site as monomers to form a dimer-DNA complex, and subsequently undergoes further oligomerization via protein-protein interactions to form a tetramer. Tetramer formation is required for a stronger repression of *hutU* promoter. Further, urocanate disrupted both protein-DNA and protein-protein interactions in a concentration dependent manner (Naren & Zhang, 2020). Similar formation of higher order oligomers by HutC protein dependent on urocanate has also been observed in *P. aeruginosa* PAO1 (Chapter 3), suggesting that the HutC mode of action and regulatory mechanism are conserved between *hutU* promoters in both the species, and presumably in others.

Genetic organization of *hut* genes is highly conserved among *Pseudomonas* spp. including *P. putida*, *P. fluorescens* SBW25, and *P. aeruginosa* PAO1 (Itoh *et al.*, 2007, Bender, 2012, Winsor *et al.*, 2016). In the above three *Pseudomonas* spp. and many others, *hutC* is divergently transcribed from the *hutF* gene, encoding for FIGLU deiminase, that catalyses the conversion of FIGLU to formylglutamate (Itoh *et al.*, 2007, Zhang & Rainey, 2007b, Bender, 2012). Gene expression studies in *P. fluorescens* SBW25 (Zhang & Rainey, 2007b) and *P.*

putida (Leidigh & Wheelis, 1973, Consevage *et al.*, 1985, Hu & Phillips, 1988) indicate that urocanate induces HutF and HutC expression, and both *hutF* and *hutC* genes are subject to negative regulation by HutC repressor protein. In both the species, the intergenic region between *hutF* and *hutC* contains a single putative HutC-binding site (Zhang & Rainey, 2007b, Allison & Phillips, 1990) that the HutC repressor protein presumably uses to regulate both genes. Currently, there is no published data on the precise mode of action of HutC on this single binding site between *hutF* and *hutC* genes.

In Chapter 3, *in silico* analysis for novel HutC-target sites in the *P. aeruginosa* PAO1 genome also identified a single putative HutC-binding site sequence between divergently transcribed *hutF* and *hutC* genes. In this study, we examined the molecular interaction between purified HutC protein and this operator site to understand the HutC mode of action on the divergently transcribed genes. Interestingly, we found that HutC interacts with this operator site as a dimer and bound a shorter region relative to the *hutU* promoter (Chapter 3). Parallel studies in *P. fluorescens* SBW25 revealed that HutC forms a hexamer with the *hutFC* regulatory DNA and binds a relatively longer region. Subsequent analysis revealed that the dissimilarities in the binding pattern were not caused by different HutC proteins from the two species. Instead, an additional but distinct HutC-binding site proximal to the *hutF* gene in *P. fluorescens* SBW25 contributed to protein oligomerization along the DNA. This novel binding site displays similarity with the NtrC-binding consensus sequence, which was designated the Pntr site, and functionally characterised in the NtrBC promoter in *P. fluorescens* SBW25 (Naren & Zhang, 2021). Further phenotypic analysis revealed that the Pntr site was significant for growth on histidine and expression of wild-type levels of HutF in *P. fluorescens* SBW25.

4.3 Results

4.3.1 Molecular interactions of HutC with P_{hutFC} DNA from *P. aeruginosa* PAO1

We examined the molecular interaction of HutC with P_{hutFC} DNA by EMSA using purified $HutC_{his6}$ protein and a 176-bp biotinylated P_{hutFC}-176 DNA probe (Fig. 4.1B). As expected, we observed a single unshifted band in lane 1 (free probe), while a $HutC_{his6}$ concentration-dependent shift in the biotin labelled probe was seen in lanes 5-8. However, addition of 20-fold molar excess of unlabelled P_{hutFC}-158 DNA probe into the reaction mixture (Fig. 4.1B, lane 10) resulted in a near elimination of the shifted complex, suggesting that this interaction is specific. Notably, $HutC_{his6}$ interaction with P_{hutFC}-176 DNA resulted in a single shifted band suggesting that HutC may bind to P_{hutFC} DNA as a dimer, given that two Phut half-sites were identified in the promoter. $HutC_{his6}$ binding affinity for the P_{hutFC} DNA was estimated from the

EMSA gel by determining the apparent dissociation constant (K_d). K_d was obtained by plotting the fractions of $HutC_{his6}$-P_{hutFC}-176 complex against $HutC_{his6}$ concentrations (Fig. 4.1C). The K_d was found to be 1.34 ± 0.11 µM [Mean ± SE].

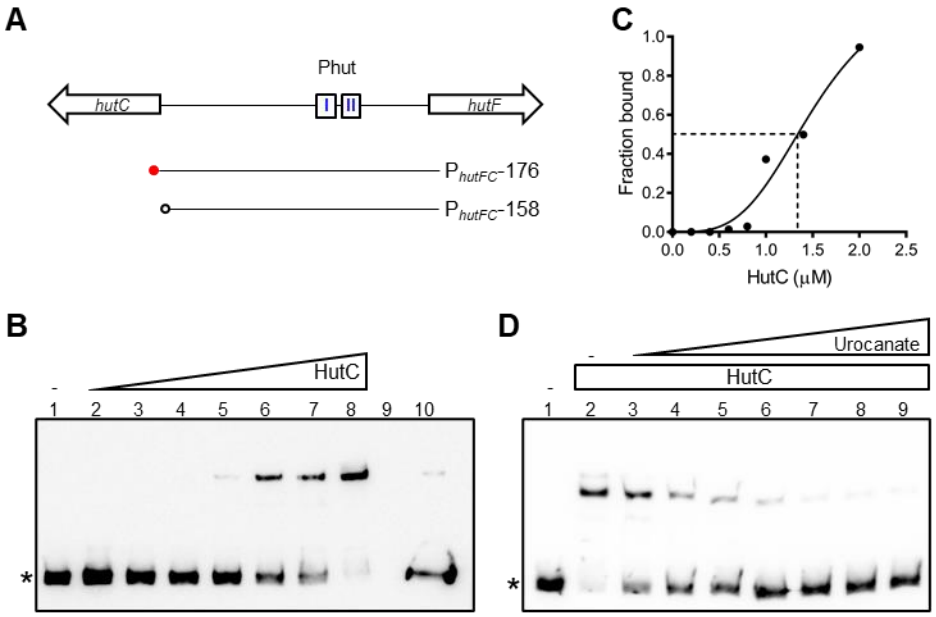

FIG 4.1 EMSA analyses of $HutC_{his6}$ interaction with P_{hutFC}-176 DNA from *P. aeruginosa* PAO1.
(A) Schematic representation of the genetic loci of divergently transcribed *hutF* and *hutC* genes, biotin labelled DNA probe used for EMSAs (red circle), and unlabelled competitor (unfilled circle). The putative Phut half-sites (Phut-I and Phut-II) are marked in blue.
(B) $HutC_{his6}$ was added at increasing concentrations of 0, 200, 400, 600, 800, 1000, 1400, and 2000 nM in lanes 1 to 8. Lane 9 is empty and lane 10 contains x20 molar excess unlabelled specific competitor.
(C) Estimation of dissociation constant (K_d) from (B). K_d was obtained by interpolation of the line of best fit.
(D) The concentration of $HutC_{his6}$ was held constant, and urocanate was added at increasing concentrations of 0, 0.05, 0.1, 0.2, 0.3, 0.4, 0.6, and 1.0 mM (lanes 2 to 9), respectively.
Asterisk denotes free probe. The biotin labelled P_{hutFC}-176 probe was used at 20 nM in the EMSAs.

Urocanate is the known physiological inducer of *hut* genes, activating *hut* expression. We next investigated the effect of urocanate on $HutC_{his6}$ interaction with P_{hutFC}-176 DNA probe by EMSA (Fig. 4.1D). $HutC_{his6}$ concentration was held constant, and urocanate was added at increasing concentrations from 0 to 1.0 mM (lanes 3-9). We observed a urocanate concentration-dependent dissociation of HutC from the $HutC_{his6}$-P_{hutFC}-176 complex. The intensity of the shifted band was minimal at urocanate concentration of 1.0 mM (lane 9). Taken together, we propose that HutC binds to P_{hutFC} DNA as a dimer and this complex is dissociated in the presence of urocanate.

4.3.2 Characterization of the stoichiometry of HutC-P_{hutFC} complex in *P. aeruginosa* PAO1

The presence of two Phut half-sites in the P_{hutFC} DNA and a single shifted band observed in the EMSA led us to propose that HutC binds to P_{hutFC} DNA as a dimer. We next performed continuous variation analysis (Job plot) to determine the stoichiometry of the HutC-P_{hutFC} complex by EMSA method (Fig. 4.2). The total molar concentration of the $HutC_{his6}$ and P_{hutFC}-176 probe was held constant at 400 nM and their molar ratio was varied. Intensities of the shifted bands were measured using ImageJ program and was plotted against $HutC_{his6}$ fraction for each Protein-DNA complex. The point of intersection of the rising and falling subsets of data gives a value of 0.650 [$HutC_{his6}$, nM], that corresponds to a ratio of 1:1.87 (P_{hutFC}-176:$HutC_{his6}$). Indeed, the result is consistent with our prediction that HutC binds to P_{hutFC} DNA as a dimer.

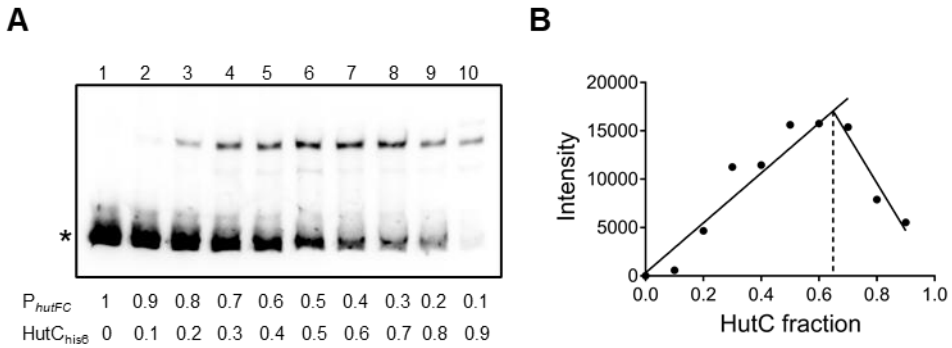

FIG 4.2 Continuous variation analysis of $HutC_{his6}$ binding to P_{hutFC} DNA from *P. aeruginosa* PAO1.
(A) EMSA showing $HutC_{his6}$ binding to P_{hutFC}-176 DNA. The total molar concentration of $HutC_{his6}$ and P_{hutFC}-176 was held constant at 400 nM and their molar ratio was varied as indicated in the figure.
(B) Analysis of the data from (A) by Job Plot method. The straight lines are the lines of best fit from linear regression analysis to the rising and falling subsets of data. The point of intersection of the lines yields a binding stoichiometry of 1:1.87.

4.3.3 Determining the HutC-binding site sequences in P_{hutFC} DNA in *P. aeruginosa* PAO1

To determine the specific HutC-binding site sequence in P_{hutFC} DNA, DNAse I footprinting was performed with purified $HutC_{his6}$ protein and a 176-bp biotinylated P_{hutFC} DNA probe (used for EMSA) from *P. aeruginosa* PAO1 (Fig. 4.3A). We observed that a 32-bp region in P_{hutFC} DNA was protected from DNAse I digestion (Fig. 4.3A, lanes 2 and 3). This protected region contains the putative Phut site (TGTA-N2-TACA) and predicted -35 and -10 elements of *hutC* and *hutF* promoters, respectively (Fig. 4.3B). The results from our *in vitro* study are consistent

with the predicted repressor role of HutC in *hut* gene expression, where HutC blocks RNA polymerase from binding to the promoter and initiating transcription by occluding the promoter.

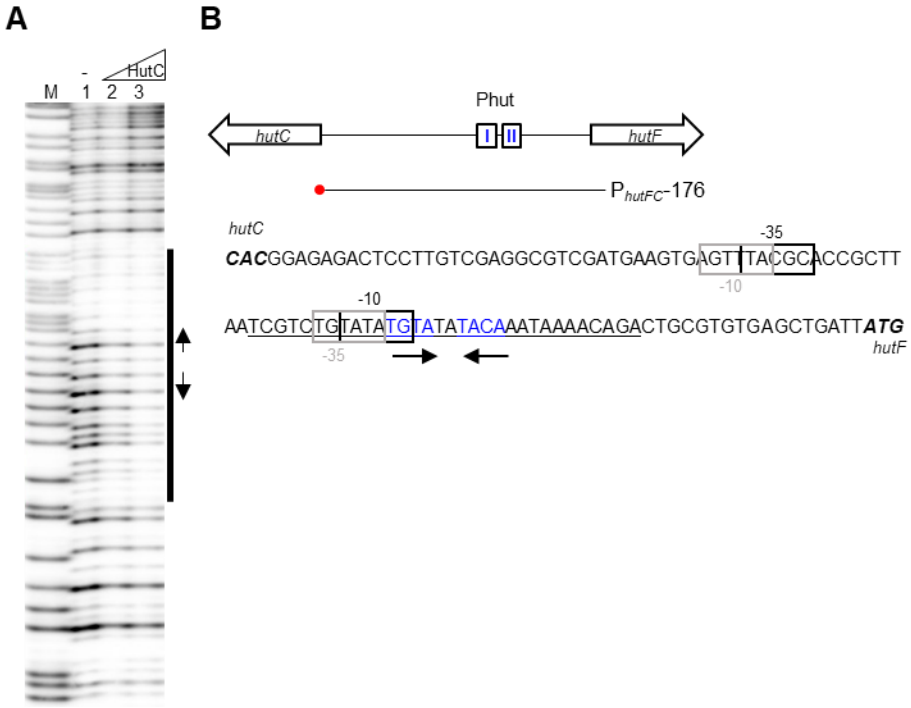

FIG 4.3 Identification of HutC-binding site sequences in P_{hutFC} DNA from *P. aeruginosa* PAO1.
(A) DNAse I footprinting was performed using $HutC_{his6}$ and biotin labelled P_{hutFC}-176 DNA probe. Lane M, G+A marker; lanes 1-3, $HutC_{his6}$ added at increasing concentrations (0, 500, and 2000 nM). The HutC-protected region and the Phut site are shown by black bar and inverted arrows, respectively.
(B) Schematic representation of the genetic loci of divergently transcribed *hutF* and *hutC* genes and biotin labelled DNA probe (red circle) used for DNAse I footprinting assay. The Phut half-sites (Phut-I and Phut-II) are marked in blue. The sequences below correspond to the *hutC-hutF* intergenic region. $HutC_{his6}$ protected region is underlined and Phut half-sites are shown by inverted arrows. Putative sigma-70 binding elements (-35 and -10 sites) of the promoters are boxed: black box – *hutF* promoter and grey box – *hutC* promoter.

4.3.4 Variations in HutC interaction with P_{hutFC} promoter DNAs from *P. fluorescens* SBW25 and *P. aeruginosa* PAO1

In a separate study, parallel work to investigate the regulatory role of HutC in *P. fluorescens* SBW25 was conducted by Naran Naren, a fellow PhD student in the Zhang lab. Intriguingly, $HutC_{his6}$ interaction with P_{hutFC} DNA from *P. fluorescens* SBW25 resulted in 4 shifted protein-DNA complexes in the EMSA; the shifted complexes corresponded to a dimer, trimer, tetramer, and hexamer, suggesting protein oligomerization with the DNA. Moreover, $HutC_{his6}$ protected a longer (68-bp) region in P_{hutFC} DNA from DNase I digestion (data not shown). The differences observed in the HutC binding pattern with P_{hutFC} DNA from *P. aeruginosa* PAO1

and *P*. *fluorescence* SBW25 prompted us to investigate if the differences were caused by $HutC_{his6}$ proteins and/or influenced by P_{hutFC} DNAs.

4.3.4.1 Molecular interactions between HutC and P_{hutFC} DNA from *P. aeruginosa* PAO1 and *P. fluorescens* SBW25

To determine if HutC protein from *P*. *aeruginosa* PAO1 or *P*. *fluorescens* SBW25 contributes to the differences in the binding pattern with their respective P_{hutFC} DNA, we examined the cross-molecular interactions between $HutC_{his6}$ proteins and P_{hutFC} DNAs from either species by means of EMSA (Fig. 4.4). $HutC_{his6}$ from both *P*. *aeruginosa* PAO1 and *P*. *fluorescens* SBW25 formed a single shifted complex with P_{hutFC} DNA from *P*. *aeruginosa* PAO1 (Fig. 4.4B & C). The migration distances of the shifted complexes with respect to the free probe were similar (5.01 and 4.86 cm) for the two $HutC_{his6}$ proteins. We have shown above that $HutC_{his6}$ binds to P_{hutFC} DNA from *P*. *aeruginosa* PAO1 as a dimer (Fig. 4.2). Thus, similar migration distances of the complexes suggest that $HutC_{his6}$ from *P*. *fluorescens* SBW25 also binds to P_{hutFC} DNA from *P*. *aeruginosa* PAO1 as a dimer.

In contrast, both the $HutC_{his6}$ proteins formed multiple shifted complexes with P_{hutFC} DNA from *P*. *fluorescens* SBW25 (Fig. 4.4D & E). Distances of each shifted complex with respect to the free probe was similar for both $HutC_{his6}$ proteins (data not shown). These indicate that both $HutC_{his6}$ proteins form similar higher order oligomers with P_{hutFC} DNA from *P*. *fluorescens* SBW25. Indeed, these results clearly demonstrate that the binding pattern of HutC with operator sites is determined by the P_{hutFC} sequences but not HutC proteins *per se*.

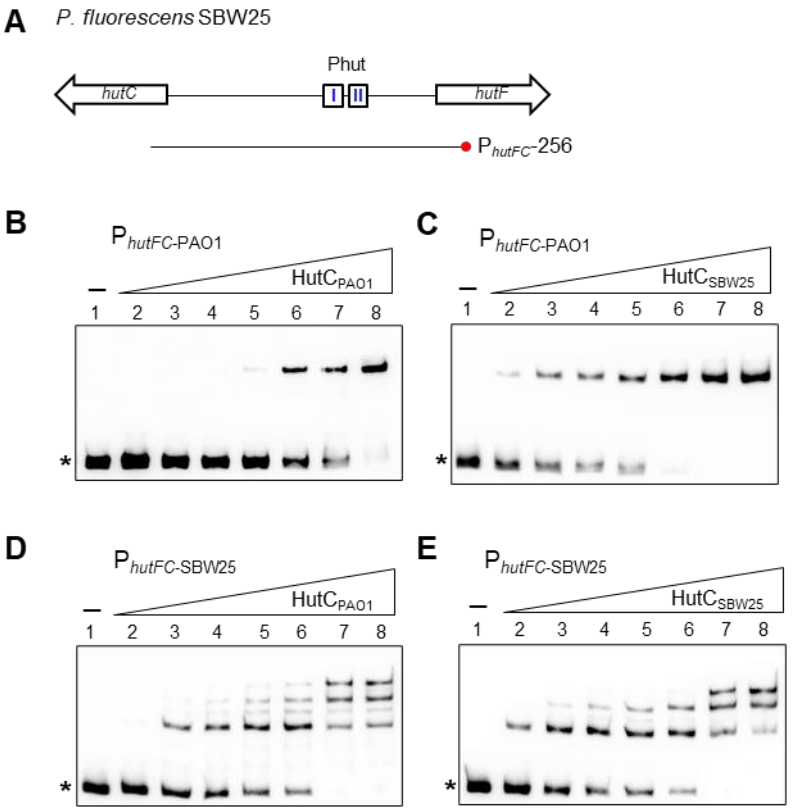

FIG 4.4 Reciprocal interactions of $HutC_{his6}$ with P_{hutFC} DNA from *P. aeruginosa* PAO1 and *P. fluorescens* SBW25.
(A) Schematic representation of the genetic loci of divergently transcribed *hutF* and *hutC* genes in *P. fluorescens* SBW25, and the biotin labelled P_{hutFC} DNA probe (red circle) used for EMSA in (D&E). Phut half-sites are marked in blue.
(B)&(C) EMSAs showing the interactions of HutC proteins from *P. aeruginosa* PAO1 ($HutC_{PAO1}$) and *P. fluorescens* SBW25 ($HutC_{SBW25}$) with P_{hutFC}-176 DNA probe from *P. aeruginosa* PAO1. $HutC_{PAO1}$ was added at concentrations of 0, 200, 400, 600, 800, 1000, 1400, and 2000 nM across lanes 1-8, respectively. $HutC_{SBW25}$ was added at concentrations of 0, 70, 140, 200, 300, 400, 600, and 800 nM across lanes 1-8, respectively.
(D)&(E) EMSAs showing the interactions of HutC proteins from *P. aeruginosa* PAO1 ($HutC_{PAO1}$) and *P. fluorescens* SBW25 ($HutC_{SBW25}$) with P_{hutFC}-256 DNA probe from *P. fluorescens* SBW25. $HutC_{PAO1}$ and $HutC_{SBW25}$ were added at concentrations of 0, 70, 140, 200, 300, 400, 600, and 800 nM across lanes 1-8, respectively.
Asterisk denotes the position of free probe.

4.3.4.2 Identification of a novel HutC-binding site in P_{hutFC} in *P. fluorescens* SBW25

Research in this section that led to the identification of a novel HutC-binding site in P_{hutFC} DNA from *P. fluorescens* SBW25 was performed by Dr Naran Naren, a fellow PhD student in Zhang lab.

The $HutC_{his6}$-binding region in the P_{hutFC} DNA of *P. fluorescens* SBW25 was carefully examined to determine the elements that may influence higher order oligomerization of $HutC_{his6}$ proteins with the DNA, resulting in multiple shifted complexes in the EMSA. Intriguingly, only a single Phut site was identified in the regulatory region (Fig. 4.5B) which ruled out the possibility that

multiple Phut sites contributed to protein oligomerization with the DNA. The sequences immediately flanking the Phut site in P_{hutFC} DNA was also identical in both *P*. *fluorescens* SBW25 and *P*. *aeruginosa* PAO1 (Fig. 4.5B). However, an imperfect inverted repeat sequence (ACACGACCGGGGTGC) displaying similarity to the NtrC-binding consensus sequence (GCACCA-N3-TGGTGC) was identified 7-bp away from the Phut site, closer to the *hutF* gene in *P*. *fluorescens* SBW25. This novel site was designated the Pntr site, and the Pntr site was absent in P_{hutFC} DNA of *P*. *aeruginosa* PAO1 (Fig. 4.5A & B). A later study from our laboratory identified that HutC can also bind to the NtrC-binding site sequence in the *ntrBC* promoter and fine-tunes *ntrBC* expression when histidine is utilized as a nitrogen source and present at high concentrations (Naren & Zhang, 2021). Together, the data led to a new hypothesis that HutC can bind to a novel Pntr site besides the Phut site in P_{hutFC} DNA of *P*. *fluorescens* SBW25. This explains the EMSA results above (Fig. 4.4D & E).

To test this prediction, the molecular interaction between $HutC_{his6}$ and a Pntr-site mutant P_{hutFC} DNA probe ($P_{hutFC\text{-}Mut1}$) was examined by EMSA. Briefly, the Pntr-site was mutated by site-directed mutagenesis, where nucleotides from both half-sites (ACACGACCGGGGTGC) were substituted with random nucleotides (AtgaGcCCGGcagaa). Consistent with our expectation, only a single shifted protein-DNA complex was observed with the $P_{hutFC\text{-}Mut1}$ probe, while multiple shifted Protein-DNA complexes were formed with the wild-type P_{hutFC} DNA probe (Fig. S4.1). This single shifted complex had similar migration distance as that of a dimer observed with wild-type P_{hutFC}, and by analogy the dimer corresponds to $HutC_{his6}$-binding with the Phut site. Indeed, elimination of the high molecular weight shifted complexes with the $P_{hutFC\text{-}Mut1}$ DNA strongly concurs with our hypothesis that HutC binds to this novel Pntr site that contributes to HutC oligomerization along the DNA.

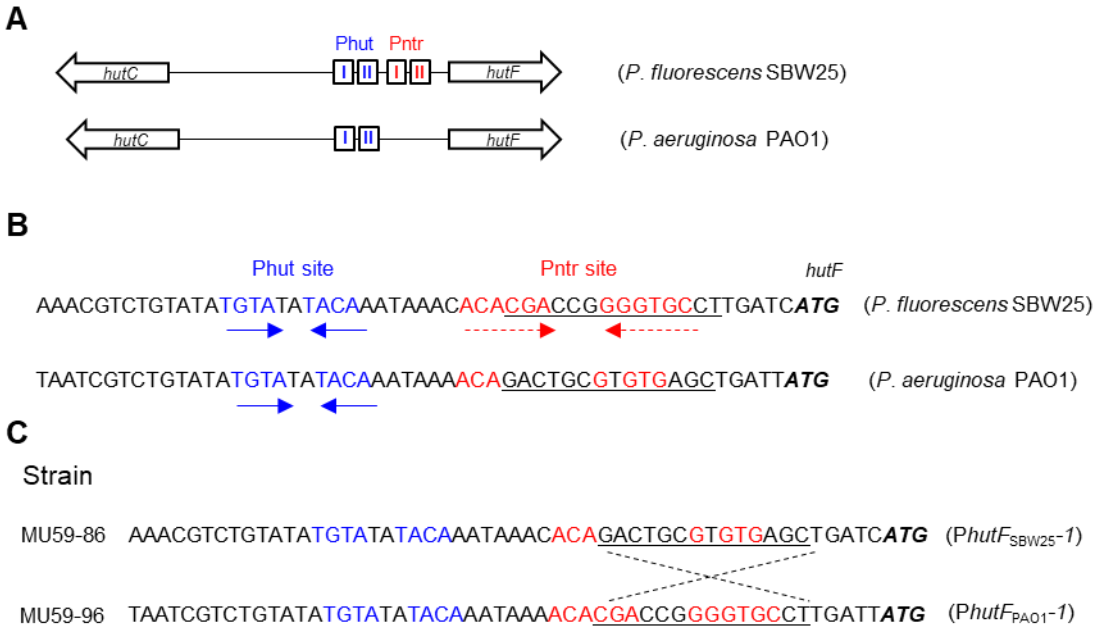

FIG 4.5 HutC regulatory element(s) in the intergenic region of *hutF* and *hutC* in *P. fluorescens* SBW25 and *P. aeruginosa* PAO1.
(A) Relative locations of the HutC-binding Phut (marked in blue) and Pntr (marked in red) half-sites between *hutF* and *hutC* genes in PAO1 and SBW25.
(B) DNA sequences (55-bp) immediate upstream of the *hutF* coding region. The canonical HutC-binding consensus sequence of the Phut half-sites are marked in blue. The sequence of the novel HutC-binding Pntr-site identified in *P. fluorescens* SBW25 is marked in red. The corresponding sequence in *P. aeruginosa* PAO1 shows poor similarity (marked in red) with the Pntr-site sequence from *P. fluorescens* SBW25.
(C) Sequence information of the Pntr-site mutant strains constructed for phenotypic analysis. A 14-bp sequence, nucleotides underlined in (B), was swapped between the wild-type promoters of *P. fluorescens* SBW25 and *P. aeruginosa* PAO1 to introduce the Pntr-site in the promoter of *hutF* in *P. aeruginosa* PAO1 (resultant strain MU59-96 [carries variant P$hutF_{PAO1}$-*1*]) and mutate the Pntr-site in the promoter *hutF* in *P. fluorescens* SBW25 (resultant strain MU59-86 [carries variant P$hutF_{SBW25}$-*1*]).

4.3.4.3 Functional characterization of the Pntr site in P_{hutFC} DNA in *Pseudomonas*

The presence of an additional HutC-binding site in the promoter of *hutF* in *P. fluorescens* SBW25 but not in *P. aeruginosa* PAO1 suggest differences in HutC-mediated regulation of *hutF* in the two species. Considering the proximity of Pntr site to *hutF* gene, we hypothesised that the Pntr site in P_{hutFC} DNA of *P. fluorescens* SBW25 confers a tight repression in *hutF* expression, which prevents *hutF* over-expression in the presence of high concentrations of histidine. This presumably circumvents toxicity from the accumulation of formylglutamate (FIGLU metabolite) resulting from imbalance between separately induced *hutF* and *hutG* expression.

To investigate the functional significance of the Pntr site in P_{hutFC} DNA, we first undertook a mutational analysis of the Pntr site to determine the associated phenotypes in both *P. fluorescens* SBW25 and *P. aeruginosa* PAO1.

4.3.5 Phenotypic analysis of the significance of Pntr site in P_{hutF} DNA in *Pseudomonas*

First, we constructed a P_{hutF} variant strain (MU59-86) of *P. fluorescens* SBW25, harbouring mutation in the Pntr site, by site-directed mutagenesis. Subsequently, a P_{hutF} variant strain (MU59-96) of *P. aeruginosa* PAO1, containing the intact Pntr site from SBW25, was also constructed by site-directed mutagenesis. To avoid any artifacts arising from random nucleotide substitutions, P_{hutF} variants were constructed by swapping regions corresponding to the Pntr site in P_{hutFC} DNA between *P. fluorescens* SBW25 and *P. aeruginosa* PAO1, leaving the flanking regions identical in both species (Fig. 4.5C).

4.3.5.1 The Pntr site in P_{hutF} promoter is required for *P. fluorescens* SBW25 to grow on histidine

To test the influence of Pntr site on histidine and urocanate (histidine metabolite) utilization, we compared the growth profiles of wild-type *P. fluorescens* SBW25 and mutant MU59-86 (P$hutF_{SBW25}$*-1* variant carrying mutation in Pntr site) on histidine and urocanate as sole sources of carbon and nitrogen (Fig. 4.6). Interestingly, we observed that mutation of the Pntr site significantly impaired growth of MU59-86 on histidine (Fig. 4.6A) as sole carbon and nitrogen source. Similarly, growth on urocanate was also significantly impaired (Fig. 4.6B). We next asked if the growth defect of MU59-86 (Pntr mutant) was caused by the over-expression of *hutF*, and the consequent accumulation of toxic formylglutamate (FG) due to the non-coordinated expression of *hutF* and *hutG* genes. HutG enzyme breaks down FG produced during histidine/urocanate catabolism. To test this, we introduced a wild-type copy of *hutF* from SBW25 ($hutF_{SBW25}$) into MU59-86 (P$hutF_{SBW25}$*-1* variant carrying mutation in Pntr site). The resultant strain MU62-23 was assayed growth on histidine and urocanate (Fig. 4.6). We observed that the $hutF_{SBW25}$ complemented strain MU62-23 restored growth on histidine and urocanate (Fig. 4.6), suggesting that mutation of the Pntr site has not resulted in over-expression of *hutF*.

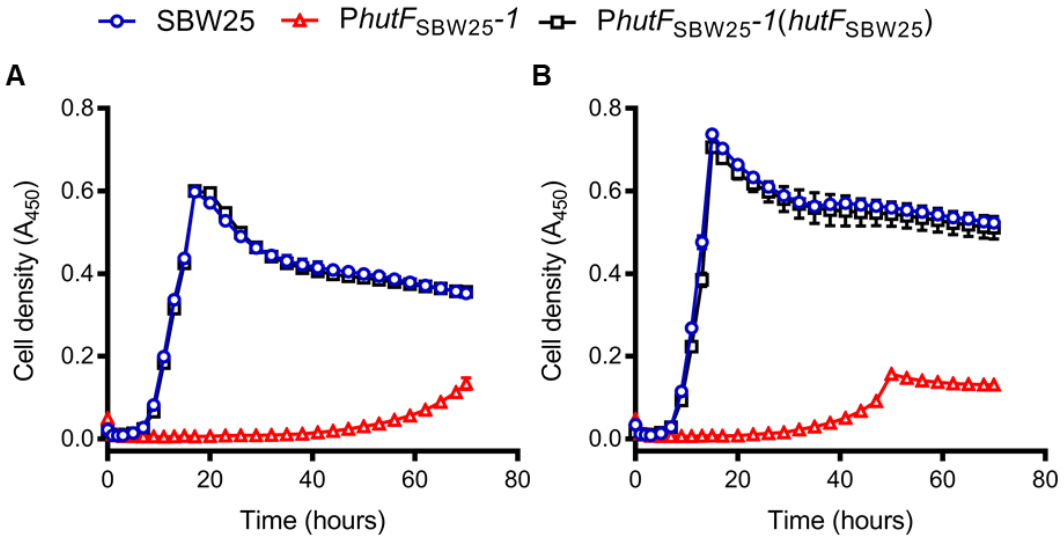

FIG 4.6 Mutation of Pntr site significantly impairs growth of *P. fluorescens* SBW25 on histidine and urocanate.
Growth dynamics of wild-type *P. fluorescens* SBW25, MU59-86 (P*hutF*$_{SBW25}$*-1* variant carrying mutation in Pntr site), and MU62-23 (*hutF*$_{SBW25}$ complemented P*hutF*$_{SBW25}$*-1* variant strain) on histidine **(A)** or urocanate **(B)** as sole source of carbon and nitrogen. Cells were grown in minimal salts medium containing histidine or urocanate at 10 mM. Data are means ± standard deviations of 4 independent cultures. Results shown are representative of 3 independent experiments. If not visible, error bars are contained within the symbol.

Next, to determine the effect of Pntr site on the utilization of histidine as a nitrogen source, we compared the growth profiles of wild-type *P. fluorescens* SBW25, MU59-86 (P*hutF*$_{SBW25}$*-1* variant carrying mutation in Pntr site), and MU35-86 (Δ*hutF*, His$^-$ phenotype) on varying concentrations of histidine as sole source of nitrogen. We observed that the Pntr site mutant strain MU59-86 was able to grow on histidine as a nitrogen source, albeit the growth was slower and reduced compared to the wild type (Fig. 4.7). However, at higher concentrations of histidine, growth of mutant MU59-86 was severely reduced and displayed an abnormal growth pattern (Fig. 4.7E & F); the growth was paused for a while before resuming. Together, the growth data suggest that mutating the Pntr-site in P$_{hutFC}$ DNA has resulted in a reduction in the *hutF*$_{SBW25}$ expression. The more pronounced growing defect at higher histidine concentrations (Fig. 4.7E & F) is possibly due to the reduced expression of *hutF*$_{SBW25}$ coupled with toxicity from the accumulation of FIGLU. We tested toxicity posed by FIGLU accumulation in a Δ*hutF* mutant (strain MU35-86) by assaying growth on glutamate supplemented with increasing concentrations of histidine. We observed that histidine has an inhibitory effect on glutamate utilization (data not shown). Of note, strain MU35-86 (Δ*hutF*) shows a minor growth (Fig. 4.7) due to NH_4^+ produced during the initial conversion of histidine to urocanate (1st step of histidine catabolism, Fig. 1.1 [Chapter 1]), which serves as a nitrogen source supporting minor growth on succinate (carbon source).

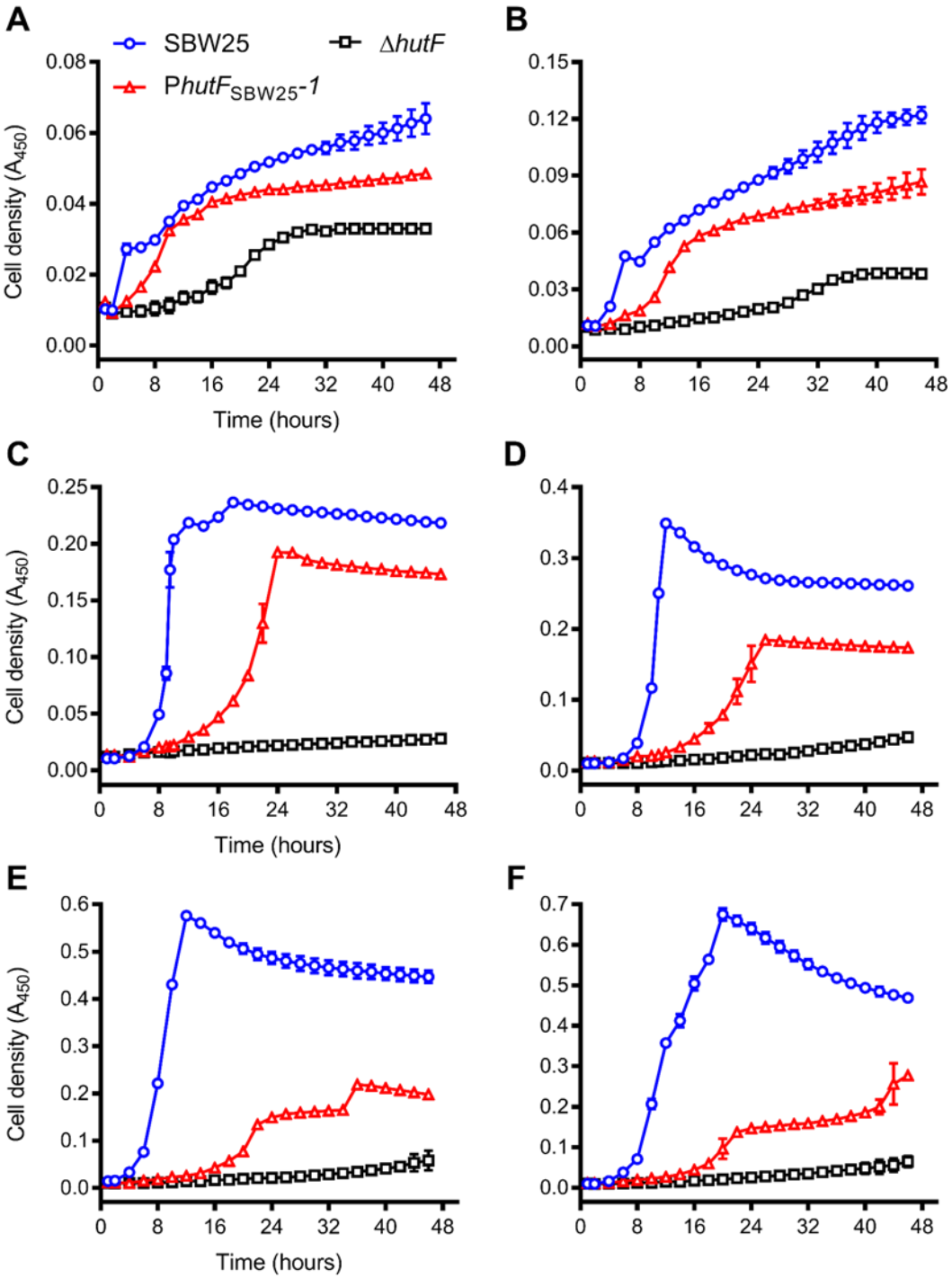

FIG 4.7 Effect of Pntr site mutation in *P. fluorescens* SBW25 growth on increasing concentrations of histidine as the sole nitrogen source.
Growth dynamics of wild-type *P. fluorescens* SBW25, MU59-86 (P*hutF*$_{SBW25}$*-1* variant carrying mutation in Pntr site), and MU35-86 (Δ*hutF*) on minimal salts succinate (5 mM) medium supplemented with histidine at concentrations of 50 µM **(A)**, 0.1 mM **(B)**, 0.5 mM **(C)**, 1.0 mM **(D)**, 5.0 mM **(E)**, and 10.0 mM **(F)**. Data are means ± standard deviations of 3-4 independent cultures. Results shown are representative of two independent experiments. If not visible, error bars are contained within the symbol.

Considering that *P. aeruginosa* PAO1 does not contain the Pntr site in P_{hutF} DNA, we asked if a $hutF_{PAO1}$ mutant (His$^-$ phenotype) could restore normal growth on histidine when complemented with $hutF_{SBW25}$*-1* (variant $hutF_{SBW25}$ that carries mutation in Pntr-site) from MU59-86 (P$hutF_{SBW25}$*-1* variant SBW25 strain). To test this, we introduced wild-type $hutF_{SBW25}$ and variant $hutF_{SBW25}$*-1* (from strain MU59-86) into a *hutF* and *figA* double deletion mutant strain MU3U3-9 (PAO1 background). The resultant strains MU64-10 (Δ*hutF* Δ*figA*::$hutF_{SBW25}$) and MU64-5 (Δ*hutF* Δ*figA*::$hutF_{SBW25}$*-1*) along with wild-type PAO1 and MU3U3-9 (Δ*hutF* Δ*figA*) were assayed growth on histidine as (i) sole source of carbon and nitrogen and (ii) sole source of nitrogen (Fig. 4.8). As expected, MU3U3-9 (Δ*hutF* Δ*figA*) was unable to grow on histidine as sole carbon and nitrogen source (Fig. 4.8A); however, the minor growth on histidine as nitrogen source (Fig. 4.8B) was supported by NH_4^+ produced during the initial conversion of histidine to urocanate. Strain MU64-10 (Δ*hutF* Δ*figA*::$hutF_{SBW25}$), carrying wild-type $hutF_{SBW25}$, displayed similar growth characteristics as the wild-type PAO1 in either growth conditions. However, strain MU64-5 (Δ*hutF* Δ*figA*::$hutF_{SBW25}$*-1*), carrying the Pntr site variant $hutF_{SBW25}$, displayed a slower growth (longer lag time) under either growth conditions.

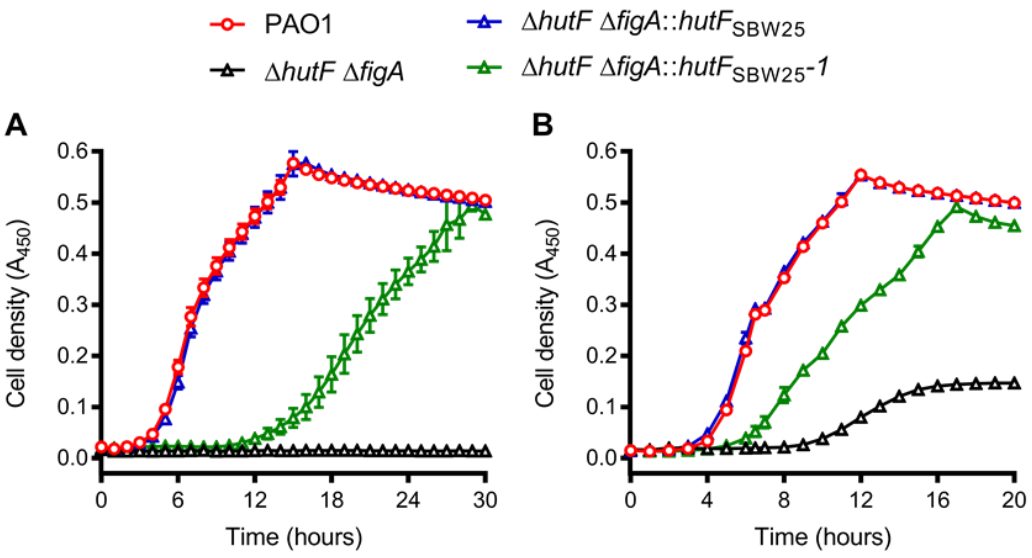

FIG 4.8 $hutF_{SBW25}$*-1* variant carrying mutation in Pntr site is functional in *P. aeruginosa* PAO1. Growth dynamics of wild-type *P. aeruginosa* PAO1 and mutants MU3U3-9 (Δ*hutF* Δ*figA*), MU64-10 (Δ*hutF* Δ*figA*::$hutF_{SBW25}$), and MU64-5 (Δ*hutF* Δ*figA*::$hutF_{SBW25}$*-1*) on histidine as sole source of carbon and nitrogen **(A)** and source of nitrogen **(B)**. Cells were grown in minimal salts medium containing histidine at 10 mM **(A)** or succinate and histidine at 5 mM each **(B)**. Data are means ± standard errors of 2 biologically independent samples (4 replicate cultures per sample). If not visible, error bars are contained within the symbol.

Intriguingly, growth of MU64-5 (PAO1 Δ*hutF* Δ*figA*::$hutF_{SBW25}$*-1*) and MU59-86 (P$hutF_{SBW25}$*-1* variant SBW25 strain), both carrying the same allele, was notably different (Fig. 4.8 and 4.6).

Although MU64-5 displayed a slower growth, growth of MU59-86 was significantly impaired. While our growth data suggest that mutation of the Pntr site has reduced the expression of *hutF*$_{SBW25}$*-1*, it also points out the possible involvement of auxiliary factors in the regulation of *hutF*$_{SBW25}$ in *P. fluorescens* SBW25.

4.3.5.2 Effect of the Pntr-site in P$_{hutF}$ DNA on histidine catabolism in *P. aeruginosa* PAO1

We next determined the effect of introducing Pntr site into P$_{hutF}$ DNA on histidine utilization in *P. aeruginosa* PAO1. First, we compared the growth dynamics of wild-type *P. aeruginosa* PAO1 and mutant strain MU59-96 (P*hutF*$_{PAO1}$*-1* variant carrying Pntr site) on histidine as sole source of carbon and nitrogen. We observed that both wild type and MU59-96 grew similarly on histidine as sole carbon and nitrogen source (Fig. 4.9A). Similar findings were also observed for growth on histidine as sole nitrogen source (Fig. 4.9B).

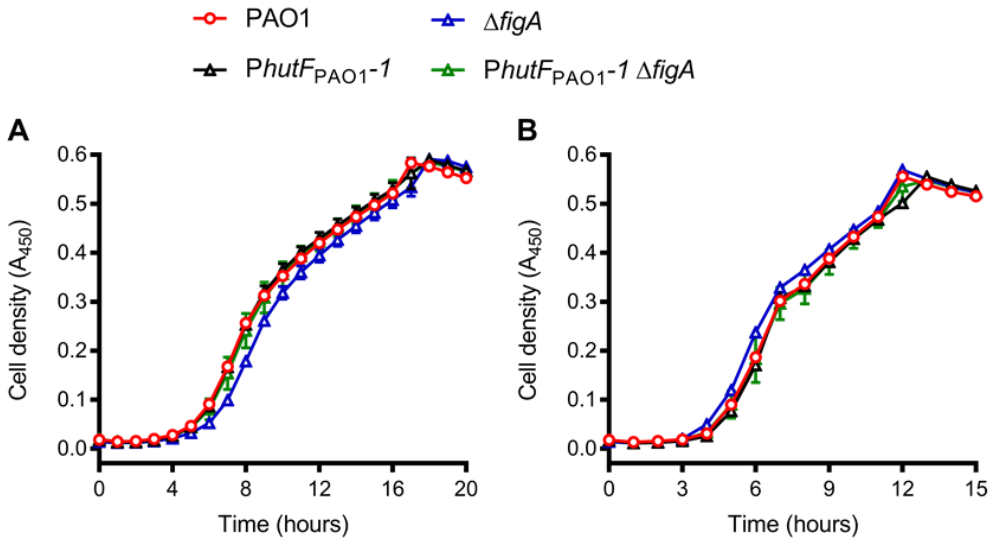

FIG 4.9 Introducing the Pntr site into P$_{hutF}$ DNA of *P. aeruginosa* PAO1 has no effect on growth on histidine.
Growth dynamics of wild-type *P. aeruginosa* PAO1, MU59-96 (P*hutF*$_{PAO1}$*-1* variant carrying Pntr site), PBR1020 (Δ*figA*), and MU63-95 (P*hutF*$_{PAO1}$*-1* variant carrying deletion of *figA*) on histidine as sole source of carbon and nitrogen **(A)** and source of nitrogen **(B)**.
Cells were grown in minimal salts medium containing histidine at 10 mM **(A)** or succinate and histidine at 5 mM each **(B)**. Data for PAO1, PBR1020 and MU59-96 are means ± standard deviations of 4 independent cultures, and data for MU63-95 represent means ± standard deviations of 3 biologically independent mutants (4 replicate cultures per mutant). If not visible, error bars are contained within the symbol.

However, MU59-96 (P*hutF*$_{PAO1}$*-1* variant carrying Pntr site) contains the intact FigA, which could potentially mask any effect caused by introducing the Pntr-site into P$_{hutF}$ DNA. Therefore, to rule out any influence of FigA on histidine catabolism via the HutFG pathway, *figA* was knocked out from MU59-96 (P*hutF*$_{PAO1}$*-1* variant carrying Pntr site) to generate strain MU63-

95 (P*hutF*$_{PAO1}$*-1* Δ*figA*). MU63-95 and PBR1020 (Δ*figA*, [control]) were then assayed growth on histidine as sole source of carbon and nitrogen. The strains MU63-95 (P*hutF*$_{PAO1}$*-1* Δ*figA*) and PBR1020 (Δ*figA*) displayed similar growth characteristics as wild type and MU59-96 (P*hutF*$_{PAO1}$*-1* variant carrying Pntr site) on histidine as sole carbon and nitrogen source (Fig. 4.9A). Similarly, no difference was observed between the mutant strains growing on histidine as nitrogen source (Fig. 4.9B). This suggests that Pntr site introduced into P_{hutF} DNA has no functional role in growth on histidine in *P*. *aeruginosa* PAO1.

4.4 Discussion

In *Pseudomonas*, *hutC* and *hutF* genes are arranged divergently, and previous gene expression studies indicate that HutC represses *hutF* expression and autorepresses its own expression (Consevage *et al.*, 1985, Hu & Phillips, 1988, Allison & Phillips, 1990, Zhang & Rainey, 2007b). This was presumably thought to be achieved through a single repressor site located in their intergenic region, but the molecular interaction of purified HutC protein with this site or the mode of action has not been previously characterized. In the present work, we showed by means of EMSA and DNase I footprinting that purified HutC protein forms a dimer with the DNA and the resulting 30-bp binding region overlaps putative -35 and -10 elements of *hutC* and *hutF* promoters, respectively, in *P*. *aeruginosa* PAO1. Urocanate was able to disrupt this binding in a concentration dependent manner. Our *in vitro* results complemented previous *in vivo* expression studies and support a molecular mechanism for HutC repressing its own and *hutF* expression through a single binding site by hindering access to RNA polymerase. However, this paradigm does not appear to be fully true for all *Pseudomonas* species. Besides the fully conserved canonical HutC-binding site (Phut site) sequence in the intergenic region of *hutC* and *hutF*, *P*. *fluorescens* SBW25 possesses an additional but distinct HutC-binding site (termed Pntr site) proximal to the *hutF* gene. The Pntr site contributed to complex HutC oligomerization and formation of HutC hexamer with the DNA, presumably via co-operative binding to two sites. Further, functional analyses of the Pntr site suggest that Pntr site is required for the wild-type level expression of *hutF* in *P*. *fluorescens* SBW25.

HutC mediates the coordinated expression of histidine catabolic genes that are transcribed from multiple transcriptional units, which otherwise have the potential to cause histidine poisoning (Bender, 2012). By autorepressing its own expression, sufficient amounts of the repressor are produced to inhibit catabolic genes upon depletion or limiting amounts of histidine or urocanate (Smith & Magasanik, 1971a). Autorepression of *hutC* is presumably weaker relative to HutC mediated repression of *hutU*. This becomes apparent from the dissimilarities in the modes of HutC interaction with the promoter regions of *hutFC* and *hutU*

(Chapter 3) in *P. aeruginosa* PAO1. Despite a high degree of conservation in the Phut sites, HutC forms a dimer with promoter *hutFC* DNA, while the interaction with *hutU* promoter (Chapter 3) presumably results in a tetramer. Higher order oligomerization of transcription factors appears to have biological significance. It has been observed that TyrR and LacI proteins form hexamers and tetramers, respectively, which enhances DNA-binding affinity or achieve a tighter repression (Chakerian & Matthews, 1992, Beckett, 2001). Consistently, we observed that HutC binds to *hutU* promoter with at least 5-fold higher affinity (Chapter 3) than *hutFC* promoter; indicating that relatively a lower amount of HutC protein is required to repress *hutU* compared to *hutC* and *hutF*. Together, HutC forming a tetramer with the *hutU* promoter suggests a stronger repression of *hutU* compared to *hutC* and *hutF*. The puzzling question then is, how the same HutC protein achieves different levels of oligomerization with almost identical Phut sites in the two promoters (*hutU* and *hutFC*). A direct repeat of the Phut half-site is present in tandem with the inverted repeat sequence in the promoter region of *hutFC* (Fig. 4.3.B), which could potentially be used for HutC binding to alternate half-sites, such that increasing the spacer nucleotides between monomer binding sites possibly inhibits further protein-protein interactions via the C-terminus.

The distinct binding pattern of HutC with *hutFC* promoter DNA from *P. fluorescens* SBW25 resulting in a hexamer was initially surprising, considering, a high degree of conservation in the Phut site sequence and immediate flanking nucleotides with *hutFC* promoter DNA from *P. aeruginosa* PAO1. First, we ruled out the possibility that different HutC proteins from two species is the contributing factor. Subsequent examination of the HutC-protected sequences in both species, and further mutational analysis confirmed that HutC also recognises a site (Pntr site) different from the Phut site. EMSA analysis indicated that this Pntr site contributed to hexamer formation in *P. fluorescens* SBW25, without which HutC appears to form a dimer with the Phut site, as observed in *P. aeruginosa* PAO1. Thus, HutC binding to the two sites (Phut and Pntr) likely promote protein-protein interactions causing an alternate oligomerization. Divergons with a secondary binding site adjacent to the main site are common among genes regulated by GntR family transcriptional regulators (Suvorova *et al.*, 2015, Lemmens *et al.*, 2019). A typical example is AraR transcriptional regulator of *B. subtilis* which negatively regulates the expression of genes involved in the utilization of L-arabinose. AraR binds cooperatively to multiple sites to achieve a tight and flexible control over the expression of arabinose utilization genes (Mota *et al.*, 1999, Mota *et al.*, 2001). Interestingly, here three binding sites appear to be involved: (i) Phut site, (ii) a direct repeat of the Phut half-site, and (iii) Pntr site.

The proximity of the Pntr site to $hutF_{SBW25}$ gene led us to hypothesize that the Pntr site may facilitate a tighter repression on $hutF_{SBW25}$ expression by HutC. This is particularly relevant

when histidine is available at high concentrations as it helps circumvent toxicity from the accumulation of formylglutamate (FG) from the non-coordinated synthesis of HutF and HutG (enzyme required for breakdown of FG). Histidine catabolism in plants has not been investigated to the best of our knowledge; however, many plant genomes contain histidase-like protein (HutH) but no recognizable urocanase (HutU). This suggests that urocanate likely accumulates on plant surfaces and is available as a nutrient source for plant bacteria such as *P*. *fluorescens* SBW25. Therefore, the Pntr site may confer a tight repression on *hut* expression to avoid histidine poisoning. However, *P*. *aeruginosa* PAO1 likely have lost the Pntr site due to the presence of *figRAT* operon. We also noted that the presence of Pntr site was disadvantageous for growth on FIGLU for both *P*. *aeruginosa* PAO1 and *P*. *fluorescens* SBW25 (containing *figRAT*), Chapter 2.

However, our current phenotypic data show that mutation of the Pntr site in *hutF* promoter of *P*. *fluorescens* SBW25 significantly impaired growth of mutant strain MU59-86 (P$hutF_{SBW25}$*-1* variant carrying mutation in Pntr site) on histidine or urocanate as sole source of carbon and nitrogen. Similarly, reduced growth phenotype was observed during growth on histidine as sole nitrogen source. The growth defect was not due to the over expression of *hutF*, resulting in toxicity from FG accumulation, but possibly due to reduced *hutF* expression. We arrived at this conclusion because, introducing a wild-type copy of the $hutF_{SBW25}$ (including the promoter) into this mutant strain MU59-86 (P$hutF_{SBW25}$*-1* variant carrying mutation in Pntr site) re-stored growth on histidine. Also, introducing a copy of the $hutF_{SBW25}$*-1* variant carrying mutation in the Pntr site in the promoter from MU59-86 into a His^- strain of *P*. *aeruginosa* PAO1 facilitated a slower growth on histidine suggesting that variant $hutF_{SBW25}$*-1* carrying the mutated Pntr site is functional, albeit expression is reduced. It appears that auxiliary factors specific to *P*. *fluorescens* SBW25 may also contribute to $hutF_{SBW25}$ expression, since a bigger growing defect was observed in mutants of *P*. *fluorescens* SBW25 compared to *P*. *aeruginosa* PAO1 (Fig. 4.6 & 4.8). Conversely, introducing the intact Pntr site from SBW25 into the native promoter of *hutF* in *P*. *aeruginosa* PAO1 appears to have no such phenotypic consequences. The growth phenotype is consistent, even if a wild-type $hutF_{SBW25}$ (including the promoter containing Pntr site) from *P*. *fluorescens* SBW25 is introduced into *P*. *aeruginosa* PAO1. These suggest that the effect of the Pntr site in *hutF* expression is more localized to the native promoter in *P*. *fluorescens* SBW25.

Based on the phenotypic data, the Pntr site appears to be significant for the activation of $hutF_{SBW25}$ in *P*. *fluorescens* SBW25. The location of the Pntr site is downstream to the -10 element of the putative $hutF_{SBW25}$ promoter, typical of a repressor that acts as a roadblock for transcribing the RNA polymerase (van Hijum *et al.*, 2009). However, it has been shown that

cis-acting proteins that bind downstream of the transcriptional initiation site are also able to activate transcription via direct contact with RNA polymerase *β* subunit; a typical example is the DnaA protein activating p_R promoter in *E*. *coli* (Szalewska-Palasz *et al.*, 1998). Considering the global regulatory role of HutC (Naren & Zhang, 2020), it would not be surprising if such a function has been evolved. Yet another possible scenario is the involvement of auxiliary factors in the regulation of $hutF_{SBW25}$, as mentioned above. Mutation of the Pntr site may have altered the structure of the promoter such that transcriptional initiation is impaired. Further gene expression studies are underway to obtain a precise role of the Pntr site in $hutF_{SBW25}$ expression in *P*. *fluorescens* SBW25.

In summary, we found significant differences in the HutC mode of action in the regulation of *hutF* and *hutC* genes in *P*. *fluorescens* SBW25 and *P*. *aeruginosa* PAO1. In *P. aeruginosa* PAO1, HutC appears to regulate both *hutC* and *hutF* gene expression via a single operator site. However, a secondary HutC-binding site is involved in the regulation of *hutF* expression in *P*. *fluorescens* SBW25, and it is functionally required for efficient utilization of histidine as a source of carbon and nitrogen.

4.5 Materials and Methods

4.5.1 Bacterial strains, plasmids, and growth conditions

Strains and plasmids used in this study are shown in Table 4.1. *E*. *coli*, *P*. *aeruginosa* PAO1, and *P*. *fluorescens* SBW25 were routinely propagated in Luria-Bertani broth (LB). *E*. *coli* and *P*. *aeruginosa* PAO1 were grown at 37°C, while *P*. *fluorescens* SBW25 was grown at 28°C. *Pseudomonas* were also grown in M9 minimal salts medium (MSM), which contained 47.8 mM Na_2HPO_4, 22 mM KH_2PO_4, 8.6 mM NaCl, and 2 mM $MgSO_4$, supplemented with carbon and nitrogen sources as indicated in the main text. *E*. *coli* DH5$\alpha\lambda_{pir}$ was used for general cloning and triparental conjugation into both *P*. *aeruginosa* PAO1 and *P*. *fluorescens* SBW25 strains. When required, antibiotics were used at the following concentrations for *E*. *coli* and *P*. *fluorescens* SBW25: 15 µg/ml tetracycline (Tc); 10 µg/ml gentamicin (Gm). For *P*. *aeruginosa*, antibiotics were used at: 100 µg/ml Tc; 20 µg/ml Gm. Spectinomycin (Sp) and nitrofurantoin (Nf) were used at 100 µg/ml for *E*. *coli*. X-gal (Melford) was used at concentrations of 60 µg/ml for blue/white screening of bacterial colonies. Succinate, histidine, and urocanate were purchased from Sigma.

Table 4.1 Bacterial strains and plasmids used in this study.

Strain or plasmid	Genotype or characteristics[a]	Reference or source
E. coli		
4A4-53	BL21-GOLD (DE3) carrying pET14b-*hutC*	Monica Gerth, unpublished
***P. aeruginosa* PAO1**		
PAO1	Wild-type strain	Lab stock
PBR1020	Δ*figA*, PAO1 devoid of PA3175	Gerth *et al.* (2012)
M3U3-9	Δ*figA* Δ*hutF*, PAO1 devoid of PA3175 and PA5106	Monica Gerth, unpublished
MU64-10	Δ*hutF* Δ*figA* carrying mini-Tn7T-Gm-GW::$hutF_{SBW25}$	This study
MU64-5	Δ*hutF* Δ*figA* carrying mini-Tn7T-Gm-GW::$hutF_{SBW25}$*-1*	This study
MU59-96	P$hutF_{PAO1}$*-1* variant of PAO1	This study
MU63-95	MU59-96 devoid of PA3175 (Δ*figA*)	This study
***P. fluorescens* SBW25**		
SBW25	Wild-type strain isolated from phyllosphere of sugar beet	Bailey *et al.* (1995)
MU35-86	Δ*hutF*, SBW25 devoid of PFLU0358	Yunhao Liu, unpublished
MU59-86	P$hutF_{SBW25}$*-1* variant of SBW25	This study
MU62-23	MU59-86 carrying mini-Tn7T-Gm-GW::$hutF_{SBW25}$	This study
Plasmids		
pRK2013	Helper plasmid, Tra^+, Km^r	Ditta *et al.* (1980)
pUX-BF13	Helper plasmid for transposition of mini-Tn7 element, Mob^+, *ori*-R6K, Ap^r	Bao *et al.* (1991)
pCR8/GW/TOPO	Cloning vector, Sp^r	Invitrogen
pCR8-P$hutFC_{SBW25}$*-1*	pCR8 containing P$hutFC_{SBW25}$*-1* promoter variant	This work
pCR8-P$hutFC_{PAO1}$*-1*	pCR8 containing P$hutFC_{PAO1}$*-1* promoter variant	This work
pCR8-$hutF_{SBW25}$*-1*	pCR8 containing $hutF_{SBW25}$*-1* variant	This work
pET14b-*hutC*	pET14b expression vector carrying *hutC* from PAO1, Amp^r	Monica Gerth, unpublished
pUIC3	Integration vector with promoterless *lacZ*, Mob^+, *ori*-R6K, Tc^r	Rainey (1999)
pUIC3-ΔPA3175	pUIC3 containing *figA* deletion fragment	Monica Gerth, unpublished
pUIC3-P$hutFC_{SBW25}$*-1*	pUIC3 containing P$hutFC_{SBW25}$*-1* promoter variant	This work
pUIC3-P$hutFC_{PAO1}$*-1*	pUIC3 containing P$hutFC_{PAO1}$*-1* promoter variant	This work
pUC18-mini-Tn7T-Gm-GW	Mini-Tn7T; GW destination vector for gene insertion in Gm^s bacteria, Ap^r, Gm^r	Choi and Schweizer (2006)
pUC18-mini-Tn7T-Gm-GW::$hutF_{SBW25}$	pUC18-mini-Tn7T-Gm-GW containing $hutF_{SBW25}$ for complementation	Yunhao Liu, unpublished
pUC18-mini-Tn7T-Gm-GW::$hutF_{SBW25}$*-1*	pUC18-mini-Tn7T-Gm-GW containing $hutF_{SBW25}$*-1* variant for complementation	This work

[a]Gm, gentamycin; Km, kanamycin; Sp, Ap, Ampicillin; Tc, tetracycline.

4.5.2 Monitoring bacterial growth kinetics

P. aeruginosa PAO1 and *P. fluorescens* SBW25 from -80°C freezer stock were cultured overnight in LB broth to similar densities. Subsequently, cultures were washed once in M9

salts and starved for 2 hours at 37°C (*P*. *aeruginosa*) or 28°C (*P*. *fluorescens*) to ensure that strains being compared were physiologically equal. The starved cells were diluted 1:100 times in 1 ml tested medium and 200 µl aliquots were transferred into a sterile clear 96-well microplate (Greiner Bio-One). Absorbance was measured at a wavelength of 450 nm as a measure of cell density using a Synergy 2 multi-detection microplate reader installed with Gen5 software (Bio-Tek). A_{450} readings were measured every 5 min following a 20 s shaking for an incubation period of 24 to 72 hours (as required) at 37°C (*P*. *aeruginosa*) or 28°C (*P*. *fluorescens*). In the growth figures for *P*. *fluorescens* SBW25, data points every 2 hours are shown for clarity. Hourly data points are shown in the growth figures for *P*. *aeruginosa* PAO1.

4.5.3 Strain construction

Standard protocols were used for the isolation of plasmid DNAs, restriction endonuclease digestion, ligation, and PCR (Sambrook *et al.*, 1989). PCRs were performed using *Taq* DNA polymerase purchased from Invitrogen Ltd. (Auckland, New Zealand). Oligonucleotide primers were synthesized by Integrated DNA Technologies Inc. (Singapore) and are shown in Table 4.2. The pCR8™/GW/TOPO® (Invitrogen) cloning kit was used for cloning *Taq* polymerase amplified PCR products into pCR8 for verifying sequence identity (Macrogen, South Korea). The desired DNA fragments were sub-cloned into appropriate expression vectors and then introduced into *P*. *aeruginosa* or *P*. *fluorescens* strains by tri-parental mating or electroporation. Transformants were selected on LB agar (1.5%) plates supplemented with antibiotics and confirmed by PCR.

The P_{hutF} Pntr site variant strains of *P*. *aeruginosa* PAO1 (MU59-96 [P$hutF_{PAO1}$*-1* variant]) and *P*. *fluorescens* SBW25 (MU59-86 [P$hutF_{SBW25}$*-1* variant]) were constructed by site-directed mutagenesis, utilizing splicing by overlap extension PCR (Horton *et al.*, 1989) in combination with a two-step allelic exchange strategy (Rainey, 1999, Zhang & Rainey, 2007b). First, P_{hutF} sequences from both *P*. *aeruginosa* PAO1 and *P*. *fluorescens* SBW25 (Winsor *et al.*, 2016) were aligned in Geneious 9.0.5 (https://www.geneious.com) using built-in clustalW alignment feature. A 14-bp sequence comprising most nucleotides of the Pntr site identified in P_{hutF} of *P*. *fluorescens* SBW25 and a 14-bp sequence in the corresponding region in P_{hutF} of *P*. *aeruginosa* PAO1 (Fig. 4.5) were artificially incorporated into primers (Table 4.2) designed for amplifying *hutF* genomic regions from *P*. *aeruginosa* PAO1 and *P*. *fluorescens* SBW25, respectively. Using wild-type genomic DNA as template, two fragments (~600-bp) were PCR amplified using oligonucleotide primers and the fragments containing complementary sequences at their ends were then joined by a third PCR. After verifying sequence identity, the fragments containing desired mutations were sub-cloned into pUIC3 (suicide vector containing promoterless *lacZ*) at the *Bgl*II site. These were then introduced into desired

recipient strains, wild-type *P*. *aeruginosa* PAO1 or wild-type *P*. *fluorescens* SBW25 by tri-parental mating with the help of pRK2013. Integration of pUIC3 into the genome via a single homologous recombination event of the cloned DNA fragment was selected on LB agar plates supplemented with Tc, Nf (to counter select *E. coli* donor cells) and X-gal (for blue/white screening). The double-cross over mutants that had lost the chromosomally integrated pUIC3-vector were selected by D-cycloserine enrichment process (Zhang & Rainey, 2007b). Of note that D-cycloserine was used at 1100 µg/ml for *P*. *aeruginosa* strains. The introduced mutations in P_{hutF} were further confirmed by sequencing the genomic region and neither *hutF* nor *hutC* was disrupted.

Genetic complementation of $hutF_{SBW25}$ and $hutF_{SBW25}$*-1* were performed by cloning the PCR amplified *hutF* coding region together with the regulatory region (template: wild-type SBW25 and MU59-86 [P$hutF_{SBW25}$*-1* variant of SBW25]) into pUC18-mini-Tn7-Gm-GW by Gateway cloning strategy. The resulting plasmid was mobilized into *P*. *fluorescens* or *P*. *aeruginosa* strains by electroporation with the help of pUX-BF13, where it is integrated into the neutral *attB* site. Transformants were selected on LB plates supplemented with Gm (20 µg/ml), and chromosomal integration downstream of *glmS* was confirmed by PCR.

Table 4.2 Oligonucleotides used in this study.

Primer name[a]	Sequence (5' - 3')[b]	Purpose
MLG036-PF	ggaattccataTGACGTCCTCTTCCTCCGA	Amplify *hutC* coding region for cloning into pET14b vector at NdeI and BamHI restriction sites. To express and purify his_6 tagged HutC protein for *in vitro* assays.
MLG037-PR	ctggatccTCATGAGCTGAAACGTCCTTCC	
PhutFC-bio1	GGAGGAAGAGGACGTCAC	Amplify *hutFC* promoter region (*P*. *aeruginosa* PAO1) for EMSA and DNAse I footprinting assays
PAO1-hutCF	aactagtGGACATTTCGCGCCCAGCCT	
Bio-F-new2	CAGCCCATCGGCGCTGACTT	Amplify *hutFC* promoter region (*P*. *fluorescens* SBW25) for EMSA and DNAse I footprinting assays
hutF-F	aactagtACAAGGGCGCCGGACTTTCG	
SPntr-1	gagatctGGTGAAATCCTGCTGCAGGT	Pntr site mutant fragment for mutating Pntr site from the *hutF* promoter in *P*. *fluorescens* SBW25
SPntr-2	tcagctcacacgcagtcTGTGTTTATTTGTATATACA	
SPntr-3	acagactgcgtgtgagcTGATCATGTCCGCTTTCTTTG	
hutC-1	agatctGAGTGGAAGCACAGGCCCA	
PPntr-1	gagatctACGATCAGCGAGTGGAACAC	Pntr site mutant fragment for inserting Pntr site into the *hutF* promoter in *P*. *aeruginosa* PAO1
PPntr-2	tcaaggcaccccggtcgTGTTTTATTTGTATATACATATAC	
PPntr-3	acacgaccggggtgcctTGATTATGTCCGCAATTTTCG	
PPntr-4	gagatctGAAGCCTGCGTGACTGTAAAG	
hutC-2	agcatgcgatcgttgacggaCTCTTGGGCTCGGCGACGA	Amplify *hutF* coding region with promoter for complementation
hutF-2	cgggatccGGTTAGCCCAGCAAATC	
SPntr-pcr	TACAAATAAACACAgactgc	Verify deletion of Pntr site from *hutF* promoter in *P*. *fluorescens* SBW25
hutC-1	agatctGAGTGGAAGCACAGGCCCA	
PPntr-pcr	ATACAAATAAAACAcgaccg	Verify insertion of Pntr site into *hutF* promoter of *P*. *aeruginosa* PAO1
PPntr-4	gagatctGAAGCCTGCGTGACTGTAAAG	
SBW25-Glms	CACCAAAGCTTTCACCACCCAA	Forward and reverse primer for verifying Tn7 integration in *P*. *fluorescens* SBW25 strains
MLG049-PR	CAGCATAACTGGACTGATTTCAG	
MLG048-PF	CAACCTGGCCAAGTCGGTCACC	Forward and reverse primer for verifying Tn7 integration in *P*. *aeruginosa* PAO1 strains
MLG049-PR	CAGCATAACTGGACTGATTTCAG	

[a]Bio – biotin labelled

[b]Restriction sites are underlined; nucleotides in lower case (excluding RE sites) are manually incorporated complementary sequences between the primer pairs

4.5.4 Statistical methods

Graphical representation of data, plots and statistical analysis were executed in Prism 7.0. The results were considered statistically significant if the *P* value was lower than 0.05, where appropriate.

4.5.5 Purification of $HutC_{his6}$ proteins from *P. aeruginosa* PAO1 and *P. fluorescens* SBW25

P. aeruginosa PAO1. Cloning of *hutC* gene from *P*. *aeruginosa* PAO1 into the expression vector pET14b was performed by a previous researcher, Dr Monica Gerth. The final construct in *E*. *coli* BL21(DE3) was available for protein expression and purification at the start of this study. Briefly, the HutC-coding region was PCR amplified from the genomic DNA and cloned

into pET14b vector at the NdeI and BamHI restriction sites, which will incorporate 6XHis affinity tags to the N-terminus of HutC when expressed. The recombinant plasmid was subsequently transformed into *E*. *coli* BL21(DE3) and $HutC_{his6}$ protein expression was induced by addition of 1 mM IPTG. The protein was purified using TALON metal affinity resin (Clontech Laboratories Inc.) (Chapter 3, Fig. S3.3).

P. *fluorescens* SBW25. The *hutC* gene from *P*. *fluorescens* SBW25 was previously cloned into the expression vector pTrc99A by Dr Naran Naren, a laboratory colleague (Naren & Zhang, 2020). Briefly, the HutC-coding region was PCR amplified from the genomic DNA using primers that incorporate 6XHis affinity tags to the N-terminus of HutC when expressed and cloned into pTrc99A vector at NcoI and HindIII sites. Subsequently, the recombinant plasmid was transformed into *E*. *coli* BL21(DE3) and $HutC_{his6}$ protein expression was induced by addition of 1 mM IPTG. The protein was purified using TALON metal affinity resin (Clontech Laboratories Inc.).

4.5.6 Electrophoretic Mobility Shift Assays (EMSAs) and dissociation constant (K_d)

EMSA. Biotin end-labeled probe DNAs were synthesised by PCR with a biotinylated primer using genomic DNA as template. Binding reactions (20 µl) were carried out by incubating $HutC_{his6}$ with probe DNA (20 nM) for at least 30 min at 23°C in a buffer (pH 7.5) containing 10 mM HEPES, 5 mM $MgCl_2$, 50 mM KCl, 1 mM dithiothreitol, and 1 µg salmon sperm DNA. The samples were subjected to electrophoresis on a 5% polyacrylamide gel at 120 V in 0.5XTBE buffer. The electrophoresis was carried out in a cold space to maintain temperatures ~4°C. Subsequently, DNA from the gel was electrophoretically transferred to a nitrocellulose membrane (Sigma Aldrich) at 80 V for 1 hour in 0.5% TBE (maintaining low temperatures) and fixed by oven baking at 80°C for 30 min. The immobilized biotin labeled DNA on the membrane was detected using the Chemiluminescent Nucleic Acid Detection kit (ThermoFisher) as per the manufacturer's instructions. The images were photographed with a LAS-4000 luminescent imager installed with ImageQuant LAS 4000 software (Fujifilm), and further analysed in ImageJ program.

Dissociation constant (K_d). Relative amounts of free probe DNA and Protein-DNA complex were quantified from the EMSA gel as band intensities using the ImageJ program. Fractions of Protein-DNA complexes were plotted against protein concentrations using a non-linear regression model specific binding with hill slope in Prism. K_d was estimated from the curve; representing protein concentration required to bind 50% of the probe DNA.

4.5.7 DNAse I footprinting analysis

Biotin end-labeled probe DNA prepared for EMSA above was also used for DNAse I footprinting assays. Binding reactions were carried out by incubating 2 µM DNA probe with $HutC_{his6}$ protein for at least 30 min at 23°C in a 50 µl reaction buffer (containing 10 mM HEPES, 5 mM $MgCl_2$, 50 mM KCl, 1 mM dithiothreitol, and 1 µg salmon sperm DNA; pH 7.5). Subsequently, 50 µl of the co-factor solution (5 mM $CaCl_2$ and 10 mM $MgCl_2$) was added to the reaction with gentle mixing. The reaction was treated with 0.02 unit of DNAse I for 6 min and digestion was terminated immediately by adding 100 µl of DNAse I stop solution [200 mM NaCl, 20 mM EDTA (pH 8), and 1% SDS]. The digested DNA fragments were purified and extracted by 1:1 phenol:chloroform treatment and ethanol precipitation at -80°C for an hour. Air-dried pellets were re-suspended in 8 µl of loading dye (95% formamide, 0.05% bromophenol blue, and 20 mM EDTA), heat denatured at 90°C for 15 min, and subjected to electrophoresis in a 6% urea-polyacrylamide sequencing gel (21 x 40 cm) in 1X TBE buffer using the Sequi-Gen GT system (Bio-Rad Laboratories Pty). The DNAs were transferred to a nitrocellulose membrane by contact blotting (performed overnight) and heat immobilized by oven-baking at 80°C for 30 min. The DNA fragments were detected using the Chemiluminescent Nucleic Acid Detection kit (ThermoFisher) as per the manufacturer's instructions. The images were photographed with a LAS-4000 luminescent imager installed with ImageQuant LAS 4000 software (Fujifilm), and further analysed in ImageJ program. A G+A marker synthesized from chemical sequencing reaction was included in the assay to help determine the footprinting site sequence.

4.6 Supplementary data

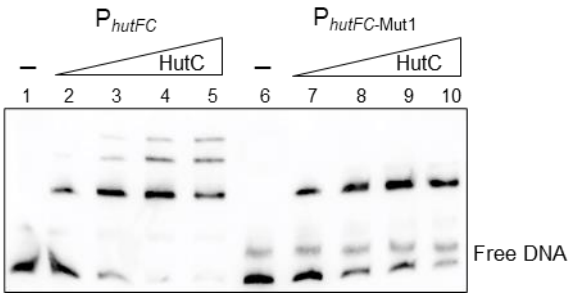

FIG S4.1 EMSA showing the significance of Pntr site in HutC binding to P_{hutFC} DNA from *P. fluorescens* SBW25. $HutC_{his6}$ was added at concentrations of 0, 73, 219, 365, and 584 nM across lanes 1-5 and lanes 6-10. The extra band seen for free $P_{hutFC\text{-}Mut1}$ DNA probe is likely caused by DNA tertiary structure; this band is absent in denatured agarose gel.

4.7 Statement of Contribution

Dr Naran Naren, a former PhD student in Zhang laboratory, performed the EMSA data shown in Fig. S4.1.

This work involved 3 recombinant plasmids and 3 mutants (unpublished) constructed by Dr Yunhao Liu and Dr Monica Gerth, prior to the start my PhD study. The specific details are provided in the list of bacterial strains and plasmids (Table 4.1).

Chapter 5
Conclusions and future perspectives

In this study, we examined the molecular basis of regulation of histidine catabolism in a human opportunistic pathogen *P. aeruginosa* PAO1. Significantly, this study strengthened our understanding of histidine catabolism in *P*. *aeruginosa* PAO1 and identified a potential mechanism for interplay of metabolism and virulence. First, we identified and characterized *figRAT* operon for the uptake and utilization of FIGLU, a histidine metabolite, likely accumulated in the host tissues. Second, we were able to show that HutC, the transcriptional regulator of *hut* operons, also plays a role in the expression of virulence factors such as antibiotic-induced biofilm formation, cell motilities, and necessary for PAO1 full virulence towards *C*. *elegans* infection model. Finally, through in vitro and phenotypic assays we demonstrated that the mode of HutC regulation of *hut* genes vary between *Pseudomonas* spp. and was critical for histidine utilization in a species dependent manner.

5.1 Identification of a new catabolic pathway for the uptake and utilization of FIGLU in *P. aeruginosa* PAO1

FIGLU is widely known as a histidine metabolite, produced during histidine catabolism, catabolized as part of histidine degradation in several Gram-negative and positive bacteria (Bender, 2012). Moreover, the differences in the number of enzymatic steps involved in the degradation of FIGLU to glutamate form the basis of the classification of histidine catabolic pathways as 4- and 5 steps in enteric bacteria and *Pseudomonas*, respectively (Itoh *et al.*, 2007, Bender, 2012). However, *P*. *aeruginosa* PAO1 contains dual enzymes for the degradation of FIGLU; one part of the 5-step *hut* pathway (*hutF*) and other (*figA*) located elsewhere in the genome with its own regulator (*figR*) capable of facilitating 4-step histidine catabolism (Marti-Arbona *et al.*, 2006, Gerth *et al.*, 2012). This was indeed surprising because the co-presence of functionally redundant enzymes for FIGLU degradation was not reported in other organisms (Bender, 2012), and the functional relevance of this additional pathway largely remained unknown.

However, our study identified a FIGLU specific transporter gene *figT* adjacent to *figRA* in *P*. *aeruginosa* PAO1. Consequently, we determined that the FigRAT system is involved in the uptake and utilization of FIGLU but not associated with histidine catabolism. An independent system for the uptake and utilization of FIGLU has not been previously described in any other organism to the best of our knowledge. In humans, FIGLU is produced as an intermediate of histidine catabolism and is coupled with folate metabolism (Solans *et al.*, 2000, Mao *et al.*,

2004). Elevated levels of urinary excretion of FIGLU occur with folate and vitamin B12 deficiencies, certain anaemia and neoplastic diseases, histidinaemia, hepatological cirrhosis, and other conditions (Hibbard, 1964, Carey *et al.*, 1964, Perry *et al.*, 1975, Majumdar *et al.*, 2017, Hilton *et al.*, 2003, Mohamed & Roberts, 1966, Luhby & Cooperman, 1964, Matsuda *et al.*, 1982). This indicates the possibility of FIGLU accumulation in various tissues and could be utilized as a nutrient source by the invading pathogen such as *P. aeruginosa*. Urinary excretion of FIGLU, associated with folate and Vitamin B12 deficiencies, also occurs in animals and fishes (Stebbings & Lewis, 1986, Quirk & Norton, 1988, Casu *et al.*, 2019). In reptiles, FIGLU appears to be the end-product of histidine catabolism (Herbert, 1968, Coulson & Hernandez, 1968). Homolog search showed that *figRAT* is highly conserved in all strains of *P. aeruginosa* and clustered in the genomes of some *Pseudomonas* spp. and a few other genera. The very high prevalence of *figRAT* in *P. aeruginosa* implies that FIGLU could be an important nutrient source providing an advantage for host colonization and causing infections. Indeed, a study that compared *P. aeruginosa* (15 human isolates) transcriptome during human infection to that of laboratory conditions identified upregulation in *figR* (>3.6-fold), *figA* (>2.8-fold), and *figT* (>1.5-fold) genes (Cornforth *et al.*, 2018).

The primary basis for the association of bacteria with eukaryotic host is to derive nutrients for their growth and proliferation. However, with trillions of commensal bacteria in the humans the invading pathogen faces tight competition for nutrients essential for survival and only those that are metabolically fit survives. For example, ability to utilize sialic acid is significant for the intestinal colonization of *V. cholerae* demonstrated in animal models (Almagro-Moreno & Boyd, 2009, McDonald *et al.*, 2016). Significantly, certain host-derived nutrients are also important for full virulence and pathogenesis of the invading pathogen. *Legionella pneumophila* is an intracellular pathogen that requires amino acid threonine of replication in phagosomes (Sauer *et al.*, 2005). Similarly, *P. aeruginosa* defective in amino acid alanine utilization displayed impaired virulence in a rat infection model (Boulette *et al.*, 2009). The rise in antibiotic resistance is a major threat to public health and require urgent development of novel therapeutics. In this regard, targeting metabolic pathways have great therapeutic potential because selection for resistance can be minimised. But this requires a deeper understanding of the metabolic pathways from a bacterial perspective. Here, we identified a system, FigRAT operon, in *P. aeruginosa* PAO1 for the uptake and utilization of FIGLU likely accumulated in the host tissues that potentially contributes to *P. aeruginosa* pathogenesis. Considering *figRAT* genes are also induced during human infection, further work is needed to determine the clinical significance of the pathway in *P. aeruginosa* infections.

5.2 Global regulatory role of HutC in *P. aeruginosa* PAO1

HutC has long been recognised as a transcriptional repressor of *hut* genes for histidine utilization in enteric bacteria and *Pseudomonas* (Itoh *et al.*, 2007, Bender, 2012). However, recent studies indicate that HutC has a significant role in gene regulation beyond histidine catabolism in some genera. HutC regulates the expression of *virB* (T4SS) operon and *btaE* (adhesin for cell attachment) in the zoonotic pathogen *Brucella abortus* (Sieira *et al.*, 2010, Sieira *et al.*, 2017). In *Yersinia pseudotuberculosis*, HutC regulates *flhDC* operon encoding for the master regulator of motility (Joshua *et al.*, 2015). A recent work from our laboratory in *P. fluorescens* SBW25, a plant-colonizing bacteria, identified that HutC regulates the expression of *ntrBC* (global regulator of cellular nitrogen metabolism) and *plcC* (phosphatidyl catabolism) genes (Naren & Zhang, 2020, Naren & Zhang, 2021).

In this study, we were able to show that HutC has a global effect in the expression of virulence traits in the human pathogen *P. aeruginosa* PAO1. HutC recognizes and binds to the promoter regions of genes encoding for virulence factors associated with tobramycin-induced biofilm formation (*arr*), motility (*bsWR*), and long-chain fatty acid utilization (*faoAB*) among others. These genes appear to be important during *P. aeruginosa* infection as they have been found induced during human infections compared to in vitro conditions. Through phenotypic analyses we confirmed that HutC plays a significant role in tobramycin-induced biofilm formation, motilities such as swimming, swarming, and twitching, and pyoverdine synthesis. Further, HutC was required for *P. aeruginosa* PAO1 full virulence towards *C. elegans* infection model. Thus, we were able to identify a new virulence factor in *P. aeruginosa* PAO1.

Our findings have significant implication in the study of host-pathogen interactions. Pathogens need to recognize suitable host to coordinate the expression of virulence and metabolic pathways for successful of colonizing of host. Host-recognition is a crucial step in infection pathogenesis and could be mediated by specific signals, such as nutrients present in the host (Galletti *et al.*, 2009, Rohmer *et al.*, 2011). In this regard, urocanate accumulated in the host tissues such as skin (Hug *et al.*, 1999, Snellman *et al.*, 1999) is a potential signal for *P. aeruginosa* colonization (Zhang *et al.*, 2014). Urocanate is also the inducer for HutC, and both urocanate and HutC may function analogous to a one-component system, presumably coordinating the expression of metabolic and virulence genes for adapting to the host environment as previously proposed (Zhang *et al.*, 2014). Here, we were able to provide empirical evidence demonstrating that HutC could regulate virulence trait expression but if this requires urocanate as a signalling molecule or nutrient source during infection needs to further be determined. However, there is some evidence that *hutU* (urocanase) and *hutH* (histidase) genes are upregulated by at least 17-fold and 30-fold, respectively, in *P. aeruginosa* exposed

to cultured human airway epithelial cells compared to laboratory growth conditions (Chugani & Greenberg, 2007). This possibly indicates that urocanate may serve as a nutrient source, and the metabolic regulator HutC may function as a dual regulator of metabolism and virulence during infection.

Further, the finding that HutC is involved in the regulation of multiple virulence traits of *P. aeruginosa* PAO1 is significant from a therapeutic perspective considering multiple-antibiotic resistance is a major public threat at present. Antivirulents targeting virulence factors (Maurice *et al.*, 2018) such as biofilm, quorum sensing, and pyoverdine have been proposed for use as monotherapies or in combination with currently available antibiotics. Therefore, by targeting HutC the global expression of virulence traits could be influenced simultaneously. Also, these strategies could be used to treat other pathogens as HutC mediated regulation of virulence genes is not restricted to *P. aeruginosa*.

However, our study has certain limitations. As a preliminary work, we investigated the effect of HutC in the expression of virulence phenotypes in a laboratory strain of *P. aeruginosa* PAO1. We need to extend our study to more virulent strains such as *P. aeruginosa* PAK and clinical isolates from burn wound infections or cystic fibrosis sputum to determine the clinical significance of our findings. Further, we were not able to provide mechanistic insights into the HutC mode of regulation of candidate genes examined in this study. HutC target-site search utilizing position weight matrix and experiments of DNA-Protein binding assays in isolation do not capture the true binding sites utilized in vivo. Therefore, high-throughput SELEX technology or Chip-Seq to pull out all HutC targets in the genome should be thought. This should be accompanied by expression studies such as RNA-seq or microarrays to understand the mechanism of gene regulation.

5.3 Distinct modes of HutC regulation of *hutF* expression in *Pseudomonas*

Transcriptional regulators bind sequences embedded in the genomic DNA in a sequence-specific manner that discern gene expression and consequent biological events (van Hijum *et al.*, 2009). Orthologs between related species generally display high conservation in binding motifs that are used to regulate genes in their regulon (Harari *et al.*, 2010). HutC orthologs from *Pseudomonas* spp. and other genera such as *Klebsiella aerogenes* and *Brucella abortus* are widely known to recognize motifs displaying high similarity to Phut site (TGTA-NN-TACA) to regulate *hut* genes (Sieira *et al.*, 2010, Naren & Zhang, 2020). However, our study showed that despite the high degree of conservation in the Phut site in *P. fluorescens* SBW25 and *P. aeruginosa* PAO1, HutC mode of regulation of *hutF* genes in the two species appear different.

We were able to show that HutC, independent of species, recognizes and binds an additional DNA sequence, Pntr site, adjacent to the Phut site in P_{hutF} DNA of *P*. *fluorescens* SBW25; contributing to HutC hexamer formation from complex protein oligomerization along the DNA. However, the Pntr site was absent in the P_{hutF} DNA in *P*. *aeruginosa* PAO1, resulting in the formation of HutC dimer with the DNA. Functional analysis indicated that Pntr site in P_{hutF} DNA of *P*. *fluorescens* SBW25 was required for growth on histidine but had negligible effects in *P*. *aeruginosa* PAO1. The inter-species differences in the HutC-binding sites presumably reflect gains and losses of binding sites during evolution, which may have been important for fine-tunning gene expression under different ecological conditions or adapt to genetic variations. Loss of the additional Pntr site may, therefore, could be associated with the gain of *figRAT* operon in *P*. *aeruginosa* PAO1.

We were able to show that HutC is a unique transcriptional regulator that can bind two distinct DNA motifs. This finding has significant implications considering that HutC has a global regulatory role in both *P*. *aeruginosa* PAO1 (this study) and *P*. *fluorescens* SBW25 (Naren & Zhang, 2020). Novel HutC-target sites in the genome was predicted by using the Position-Weight-Matrix of the canonical Phut site, and this may have missed Pntr target-sites that are part of the HutC regulon. Further work is, therefore, needed to determine the DNA-binding specificities of HutC to understand the mechanism of regulation as well as identify all potential targets. Also, in this study, we were not able to determine a precise role for the additional Pntr site in the expression of *hutF* promoter. Further expression studies are, therefore, required to understand the differences in gene expression with and without the Pntr site, and how this compares in *P*. *aeruginosa* PAO1. The findings from this work also implicate the importance of extending studies of regulation in related species as they may unravel species specific regulatory mechanisms, signal integration and facilitate use in genetic engineering such as for making biosensors (Merulla & van der Meer, 2016).

Chapter 6
Materials and Methods

This section details common experimental procedures that were not described in the "Materials and Methods" in Chapter 2, 3, and 4.

6.1 Standard Molecular Techniques, Gene cloning and Transformation

6.1.1 Polymerase Chain Reaction

6.1.1.1 Primer design

Oligonucleotide primers were designed in Geneious 9.0.5 (https://www.geneious.com) and synthesised by Integrated DNA Technologies Inc. (Singapore).

6.1.1.2 Standard PCR Reaction

The standard PCR reaction components are shown in Table 6.1. Reactions were added with 3% Dimethyl sulfoxide (DMSO), when amplifying *P. aeruginosa* PAO1 DNA. Taq polymerase, reaction buffer, and $MgCl_2$ were purchased from Invitrogen. Individual dNTPs (100 mM) were purchased from Bioline, and the dNTP mix was prepared at a final concentration of 10 mM by diluting in sterile MilliQ double distilled water. PCR reactions were carried out in a T100 thermocycler (Bio-Rad) under standard conditions, Table 6.2. Temperature gradient PCRs were performed to determine the optimum annealing temperature, when required.

Table 6.1 Standard PCR reaction.

PCR components	Volume (µl)	Final concentration
10x PCR Buffer	5	1x
$MgCl_2$ (50 mM)	1.5	1.5 mM
dNTP (10 mM)	1	0.2 mM
Primer 1 (10 µM)	1	0.2 µM
Primer 2 (10 µM)	1	0.2 µM
Taq DNA Polymerase (5U/µl)	0.2	1 U
Template DNA	5	~5-12 ng
MilliQ H_2O	35.3	

Table 6.2 PCR cycling parameters

PCR setup	Temperature °C	Duration	Cycle
Initial Denaturation	94	5 min	1
Denature template	94	45 sec	30
Anneal primers	56	45 sec	
Extension	72	30 sec/kb	
Final extension	72	10 min	1

6.1.2 Plasmid extraction

Omega bio-tek E.Z.N.A® plasmid Mini Kit I was used to extract plasmid DNA from bacterial cultures grown in LB media for 12-16 hours, following manufacturer's instructions. Plasmid from the column was eluted in sterile double distilled MilliQ water and stored at -20°C until use.

6.1.3 Restriction digestion

Restriction enzymes were purchased from Thermo Scientific™ or New England Biolabs. Digestions were carried out as per manufacturer's instructions. Reactions were incubated in a thermocycler and stopped by agarose gel purification or heat inactivation, depending on subsequent requirements.

6.1.4 DNA ligation

The insert and vector DNAs were mixed approximately at a 3:1 molar ratio in a microcentrifuge tube containing 1 µl of T4 DNA ligase (1U, Invitrogen) and 2 µl of 5x ligation reaction buffer. Sterile double distilled MilliQ water was added to a final volume of 10 µl, and the reaction was incubated overnight at 16°C in a thermocycler. 5 µl of the reaction was used for transformation.

6.1.5 Agarose gel electrophoresis

DNA fragments were separated on a gel of 1% agarose, prepared in 1x TBE Buffer (Invitrogen) containing 1x SYBR Safe™ DNA gel stain (Invitrogen). Samples were mixed with 6x DNA Loading Dye (Fermentas) and loaded into the gel along with GeneRuler 1 kb DNA ladder (Thermo Scientific™). The gels were run at 140V for 30-40 min in 1x TBE Buffer. The gels were visualized with a Safe Imager 2.0 Blue Light Transilluminator (Thermo Scientific™) and photographed with DigiDoc-It® Imaging System (UVP). When required, DNA was recovered from the gel by excising the desired bands and purified using GeneJET Gel Extraction Kit (Thermo Scientific™), as per manufacturer's instructions.

6.1.6 pCR8/GW/TOPO cloning

PCR products amplified by Taq DNA polymerase were first cloned into pCR™8 TOPO® TA vector (Invitrogen™) using the pCR™8/GW/TOPO® TA Cloning Kit to create an entry clone. After verifying sequence identity, the insert DNA was subcloned into appropriate destination vectors.

6.1.7 Preparation of chemically competent *E. coli* cells

E. coli strain from glycerol stock, stored in the -80°C freezer, was streaked onto an LB agar plate and incubated overnight at 37°C. A single colony was inoculated into a flask containing 30 ml of SOB broth and grown overnight at 37°C with shaking. 8 ml of the culture was then sub-cultured in another flask containing 200 ml of SOB broth at 37°C with shaking to an A_{600} of 0.5-0.6. The *E. coli* culture was distributed equally into 4x50 ml sterile centrifuge tubes and chilled on ice for 15 min. Cells were pelleted by centrifugation at 4000 g for 15 min at 4°C. Cells were then re-suspended in 16 ml of ice-cold transformation buffer I. Following a 15 min incubation on ice, cells were pelleted again by centrifugation and re-suspended in 2 ml of ice-cold transformation buffer II. Cells were aliquoted in 60 µl aliquots and stored at -80°C.

Transformation buffer I (250 ml)	
RbCl	3.0 g
$MnCl_2.4H_2O$	2.5 g
Potassium acetate (1M, pH 7.5)	7.g ml
$CaCl_2.2H_2O$	0.4 g
Glycerol	37.5 ml

pH was adjusted to 5.8 with 0.2 M acetic acid and the buffer was sterilized by filtration through a 0.22 µm membrane.

Transformation buffer II (250 ml)	
MOPS (0.5 M, pH 6.8)	5.0 ml
RbCl	0.3 g
$CaCl_2.2H_2O$	2.75 g
Glycerol	37.5 ml

Buffer was sterilized by filtration through a 0.22 µm membrane.

SOB medium (1 L)	
Tryptone	20.0 g
Yeast extract	5.0 g
NaCl	0.6 g
KCl	0.5 g
2 M Mg^{2+} stock	10 ml*

Sterilized by autoclaving. *2 M Mg^{2+} was filter sterilized and added into the sterilized SOB medium prior to use.

2M Mg^{2+} stock (100 ml)	
$MgCl_2$	20.3 g
$MgSO_4$	24.7 g

Sterilized by filtration through a 0.22 µm membrane

6.1.8 Preparation of electrocompetent *P. aeruginosa* PAO1

P. aeruginosa PAO1 strains from glycerol stock, stored in the -80°C freezer, were cultured overnight in LB broth at 37°C with shaking. 1.5 ml of the bacterial cultures were pelleted at 16,000 g for 1 min. The pellets were washed twice with 1 ml of sterile 300 mM Sucrose solution (stored at room temperature). Cells were re-suspended in 200 µl of the sucrose solution and separated into two 1.5 microcentrifuge tubes in equal volumes (~100 µl).

6.1.9 Preparation of electrocompetent *P. fluorescens* SBW25

P. fluorescens SBW25 strains from glycerol stock, stored in the -80°C freezer, were cultured overnight in LB broth at 28°C with shaking. 1 ml of the bacterial cultures were pelleted at 13,000 rpm for 1 min. The pellets were washed thrice with 1 ml of ice-cold sterile glycerol+HEPES buffer (10% glycerol and 1 mM HEPES). Cells were re-suspended in 100 µl of the ice-cold sterile buffer.

6.1.10 Transformation in *E. coli* using the heat-shock method

The chemically competent *E. coli* cells were thawed on ice and mixed with 2 µl of plasmid DNA or ligation mixture by gentle tapping. Following a 15-20 min incubation on ice, the cells were heat-shocked at 42°C in a water bath for 30 s. 400 µl of LB broth was immediately added and incubated at 37°C with shaking for an hour. The culture was spread on LB agar plates containing appropriate antibiotics and grown overnight at 37°C.

6.1.11 Transformation in *P. aeruginosa* PAO1 using electroporation

Freshly prepared electrocompetent *P. aeruginosa* PAO1 cells (at room temperature) were mixed with desired plasmid DNA (50~100 ng) and transferred into 0.1 cm-gap Gene Pulser/MicroPulser Elecctroporation cuvettes (Bio-Rad). Transformation was performed in Eppendorf® Electroporator 2510 at 1.8 kV. The cells were collected immediately in 600 µl of LB broth and incubated at 37°C with shaking for 1 hour. Cells were spread on LB agar plates containing antibiotics or other selective agents and incubated at 37°C for 24 hours. Colonies were purified by re-streaking on fresh LB agar plates containing appropriate selective agents. Transformants were confirmed by PCR from overnight cultures of single colony grown in LB broth.

6.1.12 Transformation in *P. fluorescens* SBW25 using electroporation

Freshly prepared electrocompetent *P. fluorescens* SBW25 cells were mixed with desired plasmid DNA (100~200 ng) and incubated on ice for 15-30 min. The cell and plasmid DNA mixtures were transferred into 0.1 cm-gap Gene Pulser/MicroPulser Elecctroporation cuvettes

(Bio-Rad) and transformation was performed in Eppendorf® Electroporator 2510 at 1.8 kV. The cells were collected immediately in 600 µl of LB broth and incubated at 28°C with shaking for 2 hours. Cells were spread on LB agar plates containing antibiotics or other selective agents and incubated at 28°C for 48 hours. Colonies were purified by re-streaking on fresh LB agar plates containing appropriate selective agents. Transformants were confirmed by PCR from overnight cultures of single colony grown in LB broth.

6.1.13 Glycerol-saline stock

Glycerol stocks of bacteria were prepared for long term storage at -80°C. Overnight cultures of bacterial strains were prepared by growing single colonies in LB broth with shaking at 28°C or 37°C. 1 ml of bacterial culture was mixed with 800 µl of sterile glycerol-saline [0.85% (w/v) NaCl, and 70% (v/v) Glycerol] solution in Nalgene™ General Long-Term Storage Cryogenic Tubes and stored at -80°C.

6.2 Mutant construction and gene complementation

Splicing by overlap extension PCR (SOE-PCR) (Horton *et al.*, 1989) technique was utilized to generate DNA fragments for chromosomal gene deletions or introducing specific mutations. Briefly, two fragments of length 500~600-bp flanking the target sites were PCR amplified using primers that leave complementary sequences of ~20-bp at the ends of each DNA fragment. Equal amounts of these fragments were used as template in a second PCR to fuse them at their complementary sites. The resulting single DNA fragment was cloned into pCR™8 TOPO® TA vector (Invitrogen™) using the pCR™8/GW/TOPO® TA Cloning Kit. After verifying sequence identity, insert DNA was sub-cloned into pUIC3 suicide vector by restriction digestion.

6.2.1 Tri-parental conjugation

6.2.1.1 *Pseudomonas aeruginosa* PAO1

Overnight cultures of *E. coli* DH5α λpir containing pUIC3+insert DNA (donor), *E. coli* DH5α containing pRK2013 plasmid (helper), and *P. aeruginosa* PAO1 strains (recipient) were prepared from -80°C freezer stocks, by growing in LB broth supplemented with appropriate antibiotics. Note that, *P. aeruginosa* PAO1 strains were grown at 43°C to minimize host restriction (Holloway, 1965). 250 µl of the recipient, donor, and helper strains, were pelleted by centrifugation at 12,000 g for 1 min. Cell pellets were washed once in 1 ml LB and re-suspended in 300 µl of LB each. All three cell cultures were mixed, pelleted a second time, and re-suspended in a final volume of ~30 µl LB. The suspension was spread on a LB agar plate with a sterile inoculating loop into a ~30 mm diameter spot until dry and incubated for 6-

8 hours at 37°C. The cells were scrapped off the plate with a sterile inoculating loop and re-suspended in 500 µl of LB. The bacterial suspension was spread over the surface of LB agar plates supplemented with tetracycline (100 µg/ml), nitrofurantoin (100 µg/ml), and X-gal (60 µg/ml) to select for transconjugants. Following a 24-h incubation at 37°C, single colonies were purified by streaking on fresh LB agar plates containing selective agents for cycloserine enrichment.

6.2.1.2 *Pseudomonas fluorescens* SBW25

Overnight cultures of *E. coli* DH5α λpir containing pUIC3+insert DNA (donor), *E. coli* DH5α containing pRK2013 plasmid (helper) and *P. fluorescens* SBW25 strains (recipient) were prepared from -80°C freezer stocks by growing in LB broth supplemented with appropriate antibiotics. 0.5 ml of the recipient cells were heat-shocked at 45°C in a water bath for 20 min. In the meantime, 0.5 ml of the donor and helper strains were pelleted by centrifugation at 13,000 rpm for 1 min and re-suspended both pellets together in a total volume of 0.5 ml LB. After heat-shock, the recipient and the donor+helper mix were pelleted, and mixed together in a total volume of 50 µl LB. The suspension was spread on a LB agar plate with a sterile inoculating loop into a ~30 mm diameter spot until dry and incubated overnight at 28°C. The cells were scrapped off the plate with a sterile inoculating loop and re-suspended in 3 ml sterile double distilled MQ water. The bacterial suspension was spread over the surface of LB agar plates supplemented with tetracycline (15 µg/ml), nitrofurantoin (100 µg/ml), and X-gal (60 µg/ml) to select for transconjugants. Following a 48-h incubation at 28°C, single colonies were purified by streaking on fresh LB agar plates containing selective agents for cycloserine enrichment.

6.2.2 Cycloserine enrichment

Desired mutant strains of *P. aeruginosa* PAO1 and *P. fluorescens* SBW25 that had lost the chromosomally integrated pUIC3-vector were selected by D-cycloserine enrichment process.

6.2.2.1 *Pseudomonas aeruginosa* PAO1

Six colonies of transconjugants (per strain) from tri-parental mating were grown overnight in 5 ml LB broth supplemented with tetracycline (20 µg/ml) at 37°C. The cultures were mixed in equal volumes and a 20 µl of the suspension was sub-cultured by growing in 400 ml LB for 24 hours with shaking at 37°C. 400 µl of the saturated culture was inoculated into fresh 20 ml pre-warmed LB and grown for 30 min with shaking at 37°C. Tetracycline was added at a final concentration of 20 µg/ml and growth was allowed to continue for another 2 hours. D-cycloserine was added at a final concentration of 1100 µg/ml and continued incubation for 4-

5 hours. 1 ml of the culture was pelleted and washed twice in sterile double distilled MilliQ water. Dilutions of the culture was spread on the surface of LB agar plates supplemented with X-gal (60 µg/ml) and incubated for 24 hourrs at 37°C. White clones were screened for mutations and loss of chromosomally integrated plasmid by PCR and sensitivity to tetracycline.

6.2.2.2 *Pseudomonas fluorescens* SBW25

Six colonies of transconjugants (per strain) from tri-parental mating were grown overnight in 5 ml LB broth supplemented with tetracycline (15 µg/ml) at 28°C. The cultures were mixed in equal volumes and a 20 µl of the suspension was sub-cultured by growing in 400 ml LB for 24 hours with shaking at 28°C. 400 µl of the saturated culture was inoculated into fresh 20 ml pre-warmed LB and grown for 30 min with shaking at 28°C. Tetracycline was added at a final concentration of 15 µg/ml and growth was allowed to continue for another 2 hours. D-cycloserine was added at a final concentration of 800 µg/ml and continued incubation for 5-6 hours. 1 ml of the culture was pelleted, washed twice in sterile double distilled MilliQ water, and re-suspended in 500 µl of sterile water. Dilutions of the culture was spread on the surface of LB agar plates supplemented with X-gal (60 µg/ml) and incubated for 48 hours at 28°C. White clones were screened for mutations and loss of chromosomally integrated plasmid by PCR and sensitivity to tetracycline.

6.2.3 Gene complementation

Desired DNA fragments were cloned into the multiple cloning site of pME6010 (Heeb *et al.*, 2000) or mini-Tn7 vectors (Choi & Schweizer, 2006) by PCR, restriction digestion, and DNA ligation as described in the previous sections. Mini-Tn7 vectors containing the desired insert DNA was introduced into the recipient strains (*P*. *aeruginosa* PAO1 or *P*. *fluorescens* SBW25) via electroporation with the help of pUX-BF13 plasmid (Bao *et al.*, 1991). pME6010 containing the desired insert DNA was introduced into the recipient strains by tri-parental mating.

6.3 β-galactosidase assays

6.3.1 Construction of transcriptional *lacZ* fusions

Promoter and gene *lacZ* fusions were constructed in pUC18-mini-Tn7TGm-*lacZ* or pUIC3 as described in each Chapter of this thesis. Briefly, the desired fragments were PCR amplified and cloned into pCR™8 TOPO® TA vector (Invitrogen™) using the pCR™8/GW/TOPO® TA Cloning Kit. After verifying sequence identity, the insert DNA was subcloned into desired plasmids and introduced into *P*. *aeruginosa* PAO1 or *P*. *fluorescens* SBW25 via electroporation or tri-parental mating.

6.3.2 β-galactosidase activity assay

The expression of *lacZ* reporter fusions were measured using 4-methylumbelliferyl-b-d-galactoside (4MUG) as the enzymatic substrate, whose cleavage produces a fluorescent molecule (4MU). *P. aeruginosa* or *P. fluorescens* strains from -80°C freezer stock were cultured overnight in LB broth with appropriate antibiotics. Cells were washed once in M9 salts and starved for 2 hours at 28°C (*P. fluorescens*) or 37°C (*P. aeruginosa*) to ensure that strains being compared were physiologically equal. The strains were inoculated into the test media at ~0.1 A_{600} and were continued to grow for a period of 24 hours. To measure *lacZ* expression, 1 ml of the culture was withdrawn at different time points and permeabilized with 20 µl of 0.1% SDS (sodium dodecyl sulfate) and 40 µl of chloroform. After thoroughly mixing the cells with permeabilization solution, samples were incubated at room temperature for 5 min. Subsequently, samples were diluted with sterile MilliQ water and a 40 µl aliquot of the sample was mixed with 160 µl of reaction cocktail. The reaction was allowed to proceed for 30 min at 37°C in a water bath and terminated by adding a 50 µl aliquot of 25% (w/v) trichloroacetic acid. The samples were cooled down by incubating on ice for 2-3 min and clarified by centrifugation at 13,000 rpm for 1 min. A 10 µl aliquot of the sample was thoroughly mixed with 990 µl of glycine-carbonate stop buffer. β-galactosidase activity was determined by measuring the fluorescence emitted by 7-hydroxy-4-methylcoumarin (4MU) at 460 nm after excitation at 365 nm using a Synergy 2 multi-detection microplate reader (Bio-Tek). Standards of 4-MU were prepared in a range of concentrations from 0 to 900 nM for estimating the concentration of 4-MU produced in the samples.

When the cells for the assay were grown in 200 µl of LB broth in 96-well microplates (Greiner Bio-One), the volume of the permeabilization solution was reduced by 5-fold.

Reaction cocktail	
Tris-HCl, pH 7.5	25 mM
NaCl	125 mM
$MgCl_2$	2 mM
β-mercaptoethanol	12 mM
4-MUG	0.3 mM*

2 mg of 4-MUG was first dissolved in 100 µl of absolute ethanol prior to adding to the solution

Glycine-carbonate stop buffer	
Glycine	133 mM
Na_2CO_3	83 mM

6.4 Protein expression and purification

6.4.1 Protein expression

E. *coli* containing the protein expression vector was grown overnight in 10 ml LB with shaking at 37°C. 8 ml of the culture was inoculated into fresh 400 ml LB and grown with shaking to an A_{600} of ~0.5 at 37°C. Protein expression was induced by the addition of 1 mM (final concentration) Isopropyl β-D-1-thiogalactopyranoside (IPTG). Protein expression was allowed to continue for 4 hours at 30°C. Cells were harvested by centrifugation at 4000 g for 20 min in 4°C. Cell pellets were stored at -20°C until use.

6.4.2 Protein purification

Cell pellets stored in -20°C were thawed on ice and resuspended in 30 ml of ice-cold lysis buffer. Lysozyme (1 mg/ml), PMSF (0.1 mM), and DNAse I (20 µg/ml) were added to the cell suspension at specified final concentrations and incubated on ice for 30 min. The resuspended cells were sonicated using MISONIX S-4000 Sonicator Ultrasonic Liquid Processor (30 s burst with 30 s pause at an amplitude of 60 mV) and pelleted by centrifugation at 4000 g for 20 min in 4°C. The supernatant was filtered through a 0.22 µm filter membrane and stored at 4°C.

Protein tagged with 6XHis affinity tags to the N-terminus were purified using TALON metal affinity resin (Clontech Laboratories Inc.). 2 ml of the TALON resin suspension in ethanol was transferred into a 30 ml centrifuge tube and pelleted for 2 min at 700 g in 4°C to remove excess ethanol. The resin was washed twice with 10 ml of ice-cold lysis buffer and gently mixed with the clarified protein solution by gentle shaking for an hour at 4°C. This facilitated binding of his-tagged proteins to the resin. The suspension was centrifuged for 5 min at 700 g in 4°C to remove the supernatant. Subsequently, the resin was washed with 10 ml ice-cold lysis buffer and resuspended in 1 ml of ice-cold lysis buffer. The resin was then loaded into a 5 ml gravity flow column and washed twice with 4 ml of lysis and wash buffers, respectively. Protein was eluted from the column in 5 ml elution buffer and stored as 500 µl aliquots at -20°C.

Lysis buffer	
HEPES, pH 7.4	20 mM
NaCl	500 mM
Imidazole	5 mM
Wash buffer	
HEPES, pH 7.4	20 mM
NaCl	500 mM
Imidazole	50 mM
Elution buffer	
HEPES, pH 7.4	20 mM
NaCl	500 mM
Imidazole	200 mM

Buffer was sterilized by filtration through a 0.22 µm membrane.

6.4.3 SDS-Polyacrylamide gel electrophoresis

Protein samples were mixed with 2x sample buffer and heated for 10 min at 95°C. The samples were clarified by centrifugation at 13,000 rpm for 1 min and loaded into the wells of a 5% stacking gel. Gel was run at 200V for 35 to 45 min using the Mini-PROTEAN Tetra cell (Bio-Rad) system until the dye reached bottom of the resolving gel. Subsequently, the gel was stained with Coomassie brilliant blue for an hour with gentle shaking and de-stained overnight at room temperature.

2x Sample buffer	
Tris-HCl, pH 6.8	125 mM
Glycerol	20%
SDS	4% (w/v)
β-mercaptoethanol	10% (w/v)
Bromophenol blue	0.02% (w/v)
10x SDS-PAGE running buffer, pH 8.3 (1 L)	
Tris base	30.3 g
Glycine	144 g
SDS	10 g
Stacking gel (5% acrylamide) (10 ml)	
Distilled water	6.1 ml
40% acrylamide/bis solution (29:1)	1.25 ml
0.5 M Tris-HCl, pH 6.8	2.5 ml
10% (w/v) SDS	0.1 ml
10% (w/v) APS	50 µl
TEMED	10 µl
Resolving gel (12% acrylamide) (10 ml)	
Distilled water	4.4 ml
40% acrylamide/bis solution (29:1)	3 ml
1.5 M Tris-HCl, pH8.8	2.5 ml
10% (w/v) SDS	0.1 ml
10% (w/v) APS	50 µl
TEMED	5 µl
Coomassie blue stain	
Coomassie brilliant blue R250	0.125%
Methanol	50%
Acetic acid	10%
De-stain solution	
Methanol	30%
Acetic acid	10%

6.4.4 Buffer exchange, protein concentration, and storage

Vivaspin® 6, 10 kDa MWCO Polyethersulfone (GE healthcare), was used to concentrate proteins and perform buffer exchange. Protein was loaded into a Vivaspin 6 concentrator, centrifuged at 4000 g in 4°C to a minimal volume of 1 ml. The concentrated protein was repeatedly diluted in a lower salt buffer solution (storage buffer) and concentrated again. Protein was stored at -20°C in 10% excess glycerol.

Storage buffer	
HEPES, pH 7.4	20 mM
NaCl	100 mM

6.4.5 Determination of protein concentration

Protein concentration was estimated by Bradford assay. A stock of BSA protein of known concentration was used as a standard to construct a standard curve for the estimation of protein concentration. 10 µl of BSA standards and protein samples were mixed with 500 µl of Quick Start™ Bradford 1x Dye Reagent (Bio-Rad) and incubated at room temperature for at least 5 min. The reactions were loaded into a 96-well microplate and absorbance was measured at 595 nm using a Synergy 2 multi-detection microplate reader (Bio-Tek). The concentration of protein was estimated from the BSA standard curve.

6.5 Electrophoretic Mobility Shift Assays (EMSAs)

6.5.1 Preparation of biotin labelled DNA probes

Biotin end-labelled probe DNAs were synthesised by PCR with a biotinylated primer using genomic DNA as template. Probes were purified by phenol:chloroform extraction followed by ethanol precipitation. An equal volume of 1:1 phenol/chloroform mixture was added into the DNA, thoroughly mixed, and centrifuged for 5 min at 10,000 rpm. The upper aqueous phase was carefully transferred into a fresh microcentrifuge tube and mixed with an equal volume of chloroform to remove residual phenol. Samples were centrifuged a second time, and the upper aqueous phase was carefully transferred into another microcentrifuge tube. $1/10^{th}$ volume of 3 M sodium acetate (pH 5.2) and 3 volumes of absolute ethanol were added to the aqueous phase and precipitated the DNA from the sample by incubating at -80°C for at least an hour. The sample DNA was pelleted by centrifugation at 15,000 g for 20 min and washed twice with 500 µl of ice-cold 70% ethanol. DNA pellets were air-dried, resuspended in 30-100 µl of DNAse free water and stored at -20°C.

6.5.2 EMSA reactions

The binding reactions (20 µl) were carried out by incubating protein with probe DNA (20 nM) for 30 min at 23°C in a buffer (pH 7.5) containing 10 mM HEPES, 5 mM $MgCl_2$, 50 mM KCl, 1 mM dithiothreitol, and 1 µg salmon sperm DNA (non-specific competitor). Reaction samples were mixed with 3 µl of loading buffer and were subjected to electrophoresis on a 5% polyacrylamide gel at 120 V for 1.5-2 hours in 0.5xTBE buffer using the Mini-PROTEAN Tetra cell (Bio-Rad) system. The gel was also pre-run in 0.5xTBE buffer at 120 V for 20 min prior to

loading the samples. Electrophoresis was carried out in a cold space to maintain low temperatures of ~4°C.

5% Native polyacrylamide gel (12 ml)	
10x TBE	0.6 ml
40% acrylamide/bis solution (60:1)	1.8 ml
50% Glycerol	1.2 ml
10% (w/v) APS	100 µl
TEMED	10 µl
Double distilled water	8.3 ml
10x EMSA Binding buffer (pH 7.5)	
HEPES	100 mM
KCl	500 mM
$MgCl_2$	50 mM
DTT	10 mM
Loading buffer	
Glycerol	60%
Bromophenol blue	0.025%
0.5x TBE buffer	
Tris-HCl, pH 8.3	50 mM
Boric acid	45 mM
EDTA	0.5 mM

6.5.3 Electroblotting and detection

The DNA from the gel was electrophoretically transferred to a nitrocellulose membrane (Sigma Aldrich) at 80 V for 1 hour in 0.5% TBE (maintaining low temperatures; ~ 4°C) and fixed by oven baking at 80°C for 30 min. The immobilized biotin labeled DNA on the membrane was detected using the Chemiluminescent Nucleic Acid Detection kit (ThermoFisher) as per the manufacturer's instructions. The images were photographed with a LAS-4000 luminescent imager installed with ImageQuant LAS 4000 software (Fujifilm), and further analysed in ImageJ program.

6.5.4 DNAse I footprinting assay

Binding reactions were carried out by incubating 2 µM DNA probe with protein for 30 min at 23°C in a 50 µl reaction buffer (containing 10 mM HEPES, 5 mM $MgCl_2$, 50 mM KCl, 1 mM dithiothreitol, and 1 µg salmon sperm DNA; pH 7.5). Subsequently, 50 µl of the co-factor solution (5 mM $CaCl_2$ and 10 mM $MgCl_2$) was added to the reaction with gentle mixing. The reaction was treated with 0.02 unit of DNAse I for 6 min and digestion was terminated immediately by adding 100 µl of DNAse I stop solution. The digested DNA fragments were purified and extracted by 1:1 phenol/chloroform treatment and ethanol precipitation at -80°C for an hour. Note that, 1 µl of glycogen was added into the samples during ethanol precipitation. Air-dried pellets were re-suspended in 8 µl of loading dye and heat denatured at

90°C for 15 min. Similarly, a G+A marker synthesized from chemical sequencing reaction was subjected to heat denaturation. The samples and G+A marker were subjected to electrophoresis on a 6% urea-polyacrylamide sequencing gel (21 x 40 cm) using the Sequi-Gen GT system (Bio-Rad Laboratories Pty). Electrophoresis was performed in 1x TBE buffer at 50W for 1.5-2 hours. The gel was pre-run for 30 min prior to loading the samples. The DNAs were transferred to a Whatman® Nytran™ SuPerCharge (SPC) nylon blotting membrane by contact blotting (performed overnight). One of the glass plates were carefully removed and the membrane was placed on the gel. Three layers of Whatman® 3MM papers were placed on top of the membrane, and subsequently the glass plate and a book weighing ~2 kg was placed on top of the other. The membrane with the DNA was heat immobilized by oven-baking at 80°C for 30 min. The DNA fragments were detected using the Chemiluminescent Nucleic Acid Detection kit (ThermoFisher) as per the manufacturer's instructions. The images were photographed with a LAS-4000 luminescent imager installed with ImageQuant LAS 4000 software (Fujifilm), and further analysed in ImageJ program.

DNAse I stop solution	
NaCl	200 mM
EDTA, pH 8.0	20 mM
SDS	1 %
6% Urea-polyacrylamide sequencing gel	
10x TBE	4 ml
40% acrylamide/bis solution (29:1)	6 ml
Urea	16.8 g
25% APS	50 µl
TEMED	50 µl
Loading dye	
Formamide	95%
Bromophenol blue	0.05%
EDTA	20 mM

6.5.5 Chemical synthesis of G+A marker

G+A marker for target DNA sequence was prepared using the Maxam-Gilbert chemical sequencing reactions. 10 µl of 20 µM biotin labelled DNA was mixed with 25 µl of formic acid and incubated for 5 min at 25˚C. The chemical reaction was stopped by adding 200 µl of hydrazine stop buffer, and the DNA was precipitated in 750 µl of ice-cold absolute ethanol. Following incubation for 2 hours at -80°C, DNA was pelleted by centrifugation for 15 min at 15,000 g in 4°C. DNA pellet was washed twice with 70% ice-cold ethanol, air-dried, and resuspended in 100 µl of freshly prepared 10% piperidine. The sample reaction was incubated for 30 min at 90°C. Subsequently, the DNA was precipitated by adding 10 µl of 3 M Sodium acetate (pH 7.0), 300 µl of ice-cold absolute ethanol, and incubation at -80°C for 2 hours. The

DNA was pelleted by centrifugation for 15 min at 15,000 g in 4°C, washed twice with 700 µl of 70% ice-cold ethanol, air-dried, and resuspended in 20 µl of the loading dye.

Hydrazine stop buffer	
Sodium Acetate, pH 7.0	300 mM
EDTA	0.1 mM
Yeast tRNA	20 µg/ml
Loading buffer	
Formamide	95%
Bromophenol blue	0.05%
EDTA	20 mM

References

Abu Kwaik, Y., and Bumann, D. (2013) Microbial quest for food in vivo: 'nutritional virulence' as an emerging paradigm. *Cell Microbiol* **15**: 882-890.

Adhin, M.R., and van Duin, J. (1990) Scanning model for translational reinitiation in eubacteria. *J Mol Biol* **213**: 811-818.

Akashi, H., and Gojobori, T. (2002) Metabolic efficiency and amino acid composition in the proteomes of *Escherichia coli* and *Bacillus subtilis*. *Proc Natl Acad Sci U S A* **99**: 3695-3700.

Allison, S.L., and Phillips, A.T. (1990) Nucleotide sequence of the gene encoding the repressor for the histidine utilization genes of *Pseudomonas putida*. *J Bacteriol* **172**: 5470-5476.

Almagro-Moreno, S., and Boyd, E.F. (2009) Sialic acid catabolism confers a competitive advantage to pathogenic *Vibrio cholerae* in the mouse intestine. *Infect Immun* **77**: 3807-3816.

Angus, B.L., Carey, A.M., Caron, D.A., Kropinski, A.M., and Hancock, R.E. (1982) Outer membrane permeability in *Pseudomonas aeruginosa:* comparison of a wild-type with an antibiotic-supersusceptible mutant. *Antimicrob Agents Chemother* **21**: 299-309.

Aravind, L., and Anantharaman, V. (2003) HutC/FarR-like bacterial transcription factors of the GntR family contain a small molecule-binding domain of the chorismate lyase fold. *FEMS Microbiol Lett* **222**: 17-23.

Arocena, G.M., Zorreguieta, A., and Sieira, R. (2012) Expression of VjbR under nutrient limitation conditions is regulated at the post-transcriptional level by specific acidic pH values and urocanic acid. *PLoS One* **7**: e35394.

Atkinson, M.R., Wray, L.V., Jr., and Fisher, S.H. (1990) Regulation of histidine and proline degradation enzymes by amino acid availability in *Bacillus subtilis*. *J Bacteriol* **172**: 4758-4765.

Baek, C.H., Wang, S., Roland, K.L., and Curtiss, R., 3rd (2009) Leucine-responsive regulatory protein (Lrp) acts as a virulence repressor in *Salmonella enterica* serovar Typhimurium. *J Bacteriol* **191**: 1278-1292.

Bailey, M.J., Lilley, A.K., Thompson, I.P., Rainey, P.B., and Ellis, R.J. (1995) Site directed chromosomal marking of a fluorescent pseudomonad isolated from the phytosphere of sugar beet; stability and potential for marker gene transfer. *Mol Ecol* **4**: 755-763.

Bailey, T.L., Boden, M., Buske, F.A., Frith, M., Grant, C.E., Clementi, L., Ren, J., Li, W.W., and Noble, W.S. (2009) MEME SUITE: tools for motif discovery and searching. *Nucleic Acids Res* **37**: W202-208.

Bailey, T.L., and Elkan, C. (1994) Fitting a mixture model by expectation maximization to discover motifs in biopolymers. *Proc Int Conf Intell Syst Mol Biol* **2**: 28-36.

Balasubramanian, D., Schneper, L., Kumari, H., and Mathee, K. (2013) A dynamic and intricate regulatory network determines *Pseudomonas aeruginosa* virulence. *Nucleic Acids Res* **41**: 1-20.

Balleza, E., Lopez-Bojorquez, L.N., Martinez-Antonio, A., Resendis-Antonio, O., Lozada-Chavez, I., Balderas-Martinez, Y.I., Encarnacion, S., and Collado-Vides, J. (2009) Regulation by transcription factors in bacteria: beyond description. *FEMS Microbiol Rev* **33**: 133-151.

Bandounas, L., Ballerstedt, H., de Winde, J.H., and Ruijssenaars, H.J. (2011) Redundancy in putrescine catabolism in solvent tolerant *Pseudomonas putida* S12. *J Biotechnol* **154**: 1-10.

Bao, Y., Lies, D.P., Fu, H., and Roberts, G.P. (1991) An improved Tn7-based system for the single-copy insertion of cloned genes into chromosomes of Gram-negative bacteria. *Gene* **109**: 167-168.

Bardoel, B.W., van der Ent, S., Pel, M.J., Tommassen, J., Pieterse, C.M., van Kessel, K.P., and van Strijp, J.A. (2011) *Pseudomonas* evades immune recognition of flagellin in both mammals and plants. *PLoS Pathog* **7**: e1002206.

Beckett, D. (2001) Regulated assembly of transcription factors and control of transcription initiation. *J Mol Biol* **314**: 335-352.

Bender, R.A. (2012) Regulation of the histidine utilization (hut) system in bacteria. *Microbiol Mol Biol Rev* **76**: 565-584.

Bortolotti, P., Hennart, B., Thieffry, C., Jausions, G., Faure, E., Grandjean, T., Thepaut, M., Dessein, R., Allorge, D., Guery, B.P., Faure, K., Kipnis, E., Toussaint, B., and Le Gouellec, A. (2016) Tryptophan catabolism in *Pseudomonas aeruginosa* and potential for inter-kingdom relationship. *BMC Microbiol* **16**: 137.

Boulette, M.L., Baynham, P.J., Jorth, P.A., Kukavica-Ibrulj, I., Longoria, A., Barrera, K., Levesque, R.C., and Whiteley, M. (2009) Characterization of alanine catabolism in *Pseudomonas aeruginosa* and its importance for proliferation in vivo. *J Bacteriol* **191**: 6329-6334.

Bowden, G., Mothibeli, M.A., Robb, F.T., and Woods, D.R. (1982) Regulation of hut enzymes and intracellular protease activities in *Vibrio alginolyticus hut* mutants. *J Gen Microbiol* **128**: 2041-2045.

Boylan, S.A., and Bender, R.A. (1984) Genetic and physical maps of *Klebsiella aerogenes* genes for histidine utilization (*hut*). *Mol Gen Genet* **193**: 99-103.

Brill, W.J., and Magasanik, B. (1969) Genetic and metabolic control of histidase and urocanase in *Salmonella typhimurium*, strain 15-59. *J Biol Chem* **244**: 5392-5402.

Brinkman, A.B., Ettema, T.J., de Vos, W.M., and van der Oost, J. (2003) The Lrp family of transcriptional regulators. *Mol Microbiol* **48**: 287-294.

Burrows, L.L. (2012) *Pseudomonas aeruginosa* twitching motility: type IV pili in action. *Annu Rev Microbiol* **66**: 493-520.

Caballero, A., Thibodeaux, B., Marquart, M., Traidej, M., and O'Callaghan, R. (2004) *Pseudomonas* keratitis: protease IV gene conservation, distribution, and production relative to virulence and other *Pseudomonas* proteases. *Invest Ophthalmol Vis Sci* **45**: 522-530.

Cabral, M.P., Soares, N.C., Aranda, J., Parreira, J.R., Rumbo, C., Poza, M., Valle, J., Calamia, V., Lasa, I., and Bou, G. (2011) Proteomic and functional analyses reveal a unique lifestyle for *Acinetobacter baumannii* biofilms and a key role for histidine metabolism. *J Proteome Res* **10**: 3399-3417.

Cameron, E.A., and Sperandio, V. (2015) Frenemies: Signaling and nutritional integration in Pathogen-Microbiota-Host interactions. *Cell Host Microbe* **18**: 275-284.

Carey, R.W., Brena, G.P., and Krant, M.J. (1964) Urinary formiminoglutamic acid excretion in patients with neoplastic disease. *Cancer* **17**: 713-722.

Casu, F., Watson, A.M., Yost, J., Leffler, J.W., Gaylord, T.G., Barrows, F.T., Sandifer, P.A., Denson, M.R., and Bearden, D.W. (2019) Investigation of graded-level soybean meal diets in red drum (*Sciaenops ocellatus*) using NMR-based metabolomics analysis. *Comp Biochem Physiol Part D Genomics Proteomics* **29**: 173-184.

Cezairliyan, B., Vinayavekhin, N., Grenfell-Lee, D., Yuen, G.J., Saghatelian, A., and Ausubel, F.M. (2013) Identification of *Pseudomonas aeruginosa* phenazines that kill *Caenorhabditis elegans*. *PLoS Pathog* **9**: e1003101.

Chakerian, A.E., and Matthews, K.S. (1992) Effect of lac repressor oligomerization on regulatory outcome. *Mol Microbiol* **6**: 963-968.

Chandler, C.E., Horspool, A.M., Hill, P.J., Wozniak, D.J., Schertzer, J.W., Rasko, D.A., and Ernst, R.K. (2019) Genomic and phenotypic diversity among ten laboratory isolates of *Pseudomonas aeruginosa* PAO1. *J Bacteriol* **201**: e00595-00518.

Chao, H., and Zhou, N.Y. (2013) GenR, an IclR-type regulator, activates and represses the transcription of gen genes involved in 3-hydroxybenzoate and gentisate catabolism in *Corynebacterium glutamicum*. *J Bacteriol* **195**: 1598-1609.

Chasin, L.A., and Magasanik, B. (1968) Induction and repression of the histidine-degrading enzymes of *Bacillus subtilis*. *J Biol Chem* **243**: 5165-5178.

Choi, K.H., and Schweizer, H.P. (2006) mini-Tn7 insertion in bacteria with single attTn7 sites: example *Pseudomonas aeruginosa*. *Nat Protoc* **1**: 153-161.

Chou, H.T., Li, J.Y., Peng, Y.C., and Lu, C.D. (2013) Molecular characterization of PauR and its role in control of putrescine and cadaverine catabolism through the gamma-glutamylation pathway in *Pseudomonas aeruginosa* PAO1. *J Bacteriol* **195**: 3906-3913.

Chouikha, I., Sturdevant, D.E., Jarrett, C., Sun, Y.C., and Hinnebusch, B.J. (2019) Differential gene expression patterns of *Yersinia pestis* and *Yersinia pseudotuberculosis* during infection and biofilm formation in the flea digestive tract. *mSystems* **4**: e00217-00218.

Chugani, S., and Greenberg, E.P. (2007) The influence of human respiratory epithelia on *Pseudomonas aeruginosa* gene expression. *Microb Pathog* **42**: 29-35.

Clatworthy, A.E., Lee, J.S., Leibman, M., Kostun, Z., Davidson, A.J., and Hung, D.T. (2009) *Pseudomonas aeruginosa* infection of zebrafish involves both host and pathogen determinants. *Infect Immun* **77**: 1293-1303.

Cohen, T.S., and Prince, A. (2012) Cystic fibrosis: a mucosal immunodeficiency syndrome. *Nat Med* **18**: 509-519.

Collier, D.N., Hager, P.W., and Phibbs, P.V., Jr. (1996) Catabolite repression control in the *Pseudomonads*. *Res Microbiol* **147**: 551-561.

Colvin, K.M., Irie, Y., Tart, C.S., Urbano, R., Whitney, J.C., Ryder, C., Howell, P.L., Wozniak, D.J., and Parsek, M.R. (2012) The Pel and Psl polysaccharides provide *Pseudomonas aeruginosa* structural redundancy within the biofilm matrix. *Environ Microbiol* **14**: 1913-1928.

Consevage, M.W., Porter, R.D., and Phillips, A.T. (1985) Cloning and expression in *Escherichia coli* of histidine utilization genes from *Pseudomonas putida*. *J Bacteriol* **162**: 138-146.

Coppens, L., and Lavigne, R. (2020) SAPPHIRE: a neural network based classifier for sigma70 promoter prediction in *Pseudomonas*. *BMC Bioinformatics* **21**: 415.

Cornforth, D.M., Dees, J.L., Ibberson, C.B., Huse, H.K., Mathiesen, I.H., Kirketerp-Moller, K., Wolcott, R.D., Rumbaugh, K.P., Bjarnsholt, T., and Whiteley, M. (2018) *Pseudomonas aeruginosa* transcriptome during human infection. *Proc Natl Acad Sci U S A* **115**: E5125-E5134.

Coulson, R.A., and Hernandez, T. (1968) Amino acid metabolism in chameleons. *Comp Biochem Physiol* **25**: 861-872.

Crooks, G.E., Hon, G., Chandonia, J.M., and Brenner, S.E. (2004) WebLogo: a sequence logo generator. *Genome Res* **14**: 1188-1190.

Cui, Y., Wang, Q., Stormo, G.D., and Calvo, J.M. (1995) A consensus sequence for binding of Lrp to DNA. *J Bacteriol* **177**: 4872-4880.

Cusumano, Z.T., Watson, M.E., Jr., and Caparon, M.G. (2014) *Streptococcus pyogenes* arginine and citrulline catabolism promotes infection and modulates innate immunity. *Infect Immun* **82**: 233-242.

D'Ari, R., Lin, R.T., and Newman, E.B. (1993) The leucine-responsive regulatory protein: more than a regulator? *Trends Biochem Sci* **18**: 260-263.

de Bentzmann, S., Roger, P., Dupuit, F., Bajolet-Laudinat, O., Fuchey, C., Plotkowski, M.C., and Puchelle, E. (1996) Asialo GM1 is a receptor for *Pseudomonas aeruginosa* adherence to regenerating respiratory epithelial cells. *Infect Immun* **64**: 1582-1588.

Diaz-Perez, A.L., Nunez, C., Meza Carmen, V., and Campos-Garcia, J. (2018) The expression of the genes involved in leucine catabolism of *Pseudomonas aeruginosa* is controlled by the transcriptional regulator LiuR and by the CbrAB/Crc system. *Res Microbiol* **169**: 324-334.

Ding, Y., Teo, J.W.P., Drautz-Moses, D.I., Schuster, S.C., Givskov, M., and Yang, L. (2018) Acquisition of resistance to carbapenem and macrolide-mediated quorum sensing inhibition by *Pseudomonas aeruginosa* via ICETn*4371* 6385. *Commun Biol* **1**: 57.

Ditta, G., Stanfield, S., Corbin, D., and Helinski, D.R. (1980) Broad host range DNA cloning system for gram-negative bacteria: construction of a gene bank of *Rhizobium meliloti*. *Proc Natl Acad Sci U S A* **77**: 7347-7351.

Drenkard, E. (2003) Antimicrobial resistance of *Pseudomonas aeruginosa* biofilms. *Microbes Infect* **5**: 1213-1219.

Eisenreich, W., Heesemann, J., Rudel, T., and Goebel, W. (2015) Metabolic adaptations of intracellullar bacterial pathogens and their mammalian host cells during infection ("Pathometabolism"). *Microbiol Spectr* **3**.

Ertugrul, B.M., Lipsky, B.A., Ture, M., and Sakarya, S. (2017) Risk factors for infection with *Pseudomonas aeruginosa* in diabetic foot infections. *J Am Podiatr Med Assoc* **107**: 483-489.

Everett, M.J., and Davies, D.T. (2021) *Pseudomonas aeruginosa* elastase (LasB) as a therapeutic target. *Drug Discov Today*.

Faure, E., Kwong, K., and Nguyen, D. (2018) *Pseudomonas aeruginosa* in chronic lung infections: How to adapt within the host? *Front Immunol* **9**: 2416.

Fisher, S.H. (1999) Regulation of nitrogen metabolism in *Bacillus subtilis*: vive la difference! *Mol Microbiol* **32**: 223-232.

Fisher, S.H., Rohrer, K., and Ferson, A.E. (1996) Role of CodY in regulation of the *Bacillus subtilis hut* operon. *J Bacteriol* **178**: 3779-3784.

Flemming, H.C., and Wingender, J. (2010) The biofilm matrix. *Nat Rev Microbiol* **8**: 623-633.

Friedberg, D., Midkiff, M., and Calvo, J.M. (2001) Global versus local regulatory roles for Lrp-related proteins: *Haemophilus influenzae* as a case study. *J Bacteriol* **183**: 4004-4011.

Gallagher, L.A., and Manoil, C. (2001) *Pseudomonas aeruginosa* PAO1 kills *Caenorhabditis elegans* by cyanide poisoning. *J Bacteriol* **183**: 6207-6214.

Galletti, R., De Lorenzo, G., and Ferrari, S. (2009) Host-derived signals activate plant innate immunity. *Plant Signal Behav* **4**: 33-34.

Gellatly, S.L., and Hancock, R.E. (2013) *Pseudomonas aeruginosa*: new insights into pathogenesis and host defenses. *Pathog Dis* **67**: 159-173.

Gerth, M.L., Ferla, M.P., and Rainey, P.B. (2012) The origin and ecological significance of multiple branches for histidine utilization in *Pseudomonas aeruginosa* PAO1. *Environ Microbiol* **14**: 1929-1940.

Gerth, M.L., Liu, Y., Jiao, W., Zhang, X.X., Baker, E.N., Lott, J.S., Rainey, P.B., and Johnston, J.M. (2017) Crystal structure of a bicupin protein HutD involved in histidine utilization in *Pseudomonas*. *Proteins* **85**: 1580-1588.

Gibbs, N.K., and Norval, M. (2011) Urocanic acid in the skin: a mixed blessing? *J Invest Dermatol* **131**: 14-17.

Glik, J., Labus, W., Kitala, D., Mikus-Zagorska, K., Roberts, C.D., Nowak, M., Kasperczyk, A., and Kawecki, M. (2018) A 2000 patient retrospective assessment of a new strategy for burn wound management in view of infection prevention and treatment. *Int Wound J* **15**: 344-349.

Goldberg, R.B., and Magasanik, B. (1975) Gene order of the histidine utilization (*hut*) operons in *Klebsiella aerogenes*. *J Bacteriol* **122**: 1025-1031.

Gomila, M., Pena, A., Mulet, M., Lalucat, J., and Garcia-Valdes, E. (2015) Phylogenomics and systematics in *Pseudomonas*. *Front Microbiol* **6**: 214.

Gorelik, M., Lunin, V.V., Skarina, T., and Savchenko, A. (2006) Structural characterization of GntR/HutC family signaling domain. *Protein Sci* **15**: 1506-1511.

Gorke, B., and Stulke, J. (2008) Carbon catabolite repression in bacteria: many ways to make the most out of nutrients. *Nat Rev Micro* **6**: 613-624.

Goss, T.J., and Bender, R.A. (1995) The nitrogen assimilation control protein, NAC, is a DNA binding transcription activator in *Klebsiella aerogenes*. *J Bacteriol* **177**: 3546-3555.

Grant, C.E., Bailey, T.L., and Noble, W.S. (2011) FIMO: scanning for occurrences of a given motif. *Bioinformatics* **27**: 1017-1018.

Guo, Z., and Houghton, J.E. (1999) PcaR-mediated activation and repression of *pca* genes from *Pseudomonas putida* are propagated by its binding to both the -35 and the -10 promoter elements. *Mol Microbiol* **32**: 253-263.

Hagen, D.C., Gerson, S.L., and Magasanik, B. (1975) Isolation of super-repressor mutants in the histidine utilization system of *Salmonella typhimurium*. *J Bacteriol* **121**: 583-593.

Hagen, D.C., and Magasanik, B. (1973) Isolation of the self-regulated repressor protein of the *Hut* operons of *Salmonella typhimurium*. *Proc Natl Acad Sci U S A* **70**: 808-812.

Hagen, D.C., and Magasanik, B. (1976) Deoxyribonucleic acid-binding studies on the *hut* repressor and mutant forms of the *hut* repressor of *Salmonella typhimurium*. *J Bacteriol* **127**: 837-847.

Hall, C.L., and Lee, V.T. (2018) Cyclic-di-GMP regulation of virulence in bacterial pathogens. *Wiley Interdiscip Rev RNA* **9**: n/a-n/a.

Hall, C.W., and Mah, T.F. (2017) Molecular mechanisms of biofilm-based antibiotic resistance and tolerance in pathogenic bacteria. *FEMS Microbiol Rev* **41**: 276-301.

Harari, O., Park, S.Y., Huang, H., Groisman, E.A., and Zwir, I. (2010) Defining the plasticity of transcription factor binding sites by Deconstructing DNA consensus sequences: the PhoP-binding sites among gamma/enterobacteria. *PLoS Comput Biol* **6**: e1000862.

Hatchette, T.F., Gupta, R., and Marrie, T.J. (2000) *Pseudomonas aeruginosa* community-acquired pneumonia in previously healthy adults: case report and review of the literature. *Clin Infect Dis* **31**: 1349-1356.

Hauser, A.R. (2009) The type III secretion system of *Pseudomonas aeruginosa*: infection by injection. *Nat Rev Microbiol* **7**: 654-665.

Haydon, D.J., and Guest, J.R. (1991) A new family of bacterial regulatory proteins. *FEMS Microbiol Lett* **63**: 291-295.

Heeb, S., Itoh, Y., Nishijyo, T., Schnider, U., Keel, C., Wade, J., Walsh, U., O'Gara, F., and Haas, D. (2000) Small, stable shuttle vectors based on the minimal pVS1 replicon for use in gram-negative, plant-associated bacteria. *Mol Plant Microbe Interact* **13**: 232-237.

Held, K., Ramage, E., Jacobs, M., Gallagher, L., and Manoil, C. (2012) Sequence-verified two-allele transposon mutant library for *Pseudomonas aeruginosa* PAO1. *J Bacteriol* **194**: 6387-6389.

Henkin, T.M. (1996) The role of CcpA transcriptional regulator in carbon metabolism in *Bacillus subtilis*. *FEMS Microbiol Lett* **135**: 9-15.

Herbert, J.D. (1968) Histidine catabolism in vivo. *Comp Biochem Physiol* **24**: 229-242.

Hernandez-Arranz, S., Moreno, R., and Rojo, F. (2013) The translational repressor Crc controls the *Pseudomonas putida* benzoate and alkane catabolic pathways using a multi-tier regulation strategy. *Environ Microbiol* **15**: 227-241.

Herrou, J., Czyz, D.M., Fiebig, A., Willett, J.W., Kim, Y., Wu, R., Babnigg, G., and Crosson, S. (2018) Molecular control of gene expression by *Brucella* BaaR, an IclR-type transcriptional repressor. *J Biol Chem* **293**: 7437-7456.

Hibbard, B.M. (1964) The role of folic acid in pregnancy; with particular reference to anaemia, abruption and abortion. *J Obstet Gynaecol Br Commonw* **71**: 529-542.

Hildebrandt, T.M., Nunes Nesi, A., Araujo, W.L., and Braun, H.P. (2015) Amino Acid Catabolism in Plants. *Mol Plant* **8**: 1563-1579.

Hilton, J.F., Christensen, K.E., Watkins, D., Raby, B.A., Renaud, Y., de la Luna, S., Estivill, X., MacKenzie, R.E., Hudson, T.J., and Rosenblatt, D.S. (2003) The molecular basis of glutamate formiminotransferase deficiency. *Hum Mutat* **22**: 67-73.

Hoffman, L.R., D'Argenio, D.A., MacCoss, M.J., Zhang, Z., Jones, R.A., and Miller, S.I. (2005) Aminoglycoside antibiotics induce bacterial biofilm formation. *Nature* **436**: 1171-1175.

Hoiby, N., Bjarnsholt, T., Givskov, M., Molin, S., and Ciofu, O. (2010) Antibiotic resistance of bacterial biofilms. *Int J Antimicrob Agents* **35**: 322-332.

Holder, I.A., Neely, A.N., and Frank, D.W. (2001) Type III secretion/intoxication system important in virulence of *Pseudomonas aeruginosa* infections in burns. *Burns* **27**: 129-130.

Holloway, B.W. (1965) Variations in restriction and modification of bacteriophage following increase of growth temperature of *Pseudomonas aeruginosa*. *Virology* **25**: 634-642.

Horton, R.M., Hunt, H.D., Ho, S.N., Pullen, J.K., and Pease, L.R. (1989) Engineering hybrid genes without the use of restriction enzymes: gene splicing by overlap extension. *Gene* **77**: 61-68.

Hu, L., Allison, S.L., and Phillips, A.T. (1989) Identification of multiple repressor recognition sites in the *hut* system of *Pseudomonas putida*. *J Bacteriol* **171**: 4189-4195.

Hu, L., Mulfinger, L.M., and Phillips, A.T. (1987) Purification and properties of formylglutamate amidohydrolase from *Pseudomonas putida*. *J Bacteriol* **169**: 4696-4702.

Hu, L., and Phillips, A.T. (1988) Organization and multiple regulation of histidine utilization genes in *Pseudomonas putida*. *J Bacteriol* **170**: 4272-4279.

Hug, D.H., Dunkerson, D.D., and Hunter, J.K. (1999) The degradation of L-histidine and trans- and cis-urocanic acid by bacteria from skin and the role of bacterial cis-urocanic acid isomerase. *J Photochem Photobiol B* **50**: 66-73.

Hug, D.H., Roth, D., and Hunter, J. (1968) Regulation of histidine catabolism by succinate in *Pseudomonas putida*. *J Bacteriol* **96**: 396-402.

Itoh, R. (1970) A comparative study of formiminotransfer from formiminoglutamic acid to tetrahydrofolic acid in animals. *Int J Biochem* **1**: 617-623.

Itoh, Y., Nishijyo, T., and Nakada, Y., (2007) Histidine catabolism and catabolite regulation. In: Pseudomonas*.* J.-L. Ramos & A. Filloux (eds). Dordrecht: Springer Netherlands, pp. 371-395.

Jacobs, M.A., Alwood, A., Thaipisuttikul, I., Spencer, D., Haugen, E., Ernst, S., Will, O., Kaul, R., Raymond, C., Levy, R., Chun-Rong, L., Guenthner, D., Bovee, D., Olson, M.V., and Manoil, C. (2003) Comprehensive transposon mutant library of *Pseudomonas aeruginosa*. *Proc Natl Acad Sci U S A* **100**: 14339-14344.

Jain, M., Ramirez, D., Seshadri, R., Cullina, J.F., Powers, C.A., Schulert, G.S., Bar-Meir, M., Sullivan, C.L., McColley, S.A., and Hauser, A.R. (2004) Type III secretion phenotypes of *Pseudomonas aeruginosa* strains change during infection of individuals with cystic fibrosis. *J Clin Microbiol* **42**: 5229-5237.

Janssen, D.B., Herst, P.M., Joosten, H.M., and van der Drift, C. (1982) Regulation of amidase formation in mutants from *Pseudomonas aeruginosa* PAO lacking glutamine synthetase activity. *Arch Microbiol* **131**: 344-346.

Jimenez, L. (2007) Microbial diversity in pharmaceutical product recalls and environments. *PDA J Pharm Sci Technol* **61**: 383-399.

Johnson, D.A., Tetu, S.G., Phillippy, K., Chen, J., Ren, Q., and Paulsen, I.T. (2008) High-throughput phenotypic characterization of *Pseudomonas aeruginosa* membrane transport genes. *PLoS Genet* **4**: e1000211.

Joshua, G.W., Atkinson, S., Goldstone, R.J., Patrick, H.L., Stabler, R.A., Purves, J., Camara, M., Williams, P., and Wren, B.W. (2015) Genome-wide evaluation of the interplay between *Caenorhabditis elegans* and *Yersinia pseudotuberculosis* during in vivo biofilm formation. *Infect Immun* **83**: 17-27.

Kaminskas, E., Kimhi, Y., and Magasanik, B. (1970) Urocanase and N-formimino-L-glutamate formiminohydrolase of *Bacillus subtilis*, two enzymes of the histidine degradation pathway. *J Biol Chem* **245**: 3536-3544.

Kanehisa, M., Furumichi, M., Tanabe, M., Sato, Y., and Morishima, K. (2017) KEGG: new perspectives on genomes, pathways, diseases and drugs. *Nucleic Acids Res* **45**: D353-D361.

Kaneko, Y., Thoendel, M., Olakanmi, O., Britigan, B.E., and Singh, P.K. (2007) The transition metal gallium disrupts *Pseudomonas aeruginosa* iron metabolism and has antimicrobial and antibiofilm activity. *J Clin Invest* **117**: 877-888.

Kang, D., Kirienko, D.R., Webster, P., Fisher, A.L., and Kirienko, N.V. (2018) Pyoverdine, a siderophore from *Pseudomonas aeruginosa*, translocates into *C. elegans*, removes iron, and activates a distinct host response. *Virulence* **9**: 804-817.

Kang, D., Revtovich, A.V., Chen, Q., Shah, K.N., Cannon, C.L., and Kirienko, N.V. (2019) Pyoverdine-dependent virulence of *Pseudomonas aeruginosa* isolates from cystic fibrosis patients. *Front Microbiol* **10**: 2048.

Kang, Y., Zarzycki-Siek, J., Walton, C.B., Norris, M.H., and Hoang, T.T. (2010) Multiple FadD acyl-CoA synthetases contribute to differential fatty acid degradation and virulence in *Pseudomonas aeruginosa*. *PLoS One* **5**: e13557.

Kariminik, A., Baseri-Salehi, M., and Kheirkhah, B. (2017) *Pseudomonas aeruginosa* quorum sensing modulates immune responses: An updated review article. *Immunol Lett* **190**: 1-6.

Kazmierczak, B.I., Schniederberend, M., and Jain, R. (2015) Cross-regulation of *Pseudomonas* motility systems: the intimate relationship between flagella, pili and virulence. *Curr Opin Microbiol* **28**: 78-82.

Kendrick, K.E., and Wheelis, M.L. (1982) Histidine dissimilation in *Streptomyces coelicolor*. *J Gen Microbiol* **128**: 2029-2040.

Khan, N.H., Ishii, Y., Kimata-Kino, N., Esaki, H., Nishino, T., Nishimura, M., and Kogure, K. (2007) Isolation of *Pseudomonas aeruginosa* from open ocean and comparison with freshwater, clinical, and animal isolates. *Microb Ecol* **53**: 173-186.

Kim, J.H., and Chambliss, G.H. (1997) Contacts between *Bacillus subtilis* catabolite regulatory protein CcpA and *amyO* target site. *Nucleic Acids Research* **25**: 3490-3496.

Kimhi, Y., and Magasanik, B. (1970) Genetic basis of histidine degradation in *Bacillus subtilis*. *J Biol Chem* **245**: 3545-3548.

Kirienko, D.R., Revtovich, A.V., Kirienko, N.V., and Blokesch, M. (2016) A high-content, phenotypic screen identifies fluorouridine as an inhibitor of pyoverdine biosynthesis and *Pseudomonas aeruginosa* virulence. *mSphere* **1**: e00217-00216.

Kirienko, N.V., Ausubel, F.M., and Ruvkun, G. (2015) Mitophagy confers resistance to siderophore-mediated killing by *Pseudomonas aeruginosa*. *Proc Natl Acad Sci U S A* **112**: 1821-1826.

Kirienko, N.V., Kirienko, D.R., Larkins-Ford, J., Wahlby, C., Ruvkun, G., and Ausubel, F.M. (2013) *Pseudomonas aeruginosa* disrupts *Caenorhabditis elegans* iron homeostasis, causing a hypoxic response and death. *Cell Host Microbe* **13**: 406-416.

Kloth, C., Schirmer, B., Munder, A., Stelzer, T., Rothschuh, J., and Seifert, R. (2018) The role of *Pseudomonas aeruginosa* ExoY in an acute mouse lung infection model. *Toxins (Basel)* **10**: 185.

Kohler, T., Curty, L.K., Barja, F., van Delden, C., and Pechere, J.C. (2000) Swarming of *Pseudomonas aeruginosa* is dependent on cell-to-cell signaling and requires flagella and pili. *J Bacteriol* **182**: 5990-5996.

Kollaran, A.M., Joge, S., Kotian, H.S., Badal, D., Prakash, D., Mishra, A., Varma, M., and Singh, V. (2019) Context-specific requirement of forty-four two-component loci in *Pseudomonas aeruginosa* swarming. *iScience* **13**: 305-317.

Koulenti, D., Lisboa, T., Brun-Buisson, C., Krueger, W., Macor, A., Sole-Violan, J., Diaz, E., Topeli, A., DeWaele, J., Carneiro, A., Martin-Loeches, I., Armaganidis, A., Rello, J., and Group, E.-V.C.S. (2009) Spectrum of practice in the diagnosis of nosocomial pneumonia in patients requiring mechanical ventilation in European intensive care units. *Crit Care Med* **37**: 2360-2368.

Krichevsky, M.I., and Love, L.L. (1964) The uptake and utilization of histidine by washed amoebae in the course of development in *Dictyostelium discoideum*. *J Gen Microbiol* **34**: 483-490.

Kroening, T.A., and Kendrick, K.E. (1987) In vivo regulation of histidine ammonia-lyase activity from *Streptomyces griseus*. *J Bacteriol* **169**: 823-829.

Kulasakara, H., Lee, V., Brencic, A., Liberati, N., Urbach, J., Miyata, S., Lee, D.G., Neely, A.N., Hyodo, M., Hayakawa, Y., Ausubel, F.M., and Lory, S. (2006) Analysis of *Pseudomonas aeruginosa* diguanylate cyclases and phosphodiesterases reveals a role for bis-(3'-5')-cyclic-GMP in virulence. *Proc Natl Acad Sci U S A* **103**: 2839-2844.

Kumarevel, T., Mizuno, H., and Kumar, P.K. (2005) Structural basis of HutP-mediated anti-termination and roles of the Mg^{2+} ion and $_{L}$-histidine ligand. *Nature* **434**: 183-191.

La Rosa, R., Johansen, H.K., and Molin, S. (2019) Adapting to the airways: metabolic requirements of *Pseudomonas aeruginosa* during the infection of cystic fibrosis patients. *Metabolites* **9**: 234.

Laarman, A.J., Bardoel, B.W., Ruyken, M., Fernie, J., Milder, F.J., van Strijp, J.A., and Rooijakkers, S.H. (2012) *Pseudomonas aeruginosa* alkaline protease blocks complement activation via the classical and lectin pathways. *J Immunol* **188**: 386-393.

Lamont, I.L., Beare, P.A., Ochsner, U., Vasil, A.I., and Vasil, M.L. (2002) Siderophore-mediated signaling regulates virulence factor production in *Pseudomonas aeruginosa*. *Proc Natl Acad Sci U S A* **99**: 7072-7077.

Lee, E.J., Cowell, B.A., Evans, D.J., and Fleiszig, S.M. (2003) Contribution of ExsA-regulated factors to corneal infection by cytotoxic and invasive *Pseudomonas aeruginosa* in a murine scarification model. *Invest Ophthalmol Vis Sci* **44**: 3892-3898.

Leidigh, B.J., and Wheelis, M.L. (1973) Genetic control of the histidine dissimilatory pathway in *Pseudomonas putida*. *Mol Gen Genet* **120**: 201-210.

Lemmens, L., Tilleman, L., De Koning, E., Valegard, K., Lindas, A.C., Van Nieuwerburgh, F., Maes, D., and Peeters, E. (2019) YtrASa, a GntR-family transcription factor, represses two genetic loci encoding membrane proteins in *Sulfolobus acidocaldarius*. *Front Microbiol* **10**: 2084.

Lenski, R.E., (1991) Chapter 9 - quantifying fitness and gene stability in microorganisms. In: Assessing Ecological Risks of Biotechnology. L.R. Ginzburg (ed). Boston: Butterworth-Heinemann, pp. 173-192.

Lessie, T.G., and Neidhardt, F.C. (1967) Formation and operation of the histidine-degrading pathway in *Pseudomonas aeruginosa*. *J Bacteriol* **93**: 1800-1810.

Liang, X., Yu, X., Pan, X., Wu, J., Duan, Y., Wang, J., and Zhou, M. (2018) A thiadiazole reduces the virulence of *Xanthomonas oryzae* pv. *oryzae* by inhibiting the histidine utilization pathway and quorum sensing. *Mol Plant Pathol* **19**: 116-128.

Lister, P.D., Wolter, D.J., and Hanson, N.D. (2009) Antibacterial-resistant *Pseudomonas aeruginosa*: clinical impact and complex regulation of chromosomally encoded resistance mechanisms. *Clin Microbiol Rev* **22**: 582-610.

Liu, Y., Gokhale, C.S., Rainey, P.B., and Zhang, X.X. (2017) Unravelling the complexity and redundancy of carbon catabolic repression in *Pseudomonas fluorescens* SBW25. *Mol Microbiol* **105**: 589-605.

Liu, Y., Rainey, P.B., and Zhang, X.X. (2014) Mini-Tn7 vectors for studying post-transcriptional gene expression in *Pseudomonas*. *J Microbiol Methods* **107**: 182-185.

Lonergan, Z.R., Palmer, L.D., and Skaar, E.P. (2020) Histidine utilization is a critical determinant of *Acinetobacter* pathogenesis. *Infect Immun* **88**: e00118-00120.

Lozada-Chavez, I., Angarica, V.E., Collado-Vides, J., and Contreras-Moreira, B. (2008) The role of DNA-binding specificity in the evolution of bacterial regulatory networks. *J Mol Biol* **379**: 627-643.

Lugtenberg, B.J., Kravchenko, L.V., and Simons, M. (1999) Tomato seed and root exudate sugars: composition, utilization by *Pseudomonas* biocontrol strains and role in rhizosphere colonization. *Environ Microbiol* **1**: 439-446.

Luhby, A.L., and Cooperman, J.M. (1964) Folic acid deficiency in man and its interrelationship with vitamin B12 metabolism. *Adv Metab Disord* **15**: 263-334.

Luhby, A.L., Cooperman, J.M., and Teller, D.N. (1959) Urinary excretion of formiminoglutamic acid: application in diagnosis of clinical folic acid deficiency. *Am J Clin Nutr* **7**: 397-406.

Lund-Palau, H., Turnbull, A.R., Bush, A., Bardin, E., Cameron, L., Soren, O., Wierre-Gore, N., Alton, E.W., Bundy, J.G., Connett, G., Faust, S.N., Filloux, A., Freemont, P., Jones, A., Khoo, V., Morales, S., Murphy, R., Pabary, R., Simbo, A., Schelenz, S., Takats, Z., Webb, J., Williams, H.D., and Davies, J.C. (2016) *Pseudomonas aeruginosa* infection in cystic fibrosis: pathophysiological mechanisms and therapeutic approaches. *Expert Rev Respir Med* **10**: 685-697.

Lundgren, B.R., Sarwar, Z., Feldman, K.S., Shoytush, J.M., and Nomura, C.T. (2019) SfnR2 regulates dimethyl sulfide-related utilization in *Pseudomonas aeruginosa* PAO1. *J Bacteriol* **201**: JB.00606-00618.

Lyczak, J.B., Cannon, C.L., and Pier, G.B. (2000) Establishment of *Pseudomonas aeruginosa* infection: lessons from a versatile opportunist. *Microbes Infect* **2**: 1051-1060.

Magasanik, B. (1955) The metabolic control of histidine assimilation and dissimilation in *Aerobacter aerogenes*. *J Biol Chem* **213**: 557-569.

Magasanik, B. (1961) Catabolite repression. *Cold Spring Harb Symp Quant Biol* **26**: 249-256.

Magasanik, B., and Bowser, H.R. (1955) The degradation of histidine by *Aerobacter aerogenes*. *J Biol Chem* **213**: 571-580.

Magasanik, B., Lund, P., Neidhardt, F.C., and Schwartz, D.T. (1965) Induction and repression of the histidine-degrading enzymes in *Aerobacter aerogenes*. *J Biol Chem* **240**: 4320-4324.

Mahajan-Miklos, S., Tan, M.-W., Rahme, L.G., and Ausubel, F.M. (1999) Molecular mechanisms of bacterial virulence elucidated using a *Pseudomonas aeruginosa–Caenorhabditis elegans* pathogenesis model. *Cell* **96**: 47-56.

Majumdar, R., Yori, A., Rush, P.W., Raymond, K., Gavrilov, D., Tortorelli, S., Matern, D., Rinaldo, P., Feldman, G.L., and Oglesbee, D. (2017) Allelic spectrum of formiminotransferase-cyclodeaminase gene variants in individuals with formiminoglutamic aciduria. *Mol Genet Genomic Med* **5**: 795-799.

Mao, Y., Vyas, N.K., Vyas, M.N., Chen, D.H., Ludtke, S.J., Chiu, W., and Quiocho, F.A. (2004) Structure of the bifunctional and Golgi-associated formiminotransferase cyclodeaminase octamer. *EMBO J* **23**: 2963-2971.

Marin, M.M., Yuste, L., and Rojo, F. (2003) Differential expression of the components of the two alkane hydroxylases from *Pseudomonas aeruginosa*. *J Bacteriol* **185**: 3232-3237.

Marti-Arbona, R., Xu, C., Steele, S., Weeks, A., Kuty, G.F., Seibert, C.M., and Raushel, F.M. (2006) Annotating enzymes of unknown function: N-formimino-L-glutamate deiminase is a member of the amidohydrolase superfamily. *Biochemistry* **45**: 1997-2005.

Matsuda, I., Matsuo, K., Endo, F., Uehara, I., Nagata, N., Jinno, Y., Chikazawa, S., Miyakita, T., and Miura, H. (1982) Skin histidase activity and urine formiminoglutamic acid (FIGLU) in patients with histidinemia found by screening newborn infants. *Clinica Chimica Acta* **119**: 319-328.

Maurice, N.M., Bedi, B., and Sadikot, R.T. (2018) *Pseudomonas aeruginosa* biofilms: host response and clinical implications in lung infections. *Am J Respir Cell Mol Biol* **58**: 428-439.

McDonald, N.D., Lubin, J.B., Chowdhury, N., and Boyd, E.F. (2016) Host-derived sialic acids are an important nutrient source required for optimal bacterial fitness in vivo. *mBio* **7**: e02237-02215.

Merulla, D., and van der Meer, J.R. (2016) Regulatable and modulable background expression control in prokaryotic synthetic circuits by auxiliary repressor binding sites. *ACS Synth Biol* **5**: 36-45.

Meyer, J.M., Neely, A., Stintzi, A., Georges, C., and Holder, I.A. (1996) Pyoverdin is essential for virulence of *Pseudomonas aeruginosa*. *Infect Immun* **64**: 518-523.

Minandri, F., Imperi, F., Frangipani, E., Bonchi, C., Visaggio, D., Facchini, M., Pasquali, P., Bragonzi, A., and Visca, P. (2016) Role of Iron uptake systems in *Pseudomonas aeruginosa* virulence and airway infection. *Infect Immun* **84**: 2324-2335.

Miyata, S., Casey, M., Frank, D.W., Ausubel, F.M., and Drenkard, E. (2003) Use of the *Galleria mellonella* caterpillar as a model host to study the role of the type III secretion system in *Pseudomonas aeruginosa* pathogenesis. *Infect Immun* **71**: 2404-2413.

Mogayzel, P.J., Jr., Naureckas, E.T., Robinson, K.A., Brady, C., Guill, M., Lahiri, T., Lubsch, L., Matsui, J., Oermann, C.M., Ratjen, F., Rosenfeld, M., Simon, R.H., Hazle, L., Sabadosa, K., Marshall, B.C., and Cystic Fibrosis Foundation Pulmonary Clinical Practice Guidelines, C. (2014) Cystic Fibrosis Foundation pulmonary guideline. Pharmacologic approaches to prevention and eradication of initial Pseudomonas aeruginosa infection. *Ann Am Thorac Soc* **11**: 1640-1650.

Mohamed, S.D., and Roberts, M. (1966) Relative importance of formiminoglutamic and urocanic acid excretion after a histidine load. *J Clin Pathol* **19**: 37-42.

Moller, S., Croning, M.D., and Apweiler, R. (2001) Evaluation of methods for the prediction of membrane spanning regions. *Bioinformatics* **17**: 646-653.

Morales-Soto, N., Anyan, M.E., Mattingly, A.E., Madukoma, C.S., Harvey, C.W., Alber, M., Deziel, E., Kearns, D.B., and Shrout, J.D. (2015) Preparation, imaging, and quantification of bacterial surface motility assays. *J Vis Exp*: 52338.

Moreno, R., Martinez-Gomariz, M., Yuste, L., Gil, C., and Rojo, F. (2009) The *Pseudomonas putida* Crc global regulator controls the hierarchical assimilation of amino acids in a complete medium: evidence from proteomic and genomic analyses. *Proteomics* **9**: 2910-2928.

Mosquera-Rendon, J., Rada-Bravo, A.M., Cardenas-Brito, S., Corredor, M., Restrepo-Pineda, E., and Benitez-Paez, A. (2016) Pangenome-wide and molecular evolution analyses of the *Pseudomonas aeruginosa* species. *BMC Genomics* **17**: 45.

Mota, L.J., Sarmento, L.M., and de Sa-Nogueira, I. (2001) Control of the arabinose regulon in *Bacillus subtilis* by AraR in vivo: crucial roles of operators, cooperativity, and DNA looping. *J Bacteriol* **183**: 4190-4201.

Mota, L.J., Tavares, P., and Sa-Nogueira, I. (1999) Mode of action of AraR, the key regulator of $_{L}$-arabinose metabolism in *Bacillus subtilis*. *Mol Microbiol* **33**: 476-489.

Nagoba, B., Davane, M., Gandhi, R., Wadher, B., Suryawanshi, N., and Selkar, S. (2017) Treatment of skin and soft tissue infections caused by *Pseudomonas aeruginosa* —A review of our experiences with citric acid over the past 20 years. *Wound Medicine* **19**: 5-9.

Naren, N., and Zhang, X.X. (2020) Global regulatory roles of the histidine-responsive transcriptional repressor HutC in *Pseudomonas fluorescens* SBW25. *J Bacteriol* **202**: e00792-00719.

Naren, N., and Zhang, X.X. (2021) Role of a local transcription factor in governing cellular carbon/nitrogen homeostasis in *Pseudomonas fluorescens*. *Nucleic Acids Res* **49**: 3204-3216.

Neidhardt, F.C., and Magasanik, B. (1957) Reversal of the glucose inhibition of histidase biosynthesis in Aerobacter aerogenes. *J Bacteriol* **73**: 253-259.

Nieuwkoop, A.J., and Bender, R.A. (1988) RNA polymerase as a repressor of transcription in the hut(P) region of mutant *Klebsiella aerogenes* histidine utilization operons. *J Bacteriol* **170**: 4986-4990.

Nieuwkoop, A.J., Boylan, S.A., and Bender, R.A. (1984) Regulation of hutUH operon expression by the catabolite gene activator protein-cyclic AMP complex in *Klebsiella aerogenes*. *J Bacteriol* **159**: 934-939.

Nishijyo, T., Haas, D., and Itoh, Y. (2001) The CbrA-CbrB two-component regulatory system controls the utilization of multiple carbon and nitrogen sources in *Pseudomonas aeruginosa*. *Mol Microbiol* **40**: 917-931.

O'Toole, G.A. (2011) Microtiter dish biofilm formation assay. *J Vis Exp*: 2437.

Oda, M., Sugishita, A., and Furukawa, K. (1988) Cloning and nucleotide sequences of histidase and regulatory genes in the *Bacillus subtilis* hut operon and positive regulation of the operon. *J Bacteriol* **170**: 3199-3205.

Osterman, I.A., Evfratov, S.A., Sergiev, P.V., and Dontsova, O.A. (2013) Comparison of mRNA features affecting translation initiation and reinitiation. *Nucleic Acids Res* **41**: 474-486.

Osuna, R., Janes, B.K., and Bender, R.A. (1994a) Roles of catabolite activator protein sites centered at -81.5 and -41.5 in the activation of the *Klebsiella aerogenes* histidine utilization operon *hutUH*. *J Bacteriol* **176**: 5513-5524.

Osuna, R., Schwacha, A., and Bender, R.A. (1994b) Identification of the *hutUH* operator (*hutUo*) from *Klebsiella aerogenes* by DNA deletion analysis. *J Bacteriol* **176**: 5525-5529.

Overhage, J., Bains, M., Brazas, M.D., and Hancock, R.E. (2008) Swarming of *Pseudomonas aeruginosa* is a complex adaptation leading to increased production of virulence factors and antibiotic resistance. *J Bacteriol* **190**: 2671-2679.

Palleroni, N.J. (2010) The *Pseudomonas* story. *Environ Microbiol* **12**: 1377-1383.

Panagea, S., Winstanley, C., Walshaw, M.J., Ledson, M.J., and Hart, C.A. (2005) Environmental contamination with an epidemic strain of *Pseudomonas aeruginosa* in a Liverpool cystic fibrosis centre, and study of its survival on dry surfaces. *J Hosp Infect* **59**: 102-107.

Panayidou, S., Georgiades, K., Christofi, T., Tamana, S., Promponas, V.J., and Apidianakis, Y. (2020) *Pseudomonas aeruginosa* core metabolism exerts a widespread growth-independent control on virulence. *Sci Rep* **10**: 9505.

Patell, S., Gu, M., Davenport, P., Givskov, M., Waite, R.D., and Welch, M. (2010) Comparative microarray analysis reveals that the core biofilm-associated transcriptome of *Pseudomonas aeruginosa* comprises relatively few genes. *Environ Microbiol Rep* **2**: 440-448.

Patriquin, G.M., Banin, E., Gilmour, C., Tuchman, R., Greenberg, E.P., and Poole, K. (2008) Influence of quorum sensing and iron on twitching motility and biofilm formation in *Pseudomonas aeruginosa*. *J Bacteriol* **190**: 662-671.

Pendleton, J.N., Gorman, S.P., and Gilmore, B.F. (2013) Clinical relevance of the ESKAPE pathogens. *Expert Rev Anti Infect Ther* **11**: 297-308.

Perry, T.L., Applegarth, D.A., Evans, M.E., Hansen, S., and Jellum, E. (1975) Metabolic studies of a family with massive formiminoglutamic aciduria. *Pediatr Res* **9**: 117-122.

Peterson, S.N., Dahlquist, F.W., and Reich, N.O. (2007) The role of high affinity non-specific DNA binding by Lrp in transcriptional regulation and DNA organization. *J Mol Biol* **369**: 1307-1317.

Phillips, A.T., and Mulfinger, L.M. (1981) Cyclic adenosine 3',5'-monophosphate levels in *Pseudomonas putida* and *Pseudomonas aeruginosa* during induction and carbon catabolite repression of histidase synthesis. *J Bacteriol* **145**: 1286-1292.

Pirnay, J.P., Matthijs, S., Colak, H., Chablain, P., Bilocq, F., Van Eldere, J., De Vos, D., Zizi, M., Triest, L., and Cornelis, P. (2005) Global *Pseudomonas aeruginosa* biodiversity as reflected in a Belgian river. *Environ Microbiol* **7**: 969-980.

Porta-de-la-Riva, M., Fontrodona, L., Villanueva, A., and Ceron, J. (2012) Basic *Caenorhabditis elegans* methods: synchronization and observation. *J Vis Exp*: e4019.

Prival, M.J., and Magasanik, B. (1971) Resistance to catabolite repression of histidase and proline oxidase during nitrogen-limited growth of *Klebsiella aerogenes*. *J Biol Chem* **246**: 6288-6296.

Pruitt, K.D., Tatusova, T., and Maglott, D.R. (2007) NCBI reference sequences (RefSeq): a curated non-redundant sequence database of genomes, transcripts and proteins. *Nucleic Acids Res* **35**: D61-65.

Quirk, M.F., and Norton, B.W. (1988) Detection of cobalt deficiency in lactating heifers and their calves. *J Agr Sci* **110**: 465-470.

Radhapriya, P., Ramachandran, A., Anandham, R., and Mahalingam, S. (2015) *Pseudomonas aeruginosa* RRALC3 enhances the biomass, nutrient and carbon contents of *Pongamia pinnata* seedlings in degraded forest soil. *PLoS One* **10**: e0139881.

Rahme, L.G., Ausubel, F.M., Cao, H., Drenkard, E., Goumnerov, B.C., Lau, G.W., Mahajan-Miklos, S., Plotnikova, J., Tan, M.W., Tsongalis, J., Walendziewicz, C.L., and Tompkins, R.G. (2000) Plants and animals share functionally common bacterial virulence factors. *Proc Natl Acad Sci U S A* **97**: 8815-8821.

Rainey, P.B. (1999) Adaptation of *Pseudomonas fluorescens* to the plant rhizosphere. *Environ Microbiol* **1**: 243-257.

Rasamiravaka, T., Labtani, Q., Duez, P., and El Jaziri, M. (2015) The formation of biofilms by *Pseudomonas aeruginosa*: a review of the natural and synthetic compounds interfering with control mechanisms. *Biomed Res Int* **2015**: 759348.

Rashid, M.H., and Kornberg, A. (2000) Inorganic polyphosphate is needed for swimming, swarming, and twitching motilities of *Pseudomonas aeruginosa*. *Proc Natl Acad Sci U S A* **97**: 4885-4890.

Recinos, D.A., Sekedat, M.D., Hernandez, A., Cohen, T.S., Sakhtah, H., Prince, A.S., Price-Whelan, A., and Dietrich, L.E. (2012) Redundant phenazine operons in *Pseudomonas aeruginosa* exhibit environment-dependent expression and differential roles in pathogenicity. *Proc Natl Acad Sci U S A* **109**: 19420-19425.

Reitzer, L. (2003) Nitrogen assimilation and global regulation in *Escherichia coli*. *Annu Rev Microbiol* **57**: 155-176.

Resch, M., Schiltz, E., Titgemeyer, F., and Muller, Y.A. (2010) Insight into the induction mechanism of the GntR/HutC bacterial transcription regulator YvoA. *Nucleic Acids Res* **38**: 2485-2497.

Rietsch, A., Wolfgang, M.C., and Mekalanos, J.J. (2004) Effect of metabolic imbalance on expression of type III secretion genes in *Pseudomonas aeruginosa*. *Infect Immun* **72**: 1383-1390.

Rigali, S., Derouaux, A., Giannotta, F., and Dusart, J. (2002) Subdivision of the helix-turn-helix GntR family of bacterial regulators in the FadR, HutC, MocR, and YtrA subfamilies. *J Biol Chem* **277**: 12507-12515.

Rigali, S., Nothaft, H., Noens, E.E., Schlicht, M., Colson, S., Muller, M., Joris, B., Koerten, H.K., Hopwood, D.A., Titgemeyer, F., and van Wezel, G.P. (2006) The sugar phosphotransferase system of *Streptomyces coelicolor* is regulated by the GntR-family regulator DasR and links *N*-acetylglucosamine metabolism to the control of development. *Mol Microbiol* **61**: 1237-1251.

Rocha, E.P. (2008) The organization of the bacterial genome. *Annu Rev Genet* **42**: 211-233.

Rodriguez, R.L., and West, R.W., Jr. (1984) Histidine operon control region of *Klebsiella pneumoniae*: analysis with an *Escherichia coli* promoter-probe plasmid vector. *J Bacteriol* **157**: 764-771.

Rohmer, L., Hocquet, D., and Miller, S.I. (2011) Are pathogenic bacteria just looking for food? Metabolism and microbial pathogenesis. *Trends Microbiol* **19**: 341-348.

Rojo, F. (2010) Carbon catabolite repression in *Pseudomonas* : optimizing metabolic versatility and interactions with the environment. *FEMS Microbiol Rev* **34**: 658-684.

Safer, D., Brenes, M., Dunipace, S., and Schad, G. (2007) Urocanic acid is a major chemoattractant for the skin-penetrating parasitic nematode *Strongyloides stercoralis*. *Proc Natl Acad Sci U S A* **104**: 1627-1630.

Sambrook, J., Fritsch, E.F., and Maniatis, T., (1989) *Molecular cloning A laboratory manual*. Cold Spring Harbour Laboratory Press, Cold Spring Harbour.

Sauer, J.D., Bachman, M.A., and Swanson, M.S. (2005) The phagosomal transporter A couples threonine acquisition to differentiation and replication of *Legionella pneumophila* in macrophages. *Proc Natl Acad Sci U S A* **102**: 9924-9929.

Sayers, E.W., Agarwala, R., Bolton, E.E., Brister, J.R., Canese, K., Clark, K., Connor, R., Fiorini, N., Funk, K., Hefferon, T., Holmes, J.B., Kim, S., Kimchi, A., Kitts, P.A.,

Lathrop, S., Lu, Z., Madden, T.L., Marchler-Bauer, A., Phan, L., Schneider, V.A., Schoch, C.L., Pruitt, K.D., and Ostell, J. (2019) Database resources of the National Center for Biotechnology Information. *Nucleic Acids Res* **47**: D23-D28.

Schlesinger, S., and Magasanik, B. (1965) Imidazolepropionate, a nonmetabolizable inducer for the histidine-degrading enzymes in *Aerobacter aerogenes*. *J Biol Chem* **240**: 4325-4330.

Schlesinger, S., Scotto, P., and Magasanik, B. (1965) Exogenous and endogenous induction of the histidine-degrading enzymes in *Aerobacter aerogenes*. *J Biol Chem* **240**: 4331-4337.

Schröder, J., Maus, I., Meyer, K., Wördemann, S., Blom, J., Jaenicke, S., Schneider, J., Trost, E., and Tauch, A. (2012) Complete genome sequence, lifestyle, and multi-drug resistance of the human pathogen *Corynebacterium resistens* DSM 45100 isolated from blood samples of a leukemia patient. *BMC Genomics* **13**: 141.

Schroder, J., Maus, I., Ostermann, A.L., Kogler, A.C., and Tauch, A. (2012) Binding of the IclR-type regulator HutR in the histidine utilization (*hut*) gene cluster of the human pathogen *Corynebacterium resistens* DSM 45100. *FEMS Microbiol Lett* **331**: 136-143.

Schwacha, A., and Bender, R.A. (1990) Nucleotide sequence of the gene encoding the repressor for the histidine utilization genes of *Klebsiella aerogenes*. *J Bacteriol* **172**: 5477-5481.

Schwacha, A., Cohen, J.A., Gehring, K.B., and Bender, R.A. (1990) Tn*1000*-mediated insertion mutagenesis of the histidine utilization (*hut*) gene cluster from *Klebsiella aerogenes*: genetic analysis of *hut* and unusual target specificity of Tn*1000*. *J Bacteriol* **172**: 5991-5998.

Shatalin, K., Shatalina, E., Mironov, A., and Nudler, E. (2011) H_2S: a universal defense against antibiotics in bacteria. *Science* **334**: 986-990.

Shaw, E., and Wuest, W.M. (2020) Virulence attenuating combination therapy: a potential multi-target synergy approach to treat *Pseudomonas aeruginosa* infections in cystic fibrosis patients. *RSC Med Chem* **11**: 358-369.

Shen, D.K., Filopon, D., Chaker, H., Boullanger, S., Derouazi, M., Polack, B., and Toussaint, B. (2008) High-cell-density regulation of the *Pseudomonas aeruginosa* type III secretion system: implications for tryptophan catabolites. *Microbiology (Reading)* **154**: 2195-2208.

Sieira, R., Arocena, G.M., Bukata, L., Comerci, D.J., and Ugalde, R.A. (2010) Metabolic control of virulence genes in *Brucella abortus*: HutC coordinates *virB* expression and the histidine utilization pathway by direct binding to both promoters. *J Bacteriol* **192**: 217-224.

Sieira, R., Bialer, M.G., Roset, M.S., Ruiz-Ranwez, V., Langer, T., Arocena, G.M., Mancini, E., and Zorreguieta, A. (2017) Combinatorial control of adhesion of *Brucella abortus* 2308 to host cells by transcriptional rewiring of the trimeric autotransporter *btaE* gene. *Mol Microbiol* **103**: 553-565.

Silby, M.W., Winstanley, C., Godfrey, S.A., Levy, S.B., and Jackson, R.W. (2011) *Pseudomonas* genomes: diverse and adaptable. *FEMS Microbiol Rev* **35**: 652-680.

Smith, G.R., Halpern, Y.S., and Magasanik, B. (1971) Genetic and metabolic control of enzymes responsible for histidine degradation in *Salmonella typhimurium*. 4-imidazolone-5-propionate amidohydrolase and N-formimino-L-glutamate formiminohydrolase. *J Biol Chem* **246**: 3320-3329.

Smith, G.R., and Magasanik, B. (1971a) Nature and self-regulated synthesis of the repressor of the *hut* operons in *Salmonella typhimurium*. *Proc Natl Acad Sci U S A* **68**: 1493-1497.

Smith, G.R., and Magasanik, B. (1971b) The two operons of the histidine utilization system in *Salmonella typhimurium*. *J Biol Chem* **246**: 3330-3341.

Snellman, E., Jansen, C.T., Rantanen, T., and Pasanen, P. (1999) Epidermal urocanic acid concentration and photoisomerization reactivity in patients with cutaneous malignant melanoma or basal cell carcinoma. *Acta Derm Venereol* **79**: 200-203.

Solans, A., Estivill, X., and de la Luna, S. (2000) Cloning and characterization of human FTCD on 21q22.3, a candidate gene for glutamate formiminotransferase deficiency. *Cytogenet Cell Genet* **88**: 43-49.

Somers, E., Vanderleyden, J., and Srinivasan, M. (2004) Rhizosphere bacterial signalling: A love parade beneath our feet. *Crit Rev Microbiol* **30**: 205-240.

Sonnleitner, E., Abdou, L., and Haas, D. (2009) Small RNA as global regulator of carbon catabolite repression in *Pseudomonas aeruginosa*. *Proc Natl Acad Sci U S A* **106**: 21866-21871.

Sonnleitner, E., and Blasi, U. (2014) Regulation of Hfq by the RNA CrcZ in *Pseudomonas aeruginosa* carbon catabolite repression. *PLoS Genet* **10**: e1004440.

Sonnleitner, E., Prindl, K., and Blasi, U. (2017) The *Pseudomonas aeruginosa* CrcZ RNA interferes with Hfq-mediated riboregulation. *PLoS One* **12**: e0180887.

Sonnleitner, E., Valentini, M., Wenner, N., Haichar, F.Z., Haas, D., and Lapouge, K. (2012) Novel targets of the CbrAB/Crc carbon catabolite control system revealed by transcript abundance in *Pseudomonas aeruginosa*. *PLoS One* **7**: e44637.

Sonnleitner, E., Wulf, A., Campagne, S., Pei, X.Y., Wolfinger, M.T., Forlani, G., Prindl, K., Abdou, L., Resch, A., Allain, F.H., Luisi, B.F., Urlaub, H., and Blasi, U. (2018) Interplay between the catabolite repression control protein Crc, Hfq and RNA in Hfq-dependent translational regulation in *Pseudomonas aeruginosa*. *Nucleic Acids Res* **46**: 1470-1485.

Sprouffske, K., and Wagner, A. (2016) Growthcurver: an R package for obtaining interpretable metrics from microbial growth curves. *BMC Bioinformatics* **17**: 172.

Stebbings, R.S., and Lewis, G. (1986) Cobalt deficiency and urinary formiminoglutamic acid in lambs. *Br Vet J* **142**: 270-274.

Stover, C.K., Pham, X.Q., Erwin, A.L., Mizoguchi, S.D., Warrener, P., Hickey, M.J., Brinkman, F.S., Hufnagle, W.O., Kowalik, D.J., Lagrou, M., Garber, R.L., Goltry, L., Tolentino, E., Westbrock-Wadman, S., Yuan, Y., Brody, L.L., Coulter, S.N., Folger, K.R., Kas, A., Larbig, K., Lim, R., Smith, K., Spencer, D., Wong, G.K., Wu, Z., Paulsen, I.T., Reizer, J., Saier, M.H., Hancock, R.E., Lory, S., and Olson, M.V.

(2000) Complete genome sequence of *Pseudomonas aeruginosa* PAO1, an opportunistic pathogen. *Nature* **406**: 959-964.

Streeter, K., and Katouli, M. (2016) *Pseudomonas aeruginosa*: a review of their pathogenesis and prevalence in clinical settings and the environment. *Infection, Epidemiology and Medicine* **2**: 25-32.

Suvorova, I.A., Korostelev, Y.D., and Gelfand, M.S. (2015) GntR family of bacterial transcription factors and their DNA binding motifs: structure, positioning and co-evolution. *PLoS One* **10**: e0132618.

Szalewska-Palasz, A., Wegrzyn, A., Blaszczak, A., Taylor, K., and Wegrzyn, G. (1998) DnaA-stimulated transcriptional activation of orilambda: *Escherichia coli* RNA polymerase beta subunit as a transcriptional activator contact site. *Proc Natl Acad Sci U S A* **95**: 4241-4246.

Tabor, H., and Mehler, A.H. (1954) Isolation of N-formyl-L-glutamic acid as an intermediate in the enzymatic degradation of L-histidine. *J Biol Chem* **210**: 559-568.

Takase, H., Nitanai, H., Hoshino, K., and Otani, T. (2000) Impact of siderophore production on *Pseudomonas aeruginosa* infections in immunosuppressed mice. *Infect Immun* **68**: 1834-1839.

Tan, M.W., and Ausubel, F.M. (2000) *Caenorhabditis elegans*: a model genetic host to study *Pseudomonas aeruginosa* pathogenesis. *Curr Opin Microbiol* **3**: 29-34.

Tan, M.W., Mahajan-Miklos, S., and Ausubel, F.M. (1999) Killing of *Caenorhabditis elegans* by *Pseudomonas aeruginosa* used to model mammalian bacterial pathogenesis. *Proc Natl Acad Sci U S A* **96**: 715-720.

Tart, A.H., Blanks, M.J., and Wozniak, D.J. (2006) The AlgT-dependent transcriptional regulator AmrZ (AlgZ) inhibits flagellum biosynthesis in mucoid, nonmotile *Pseudomonas aeruginosa* cystic fibrosis isolates. *J Bacteriol* **188**: 6483-6489.

Turner, K.H., Everett, J., Trivedi, U., Rumbaugh, K.P., and Whiteley, M. (2014) Requirements for *Pseudomonas aeruginosa* acute burn and chronic surgical wound infection. *PLoS Genet* **10**: e1004518.

Valentini, M., Garcia-Maurino, S.M., Perez-Martinez, I., Santero, E., Canosa, I., and Lapouge, K. (2014) Hierarchical management of carbon sources is regulated similarly by the CbrA/B systems in *Pseudomonas aeruginosa* and *Pseudomonas putida*. *Microbiology (Reading)* **160**: 2243-2252.

Vallet-Gely, I., Sharp, J.S., and Dove, S.L. (2007) Local and global regulators linking anaerobiosis to *cupA* fimbrial gene expression in *Pseudomonas aeruginosa*. *J Bacteriol* **189**: 8667-8676.

Vallet, I., Olson, J.W., Lory, S., Lazdunski, A., and Filloux, A. (2001) The chaperone/usher pathways of *Pseudomonas aeruginosa*: identification of fimbrial gene clusters (*cup*) and their involvement in biofilm formation. *Proc Natl Acad Sci U S A* **98**: 6911-6916.

Valot, B., Guyeux, C., Rolland, J.Y., Mazouzi, K., Bertrand, X., and Hocquet, D. (2015) What it takes to be a *Pseudomonas aeruginosa*? The core genome of the opportunistic pathogen updated. *PLoS One* **10**: e0126468.

van Hijum, S.A., Medema, M.H., and Kuipers, O.P. (2009) Mechanisms and evolution of control logic in prokaryotic transcriptional regulation. *Microbiol Mol Biol Rev* **73**: 481-509, Table of Contents.

Vance, R.E., Rietsch, A., and Mekalanos, J.J. (2005) Role of the type III secreted exoenzymes S, T, and Y in systemic spread of *Pseudomonas aeruginosa* PAO1 in vivo. *Infect Immun* **73**: 1706-1713.

Waite, R.D., Rose, R.S., Rangarajan, M., Aduse-Opoku, J., Hashim, A., and Curtis, M.A. (2012) *Pseudomonas aeruginosa* possesses two putative type I signal peptidases, LepB and PA1303, each with distinct roles in physiology and virulence. *J Bacteriol* **194**: 4521-4536.

Walker, T.S., Bais, H.P., Deziel, E., Schweizer, H.P., Rahme, L.G., Fall, R., and Vivanco, J.M. (2004) *Pseudomonas aeruginosa*-plant root interactions. Pathogenicity, biofilm formation, and root exudation. *Plant Physiol* **134**: 320-331.

Wang, C., Ye, F., Kumar, V., Gao, Y.G., and Zhang, L.H. (2014) BswR controls bacterial motility and biofilm formation in *Pseudomonas aeruginosa* through modulation of the small RNA rsmZ. *Nucleic Acids Res* **42**: 4563-4576.

Weiser, R., Green, A.E., Bull, M.J., Cunningham-Oakes, E., Jolley, K.A., Maiden, M.C.J., Hall, A.J., Winstanley, C., Weightman, A.J., Donoghue, D., Amezquita, A., Connor, T.R., and Mahenthiralingam, E. (2019) Not all *Pseudomonas aeruginosa* are equal: strains from industrial sources possess uniquely large multireplicon genomes. *Microb Genom* **5**.

Winsor, G.L., Griffiths, E.J., Lo, R., Dhillon, B.K., Shay, J.A., and Brinkman, F.S. (2016) Enhanced annotations and features for comparing thousands of *Pseudomonas* genomes in the Pseudomonas genome database. *Nucleic Acids Res* **44**: D646-653.

Winstanley, C., O'Brien, S., and Brockhurst, M.A. (2016) *Pseudomonas aeruginosa* evolutionary adaptation and diversification in cystic fibrosis chronic lung infections. *Trends Microbiol* **24**: 327-337.

Wirebrand, L., Madhushani, A.W.K., Irie, Y., and Shingler, V. (2018) Multiple Hfq-Crc target sites are required to impose catabolite repression on (methyl)phenol metabolism in *Pseudomonas putida* CF600. *Environ Microbiol* **20**: 186-199.

Wolfgang, M.C., Kulasekara, B.R., Liang, X., Boyd, D., Wu, K., Yang, Q., Miyada, C.G., and Lory, S. (2003) Conservation of genome content and virulence determinants among clinical and environmental isolates of *Pseudomonas aeruginosa*. *Proc Natl Acad Sci U S A* **100**: 8484-8489.

Wray, L.V., Jr., and Fisher, S.H. (1994) Analysis of *Bacillus subtilis hut* operon expression indicates that histidine-dependent induction is mediated primarily by transcriptional antitermination and that amino acid repression is mediated by two mechanisms: regulation of transcription initiation and inhibition of histidine transport. *J Bacteriol* **176**: 5466-5473.

Wray, L.V., Jr., Pettengill, F.K., and Fisher, S.H. (1994) Catabolite repression of the *Bacillus subtilis hut* operon requires a cis-acting site located downstream of the transcription initiation site. *J Bacteriol* **176**: 1894-1902.

Yahr, T.L., and Parsek, M.R., (2006) *Pseudomonas aeruginosa*. In: The Prokaryotes: Volume 6: Proteobacteria: Gamma Subclass. M. Dworkin, S. Falkow, E. Rosenberg, K.-H. Schleifer & E. Stackebrandt (eds). New York, NY: Springer New York, pp. 704-713.

Yao, X., He, W., and Lu, C.D. (2011) Functional characterization of seven gamma-Glutamylpolyamine synthetase genes and the *bauRABCD* locus for polyamine and beta-alanine utilization in *Pseudomonas aeruginosa* PAO1. *J Bacteriol* **193**: 3923-3930.

Yeung, A.T., Torfs, E.C., Jamshidi, F., Bains, M., Wiegand, I., Hancock, R.E., and Overhage, J. (2009) Swarming of *Pseudomonas aeruginosa* is controlled by a broad spectrum of transcriptional regulators, including MetR. *J Bacteriol* **191**: 5592-5602.

Yoshida, K., Sano, H., Seki, S., Oda, M., Fujimura, M., and Fujita, Y. (1995) Cloning and sequencing of a 29 kb region of the *Bacillus subtilis* genome containing the *hut* and *wapA* loci. *Microbiology (Reading)* **141 (Pt 2)**: 337-343.

Young, A.T., Ly, K.N., Wilson, C., Lehnert, K., Snell, R.G., Reid, S.J., and Jacobsen, J.C. (2018) Modelling brain dopamine-serotonin vesicular transport disease in *Caenorhabditis elegans*. *Dis Model Mech* **11**: dmm035709.

Yuji, N. (2010) Identification of the transcriptional regulatory gene of histidase and urocanase in *Pseudomonas aeruginosa* -Regulation of histidase and urocanase expression. *Aino journal*.

Zhang, X.X., Chang, H., Tran, S.L., Gauntlett, J.C., Cook, G.M., and Rainey, P.B. (2012) Variation in transport explains polymorphism of histidine and urocanate utilization in a natural *Pseudomonas* population. *Environ Microbiol* **14**: 1941-1951.

Zhang, X.X., George, A., Bailey, M.J., and Rainey, P.B. (2006) The histidine utilization *(hut)* genes of *Pseudomonas fluorescens* SBW25 are active on plant surfaces, but are not required for competitive colonization of sugar beet seedlings. *Microbiology (Reading)* **152**: 1867-1875.

Zhang, X.X., and Rainey, P.B. (2007a) Construction and validation of a neutrally-marked strain of *Pseudomonas fluorescens* SBW25. *J Microbiol Methods* **71**: 78-81.

Zhang, X.X., and Rainey, P.B. (2007b) Genetic analysis of the histidine utilization (*hut*) genes in *Pseudomonas fluorescens* SBW25. *Genetics* **176**: 2165-2176.

Zhang, X.X., and Rainey, P.B. (2008) Dual involvement of CbrAB and NtrBC in the regulation of histidine utilization in *Pseudomonas fluorescens* SBW25. *Genetics* **178**: 185-195.

Zhang, X.X., and Rainey, P.B. (2013) Exploring the sociobiology of pyoverdin-producing *Pseudomonas*. *Evolution* **67**: 3161-3174.

Zhang, X.X., Ritchie, S.R., and Rainey, P.B. (2014) Urocanate as a potential signaling molecule for bacterial recognition of eukaryotic hosts. *Cell Mol Life Sci* **71**: 541-547.